Systemic Analysis of the Radiation- and Oxidation-induced Cellular Signaling Response

Dissertation

zur

Erlangung der naturwissenschaftlichen Doktorwürde

(Dr. sc. nat.)

vorgelegt der

Mathematisch-naturwissenschaftlichen Fakultät

der

Universität Zürich

von

Andrej Bluwstein

aus

Deutschland

Promotionskomitee

Prof. Dr. Dr. Michael O. Hottiger

(Leiter der Dissertation)

Prof. Dr. Alessandro A. Sartori

(Vorsitzender des Komitees)

Prof. Dr. Lars E. French

Dr. Markus Ehrat

Zürich 2013

Summary

DNA is under constant attack by various genotoxins from the environment or from within the cell. To preserve genome integrity and prevent propagation of mutations into progeny, a major goal is to recognize genotoxic stress and to respond in an appropriate manner. The cellular response to a specific genotoxic stress is regulated by different enzymes, which fine-tune a sophisticated network of intracellular signaling cascades. Understanding the complexity of genotoxic stress-induced signaling events in cells could assist the development of new treatment strategies for the therapy of tumors.

The aims of this thesis were to understand i) the resistance of human primary fibroblasts towards high doses of ionizing radiation (IR) and ii) the mechanism of ARTD1 activation upon oxidative stress. Based on a kinetic network analysis by protein microarrays, we observed IR-induced phosphorylation of PKC family members, which fostered pro-survival signaling of human fibroblasts via CREB and Bad phosphorylation. Inhibition or knockdown of PKC family members induced a transition from IR-induced senescence to apoptosis, which was accompanied by p53 and Bad stabilization, cleavage of ARTD1 and enhanced DNA fragmentation, and thus indicated a PKC-dependent molecular survival mechanism. A similar network analysis in combination with an inhibitor screen was employed to identify positive and negative regulators of poly-ADP-ribose (PAR) formation upon H_2O_2. Validation of candidates revealed enhanced and reduced activation of ARTD1 by CaMKIIδ and the calcium-independent PKCδ, respectively. Importantly, PAR formation was abolished upon the depletion of calcium-dependent PKC family members (e.g., PKCα), thus revealing a dual role of PKC in regulating ARTD1 activity upon H_2O_2 exposure. Finally, we confirmed that oxidative stress activates PLC and subsequently IP3R/RYR receptors and thereby leads to calcium release from the ER, which is required for PAR formation. Chelation of calcium not only prevented PAR formation, but also reduced DNA single-strand break formation, indicating a correlation between calcium-dependent PAR formation and DNA damage.

In summary, these studies highlighted the importance of cytoplasmic signaling at the forefront of the response to irradiation and oxidative stress. The activation of the nuclear genotoxic stress response and the regulation of cell fate thus rely on these signal responses.

Zusammenfassung

DNA ist ständig den schädigenden Einflüssen genotoxischer Substanzen aus der Umwelt und der Zelle ausgesetzt. Um die Integrität des Genoms zu wahren und die Vererbung von Mutationen zu verhindern, ist es das Ziel genotoxische Stressfaktoren zu erkennen und darauf entsprechend zu antworten. Die Antwort auf genotoxischen Stress ist durch die Aktivierung eines ausgeklügelten Netzwerks von verschiedenen Signalkaskaden gesteuert. Das Verständnis der Komplexität der Signalvermittlung als Antwort auf genotoxischen Stress ist für die Entwicklung neuer Behandlungsstrategien für die Therapie von Tumoren von Bedeutung.

Die wichtigsten Ziele dieser Dissertation waren das Verständnis i) der Radioresistenz humaner, primärer Fibroblasten als Antwort auf hohe Dosen ionisierender Strahlung (IS) und ii) des Mechanismus der Aktivierung von ARTD1 als Antwort auf oxidativen Stress. Basierend auf der kinetischen Netzwerkanalyse konnten wir die IS-abhängige Phosphorylierung von Mitgliedern der PKC Familie beobachten, welche das Überleben der humanen Fibroblasten mittels Phosphorylierung von CREB und Bad förderten. Die Inhibierung oder Reduktion von PKCs hat zu einer Verschiebung der Antwort auf Bestrahlung von Seneszenz zum Zelltod geführt. Für diese Veränderung waren die Stabilisierung von p53 und Bad, die Spaltung von ARTD1 und die Fragmentierung von DNA ausschlaggebend. Basierend auf der Netzwerkanalyse und einem pharmakologischen Screen haben wir positive und negative Regulatoren der poly-ADP-ribose (PAR) Bildung als Antwort auf oxidativen Stress entdeckt. Funktionelle Validierung der Kandidaten hat ergeben, dass ARTD1 durch CaMKIIδ und PKCδ positiv und negativ reguliert wird. Ausschlaggebend konnten wir mit Hilfe der Reduktion von Kalzium-abhängigen PKC Mitgliedern (PKCα) die Inhibierung und damit duale Regulierung der ARTD1 Aktivität durch PKC zeigen. Schlussendlich haben wir funktionell bestätigt, dass oxidativer Stress zum Kalziumausstrom aus dem ER mittels PLC und IP3R/RYR führt, was eine Voraussetzung für die PAR Bildung war. Die Komplexierung von Kalzium hat nicht nur zur Inhibierung von PAR, sondern auch zur Reduktion von Einzelstrang-Brüchen der DNA geführt.

Zusammenfassend haben diese Studien die Bedeutung zytoplasmatischer Signalwege als erste Antwort auf zellulären Stress durch Bestrahlung oder oxidativen Stress herausgestellt. Die Aktivierung der nukleären, genotoxischen Stressantwort und die Regulation des Zellzustands hängt somit entscheidend von diesen Signalkaskaden ab.

Table of contents

Abbreviations

53BP1	Tumor suppressor p53-binding protein 1
ADP	Adenosine diphosphate
ADPR	Adenosine diphosphate ribose
AIF	Apoptosis inducing factor
ARTD1	ADP-ribosyltransferase Diphtheria toxin-like 1
ASK1	Apoptosis signal-regulating kinase 1
JNK	c-Jun N-terminal kinase
ATF4	Activating transcription factor 4
ATF6	Activating transcription factor 6
ATM	Ataxiatelangiectasia mutated
ATP	Adenosine-5'-triphosphate
ATR	Ataxia telangiectasia and Rad3-related protein
Bad	BCL2-associated agonist of cell death
Bak	BCL2-antagonist/killer 1
Bcl-2	B-cell lymphoma 2
BER	Base excision repair
BIM	Bisindolylmaleimide
BiP	Binding immunoglobulin protein
BRCA1	Breast cancer type 1 susceptibility protein
cADPR	Cyclic adenosine diphosphate ribose
CaM	Calmodulin (Ca^{2+}-modulated protein)
CaMKII	Ca^{2+}/calmodulin-dependent protein kinases II
CD38	Cluster of differentiation 38
CDK	Cyclin-dependent kinases
Chk1/2	Checkpoint kinase-1/2
CICR	Ca^{2+} induced Ca^{2+} release
CREB	Cyclic AMP-responsive element-binding protein
Cys	Cysteine
DAG	Diacylglycerol
DDR	DNA damage response
DNA	Deoxyribonucleic acid
DNA-PK	DNA-dependent protein kinase
DNA-PKcs	DNA-dependent protein kinase, catalytic subunit
DSB	DNA double-strand break
ECM	Extracellular matrix
ER	Endoplasmic reticulum
ERAD	Endoplasmic-reticulum-associated protein degradation
ERK	Extracellular-signal regulated kinase
ERO1	ER oxidoreductin 1
GAPDH	Glycerinaldehyd-3-phosphat-Dehydrogenase
NER	Nucleotide excision repair
Glu	Glutamate
GPCR	G protein-coupled receptor
GPX	Glutathione peroxidase
GRP78	78 kDa glucose-regulated protein
GS-lyation	Glutathionylation
GSSG	Glutathione disulfide (oxidized)
GSH	Glutathione (reduced)

GST	Glutathione S-transferase
H2A.X	H2A histone family, member X
H_2O_2	Hydrogen peroxide
H3	H3 histone
HO	Hydroxyl
HR	Homologous recombination
InsP3R	Inositol trisphosphate receptor
IP3	Inositol trisphosphate
IP3R	Inositol trisphosphate receptor
IR	Ionizing radiation
KO	Knockout
Lys	Lysine
MAPK	Mitogen-activated protein kinases
MDC1	Mediator of DNA damage checkpoint protein 1
MEK	Dual specificity mitogen-activated protein kinase kinase 1
Met	Methionine
MRN	Mre11, Rad50 and Nbs1
mTOR	Mammalian target of rapamycin
mTORC2	Mammalian target of rapamycin complex 2
NAADP	Nicotinic acid adenine dinucleotide phosphate
NAD^+/NADH	Nicotinamide adenine dinucleotide
$NADP^+$/NADPH	Nicotinamide adenine dinucleotide phosphate
NF-κB	Nuclear factor kappa-light-chain-enhancer of activated B cells
NHEJ	Non-homologous end joining
NMDA	N-methyl-D-aspartate
NO	Nitric oxide
NO_3^-	Nitrate
O2-	Superoxide
PAR	Poly-Adenosine diphosphate ribose
PDI	Protein disulfide isomerase
PDK1	3-phosphoinositide-dependent protein kinase
PHD	Plant Homeo Domain
PI-3	Phosphatidylinositide 3
PI3K	Phosphatidylinositol 3- and 4-kinase
PIKK	Phosphatidylinositol 3-kinase-related kinase
PIP_2	Phosphatidylinositol 4,5-bisphosphate
PIP_3	Phosphatidylinositol (3,4,5)-trisphosphate
PKB	Protein kinase B
PKC	Protein Kinase C
PLC	Phospholipase C
PMA	Phorbol-12-myristat-13-acetat
Pol	Polymerase
PS	Phosphatidylserine
PTB	Phosphotyrosine-binding domain
PTM	Posttranslational modification
PTP	Protein tyrosine phosphatase
RAS	Rat sarcoma
Rb	Retinoblastoma
RNA	Ribonucleic acid
RNA Pol II	RNA-Polymerase II
ROS	reactive oxygen species

RTK	Receptor tyrosine kinase
RYR	Ryanodine receptor
SERCA	Sarcoplasmic reticulum
SH2/3	Src Homology 2/3
SOD	Superoxide dismutase
SSB	Single-strand break
STAT	Signal Transducer and Activator of Transcription
TCA cycle	Tricarboxylic acid cycle
TCR	Transcription coupled repair
TLS	Translesion synthesis
TRPM2	Transient receptor potential cation channel, subfamily M, member 2
Trx	Thioredoxin
TrxR	Thioredoxin reductase
Tyr	Tyrosine
UPR	Unfolded protein response
UV	Ultraviolet
VDAC	Voltage-dependent anion channel
Zn^{2+}	Zinc
γH2A.X	Gamma-H2A histone family, member X

1. Introduction

1.1 Signaling

Higher organisms are constantly exposed to environmental (extrinsic) and endogenous (intrinsic) changes. They need to react to these changes in a fast and appropriate (reproducible) manner. Signaling is a cellular language which was optimized through evolution for exactly those purposes (*1*). Cells communicate via receptor mediated signaling over short (paracrine signaling) or long (endocrine signaling) distances. Cellular signaling events depend on second messengers, allosteric mechanisms, positive and negative regulatory events, as well as the subcellular localization of molecules. One important mechanism to pass the signal on is by regulated modification of proteins with chemical groups (posttranslational modifications) during or after their synthesis. Phosphorylation is an important posttranslational modification of proteins, during which they receive a phosphate group. This phosphate group is able to change the protein structure due to its highly negative charge, and in the case of enzymes it can affect their catalytic activity (*2, 3*). Once transduced into the cell, the signal must be propagated into the nucleus to allow the cell to react on the extracellular stimulus by activating gene transcription. Gene transcription is a way to transform the signaling into molecular building blocks, such as proteins or RNAs, which are essentially required for a physiological response to the stimuli.

Feedback loops are an important feature of cellular signaling allowing the fine-tuning of the system (*4*). There are two general types of feedback mechanisms. The first one relies on the presence of components which undergo posttranslational modifications for immediate modification of the output (*5*). The second relies on newly synthesized components (induced early genes / delayed early genes) for better temporal system control and robustness (*1*).

1.1.1 Principles of cellular kinase signaling

To coordinate and integrate highly complex cellular process decisions including cell growth, proliferation, differentiation and apoptosis, multicellular organisms have developed sophisticated networks based on phosphorylation events of proteins in all

cellular compartments from the cellular membrane to the nucleus (*6*). Extracellular stimuli are perceived at the cell membrane via receptor protein-tyrosine kinases (RPTKs or shortly RTKs). RTKs are integral trans-membrane fusion proteins consisting of a highly variable extracellular domain and a conserved cytoplasmic protein kinase domain (*7*). Extracellular or environmental signals in form of peptide- or steroid-based ligands stimulate the activity of RTKs by direct interaction with the extracellular-ligand binding domain (e.g., regulation of blood sugar through activation of the insulin receptor (RTK) by insulin (ligand)) (*8*). Ligand binding induces dimerization of the RTK leading to its enzymatic activation and auto-phosphorylation of Tyr residues outside the kinase domain in its cytoplasmic region (*9*). Phosphorylated Tyr is an important mark to further stimulate a cascade which is mediated by protein-protein interactions via SH2/3 or PTB domain-containing adaptors (*10*). Adaptor proteins recruit effector proteins to the RTK in a phosphorylation dependent manner, for instance, cellular kinases which in turn become active and initiate a phosphorylation cascade. In the case of mitogen activated protein kinase (MAPK) signaling, multiple phosphorylation events result in the activation of a terminal kinase (ERK, p38 or JNK) which translocates into the nucleus and drives gene expression (*11*). A vast number of nuclear transcription factors regulates the physiological outcome of the different MAPK circuits, ranging from cell growth, division, proliferation, cell cycle arrest and apoptosis (*12*). Signal transduction can also be achieved via signaling molecules which contain phospholipid-binding domains (PHD, pleckstrin homology domain), as in the case of protein kinase B (PKB, also called AKT) activation by the phosphoinositide-dependent kinase-1 (PDK1) (*13*). Recruitment of AKT and PDK1 to the cell membrane via their PHD domains brings PDK1 in close proximity to AKT, leading to AKT activation by phosphorylation through PDK1 (*14*). Alternatively, signal transduction can be achieved by direct or indirect activation of transcription factors in the cytoplasm as in the case of STAT or NF-κB signaling, or through phospholipid-derived second messengers and receptor induced cytoplasmic and nuclear calcium (Ca^{2+}) shifts (*15-17*) (see 1.4).

1.1.2 Evolution of regulatory mechanisms of kinase signaling

In the course of the evolution from unicellular to multicellular organisms, signal transduction evolved into a multilayered highly interconnected system that allows

higher organisms to quickly adapt to environmental signals (*18*). One crucial event was the evolution of RTKs, which are exclusively found in multicellular organisms and are believed to be a product of repeated gene fusion events between primordial binding proteins and intracellular tyrosine kinases. To reach the full complexity of multicellular signaling networks, RTKs and cellular signaling molecules encountered duplication of their encoding genes, allowing the expression of slightly different proteins, which resulted in dense interconnections (formation of hubs or nodes) and novel regulatory mechanisms such as feedback loops (*19*). The modular composition of molecules is another way to involve the same protein for different changing environments. One example is the utilization of PI3 kinases for mediating metabolic signaling in response to insulin and at the same time for activating cell proliferation in response to growth factors in one and the same cell, a process which can only be achieved by tethering PI3K via different adaptor proteins to different RTKs (*6*). Modularity enables thus reutilization of genetic circuits (PI3K signaling) in different biological settings (metabolism vs. proliferation). The much larger number of different RTKs in vertebrates (58) as compared to nematodes (12) indicates how higher organisms managed to evolve complex multilayered and interconnected signaling networks at a comparable genome size.

1.1.3 Regulation of signaling by Protein kinase C (PKC)

An important kinase, which is modulated by Ca^{2+} and PLC-dependent generation of diacylglycerol (DAG, also called DG), is the protein kinase C (PKC). The PKC family comprises 10 members, which are classified into three groups based on their domain composition (*20*). PKCα, -βI/II and -γ belong to the conventional group, PKCδ, -ε, -η and -θ to the novel group, and finally PKCζ and -ι to the atypical group (Fig. 1). The basic structure is composed of a N-terminal regulatory domain followed by the kinase and carboxyterminal (CT) domain. The regulatory domain is subdivided into the C1 and C2 domain, which can bind DAG or Ca^{2+}, respectively (Fig. 1). The regulatory domain is the basis for distinguishing different PKC groups and determines the activation pattern: conventional PKCs are potently induced by Ca^{2+} and DAG, novel PKCs by DAG, and atypical PKCs lacking the C1 and C2 domains are activated by an independent mechanism (*20*). For complete activation all groups are matured by PDK1-dependent phosphorylation in the activation loop of the catalytic domain (*21*),

and the mammalian target of rapamycin 2 (mTORC2) kinase complex phosphorylates PKCs in the CT domain (*22*). Interestingly, in absence of maturation PKCs undergo complete proteolytic degradation, pointing at a tightly regulated mechanism of preventing signal transduction leakage (*22, 23*). A mature PKC can be eventually fully activated by secondary messengers. Signal-dependent increase in cytosolic Ca^{2+} mediated by IP3-dependent store depletion of the ER (see chapter 1.4) is bound by the C2 domain of conventional PKCs (α-γ) and leads to their translocation to the cell membrane (*24*). At the cell membrane its C1 domain interacts with membrane-bound DAG, which has been generated trough stimulus dependent PIP_3 cleavage by PLC. Mature and activated PKC is subsequently able to target substrate proteins by phosphorylation.

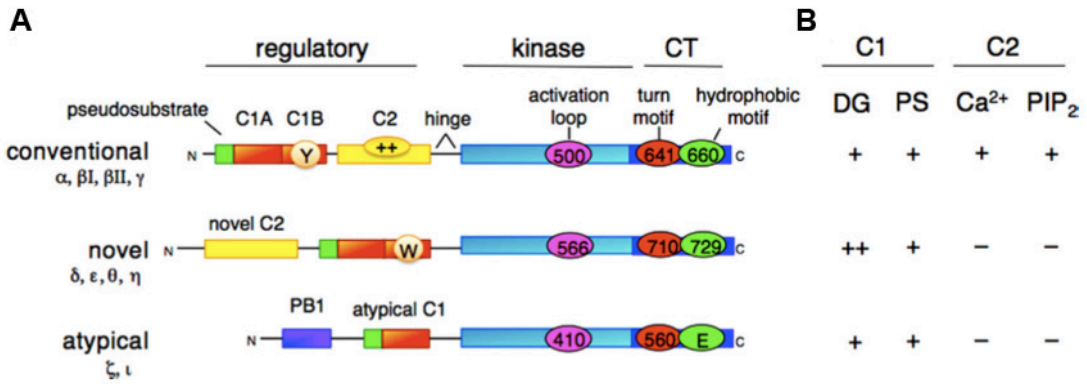

Figure 1. Protein kinase C (PKC) family members. **A:** Domain structure of PKC family members, showing pseudosubstrate (green rectangle), C1 domain [orange rectangle; Y/W switch that determines affinity for diacylglycerol (DG)-containing membranes depicted by circle in C1B domain], C2 domain [yellow rectangle; basic patch that governs binding to PIP2 (phosphatidylinositol-4,5-bisphosphate), marked by oval with ++], connecting hinge segment, kinase domain (cyan), and carboxyl-terminal tail (CT; dark blue rectangle). The 3 priming phosphorylations in the kinase domain and CT are indicated with numbering for PKCβII, PKC ε , and PKCζ (note atypical PKC isozymes have Glu at phosphor-acceptor position of hydrophobic motif). **B:** Dependence of PKC members on C1 domain cofactors, DG, and phosphatidylserine (PS) and C2 domain cofactors Ca^{2+} and PIP2. (Adapted from (*20*))

In contrast, novel PKCs (δ-θ) do not require Ca^{2+} for their translocation to the membrane because the loss of a C2 domain improved the affinity of their C1 domain towards DAG, thus making the novel PKC group independent of Ca^{2+} (*25*).

Negative regulation of PKCs is achieved by proteolytic degradation upon sustained stimulation (*26*). *In vitro* such degradation can be mimicked by prolonged activation with phorbol-esters such as phorbol 12-myristate 13-acetate (PMA) (*27, 28*). The presence of PMA on one hand activates PKCs by mimicking the presence of DAG. Prolonged activation, on the other hand induces dephosphorylation of the PKC's priming phosphate groups, leading to quick proteolytic degradation.

Cellular processes regulated by PKC signaling have been widely studied using small molecule ATP-competitive inhibitors, including the Bisindolylmaleimide (BIM) class of highly potent (nM range) and selective inhibitors (*29*). Interestingly, inhibition of PKCs by ATP competitive inhibitors such as BIM-1 (GF109203X) led to retention and even increase of the phosphorylation at the priming sites (*30*). One possible explanation is the increased protein stability in the presence of PKC inhibitors leading to increased priming, therefore also suggesting an induced-fit model of PKC priming in presence of ATP bound in the catalytic cleft. As mentioned above, priming is crucial for full activation of PKC, however, the substitution of ATP by ATP-competitive inhibitors is preventing any downstream signaling due to the absence of ATP as a substrate.

1.2 Genotoxic stress

Cells are constantly harmed by DNA damaging agents from external and endogenous sources and must protect their genetic information in order to assure faithful reproduction and genomic stability, otherwise this would lead to malignancies such as cancer (*31*) (see also 1.2.4). Typical genome hazards from external sources include UV and ionizing radiation (IR), as well as anthropogenic release of chemicals into the environment (e.g., cigarette smoke is responsible for the majority of lung cancers in man and women in the US) (*32*). Endogenous sources include byproducts of aerobic metabolism such as ROS (superoxide anions, hydroxyl radicals and hydrogen peroxide) derived from oxidative respiration and lipid peroxidation, as well as spontaneous disintegration of DNA bonds and replication errors under physiological conditions (*31*). Genotoxic stress is a life-threatening event for organisms as it alters the content and organization of the genetic material. The cellular responses to this danger are diverse and culminate in the activation of cell-cycle checkpoints and DNA repair pathways, or, in certain contexts, initiation of apoptotic programs (*31, 33, 34*). Regulation of these processes is accompanied by changes of the proteome, including altered protein expression levels or induced post-translational modifications.

1.2.1 Different types of DNA damage induce distinct repair responses

On the level of the DNA, damaging agents induce different types of DNA breaks and lesions, which require sophisticated repair machineries to prevent inheritance of lesions into the next generation (*31*) (Fig. 2).

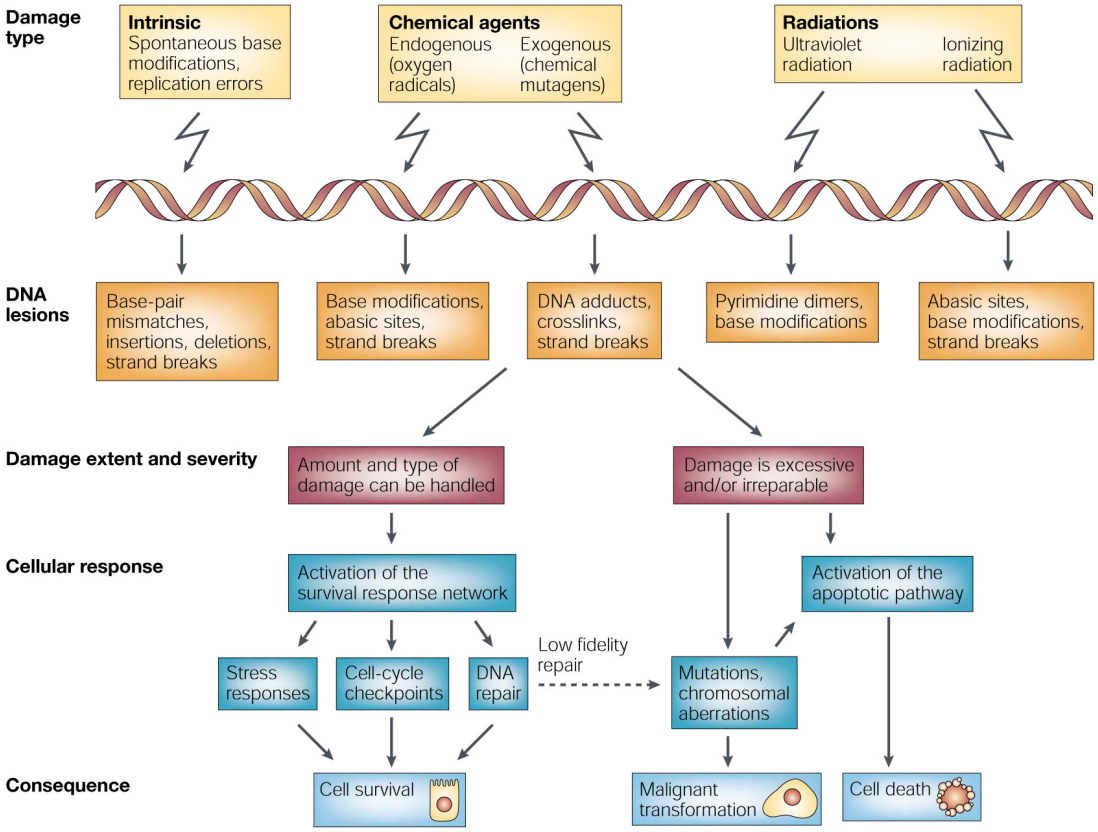

Figure 2. Cellular responses to DNA damage (*35*).

In general, different types of DNA lesions may block transcription, which can only be resumed by transcription-coupled repair (TCR) via RNA Pol II displacement and subsequent recruitment of the repair machinery (*36*). Global genome nucleotide-excision repair (ggNER) is another sub-pathway activated in response to bulky DNA lesions upon UV-damage, and follows a similar repair mechanism as in case of TCR. Interestingly, somatic mutations which occur in one of the repair machinery members of ggNER or TCR pathways strongly predispose individuals to sun-induced skin cancer (*31*). On the other hand, DNA damage may also block DNA replication. In that case, particular translesion synthesis (TLS) DNA polymerases (Rev1, Pol ζ, Pol κ, Pol η, and Pol ι) bypass the damage and thereby promote replication at the expense of introducing new mutations due to its flexible base-pairing properties (*37*).

In the case of oxidative DNA damage, formation of DNA strand adducts through oxygenation (8-Oxo-guanine), deamination (of all bases), hydroxylation (8-hydroxylated guanine) or methylation (O-6-Methylguanine) as well as direct formation of DNA single-strand breaks (SSBs) make up the majority of lesions, which are potent inducers of the base-excision repair pathway (BER) (*38, 39*). As in the case of NER, mutations in SSB repair pathways are linked to different diseases, such as cancer and neurodegenerative diseases (*40*).

The most cytotoxic but also mutagenic DNA lesions are DNA double strand breaks (DSBs). DSBs are typically induced upon high energy IR with X- and γ-rays (*41*) (see also 1.2.2). While naturally occurring radioisotopes or cosmic ray particles are responsible for γ-rays, X-ray photons can be generated artificially in a vacuum tube by electron acceleration against a metal anode. X-rays are used for many biological and medical applications, such as the determination of protein structure by X-ray crystallography or in diagnostic radiography and external-beam radiotherapy in medical care (*42-44*). Finally, DSBs are also formed during replication of SSBs in response to DNA replication fork collapses (*45*). Independent of the source, once DSBs are formed, the cell tries to restore genomic integrity in many ways, including checkpoint / transcriptional activation as well as induction of cell death (apoptosis) in cases of severe DNA damage. All of the previously mentioned DNA repair responses, also termed the DNA damage response (DDR), are however activated with the central goal to repair the damaged DNA and to facilitate DNA replication (*46*). DSBs can be either sealed by non-homologous end joining (NHEJ), which is on the one hand error prone but active in all phases of the cell cycle (*47, 48*). Alternatively, if the damage is encountered in the S/G2/M phase, DSBs can be repaired by homologous recombination (HR), which relies on the presence of sister chromatids and is thus less error-prone than NHEJ (*35, 47, 49*).

1.2.2 DNA double strand break-induced ATM signaling

Besides the induction of repair, DSBs also activate a signal transduction cascade, which is orchestrated by the ATM kinase as well as its close homologues ATR and DNA-PKcs with partly redundant functions (*46, 50, 51*). ATM belongs to a family of PI3K like kinases (PIKKs) together with ataxia-telangiectasia and Rad3-related (ATR), the catalytic subunit of DNA-PK (DNA-PKcs) as well as other PIKKs

(hSMG-1, mTOR and TRRAP), which either have a minor or no role in the DDR (*52*). While DNA-PKcs is a repair factor of the NHEJ pathway, the ATR kinase plays a role in the surveillance of replication stress and critically regulates maintenance of DNA replication. ATR knockout mice show embryonic lethality and patients with mutations in this gene develop syndromes which are characterized by growth retardation, dwarfism, microcephaly and mental retardation, as well as defects in the DDR (*53, 54*). These studies indicate ATR's crucial role in developmental processes, while a recent study could also show ATR's involvement in the classical DSB-induced DDR (*55*). Even though the precise mechanism of ATM activation upon DSBs is under debate, the DSB-sensing MRN-complex seems to be at the forefront, at least when it comes to complete activation of the kinase (*56-59*). However, a recent study could also show a direct mechanism of ATM activation in the presence of H_2O_2 but independent of double strand DNA damages (*60*). Oxidation of a critical Cys residue leads to homo-dimerization via disulfide bond formation and activation in the absence of MRN and DNA (*61*). Independent of the precise mechanism, once activated ATM initiates a classical phosphorylation cascade leading to cell cycle arrest, transcriptional changes, repair and in some cases apoptosis (*50*). Several proteomic studies recently described the complex network of ATM-regulated downstream targets in response to DSB-inducing agents (*62, 63*).

One of the early-induced targets is H2A.X, which is phosphorylated by ATM (but also by other PIKKs of the DDR) at Ser197 in the SQ motif (γ-H2A.X) and serves as a well-accepted marker of DSB-induced DNA damage sites (*41, 64-66*). Despite a clear mechanism of its activation, the role of H2A.X in the DDR is still obscure. One recent study showed the necessity of phosphorylated H2A.X in the recruitment of MDC1 (*67*). MDC1 on the other hand is crucial for the juxtaposition of ATM in close proximity to non-phosphorylated H2A.X as shown by a study using MDC KO mice (*68*). Close proximity lead to ATM-dependent spreading of γ-H2A.X around the break sites. This implicates a positive feedback loop, which completes the recognition of DSBs and thus indicates γ-H2A.X's role in facilitating the recognition of DSBs. Moreover, indirectly one can argue that γ-H2A.X must serve as a platform for the recruitment of DDR factors, since the knockdown of MDC1 prevents recruitment of important DDR sensors and repair factors to sites of DNA damage (*69*). Besides phosphorylation, ubiquitylation has also been shown to be a crucial early modification of H2A.X, facilitating the recruitment of BRCA1 and 53BP1 which are important

repair factors involved in the repair of DSBs by the HR pathway (*70*). To describe a general picture of epigenetic changes induced upon DNA damage, Steve Jackson's lab performed a small-scale screen using PTM-specific histone antibodies (*71*). Interestingly, most of the well-known histone marks involved in epigenetic silencing or activation of gene expression remained unchanged upon treatment with a DNA intercalating DSB-inducing agent. However, the two new acetylation sites H3K9ac and H3K56ac could be added to the DDR-dependent histone code and were decreased upon DSB-induction. Interestingly, previously believed DDR-dependent changes like H3S10p, H3S28p and H3.3S31p were shown to be a consequence of DDR-dependent cell cycle changes rather than a direct DDR-dependent signaling mediated event. The absence of DDR induced histone mark changes could be also shown by yet another study on DSB-induced H3K79me changes (*72*). Even though crucial for the recruitment of the HR repair factor 53BP1 to DNA damage sites, methylation of H3 at Lys79 was not induced directly by DSBs. One explanation could be the induction of higher-order chromatin structure changes upon DNA breaks, which indirectly lead to H3K79 methylation and recruitment of 53BP1 to methylated histones residing at DNA breaks. Acetylation and methylation of non-histone substrates have also been described to be under control of the DDR (*73-76*).

Until recently, DDR-induced signaling events have been traditionally placed downstream of the induction of DNA breaks and the research focus has been majorly set on signaling-dependent regulation of processes in the nucleus. New sophisticated proteomics and bioinformatics studies, however, expanded the DDR signaling network to the cytoplasm (*62, 63, 77-80*). Indeed, targeted approaches have identified many canonical cytoplasmic signaling pathways that are regulated by the DDR (e.g., NF-κB pathway (*81-83*), MEK-ERK pathway (*84, 85*), AKT/PKB pathway (*86*), p38-MAPKAP2 pathway (*87, 88*) and many more (*89*)). Comparison between different types of post-translational modifications, induced by the ATM-mediated DDR, could show that phosphorylation events are predominant over acetylation of proteins, arguably pointing to kinase-dependent signal transduction as the crucial outcome of the DDR (*78*).

1.2.3 ATM-induced cell cycle arrest

The major outcome of ATM activation, besides γ-H2A.X formation, is the activation of checkpoints for cell cycle arrest upon DNA damage (*35*). Cell cycle transition into S-phase is a two-waved G1 checkpoint response (*90*). However, a very early response regulated by DDR can also affect the phosphorylation status of the retinoblastoma protein (Rb), which controls transition through the restriction point in G1 via E2F. Rb is usually kept phosphorylated by the CDK4/6-Cyclin D complex, which releases E2F and drives cell cycle transition through the restriction point (*91*). However, upon starvation as well as under stress conditions, such as genotoxic stress, Cyclin D is phosphorylated on Thr286. Consequently, Cyclin D is degraded and Rb becomes hypo-phosphorylated, which keeps E2F in an inhibitory grip and blocks transition through the restriction point (*91, 92*). The first wave of the DDR-dependent G1/S arrest relies on Chk1/2 dependent phosphorylation of Cdc25A, leading to its ubiquitinylation-dependent proteasomal degradation (*93*). Cdc25A is a phosphatase which targets CDK2 for dephosphorylation on Tyr15. Tyr15 phosphorylation on the other hand, is an inhibitory modification, which prevents activation of the Cyclin E-CDK2 complex. Consequently, degradation of Cdc25A keeps CDK2 modified in an inhibited state, thus blocking early G1/S transition in a fast and highly regulated manner without the need for time consuming transcriptional changes (*90*). In parallel, the DDR induces a second signaling cascade, which relies on the stabilization of p53 by phosphorylation and thus leads to transcription of the general CDK inhibitor p21 (*94*). In response to severe DNA damage, a permanent cell cycle arrest in G1 can be established by $p16^{Ink4a}$, which is a CDK4/6 inhibitor (*95, 96*). The state of permanent cell cycle arrest is called senescence and is believed to be a crucial mechanism for cancer prevention (*97*). Besides a G1/S cell cycle arrest, the DDR can also induce an intra-S-phase or G2/M checkpoint. Like for the G1/S arrest, the G2/M checkpoint relies on the action of Cdc25 phosphatases, but Cdc25B and C are functionally inactivated in order to preserve an inhibitory phosphorylation on CDK1 (*98*). CDK1 can also be directly phosphorylated on the inhibitory site Ser15 (like CDK2), which prevents complex formation between CDK1 and Cyclin B and thus arrests the cell cycle in G2/M (*99*).

1.2.4 DNA damage and cancer

DNA damage and subsequent mutation of the information is the first step in tumor formation because it enables the evolution of the six hallmarks of cancer (*97*). Cancer development or malignant transformation of benign tissue relies on a set of hallmark capabilities, which initiate tumor growth and drive metastatic dissemination (*97*). Sustained proliferation through reprogramming of cellular signaling is one of the hallmarks of cancer.

Two classes of cancer genes are affected by mutations: the so-called "gatekeepers" and "caretakers" (*100*). Gatekeepers combine oncogenes and tumor suppressor genes, which in case of gain-of-function (oncogenes) or loss-of-function (suppressors) mutations all increase tumor cell growth and proliferation. Caretakers, on the other hand, code for repair proteins of DNA repair pathways (Chapter 1.2.1) and, as the name implicates, try to maintain or take care of the genome integrity, which is constantly endangered from endogenous and exogenous DNA damaging sources. In contrast to caretakers, only mutations in gatekeepers affect net cell growth and therefore are the main drivers for the establishment of the hallmarks (*101*). On the other hand, only the presence of mutated caretakers predisposes cells to become cancer cells. Indeed, all of the known caretaker gene mutations have been shown to occur in the germ line and, based on the multiple-hit theory, are usually the first hit in cancer progression (*102*).

1.3 Oxidative stress

Oxidative stress is caused by environmental factors (pollutants such as cigarette smoke, high doses of radiation), as well as due to endogenous oxygen metabolism (aerobic respiration in mitochondria, different oxidases, cytochrome P450 family or NO synthases) (*103*). The production of superoxide anions (O_2^-) during aerobic respiration in mitochondria is the major source of endogenous ROS, and the mitochondrial superoxide dismutase (SOD) converts O_2^- into hydrogen peroxide (H_2O_2). H_2O_2 is membrane permeable and further ionized to highly reactive hydroxyl (HO) radicals in the presence of iron (Fenton reaction). Cytoplasmic accumulation of ROS induces oxidative stress conditions which, as described in chapter 1.3.1, can cause ER-stress induced unfolded protein response (UPR), lipid peroxidation in

presence of trace metals, as well as harm genomic integrity due to the introduction of oxidative DNA base lesions as well as the direct induction of SSBs.

1.3.1 Reactive oxygen species (ROS) and their role in cellular signaling

Even though discussed so far controversial, there is a growing body of evidence which indicates the potential role of ROS in regulating cellular signaling events (*104, 105*). The basis for the skepticism stems from the fact that ROS is highly reactive and thus leads to oxidation of organic macromolecules (proteins, lipids, DNA) and induces cytotoxicity in an uncontrollable manner. Even though true for free radical oxidants, for instance superoxide (O_2^-), nitric oxide (NO) or hydroxyl (HO) radicals, hydrogen peroxide (H_2O_2) as well as superoxide anions (O_2^-) exhibit lower reactivity with macromolecules. In fact, free radical chain reactions in cellular systems are kept at a very low level, and in the presence of detoxifying enzymes (e.g., SOD) the balance is shifted to less reactive, non-radical O_2^-, H_2O_2 or peroxynitrite (NO_3^-) (*106-108*). Interestingly, signaling mediated by O_2^- or H_2O_2 can directly involve oxidation of regulatory Cys residues in a protein, as has been shown for the bacterial transcription factor SoxR, the molecular H_2O_2 sensor OxyR and the molecular chaperone Hsp33 (*109-112*). In the case of SoxR, oxidation of 2Fe-2S clusters leads to a conformational change and binding to a DNA-operator, which results in gene expression. The presence of heat and H_2O_2 activate Hsp33, which is a redox-regulated chaperone expressed in *E. coli* (*112*). Hsp33 contains a tetrahedral Zn^{2+} which is coordinated by a four-Cys zinc-binding motif. Under reducing conditions, Cys-bound Zn^{2+} keeps Hsp33 in an inactive conformation. In the presence of H_2O_2, Cys oxidation leads to disulfide bond formation and repulsion of the Zn^{2+}, which results in an active chaperone (*113*). Redox-regulated signal transduction proteins were also found in higher eukaryotes (*105, 106*). Reversible oxidation-reduction of Cys and potentially also Met residues can, for example, regulate the enzymatic activity as an "on-off" switch, enhance or reduce the enzymatic activity (allosteric regulation), or change macromolecular interactions. In all cases, the protein function can be modulated by direct oxidation of Cys to form disulfide bond formation, S-Glutathionylation (GS-lyation) and S-Nitrosylation (*114*). Examples for on-off switches include direct oxidation of protein tyrosine phosphatase-1B, GS-lyation of GAPDH, NF-κB and caspase 3 (*115-118*). Moreover, Cys residues have been found in detoxifying enzymes such as glutathione transferase (GST), cytochrom P450, thioredoxin (Trx), as well as

peroxiredoxin (Prx). Allosteric regulation of enzymes by redox-dependent mechanisms has been shown for different signal transduction factors, such as RAS or NMDA-receptor (*119, 120*). Thanks to modern proteomics analysis by mass spectrometry, many more redox-regulated proteins have been identified and the already huge list of redox-regulated proteins has been significantly extended (*121, 122*).

1.3.2 Cellular redox-system and antioxidant response

To counteract oxidative stress conditions, cells have evolved antioxidant defense mechanisms comprised of scavenging enzymes such as superoxide dismutase (SOD), glutathione peroxidase (GPX), catalase and thioredoxin reductase (TrxR) (*106*) In addition, radical-scavenging chemicals such as Vitamin E and C can provide another protection against ROS (*123*). Several redox systems (e.g., NAD^+/NADH, $NADP^+$/NADPH, and oxidized glutathione/reduced glutathione (GSSG/GSH)) keep the cytosol in a reduced state and ensure redox homeostasis despite the presence of ROS (*124*). Reducing conditions in the cytosol are very important to maintain cysteine residues in their reduced state, which conserves many proteins in their three-dimensional confirmation. By contrast, the ER has an oxidizing milieu which is required for disulfide bond formation of nascent polypeptide chains during protein biosynthesis (*125*). One way to keep the ER in an oxidized state is to maintain a smaller GSH/GSSG ratio. Indeed the ratio of GSH/GSSG in the ER is between 1:1 and 1:3 and thus about 30 times smaller than in the cytosol (30:1 to 100:1) (*126*). Even though the mechanism of increased GSSG maintenance in the ER is still under debate, one proposal is based on the function of ER oxidoreductin 1 (Ero1) (*125*). Ero1 assists protein disulfide isomerase (PDI) in disulfide bond formation of nascent polypeptides and generates ROS as a byproduct by transferring electrons from PDI to molecular oxygen (*127*). Detoxification of ROS in presence of GSH would eventually accumulate GSSG and maintain an oxidizing milieu.

1.3.3 Involvement of the Endoplasmic reticulum (ER) during oxidative stress

The endoplasmic reticulum (ER) is a cellular organelle that is organized in a tubular and sac-shaped structure and is responsible for the biosynthesis, folding, assembly and post-translational modifications of cellular proteins (*128*). In addition, it also serves as a major intracellular Ca^{2+} store, which makes it an important signaling regulator through the dynamic release of this second messenger (*17*) (see chapter 1.4). Stress conditions such as oxidative stress lead to increased protein miss-folding and result in ER-stress and an unfolded protein response (UPR) when the folding capacity of the ER is exceeded (*129*). UPR regulates a signaling cascade, majorly aiming to reverse these stress conditions. This cascade is based on ER stress protein-sensors (e.g., IRE1α, PERK and ATF6), which are kept inactive by interacting with the abundant ER chaperone BiP (immunoglobulin-heavy-chain-binding protein, also called GRP78). Upon ER-stress, however, BiP is rapidly sequestered from the sensors through the interaction with misfolded polypeptides, thus leading to the activation of the ER-stress sensors (*130*). Major physiological outcomes of these activation events include ATF4 mediated transcriptional expression of UPR-target genes, involved in amino-acid biosynthesis and antioxidant response, as well as ATF6 and XBP1 mediated transcriptional expression of genes encoding ER chaperones and enzymes that promote protein folding, maturation, secretion and ER-associated protein degradation (ERAD) (*131, 132*). However, if the cell fails to resolve the ER stress condition, extended activation of the ER-stress sensors ATF6 and PERK induce the transcription of CCAAT/enhancer-binding protein (CHOP), which is the main apoptosis mediator of the UPR (*124*). Other pro-apoptotic pathways in response to UPR include Bak/Bax-regulated Ca^{2+} release from the ER, IRE1α induction of the pro-apoptotic ASK1/JNK pathway, and cleavage-dependent activation of pro-caspase 12 (inflammatory pro-caspase). Reduction of the ER-stress by reversing incorrect protein folding and recycling misfolded proteins by proteasomal degradation is crucial for cell survival and growth (*133*). Moreover, if the balance is shifted towards irreparable conditions, the ER is also able to generate ROS production. Mechanisms of ROS production include refolding under oxidizing conditions by PDI and Ero1, increased aerobic respiration, and Ca^{2+} leakage from the ER (*124, 134, 135*). In all cases, either ER-based or generated by the Mitochondria, ROS production is a threat to genomic integrity and for the sake of genome stability programmed cell death is a typical consequence as a last resort (*136*).

1.4 Calcium (Ca^{2+}) signaling

Ca^{2+} as a second messenger is an important player in intra- and extracellular signaling events (*17, 137*). In a resting cell, Ca^{2+} is maintained at low cytosolic concentrations of about 100 nM, while in response to stimuli its levels can reach up to 1000 nM (10 fold increase) (*137*). Furthermore, its concentration in the extracellular matrix is in the mM range and the cell invests a lot of energy in extruding Ca^{2+} from the cytosol. Keeping cytosolic Ca^{2+} levels at a very minimum is important, since Ca^{2+} levels above a particular threshold are potent inducers of apoptosis (*138*) (see chapter 1.4.2). Even though the induction of apoptosis is a major function of Ca^{2+} signaling, it also regulates many cellular and physiological functions that are important for living cells, such as fertilization of mammalian eggs as well as during embryonic development of zebrafish, *Xenopus* and *Drosophila* embryos (*139-142*). Mammalian physiological processes include Ca^{2+} dependent regulation of cardiac muscle contraction (*143*) and neuronal function (*144*). On the cellular level Ca^{2+} regulates cell differentiation (*145*), the cell cycle and proliferation (*146*), and transcriptional activation (*147-149*). Its deregulation has also been reported to cause cancer (*150, 151*).

1.4.1 Regulation of intracellular Ca^{2+} levels

Depending on the stimulus, Ca^{2+} can be either released from external (extra-cellular medium) or internal stores of which ER is the major source. The Ca^{2+} concentrations in the ER are around 100 μM and the two major ion channels regulating its release are inositol-1,4,5-trisphosphate receptor (IP3R) and ryanodine receptor (RYR) (*152*). Depending on the stimulus, these channels are activated by different secondary messengers in which Ca^{2+} itself is an important regulator. The so-called Ca^{2+} induced Ca^{2+} release (CICR) is a mechanism through which changes of ER-luminal or cytosolic Ca^{2+} can sensitize IP3Rs or RYRs and either act inhibitory or stimulatory, depending on the concentration of the secondary messenger. For IP3R concentrations below 300 nM are stimulatory, while concentrations above 300 - 500 nM are inhibitory (*153*). However, for complete activation, IP3R has to be stimulated by the IP3 secondary messenger (*138*). In response to extracellular stimuli, for instance growth factors, G protein-coupled receptors (GPCRs) or RTKs activate PLC (β in

case of GPCR or γ in case of RTK), which in turn performs cleavage of PIP2 and thus generates the previously mentioned IP3 as well as diacylglycerol (DAG) secondary messengers (*154*) (Fig. 3). Activation of other PLC isoforms can be achieved by elevated cytosolic Ca^{2+} levels (PLCδ pumped in from the ECM or mitochondria) or through activation by RAS (PLCε) (*17, 155*). Interestingly, IP3R changes its sensitivity to Ca^{2+} upon binding of IP3 and becomes insensitive to inhibition by Ca^{2+} (*138*). Hence, activation of IP3R by IP3 causes complete store depletion, which can only be prevented by a decline of the external stimulus.

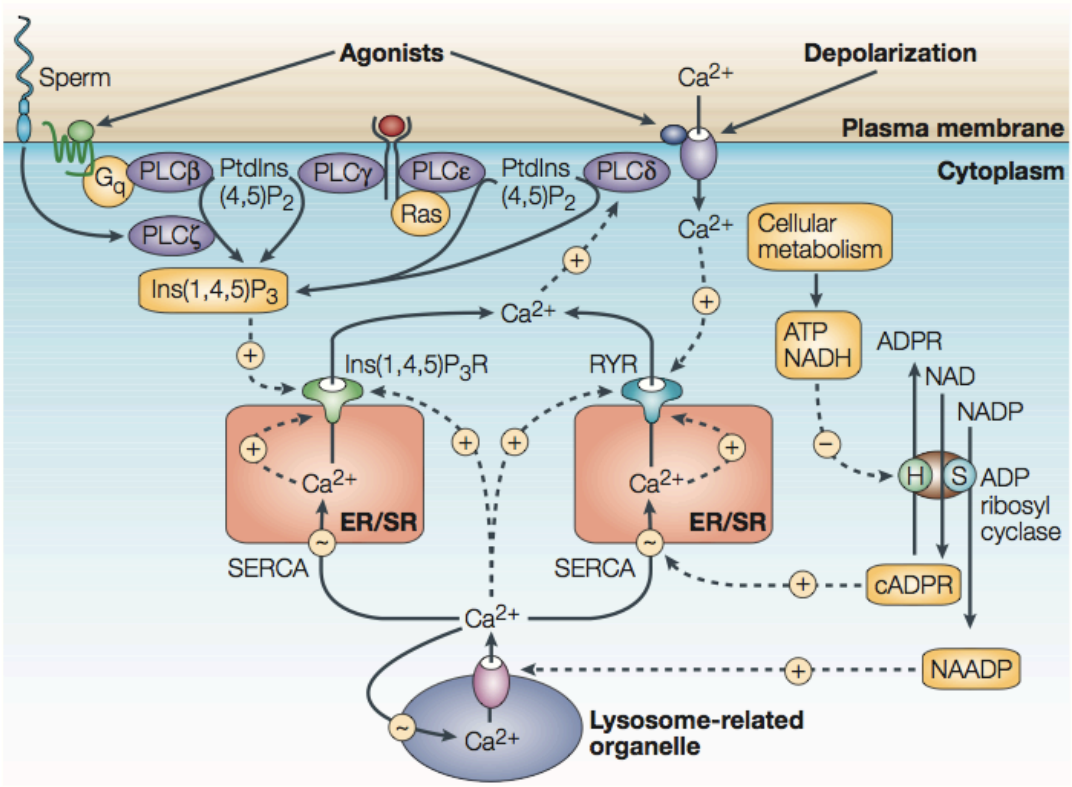

Figure 3. Calcium-mobilizing messengers and modulators. Ca2+ release is regulated by various second messengers or modulators from internal stores by the inositol-1,4,5-trisphosphate receptor (Ins(1,4,5)P3R) or the ryanodine receptor (RYR). Activation of these channels is sensitive to factors from the cytosol and from the endoplasmic/sarcoplasmic reticulum (ER/SR). The Ins(1,4,5)P3R is regulated by inositol-1,4,5-trisphosphate (Ins(1,4,5)P3 and phospholipase C (PLC; β, δ, ε, γ and ζ). The nucleotides cyclic ADP ribose (cADPR) and nicotinic acid adenine dinucleotide phosphate (NAADP) are produced by the synthase and hydrolase activity of ADP ribosyl cyclase, which is sensitive to the cellular metabolism. cADPR is described to regulate the sarco(endo)plasmic reticulum Ca2+-ATPase (SERCA) pump, which regulates the uptake of Ca2+ into the lumen of the ER, resulting in sensitization of the RYR. NAADP has an impact on a channel, located on a lysosomal-like organelle to release Ca2+ that can either stimulate the Ins(1,4,5)P3R or the RYR directly, or indirectly by increasing Ca2+ levels in the lumen of the ER (*17*).

In contrast, RYRs are sensitized to elevated Ca^{2+} levels by cyclic-ADP-ribose (cADPR). CD38 (ADP-ribosyl cyclase) uses NAD^+ as a substrate to generate cADPR,

but is also able to hydrolyze cADPR to ADP-ribose (ADPR) (*156*) (Fig. 3). ADPR in turn has been previously shown to activate the melastatin-related transient receptor potential channel 2 (TRPM2) channel and to induce Ca^{2+} influx into the cytosol (*157*). Interestingly, low concentrations of cADPR (around 10 μM) only sensitize TRPM2, and ADPR is required for full activation. On the other hand, cADPR concentrations above 100 μM are sufficient to fully activate TRPM2 in the absence of ADPR (*158*). Altogether, these data indicate a fine-tuning mechanism for Ca^{2+} influx, which involves CD38-induced potentiation of TRPM2 via cADPR and ADPR and consecutive stimulation of ER-based Ca^{2+} channels (RYR or IP3R). Even though crucial for RYRs potentiation, additional Ca^{2+} signaling modulators besides cADPR, for example CaM/CaMKII, FK-506-binding proteins, mAKAP/PKA, P130/calcineurin and many more, were shown to regulate the channel (*159*). Other channels, which regulate Ca^{2+} entry into the cytosol, include voltage-operated channels (VOCs), receptor-operated channels (ROCs), store-operated channels (SOCs) and, as already mentioned above, transient receptor potential (TRP) channels, most of which are involved in regulating Ca^{2+} entry from the ECM (*17, 160*). Once Ca^{2+} has reached a cytosolic threshold concentration, different signaling events and outcomes (mentioned above and in chapter 1.4.2 and 1.4.3) are initiated.

1.4.2 Ca^{2+} release and mitochondria

In response to stress conditions such as ER- and oxidative stress (chapter 1.3), Ca^{2+} fluxes from the ECM and intracellular stores (ER) can rise cytosolic Ca^{2+} in the μM range. A major outcome of increased cytosolic Ca^{2+} levels is permeabilization of the mitochondrial membrane leading to membrane swelling, rupture and opening of the mitochondrial permeability transition pore (PTP), which subsequently leads to apoptosis (*161*). In fact cross talk between mitochondrial and ER Ca^{2+} flux exists, which can induce a vicious circle if initiated by stress stimuli such as ER-stress or oxidative stress (*124*). As previously mentioned in chapter 1.3, oxidative stress can overload the ER with unfolded proteins, leading to increased ROS production as a byproduct of the refolding machinery. A positive feedback loop enhances the UPR, thus leading to Ca^{2+} leakage from the ER. The close proximity of ER to mitochondrial outer membrane leads to Ca^{2+} uptake by the mitochondria, while a major role is attributed to the voltage-dependent anion channels (VDACs) in regulating this uptake process (*162*). Furthermore, the anti-apoptotic protein Bcl-2 has been shown to

regulate Ca^{2+} release from the ER, thus preventing mitochondrial Ca^{2+} overload and apoptosis (*163*). By contrast, Bax, a pro-apoptotic member of the BH3-only family, was shown to regulate the opposite effect by increasing Ca^{2+} availability and inducing PTP (*164, 165*). Nevertheless, increased amount of Ca^{2+} in the mitochondria stimulates the TCA (Krebs cycle) and thereby increases oxygen consumption and subsequently ROS generation as a byproduct of oxidative phosphorylation (see chapter 1.3). Release of ROS into the cytosol enhances ER stress, thus closing the vicious circle, which eventually leads to the opening of the mitochondrial PTP and release of apoptosis inducing factors such as cytochrome c, AIF or SMAC/DIABLO, which in most cases induce apoptosis in a Caspase-dependent manner (*138*).

1.4.3 Ca^{2+} signaling through calcium/calmodulin-dependent kinase II (CaMKII)

Ca^{2+} initiates signaling events also through so-called Ca^{2+} binding proteins (*166*). EF-hand proteins are the major Ca^{2+} binding proteins (*167*) and consist of a helix-turn-helix motif, which stabilizes one Ca^{2+} atom by 7 negatively charged oxygen atoms usually originating from aspartic or glutamic acids. One important EF-hand containing Ca^{2+} binding protein is calmodulin (CaM), which is a ubiquitous adaptor protein present in the cytosol with the only purpose to propagate signaling initiated by Ca^{2+} influx (*168*). Upon the binding of Ca^{2+}, CaM undergoes major conformational changes, which expose its hydrophobic surface and allow interaction with other proteins. Bound to CaM, these proteins become more active, dimerize or form complexes with other proteins. A recent proteome screen increased the quickly growing list of CaM-binding proteins (*169*). Maybe one of the best-characterized CaM target proteins is CaMKII, which belongs to the family of calmodulin-dependent kinases (CaMKI-IV) (*170*) (Fig. 4). All CaMKs are Ser/Thr kinases, preferentially phosphorylating their target proteins on Ser or Thr of the Arg-X-X-Ser/Thr consensus motif (*171*). Structurally, CaMKs are composed of a N-terminal bi-lobed catalytic domain followed by a regulatory domain, which includes an autoinhibitory and CaM binding domain. Apart from other CaMK members, CaMKII possess a C-terminal association domain, which allows it to form homo-dodecamers leading to the assembly of a twelve-subunit holoenzyme (*172-174*) (Fig. 4A). Once bound to CaM, CaMK's catalytic domain is relieved from its autoinhibition. In case of CaMKII, autophosphorylation on Thr286 (alpha) or Thr287 (in beta, gamma or delta) increases

the affinity for CaM by more than 1000-fold and generates Ca^{2+}-independent or autonomous activity (*175, 176*) (Fig. 4B).

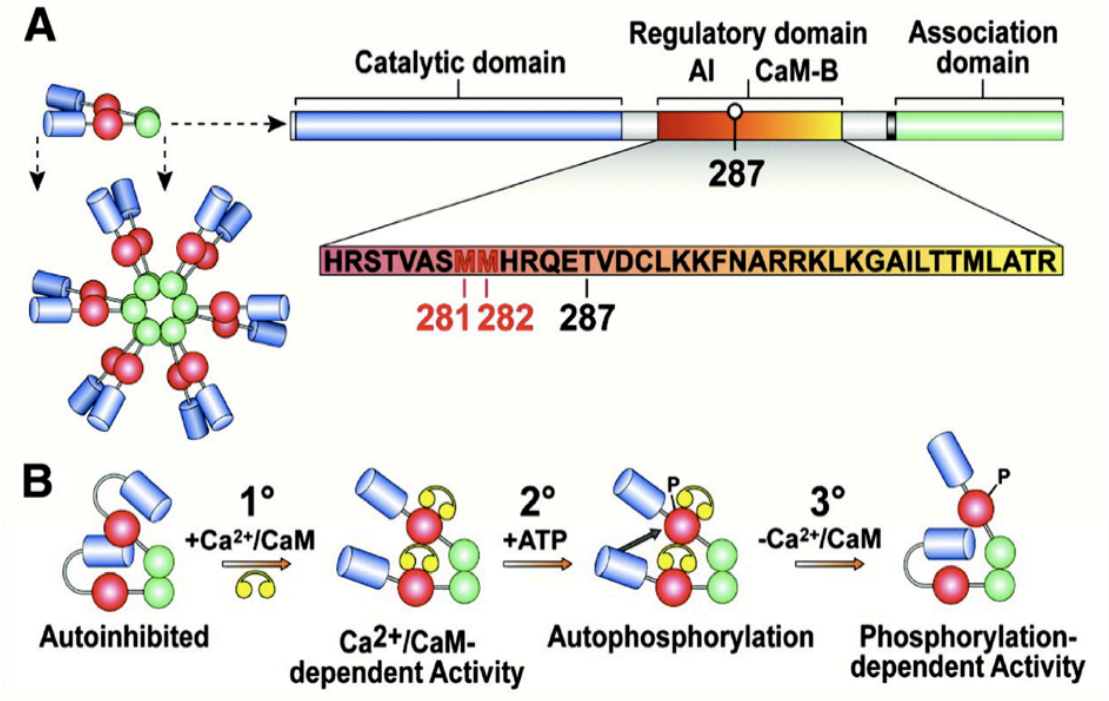

Figure 4. Structure and function of calcium/calmodulin-dependent kinase II (CaMKII) (*177*)**.** (See text for explanations)

CaMKII alpha and beta are predominantly found in the brain, while gamma and delta are expressed throughout the body (*178*). Due to its high presence in the brain (CaMKII alpha and beta) which can reach up to 2% of the whole brain mass, CaMKII's major role is the regulation of synaptic and behavioral plasticity and a recently discussed crucial function in memory regulation (*179, 180*). On the molecular level, CaMKII and especially its closely-related cousin CaMKIV, have been shown to regulate proliferation by targeting cytoplasmic and nuclear transcription factors such as CREB, CREB-binding protein (CBP) ATF, CEBPβ and SRF (*137, 148, 181*). CaMKII was shown to interact and phosphorylate the signal transducers and activators of transcription 1 (Stat1) in response to increased cytosolic Ca^{2+} flux induced by IFN-γ (*182*). Complexation of Ca^{2+} by BAPTA (specific intracellular Ca^{2+} chelator) prevented Stat1 phosphorylation and target gene expression of interferon regulatory factor 1 (IRF-1).

1.5 Nuclear ADP-ribosylation in higher organisms

1.5.1 ADP-ribosyltransferases

Poly-ADP-ribose (PAR) is a sugar-based polymer, consisting of covalently linked ADP-ribose units and an important nuclear post-translational protein modification, which is majorly involved in chromatin-associated processes (*183-187*). PAR is synthesized by a few members of the ARTD family (ADP-ribosyltransferase diphtheria toxin-like, originally PARP), consisting of 18 mammalian ARTDs which all share the catalytic ART domain, required for ADP-ribosylation (*188*). While the majority of the ARTD family members are only able to catalyze protein mono-ADP-riboslyation, some ARTDs have been reported to synthesize PAR through automodification or transmodificion (i.e. modification of target proteins). The first 6 ARTD family members (ARTD1-6) are further subdivided into 3 subgroups according to their sequences of the catalytic domain, type of their catalytic activity, localization and function (*187*). Members of subgroup 1, including ARTD1-3 (originally PARP1-3), are characterized by their WGR domain and their ability to synthesize large branched PAR polymer in response to various types of stress conditions (*184, 187, 189*). Based on *in vitro* studies by Altmeyer et al, ARTD3 was not able to synthesize PAR, in strong contrast to ARTD1 and 2, which showed clear PAR-modification ability *in vitro* (*190*). Other groups have reported a catalytically active mono-ADP-ribosylating ARTD3, being readily induced by DNA-breaks *in vitro* (*191, 192*). It remains to be clarified, whether ARTD3 is active as a PAR-forming enzyme *in vivo*. Subgroup 2 consists of the single member ARTD4 (originally vault-PARP), which is localized in the cytoplasm as a component of the vault particle, as well as the nucleus associating with the mitotic spindle (*193*). ARTD4 possesses poly-ADP-ribosylation activity and its only function, so far reported, has been linked to increased carcinogen-induced tumorigenesis based on studies with ARTD4 KO mice (*194*). Subgroup 3 consists of the two members ARTD5 (tankyrase-1) and ARTD6 (tankyrase-2a). These two members possess oligo-ADP-ribosyltransferase activity and were identified as components of the telomeric complex (*195*), suggesting their crucial role in the cell cycle, especially during mitosis by regulating the spindle structure (*196*).

1.5.2 ARTD1- structural aspects

The best-characterized ARTD family member of the "bona-fide" poly-ADP-ribosyltransferase subfamily is ARTD1 (*184, 187*). ARTD1 is a 116-kDa nuclear enzyme consisting of an N-terminal DNA-binding domain (DBD), followed by a central automodification domain (AMD) and a C-terminal catalytic domain (CD or CAT) (Fig. 5).

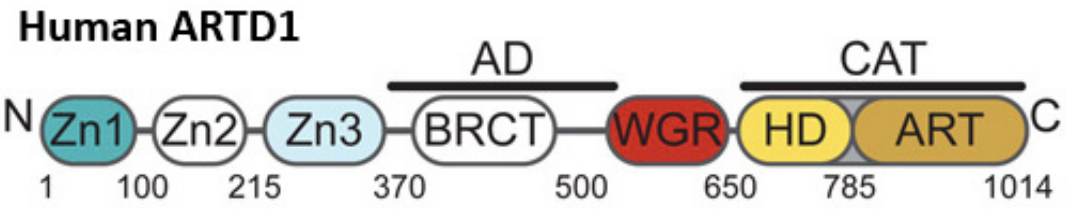

Figure 5. Modular domain architecture of human ARTD1. (Adapted from (*197*))

The DBD is composed out of two zinc fingers and one zinc binding domain (ZF1/2, ZBD or ZF3), a bipartite nuclear localizing sequence (NLS) and a Caspase-3 cleavage site lying between the two ZFs and the ZBD. Based on structural studies, all three zinc binding domains are involved in recognizing DNA breaks or altered chromatin structure, leading to enhanced catalytic activity of ARTD1 (see below) (*197, 198*). The ZBD is believed to regulate chromatin compaction, besides its major role in triggering ARTD1's catalytic activity (*199*). The AMD contains a BRCT (BRCA1 C-terminus) fold, which is believed to mediate phosphorylation-dependent protein-protein interactions involved in cell cycle and DNA repair processes (*200*). Finally, the CD domain is composed of the NAD^+ binding motif, also termed as PARP signature motif as well as the WGR domain. Based on a recently revealed structure of the ZF1/2/ZBD-WGR-CAT bound to a DSB, WGR was shown to be involved in DNA break-induced remodeling of an inhibitory helical domain (HD) near the active site, eventually triggering ARTD1 activity (*197*).

1.5.3 Poly-ADP-ribosylation cycle, PAR substrates and PAR hydrolases

In response to genotoxic stress, including oxidative and alkylation stress, ARTD1 catalyzes the formation of PAR using NAD^+ as a substrate (*186*). PAR is a

heterogeneous linear or branched polymer of ADP-ribose (ADPr) units, linked by a α(1→2) O-glycosidic bond, reaching a size of 200 - 400 ADPr units. Branching occurs every 20-50 elongation reactions (*201*). The PAR cycle is dived into five major steps, with i) Initiation; covalent auto-mono-ADP-ribosylation of the catalytic domain, ii) Trans-ADP-ribosylation; the instable initiation adduct is immediately trans-ADP-ribosylated to a more stable amino acid residue in the automodification domain of ARTD1 or on acceptor proteins by trans-ADP-ribosylation, iii) Elongation; polymer elongation involves the catalysis of a 2'–1" glycosidic bond, whereby the postulated covalently bound mono-ADP-ribose serves as a starting unit, iv) Branching of the polymer, v) Release of the enzyme-bound branched poly-ADP-ribose, either through poly-ADP-ribose-glycohydrolase activities (PARG)) or a putative intrinsic poly-ADP-ribosyl-protein-hydrolase activity. Glutamic acid (Glu) residues were early shown to serve as acceptor sites for ADPr, however, recent studies by the Hottiger and Poirier lab were able to pin-point lysines (Lys) as well as arginines (Arg) as novel acceptor sites for automodified ADPr by mass-spectrometry (*190, 202-205*). The major cellular substrate for PAR-modification is ARTD1 itself (*190*). Other well-described ARTD1 target proteins are histones, transcription factors and DNA-repair proteins (*185, 206, 207*). As already mentioned above, once formed, PAR is very quickly degraded with a predicted half-life of about 5 min in cells. Major PAR degrading enzymes belong to the family of endo- and exo- poly(ADP-ribose) glycohydrolases (PARG) family, including two cytoplasmic ($PARG_{99}$ and $PARG_{102}$) and one nuclear ($PARG_{110}$) localized members (*208*). Recently another member of PAR catabolizing enzymes, ADP-ribosyl hydrolase 3 (ARH3), joined the family of PAR degrading catabolizing enzymes (*209*).

1.5.4 DNA dependent activation of ARTD1

ARTD1 has been recently coined as "cellular rheostat", integrating different types and levels of stress conditions and initiating different cellular responses (*184*). In response to mild or moderate stress it regulates transcription and DNA repair, while upon severe and sustained stress conditions, hyper-activation of ARTD1 leads to apoptosis or necrosis (*210, 211*). Independent of the cellular outcome, its activation strongly depends on genotoxic stress (*187*). *In vitro*, ARTD1 activity is readily induced in presence of naked double and to a lesser extent single-stranded DNA (*190, 212*). A series of studies could also show ARTD1 automodification in presence of double-

stranded DNA hairpins, cruciforms and loops, indicating activation of ARTD1 by high-order DNA structure in a DNA damage independent manner (*213, 214*). Based on early studies both N-terminal zinc fingers (ZF1 and ZF2) were shown to be required for its enzymatic activity in presence of broken DNA, however with opposite results regarding the DNA specificity of each ZF (*215, 216*). In response to DSBs, ZF1/ZBD and WGR-CAT were shown by the Hottiger and Pascal lab to be essential and sufficient for ARTD1 activity *in vitro* (*190, 199*). In contrast to that, both N-terminal zinc fingers (ZF1 and ZF2) were required and sufficient for the activation of ARTD1 in presence of DSBs and SSBs as confirmed by the Oliver lab (*198*).

Many studies in the past were able to link ARTD1 activity to genotoxic stress in cells (*45*). Upon laser irradiation-induced DNA damage, ARTD1 is quickly recruited to sites of damage in a DBD-dependent manner and is required for the recruitment of ARTD2 and XRCC1, as shown by live cell microscopy using ARTD1 KO and enzymatically inactive mutants (*217*). Interestingly, recruitment was followed by dissociation, which was dependent on the enzymatic activity of ARTD1. These findings are in agreement with two recent studies, providing experimental evidences for the entrapment of ARTD1 and ARTD2 at DNA break sites in presence of PARP inhibitors, thus speaking for a role of PAR in regulating the chromatin compaction (*218, 219*). Altogether, these data contributed to the present model, which places ARTD1 activation downstream of DNA break recognition. Its activation leads subsequently to automodification, relaxation of the chromatin and a possible recruitment of the repair machinery to a DNA break. However, its role in break sensing was challenged by a recent study, showing ARTD1-independent recruitment of the BER machinery (XRCC1, Pol β) to the chromatin in response to H_2O_2 doses, that would not exceed the repair capacity of the cells, as confirmed by alkaline Comet assay and γH2AX staining (*220*). It still remains to be clarified which precise role ARTD1 is playing in DNA repair or genome instability upon genotoxic stress. Its role in genome stability is supported by studies based on ARTD1 $^{-/-}$ mice, which are viable, but sensitive to genotoxic stress (*221-223*).

1.5.5 DNA-independent activation of ARTD1

So far, DNA-dependent activation of ARTD1 could only be confirmed *in vitro* (*190, 197, 198, 212*), or indirectly upon genotoxic stress (*184*). Nucleosomes (intact DNA wrapped around core histones) were however also sufficient to induce ARTD1

activity and in fact led even to a stronger activation in comparison to activation by DNA fragments (*224*). Indeed, there is a growing body of evidences, indicating involvement of intracellular signaling in the activation of ARTD1 in a DNA break-independent manner, but dependent on either protein complex formation or post-translational modifications (*225*). Among the early observations, Ca^{2+} signaling has been placed upstream of ARTD1 activity in response to peroxynitrite (ONOO) treatment (*226*). Sequestration of ONOO-induced Ca^{2+} mobilization by Ca^{2+} chelators not only reduced PAR formation, but also decreased the induction of SSBs, indicating Ca^{2+}-dependent regulation of ARTD1 activity as well as DNA SSB formation. Paradoxically, Ca^{2+} sequestration lead to increased internucleosomal DNA cleavage upon ONOO exposure, while at the same time protecting cells from cytotoxicity (*226*).

Ca^{2+}-dependent stimulation of ARTD1 activity was also reported in response to β-lapachone, which is an NQO1-dependent ROS producer (*227*). Interestingly, studies from the Althaus lab could provide evidences for ARTD1-dependent Ca^{2+} regulation in response to lethal hydrogen peroxide doses, thus placing Ca^{2+} downstream of hydrogen peroxide induced ARTD1 activity (*228, 229*). Independent of the discrepancies regarding the physiological outcome in response to Ca^{2+} mobilization upon oxidative stress, the exact mechanism of Ca^{2+} dependent regulation of ARTD1 activity is missing. One proposal came from the Cohen-Armon lab, showing ARTD1 activation by PLC-IP3-dependent Ca^{2+} mobilization in a DNA-independent manner (*230*), however not providing the direct link from Ca^{2+} mobilization to ARTD1 activity. One potential link could be shown by two recent studies, identifying calcium/calmodulin-dependent kinase II (CaMKII) as a positive regulator of ARTD1 activity in neurons (*231, 232*). In both studies, CamKII directly modified ARTD1 by phosphorylation consequently leading to its activation. Positive regulation of ARTD1 activity was also described for the extracellular signal-regulated kinase (ERK) (*233-235*) as well as for c-Jun N-terminal kinase (JNK) (*236*), while negative regulation of ARTD1 by kinase-dependent phosphorylation was described to be under control of protein kinase C (PKC) (*237-239*).

2. Aim of the thesis

Cells are constantly harmed by DNA damaging agents from external and endogenous sources and must protect its genetic information in order to assure faithful reproduction and genomic stability, which otherwise would lead to malignancies such as cancer. The response of cells to genotoxic stress is regulated by a sophisticated network of signal cascades. The aim of this thesis was to elucidate the components regulating cellular response to two different genotoxic stress conditions.

Primary human fibroblasts are able to withstand high doses of ionizing radiation and prevent radiation-induced apoptosis. However the underlying mechanism of radio-resistance remained unclear until now. The first goal of this thesis was to describe a kinetic signaling network and functionally identify signaling components which are important for survival of primary human fibroblasts in response to high doses or ionizing radiation.

ARTD1 is a nuclear chromatin associated protein and its enzymatic activity is strongly induced upon DNA *in vitro*. ARTD1 is also strongly activated upon oxidative stress in fibroblast. Whether theses two observations are functionally interconnected remains to be defined. The second goal of this thesis was to describe the H_2O_2-induced signaling network and to functionally characterize regulatory mechanisms of nuclear poly-ADP-ribosylation formation in response to H_2O_2.

3. Results

3.1 Overview of the published results

3.1.1 PKC signaling prevents irradiation-induced apoptosis of primary human fibroblasts

Authors: **Andrej Bluwstein,** Nitin Kumar, Karolin Léger, Jens Traenkle, Jan van Oostrum, Hubert Rehrauer, Michael Baudis, Michael O. Hottiger

Journal: Cell Death and Disease

Contribution: Planning, performing and evaluating the experiments. Preparation of the figures and revision of the manuscript. NK and HR analysed protein microarray data. KL generated and analysed quantitative PCR data. JT, JvO, HR, MB and MOH supervised the study.

3.1.2 Opposite regulation of ADP-ribosylation by PKC signaling: ARTD1 is activated by PKCα and inactivated by PKCδ

Authors: **Andrej Bluwstein**, Nitin Kumar, Nicole Grosse, Jens Traenkle, Barbara van Loon, Michael Baudis, Michael O. Hottiger

Journal: Manuscript submitted

Contribution: Planning, performing and evaluating the experiments. Preparation of the figures and revision of the manuscript. NK analysed protein microarray data. NG performed and analysed comet assay. JT, BvL, MB and MOH supervised the study.

3.1.3 Oxidative stress induced poly-ADP-ribose formation is initiated by a calcium-dependent nuclease

Authors: **Andrej Bluwstein**, Nicole Grosse, Karolin Léger, Barbara van Loon, Michael O. Hottiger

Journal: Manuscript in preparation

Contribution: Planning, performing and evaluating the experiments. Preparation of the figures and revision of the manuscript. NG performed and analysed comet assay. KL generated and analysed quantitative PCR data. BvL and MOH supervised the study.

3.1.1 *PKC signaling prevents irradiation-induced apoptosis of primary human fibroblasts*

Citation: Cell Death and Disease (2013) 4, e498; doi:10.1038/cddis.2013.15

www.nature.com/cddis

PKC signaling prevents irradiation-induced apoptosis of primary human fibroblasts

A Bluwstein[1,2], N Kumar[3], K Léger[1,2], J Traenkle[4], J van Oostrum[5], H Rehrauer[6], M Baudis[3] and MO Hottiger*[,1]

Primary cells respond to irradiation by activation of the DNA damage response and cell cycle arrest, which eventually leads to senescence or apoptosis. It is not clear in detail which signaling pathways or networks regulate the induction of either apoptosis or senescence. Primary human fibroblasts are able to withstand high doses of irradiation and to prevent irradiation-induced apoptosis. However, the underlying regulatory basis for this phenotype is not well understood. Here, a kinetic network analysis based on reverse phase protein arrays (RPPAs) in combination with extensive western blot and cell culture analyses was employed to decipher the cytoplasmic and nuclear signaling networks and to identify possible antiapoptotic pathways. This analysis identified activation of known DNA damage response pathways (e.g., phosphorylation of MKK3/6, p38, MK2, Hsp27, p53 and Chk1) as well as of prosurvival (e.g., MEK-ERK, cAMP response element-binding protein (CREB), protein kinase C (PKC)) and antiapoptotic markers (e.g., Bad, Bcl-2). Interestingly, PKC family members were activated early upon irradiation, suggesting a regulatory function in the ionizing radiation (IR) response of these cells. Inhibition or downregulation of PKC in primary human fibroblasts caused IR-dependent downregulation of the identified prosurvival (CREB phosphorylation) and antiapoptotic (Bad phosphorylation, Bcl-2) markers and thus lead to a proliferation stop and to apoptosis. Taken together, our analysis suggests that cytoplasmic PKC signaling conditions IR-stressed MRC-5 and IMR-90 cells to prevent irradiation-induced apoptosis. These findings contribute to the understanding of the cellular and nuclear IR response and may thus eventually improve the efficacy of radiotherapy and help overcome tumor radioresistance.

Cell Death and Disease (2013) **4**, e498; doi:10.1038/cddis.2013.15; published online 14 February 2013
Subject Category: Cancer

Genotoxic stress such as ionizing radiation (IR) causes DNA damage and thereby induces diverse cellular responses such as cell cycle arrest and the activation of the DNA damage response (DDR) pathways to deal with this threat.[1] These complex DDRs are regulated by the PI3K-like kinases ATM, ATR and DNA-PK, which regulate downstream effectors that induce cell cycle checkpoints via phosphorylation of checkpoint kinases (Chk1/2), phosphatases (Cdc25) as well as stabilization of p53 and activation of the p16INK4a-Rb pathway to delay progression into the S phase or mitosis.[2] Following the detection of DNA breaks, ATM initiates a nuclear signaling cascade, leading to the phosphorylation of protein substrates such as histone H2A.X, which is thus modified into γH2A.X and sensitively marks individual DNA breaks.[3] Depending on the cell type, prolonged cell cycle arrest and extensive DNA damage leads to apoptosis or senescence,[4–6] but the molecular mechanism leading to either of these outcomes is not understood in detail. Recent large-scale network analyses have extended our understanding not only of genotoxic stress signaling and identified new phosphorylation but also of acetylation sites and target proteins mainly in the nucleus.[7–11] Reverse phase protein arrays (RPPA) represent a powerful technology for the sensitive detection and high-throughput quantification of protein changes at the single-cell level in a multiplex setting.[12,13] Protein arrays have already been applied to study changed expression levels or post-translational modification status of proteins in cellular stress conditions or in normal and cancerous prostate and ovarian tissue.[10,13–15]

Depending on the cell type, IR induces different responses and proteome changes. MRC-5 primary human lung fibroblasts were used in this study as a model cell strain, because these cells tolerate IR doses up to 80 Gy and do not induce apoptosis.[16,17] Here, we applied the RPPA technology to study IR-induced stress pathways in primary cells on a 'signalosome level' by analyzing cellular candidate markers. The RPPAs were probed with 165 different antibodies to quantify the major components and post-translational modifications of nuclear and cytoplasmic stress signaling events. Besides classical components of the DDR, such as protein level and phosphorylation changes in Chk1, p53, p21 and cyclin D1, as well as activation of the MEK-ERK, p38-Hsp27

[1]Institute of Veterinary Biochemistry and Molecular Biology (IVBMB), University of Zurich, Winterthurerstrasse 190, Zurich, Switzerland; [2]Cancer Biology PhD Program, Life Science Zurich Graduate School, University of Zurich, Winterthurerstrasse 190, Zürich, Switzerland; [3]Institute for Molecular Life Science (IMLS) and Swiss Institute of Bioinformatics (SIB), University of Zurich, Winterthurerstrasse 190, Zurich, Switzerland; [4]Bayer Technology Services GmbH, Zeptosens Platform, Leverkusen, Germany; [5]Luxembourg Clinical Proteomics Center, CRP-Santé, Strassen, Luxembourg and [6]Functional Genomics Center Zurich (FGCZ), University of Zurich, Zurich, Switzerland
*Corresponding author: MO Hottiger, Institute of Veterinary Biochemistry and Molecular Biology (IVBMB), University of Zurich, Winterthurerstrasse 190, Zurich 8057 Switzerland. Tel: +41 44 6355474; Fax: +41 44 6356840; E-mail: hottiger@vetbio.uzh.ch
Keywords: apoptosis; DNA damage response; PKC signaling; primary human fibroblast; radiation sensitivity; reverse phase protein array
Abbreviations: CREB, cAMP response element-binding protein; DDR, DNA damage response; DNA, deoxyribonucleic acid; IgG, immunoglobulin G; IR, ionizing radiation; NHF, normal human fibroblast; PKC, protein kinase C; RPPA, reverse phase protein array
Received 26.09.12; revised 21.12.12; accepted 02.01.13; Edited by A Stephanou

and LKB-AMPK pathways, the RPPA analysis described here also identified specific components of the cellular IR response involved in antiapoptotic and prosurvival signaling. Among these changes was also the activation of PKC family members. The PKC signaling pathway is known to integrate extracellular signals, calcium and secondary lipid messengers (diacylglycerol, phosphatidylserine), to regulate diverse cellular responses, including apoptosis or survival during genotoxic stress.[18–20] We found that experimental inhibition or downregulation of PKC led to downregulation of prosurvival (cAMP response element-binding protein (CREB) phosphorylation) and antiapoptotic (Bad phosphorylation, Bcl-2) markers upon IR treatment and thus lead to apoptosis in normal human MRC-5 and IMR-90 fibroblasts (normal human fibroblasts (NHFs)). These results thus implicated significantly changed kinetics of prosurvival (CREB phosphorylation) and antiapoptotic (Bad phosphorylation, Bcl-2) key determinants in the ability to prevent apoptosis upon severe DNA damage. IR-induced PKC signaling is thus defined as the mechanism that prevents IR-induced apoptosis.

Results

IR induces a DDR and senescence in MRC-5 fibroblasts. To induce DNA damage, primary human MRC-5 fibroblasts were irradiated with doses of 10 and 40 Gy. Both doses induced key components of the classical DDR, including phosphorylation of ATM at serine 1981 (pS1981), of Chk1 at serine 345 (pS345), of H2A.X at serine 139 (pS139) and stabilization of p53 protein levels (Figure 1a). The IR doses were chosen based on preliminary experiments and reflect the high capacity to repair IR-induced DNA damage of MRC-5 cells, which have been shown to efficiently remove DNA strand breaks (DSBs) up to IR doses of 80 Gy[16] and to enter the senescent state upon treatment with various stress stimuli.[21] In agreement with these findings, irradiation of MRC-5 cells with IR doses between 4 and 10 Gy induced a dose-dependent increase and time-dependent decrease of H2A.X pS139 that was mediated by ATM and DNA-PK (Figures 1b and c). The majority of DSBs was repaired within 8 h post-irradiation as indicated by the reduction of γH2AX foci and the remaining γH2AX foci continued to be repaired 24–48 h following IR treatment (Supplementary Figures S1a and b).

The strong reduction in colony formation of single cells after 10 days and the appearance of β-galactosidase-positive cells (MRC-5 and IMR-90) by 72 h after irradiation indicated growth arrest and induction of cell senescence (Supplementary Figures S1c and d), which was further supported by elevated p21 gene expression as well as p21 and p16 protein levels in MRC-5 and IMR-90 primary fibroblasts (Supplementary Figures S1e–g). Irradiation caused only a slight increase in the G2/M cell cycle population, but this effect was intensified upon ATM inhibition, suggesting that the efficient DDR prevented a more pronounced effect on cell cycle progression of irradiated MRC-5 cells (Supplementary Figures S2a–d). Cells did not exhibit elevated apoptosis even at the 8 h time point after 40 Gy irradiation, as indicated by the stable fraction of Annexin V-positive cells and undetectable expression of NOXA, PUMA and Bax (relative to a significant increase after staurosporine or cycloheximide treatment; Supplementary Figures S3a–d).

These results documented the suitability of 10 and 40 Gy IR to induce non-lethal, but senescence responses in primary fibroblasts.

IR induces significant proteome changes in MRC-5 fibroblasts. To quantify the kinetic proteome changes upon IR, MRC-5 fibroblasts were harvested at the 0.5, 2, 4 and 8 h time points after IR exposure (10 and 40 Gy) and RPPA analysis was performed (Figure 2a and Supplementary Figure S4). The time points were chosen based on the observed kinetics of γH2AX activation (Figure 1b) and were similar to those used in earlier studies.[7] The protein arrays were probed with 165 validated antibodies that specifically recognize the activation state of crucial proteins of all major signaling pathways. Only antibodies previously assessed and certified for commercial RPPA analysis services (identifying only one single band in a conventional western blot) were used and the spotted protein samples were diluted to increase the dynamic range for protein detection.[13] All quantitative RPPA data of three independent biological experiments (eight technical replicates) were subjected to stringent statistical analysis (ANOVA: $P<0.05$ and fold change cutoff: fold change $\geq 1.5 \times$ S.D.) (Supplementary Figures S5–9). Altogether, 90 unique proteome changes were either significant based on ANOVA and/or passed the $1.5 \times$ S.D. cutoff (Supplementary Figures S6 and 7 and Supplementary Table).

Clustering analysis identifies early cytoplasmic signals and subsequent activation of classical DDR proteins. The analysis described here identified distinct clusters based on the temporal up- and downregulation of specific proteins or protein modifications. In general, treatment of MRC-5 fibroblasts with 40 Gy induced more distinct clusters as compared with 10 Gy irradiation and three broad groups were apparent (Figures 2b and c and Supplementary Figures S10a and -b). The earliest changes affected many cytoplasmic proteins such as MEK1/2 (pS217/222, pS221/226), ERK1/2 (pT202/185, pY204/187), LKB (pS428) and cyclin D1 (pT286), which were sharply induced at 0.5 h after irradiation and relaxed to much lower and constant levels thereafter (cluster 1; Figure 2c and Supplementary Figure S10b). Following this first wave of protein changes, a cluster with a distinct maximum at 2 h after 40 Gy IR appeared (clusters 2 and 5). The protein changes that appeared at later time points after 40 Gy IR comprised changes that were upregulated throughout the entire IR response or specifically increased by the higher IR dose (clusters 3 and 4). The consecutive activation and inactivation of different groups of proteins indicated a signaling cascade that progresses from the cytoplasm (early activation of MEK1/2, ERK1/2, LKB) to the nucleus (delayed activation of classical nuclear DDR proteins such as Chk1, p53, p21, MAPKAP2, Hsp27).

Validation of RPPA analysis confirms upregulation of known DDR pathways and identifies pRb downregulation. The detection of many classical DDR proteome

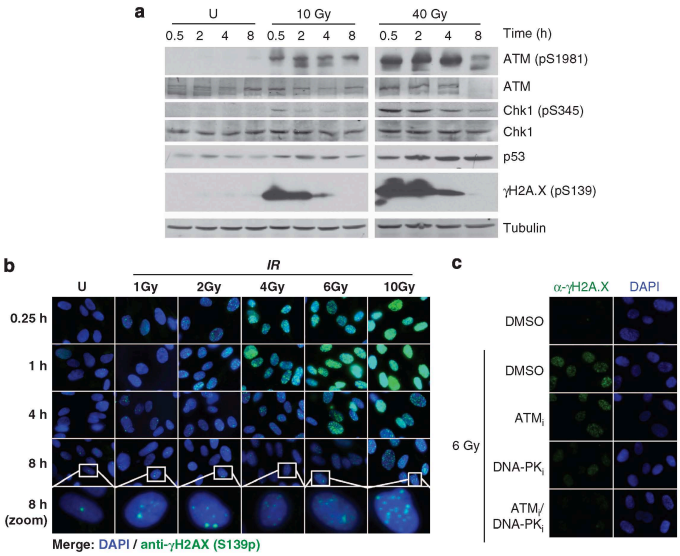

Figure 1 Induction of the DRR and efficient repair of IR-induced DNA breaks over 48 h in NHFs. (**a**) Western blot analysis of irradiated MRC-5 cells after recovery from IR for 0.5–8 h. (**b**) Immunofluorescence staining of MRC-5 cells irradiated with X-ray doses of 1–10 Gy or left untreated (U) and recovered for 15 min–8 h. (**c**) MRC-5 cells were pretreated with 10 μM KU-55933 (ATMi) and/or 10 μM Nu7441 (DNA-PKi) before irradiation with 6 Gy, or left untreated (U) as a control. Cells were stained with anti-γH2A.X (phospho-Ser139) 1 h post-irradiation. ATM, Ataxia-telangiectasia mutated; Chk, checkpoint kinase; DAPI, 4′,6-diamidino-2-phenylindole; DNA-PK, DNA protein kinase; DMSO, dimethyl sulfoxide

changes upon both 10 and 40 Gy IR validated the RPPA analysis of IR-treated MRC-5 fibroblasts. Known proteome changes of the DDR pathway included higher total amounts of p53 and p21 as well as increased levels of phosphorylated p38 MAPK (pT180, pY182), Hsp27 (pS78), p53 (pS15) and Chk1 (pS345) (clusters 1–3 for 10 Gy and clusters 2–5 for 40 Gy; Figures 2b and c and Supplementary Figures S10a and -b). In addition, Chk1 phosphorylation upon 10 and 40 Gy IR was confirmed by western blot analysis (Figure 1a and Supplementary Figure S10c). Levels of Chk1 phosphorylation determined by RPPA and western blot analysis showed similar kinetics (early increase after 30 min recovery from IR followed by a decline over the 8 h time course) and thus confirmed the validity of the RPPA approach. IR-induced Chk2 phosphorylation could only be shown by western blotting because of its poor antibody performance on the arrays (Supplementary Figure S10f). Even though ANOVA ($P<0.05$) and fold cutoff (S.D. = 1.5) analysis did not reveal significantly changed phosphorylation of the classical DDR marker H2A.X (pS139) in response to 10 Gy, at the 2 h time point, the Student's *t*-test showed a significantly increased H2A.X phosphorylation ($P<0.05$) (Supplementary Figures S7 and 8). The kinetics of H2A.X phosphorylation upon 10 and 40 Gy correlated well, but the higher dose resulted in a stronger fold induction (Supplementary Figures S8 and 9). In agreement with previously published studies,[22] activation of the cytoplasmic stress kinase p38 MAPK and its downstream effector, the small heat-shock protein Hsp27, were both ATM-dependent as confirmed by western blotting and ATM inhibitor studies (Supplementary Figure S10d). Other proteome changes that were also analyzed by western blotting similarly confirmed the RPPA results, albeit western blotting revealed higher fold changes. Temporarily increased levels of p53, which is the main target for ATM in response to IR,[2] correlated with delayed upregulation of p21 (clusters 1 and 2 for 10 Gy; Figure 2b). Surprisingly, the important cell cycle regulator retinoblastoma protein (pRb) was significantly downregulated upon 10 Gy irradiation (cluster 5; Figure 2b), representing a proteome change that has not been implicated in the IR response previously. The RPPA-based pRb quantification correlated strongly with results obtained by western blotting (Supplementary Figures S10e and f), supporting *in vivo* pRb downregulation upon IR in MRC-5 fibroblasts. In contrast to total pRb levels, the phosphorylation of pRb at S780 (relative to total pRb) increased upon 10 Gy after 8 h and already after 2 h following irradiation with 40 Gy (Supplementary Figure S10f). In line with this finding, a strong cell-cycle effect was not observed 24–48 h after irradiation compared with a clear accumulation of cells at the G1/S boundary upon hydroxyurea treatment (Supplementary Figure S2), suggesting that the pRb changes may be important for the maintenance of cell cycle progression during the immediate IR response.

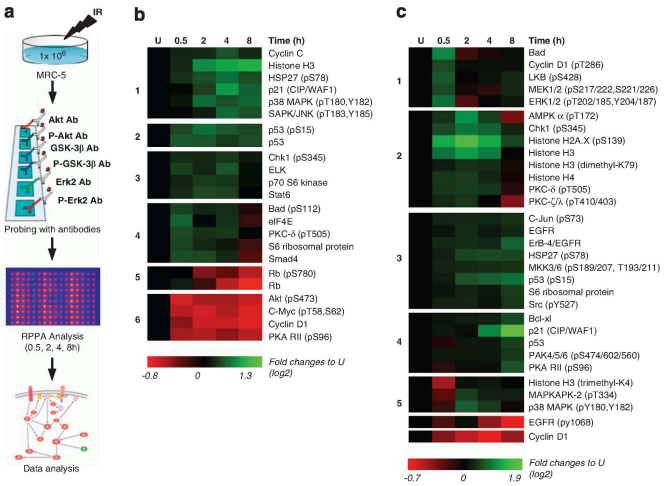

Figure 2 Identification of significant proteome changes in response to IR. (**a**) Workflow for the characterization of IR-induced proteome changes by RPPA. MRC-5 cells were left untreated (U) or irradiated in biological triplicates with 10 or 40 Gy. At different time points, cell lysates were prepared and spotted in equal amounts on hydrophobic glass slides. Each array was incubated with a different primary antibody, directed against a protein of interest and a secondary fluorophore-labeled antibody. Relative fluorescence intensities were quantified and used for statistical data analysis to identify significant proteome changes in response to irradiation. (**b** and **c**) Time-profile clustering of IR-dependent proteome changes (analysis of variance (ANOVA), $P<0.05$; 1.5 S.D. cutoff) using Self-Organizing Tree Algorithm (SOTA) showing protein expression and modification (e.g., phosphorylation) in green or downregulation and de-modification (e.g., de-phosphorylation) in red. (**b**) Clustering of proteome changes upon irradiation with 10 Gy. (**c**) Clustering analysis of IR-dependent proteome changes upon 40 Gy treatment. AMPK, AMP-activated protein kinase; Bad, Bcl2 antagonist of cell death; EGFR, epidermal growth factor receptor; eIF4E, Eukaryotic initiation factor eIF4E like protein; ERK, extracellular signal-regulated kinase; Hsp, heat-shock protein; JNK, c-Jun NH2-terminal kinase; MAPK, mitogen-activated protein kinase; MEK, MAPK/ERK kinase; PAK, p21-activated kinase; PKA RII, cAMP-dependent protein kinase type II regulatory subunit; PKC, protein kinase C; Rb, Retinoblastoma-associated protein; SAPK, stress-activated protein kinase; SMAD, Homolog of mothers against decapentaplegic homolog from *Drosophila* and SMA from *Caenorhabditis elegans*; Stat6, signal transducer and activator of transcription 6

The role of the p53 pathway in DDR and its function as a 'guardian of the genome'[23,24] is emphasized by the fact that it was significantly over-represented among the proteins responding to both 10 and 40 Gy IR (Figure 3a), and by its many interactions (more than 14 interactions) in the predicted protein network (Figure 3b and Supplementary Figure S10g). The agreement of the RPPA analysis with western blot quantifications, as well as the identification of the known key players in the DDR, confirmed the validity of the RPPA approach described here and proved that the IR-treated cells used in these experiments launched a classical DDR.

IR upregulates antiapoptotic and prosurvival markers in MRC-5 cells. The kinetic RPPA analysis described here also revealed many new cytoplasmic factors, which were further analyzed in more detail. The here identified changes included prosurvival signals CREB (pS133) as well as MEK1/2 (pS217/222, pS221/226), ERK1/2 (pT202/185, pY204/187) and AMPK (pT172) for 40 Gy only, antiapoptotic markers (Bad pS112 and pS136, Bcl-2 pS70 for 10 Gy only) as well as a cluster comprising protein kinase C (PKC) family members. The changes in PKC family members included the phosphorylation of the novel PKC-δ (pT505) and of the atypical PKCζ/λ (pT410/403) in the activation loop (Figures 2b and c), which marks the activated state of these two PKC isoforms.[25]

These analyses suggested that IR treatment of primary fibroblasts activates not only the classical DDR pathways MEK-ERK and p38-Hsp27 but that also the cytoplasmic PKC signaling and specific antiapoptotic and prosurvival factors were regulated. It is thus possible that PKC signaling is involved in mediating the high IR resistance of MRC-5 and IMR-90 cells by preventing apoptosis and stimulating prosurvival factors.

Inhibitor screen identifies PKC signaling as important for IR resistance. To elucidate whether PKC or other main signaling cascades regulate cell viability in NHFs upon IR treatment, a radiosensitivity screen with inhibitors specific for key components of the MEK-ERK, p38, JNK or PKC pathways was performed (Figure 4 and Supplementary Figures S11a–e). While JNK inhibitors had only a weak effect on cell viability, inhibition of MEK and p38 affected cell proliferation, but independent of IR (i.e., similar effect in treated and untreated cells). Interestingly, already 48 h after the cotreatment with either one of two PKC inhibitors (GF109203X or Ro-318220) and with IR, MRC-5 cells showed a significant reduction in cell viability compared with cells treated with DMSO (the solvent) or with IR alone (Figure 4 and Supplementary Figure S11). The NHF strain IMR-90 behaved similarly and showed a significant reduction

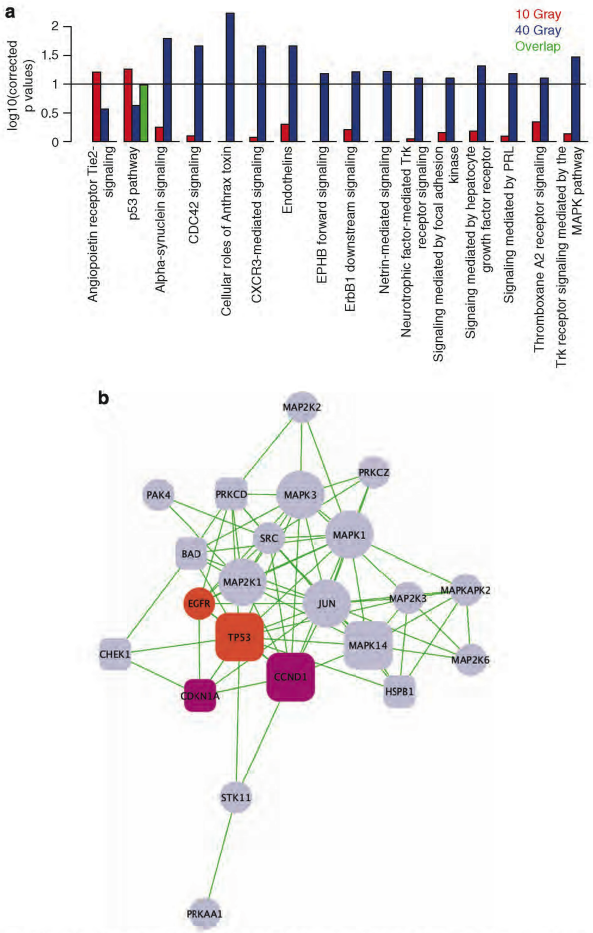

Figure 3 Pathway and protein–protein interaction analysis of significant IR-induced proteome changes. (**a**) Enrichment of pathways from the pathway interaction database (PID) with significant proteome changes (analysis of variance (ANOVA), $P<0.05$; 1.5 S.D.) induced by 10 Gy only (red), 40 Gy only (blue) and overlapping changes (green) using Fisher's exact test. (FDR-corrected *P*-value cutoff = 0.1). (**b**) Protein–protein interaction analysis of significant proteome changes induced by 40 Gy using STRING, with a STRING score cutoff >0.7. Colors indicate phosphorylation (light blue), total protein changes (violet), phosphorylation and total protein changes (orange). Circles represent unique changes and squares overlapping changes. Large symbols indicate proteins that interact with more than 14 members. BAD, Bcl2 antagonist of cell death; CCND, Cyclin D; CDC42, Cell division control protein 42 homolog; CDKN1A, Cyclin-dependent kinase inhibitor 1A (p21); CHEK1, Checkpoint kinase-1; CXCR3, C-X-C chemokine receptor type 3; EGFR, Epidermal growth factor receptor; EPHB, Ephrin type-B receptor; ErbB, Epidermal growth factor receptor; HSPB, Heat shock protein beta; MAP2K1, Dual specificity mitogen-activated protein kinase kinase 1 (MEK1); MAP2K2, Dual specificity mitogen-activated protein kinase kinase 2 (MEK2); MAP2K3, Dual specificity mitogen-activated protein kinase kinase 3 (MKK3); MAP2K6, Dual specificity mitogen-activated protein kinase kinase 6 (MKK6); MAPK, mitogen-activated protein kinase; MAPK1, Mitogen-activated protein kinase 1 (ERK-2); MAPK3, Mitogen-activated protein kinase 3 (ERK-1); MAPKAP2, MAP kinase-activated protein kinase 2 (MK2); PAK, p21-activated kinase; PRKAA1, 5'-AMP-activated protein kinase catalytic subunit alpha-1 (AMPK1); PRKCD, protien kinase C delta type; PRKCZ, Protein kinase C zeta type; PRL, prolactin; SRC, Proto-oncogene tyrosine-protein kinase Src; STK11, Serine/threonine-protein kinase STK11 (LKB1); Trk, tropomyosin-receptor-kinase.

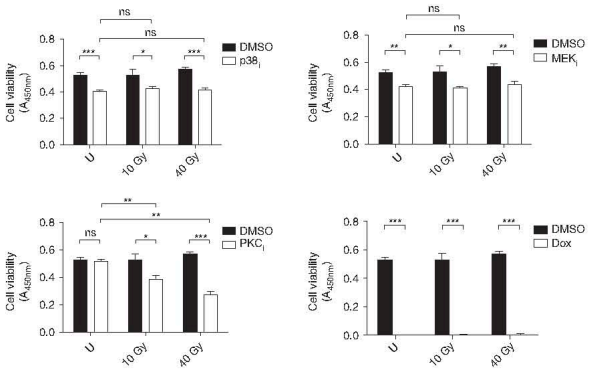

Figure 4 PKC inhibition sensitizes MRC-5 to 10 and 40 Gy after 48 h. Cell viability assay (WST-1) of MRC-5, pretreated with p38 (SB203580, 10 μM), MEK (PD98059, 20 μM) or PKC inhibitor (GF109203X, 10 μM) and as a positive control for cell death with doxorubicin (Dox, 1 μg/ml) for 2 h before IR and recovery for the indicated time points ($n=3$). DMSO, dimethyl sulfoxide; MEK, mitogen-activated protein kinase/extracellular signal-regulated kinase kinase; NS, nonsignificant; PKC, protein kinase C; U, untreated; $^{*}p<0.05$; $^{**}p<0.01$; $^{***}p<0.001$

in growth when treated with the PKC inhibitor GF109203X (2.5 μM) and either 10 or 40 Gy irradiation (Supplementary Figures S12a–c). These results implicated PKC activity and signaling in the radiosensitivity of MRC-5 and IMR-90 cells.

Inhibition or downregulation of PKC directs cells towards apoptosis. To confirm and validate PKC activation upon IR, western blot analyses were performed. In agreement with the RPPA results and the inhibitor studies, phosphorylation of PKCζ/λ (pT410/pT403) as well as of PKCβ (pT641) were confirmed to be increased upon IR (Figures 5a and b). To further characterize the mechanism of the PKC-dependent reduction in cell viability, one prosurvival (CREB phosphorylation)[26] and one antiapoptotic marker (phosphorylation of Bad)[27] was analyzed in more detail by western blotting (Figures 5c–e). In combination with IR treatment, PKC inhibition or downregulation caused strongly reduced phosphorylation of CREB (pS133) and Bad (pS136), while the total protein levels were only marginally affected (Figures 5c and d for MRC-5; Figure 5e for IMR-90). Interestingly, ATM (pS1981) was not affected by PKC inhibition (Figures 5c and e) and did not affect CREB phosphorylation or protein levels (Figure 5c), suggesting that the PKC pathway is activated independent of the classical DDR.

Although primary human fibroblasts are known to undergo senescence as a response to irradiation, the reduced phosphorylation of CREB and Bad, as well as the reduced cell viability, upon IR treatment and PKC inhibition or downregulation indicated the induction of apoptosis.[28,29] It was therefore assessed whether irradiation and PKC inhibition affects senescence and possibly induces apoptosis. Upon PKC inhibition and irradiation with 10 or 40 Gy, MRC-5 and IMR-90 cells both showed reduced β-galactosidase staining as compared with the DMSO-treated control, which is indicative of reduced senescence (Figure 5f and Supplementary Figure S13a). Using an alternative senescence marker, reduced p16 protein levels upon irradiation, in combination with PKC inhibition or downregulation, could be confirmed in MRC-5 cells (Figure 5h). The p16 levels were not significantly reduced in IMR-90 cells in response to IR and PKC inhibition; however; the significant reduction in p21 protein levels (Supplementary Figures S13b and c) was another alternative indicator for cellular senescence.[30] In contrast, in the presence of PKC inhibitors, IR treatment led to induced levels of the proapoptotic marker Bad and reduced amounts of the antiapoptotic marker Bcl-2, persistently increased p53 protein levels (in addition to the temporary p53 stabilization observed as a response to IR alone) and ARTD1 (PARP-1) cleavage (reduction in ARTD1 full-length levels and accumulation of the 89 kDa cleavage fragment), all suggestive of a switch from senescence to apoptosis, specifically upon IR in combination with PKC inhibitor treatment or PKC knockdown after 48 h of IR recovery (Figures 5g and h). Reduced ARTD1 levels and an increased sub-G1 cell population in the NHF strain IMR-90 also confirmed the findings with the MRC-5 strain (Supplementary Figures S13b–f), in addition to the reduced senescence and cell viability upon IR treatment in combination with PKC inhibition.

In summary, these results demonstrated the IR-dependent activation of cytoplasmic PKC signaling and discovered the consecutive PKC-dependent activation of prosurvival signaling mediated via CREB and Bcl-2 as well as the inactivation of proapoptotic pathways (Bad), which direct normal human MRC-5 and IMR-90 fibroblasts towards senescence and prevent IR-induced apoptosis (Figure 6). Activation of cytoplasmic PKC signaling upon IR is thus a novel mechanism that orchestrates the different IR-induced responses to ensure cell survival of primary human fibroblasts.

Discussion

Human primary fibroblasts such as MRC-5 cells are able to repair DNA damage induced by IR doses up to 80 Gy.[16,17] However, it was so far not clear how MRC-5 fibroblasts prevent

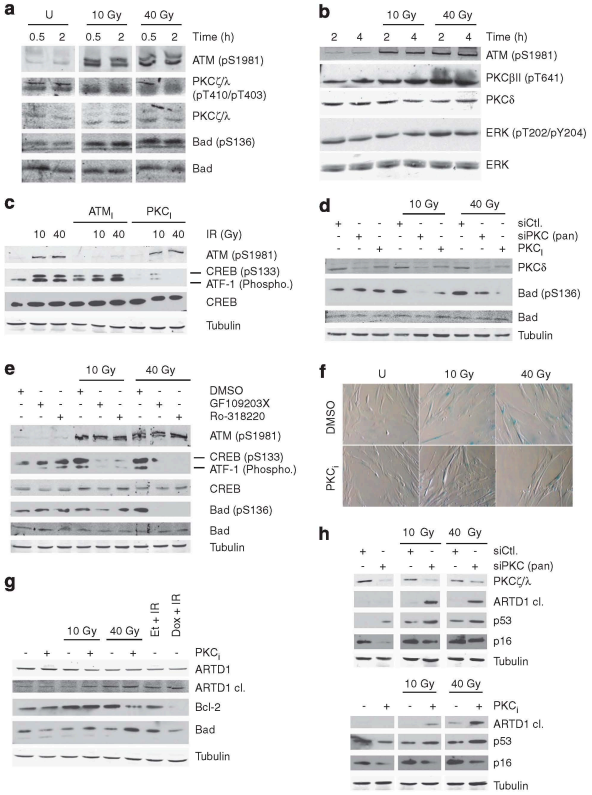

Figure 5 Inhibition or downregulation of PKC reduces prosurvival signaling in NHFs. Phosphorylation of PKCζ/λ and Bad (**a**) or PKCβII and ERK (**b**) in response to IR. Western blot analysis of irradiated MRC-5 cells after recovery for 0.5–2 or 2–4 h following IR. Total PKCζ/λ and Bad (**a**) or total PKCδ and ERK (**b**) were used as loading control. (**c**) Phosphorylation of CREB and ATF-1 is downstream of PKC activation in response to IR. Western blot analysis of irradiated MRC-5 cells (4 h recovery) that were treated either with the PKC-specific inhibitor Ro-318220 (5 μM, added before irradiation) or with the ATM inhibitor KU-55933 (10 μM, added before irradiation). Tubulin was used as loading control. (**d**) Phosphorylation of Bad is downstream of PKC activation in response to IR. Western blot analysis of irradiated MRC-5 cells (4 h recovery) that were exposed to the PKC-specific inhibitor GF109203X (5 μM, for 2 h) or siPKC pan. (**e**) Phosphorylation of CREB, ATF-1 and Bad is downstream of PKC activation in response to IR. Western blot analysis of irradiated IMR-90 cells (4 h recovery) that were treated with GF109203X or Ro-318220 (2.5 μM, 2 h pre-incubation before irradiation). Tubulin was used as loading control. (**f**) Pharmacological inhibition of PKC reduces senescence associated β-galactosidase (β-gal) staining. SA-β-gal staining of irradiated MRC-5 in presence of PKC inhibitor (GF109203X, 5 μM, 72 h recovery) with untreated (U) as control. (**g**) Pharmacological inhibition of PKC (GF109203X, 5 μM) leads to ARTD1 cleavage, Bcl-2 downregulation and Bad upregulation 48 h after IR. (**h**) Knockdown of PKC leads to increased p53 stabilization and reduced p16 protein levels as well as increased ARTD1 cleavage in response to 10 and 40 Gy at 48 h after IR. Western blot analysis of irradiated MRC-5, transfected either with siPKC pan or scrambled siRNA as control for 3 days before IR. Tubulin was used as loading control. ARTD1, ADP-ribosyltransferase diphtheria toxin-like 1; ATF, cyclic AMP-dependent transcription factor 1; ATM, ataxia–telangiectasia mutated; Bad, Bcl2 antagonist of cell death; Bcl-2, B-cell lymphoma 2; CREB, cAMP response element-binding protein; DMSO, dimethyl sulfoxide; ERK, extracellular signal-regulated kinase; Et, etoposide; PKC, protein kinase C

apoptosis, which is induced at much lower IR doses in other cell types.[31] Understanding the dynamics of *in vivo* signaling events in response to IR in human primary fibroblast may thus reveal medically relevant IR resistance mechanisms.

The network analysis of IR-induced proteome changes in MRC-5 fibroblasts presented here identified upregulation of known DDR factors (H2AX, p53, p21, MKK3/6, p38, MK2, Hsp27, Chk2) only 2–8 h after irradiation (Supplementary Table). In contrast, growth factor- and cytokine-dependent signaling pathways including members of the MAPK family (MEK/ERK), PKC family (PKCδ, PKCζ/λ, PKCβII) as well as anti- and proapoptotic Bcl-2 family members (Bcl-2, Bad) tended to respond with faster kinetics and thus indicated that cytoplasmic signaling events are upstream of the canonical DDR. Indeed, an increasing body of evidence implicates an IR-dependent cytoplasmic signaling network in regulating

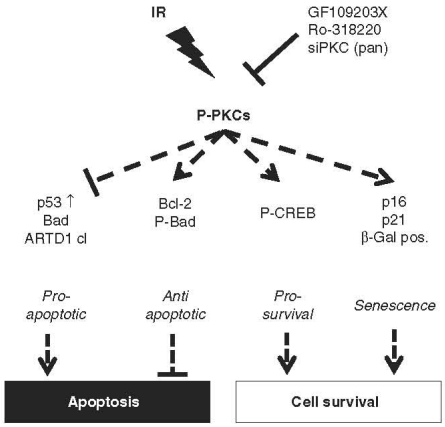

Figure 6 Model of PKC-dependent cellular prosurvival signaling in response to IR. IR-induced PKC signaling orchestrates cell survival via upregulation of Bcl-2 and phosphorylation of Bad and CREB. Hypersensitization with PKC inhibitors (GF109203X, Ro-318220) and genetic knock down (siPKC pan) leads to IR-induced activation of apoptosis mediated by p53 stabilization, upregulation of Bad and ARTD1 cleavage, as well as reduced senescence mediated via decrease in p21 protein levels and reduced β-galactosidase (β-Gal) activity in response to IR. ARTD1, ADP-ribosyltransferase diphtheria toxin-like 1; Bad, Bcl2 antagonist of cell death; Bcl-2, B-cell lymphoma 2; CREB, cAMP response element-binding protein

DNA break repair.[32] Although RPPA analysis is restricted by antibody performance and reduced dynamic range, western blotting confirmed the tested proteome changes discovered by RPPA analysis, supporting the stringent statistical analysis. However, western blotting indicated that RPPA analysis usually underestimated the IR-induced proteome changes.

Most proteome changes, in particular upon 40 Gy IR, affected mitogenic signaling events controlling cell survival (MKK3/6-p38-MK2 pathway, MEK-ERK pathway, LKB-AMPK pathway, PKC-Bad pathway). Previously published results have demonstrated p38-MK2 pathway activation and subsequent cell cycle arrest in G2/M in response to UV irradiation, thus protecting DNA damaged cell from entering mitosis, which would lead to a mitotic catastrophe and eventually to apoptosis.[33,34] In agreement with these findings, in response to 10 and even more pronounced upon 40 Gy, we could show activation of the major p38-MK2 pathway components, with phosphorylation of MKK3/6, p38, MAPKAP-2 (MK2) and Hsp27, besides the slight increase in the percentage of the G2/M cell cycle population 24–48 h after IR recovery (Supplementary Figures S2 and S7).

The most important finding of this systematic RPPA analysis is the identification of PKC as a key player that orchestrates the downstream signaling pathways regulating apoptosis and cell survival (Figure 6). IR-dependent PKC activation regulated Bad, Bcl-2 and CREB to prevent apoptosis and to induce prosurvival signaling. Whether PKC family members directly phosphorylate the identified downstream proteins or rather indirectly affect their activation is currently not known. Interestingly, PKCs are known to translocate to the nucleus[35] and all identified regulatory components (Bad, Bcl-2, CREB) contain putative target sites for phosphorylation by PKC.[36] PKC inhibitors, or PKC downregulation before IR treatment, downregulated antiapoptotic factors (Bad phosphorylation, Bcl-2) and induced apoptosis (ARTD1 cleavage, increased p53 stabilization, Bad upregulation, increased sub-G1 population and decline in cell number). Sensitization of primary fibroblasts by PKC inhibitors or downregulation thus induced an apoptotic program that is mediated by effects on CREB, Bad and proapoptotic genes. PKC-dependent regulation of cell survival, apoptosis as well as cell cycle progression is thus proposed as a part of the mechanism by which primary fibroblasts resist high IR doses and circumvent apoptosis, which is in agreement with the high DNA repair efficiency and the PKC-dependent regulation of p53 function.[16,37] The inhibitor and siRNA experiments described here imply PKC signaling in the prevention of apoptosis in human primary MRC-5 and IMR-90 fibroblasts. However, these analyses do not identify which PKC family member mediates the observed phenotypes. The RPPA analysis identified PKCδ activation, which was previously shown to be induced upon DNA damage[38] and linked to pro- and antiapoptotic functions (Basu and Pal[39] and many reference therein). Future studies on the upstream regulators relevant for PKC activation upon IR in MRC-5 and IMR-90 cells will identify the required cofactors and signaling components and thereby indicate which PKC subgroup mediates the antiapoptotic function. Taken together, our findings provide the cellular mechanism, which is responsible for this phenotype and may thus open up possiblities for new treatment schemes of highly IR-resistant tumors.

This result has not only important implications for our understanding of the IR response but also for the comprehension of nuclear regulatory events and supports the concept of the cellular, in contrast to the nuclear, radiation response.[40] Cellular stress such as IR is perceived at the plasma membrane and in the cytoplasm and initiates cytoplasmic signaling pathways that consecutively control nuclear events such as DNA repair. This is also suggested by the induction of IR-induced signaling in cells exposed to IR conditioned medium, which is termed the 'bystander effect'.[41] The classical DDR, comprised of nuclear events regulating cell cycle progression and DNA repair, is thus preceded and controlled by the cytoplasmic radiation response, which is mediated by the PKC signaling pathway as well as other signaling pathways such as the MEK-ERK pathway.

This RPPA network analysis of IR-induced signaling identified a new, cytoplasmic, PKC-dependent regulatory mechanism that conditions stressed cells by preventing apoptosis. The PKC-dependent induction of prosurvival signaling and evasion of apoptosis is thus a mechanism, which renders primary human fibroblasts resistant to high doses of IR, and may thereby protect the microenvironment and permit survival of tumors. Our results thus provide an explanation for the cellular response to severe irradiation stress and will therefore help optimize and improve radiotherapy.

Materials and Methods

Cell culture, IR treatment, siRNA transfection, lysis, viability and senescence assays. The MRC-5 and IMR-90 human lung fibroblast cell strains[42,43] were obtained from the American Type Culture Collection and cultured in supplemented MEM (Invitrogen; Life Technologies, Carlsbad, CA, USA). Cells were exposed to IR using an X-ray generator (Pantak Seifert X-ray System, Ahrensburg, Germany; 120 kV; 19 mA; aluminum filter; 3.11 Gy/min) and recovered for different time periods. Inhibitor treatment was performed as indicated in the figure legends before the exposure to IR. To reduce PKC expression, 1×10^5 MRC-5 cells were transfected using human siPKC pan (Santa Cruz Biotechnology, Dallas, TX, USA; sc-29449) over 3 and 4 days, before irradiation. Whole cell extracts were prepared with Zeptosens Cell Lysis Buffer CLB1 (Bayer Technology Services GmbH, Leverkusen, Germany) or RIPA lysis buffer and total protein concentration was determined using the standard Lowry method. Cell viability was determined by seeding 2×10^3 cells in 96-well plates overnight before irradiation or drug treatment. Cell viability was quantified using the WST-1 proliferation reagent (Roche, Basel, Switzerland) or alamarBlue cell viability assay (Invitrogen) and a plate reader (Tecan, Männedorf, Switzerland). The clonogenic and senescence assays were performed as described elsewhere.[44,45]

Reverse phase protein arrays. RPPA were prepared as described.[46] In brief, whole cell extracts were spotted onto hydrophobically coated Zeptosens Chips (Bayer Technology Services GmbH). Serially diluted lysates (100, 75, 50 and 25%) were arrayed in duplicates onto hydrophobic Zeptosens Chips using the Nanoplotter NP2.0 (GeSiM; Gesellschaft für Silizium-Mikrosysteme mbH, Grosserkmannsdorf, Germany), followed by blocking in an ultrasonic nebulizer (ZeptoFOG; Bayer Technology Services GmbH). Antibody incubation, microarray data acquisition (ZeptoREADER; Bayer Technology Services GmbH) and data analysis (ZeptoVIEW version 3.1.0.2; Bayer Technology Services GmbH) was performed exactly as described.[47] The eight data points (100, 75, 50 and 25% lysate amount in duplicates) were fitted using a weighted linear least-squares fit[48] and the relative fluorescence intensity determined by interpolating at the median protein concentration or modification. To correct for small variations in protein content, relative intensities were normalized to the signals of β-catenin, which did not show any significant variation (ANOVA, $P<0.05$; $1.5 \times$ S.D.) in response to IR over indicated time points.

Significance and clustering analysis. To identify significant proteome changes in response to IR, relative fluorescence intensities were imported to MeV version 4.6.[49] Relative fluorescence intensities were log 2 transformed and normalized, before performing statistical analysis using one-way ANOVA as described in Zar.[50] The mean transformed fluorescence intensities for group 1 (untreated: 0.5, 2, 4 and 8 h), group 2 (biological triplicates of 10 or 40 Gy at 0.5 h), group 3 (biological triplicates of 10 or 40 Gy at 2 h), group 4 (biological triplicates of 10 or 40 Gy at 4 h) and group 5 (biological triplicates of 10 or 40 Gy at 8 h) were compared using F-statistics with $P<0.05$. Owing to technical problems during preparation of the serial dilution of the whole cell extracts, two biological replicates for the 8 h time point of 10 Gy irradiated samples (10 Gy at 8 h) and one biological replicate for the 2 and 8 h time point of 40 Gy irradiated samples (40 Gy at 2 h and 40 Gy at 8 h) were excluded from the statistical analysis. For fold-change analysis, transformed means of the biological replicates were normalized to the untreated sample (set as 1) and proteome changes were filtered (cutoff set at $1.5 \times$ S.D. equal to $\log 2 > 0.27 / < -0.27$ for 10 Gy or $\log 2 > 0.29 / < -0.29$ for 40 Gy). Significant proteome changes in response to IR were selected, if significant by one-way ANOVA ($P<0.05$) and fold cutoff ($1.5 \times$ S.D.). Alternatively, significance analysis was performed using two-tailed Student's *t*-test ($P<0.05$). Similar profiles of the fold changes over time were identified by clustering analysis using the Self Organizing Tree Algorithm[51] and default parameters of MeV version 4.6.[49]

Pathway and network analysis. Gene pathway membership data were obtained from protein interaction database, PID[52] and KEGG.[53] A total of 200 and 211 pathways were obtained from PID and KEGG, respectively. For statistical analysis, all analyzed proteins in this study (unique IDs) were set as the background list and all pathways consisting of more than five proteins from the background list were considered for statistical analysis by Fisher's exact test, resulting in a total of 93 pathways from PID and 63 from KEGG. Fisher's exact test was performed to identify pathways significantly affected by proteins (modifications) altered in response to irradiation (significant by ANOVA and fold change) using the R statistical framework.[54] To account for multiple testing, *P*-values were corrected for false discovery rates (FDRs) using Benjamini–Hochberg correction. We have used an FDR-corrected *P*-value cutoff of 0.1 to identify pathways significantly affected by proteome changes.

Significant proteome changes, identified by statistical (ANOVA) and fold-change analysis (log 2 cutoff) were subjected to protein–protein interaction analysis using STRING (v. 9.0, http://www.string-db.org/).[55] Only interactions with a STRING score of 0.7 and above were further analyzed using Cytoscape (http://www.cytoscape.org/).[56]

Immunoblotting. For western blot analysis, proteins were separated by SDS-PAGE gel electrophoresis and bands were visualized by using either horseradish peroxidase-conjugated antibodies (1 : 5000; GE Healthcare, Life Sciences, Uppsala, Sweden) and ECL detection (GE Healthcare) or IR-dye-conjugated antibodies (1 : 15 000; LI-COR Biosciences) and detection by the Odyssey infrared imaging system (LI-COR Biosciences, Lincoln, NE, USA). For quantification, bands were analyzed by ImageJ 1.46 (ref. 57) and the Odyssey imaging software (LI-COR Biosciences).

Antibodies used for western blotting were anti-ATM (GeneTex, Irvine, CA, USA), anti-ATM Phospho (pS1981) (Epitomics-an Abcam Company, Burlingame, CA, USA), anti-Bad (CST), anti-Bad Phospho (pS136) (Cell Signaling Technology (CST), Danvers, MA, USA), anti-Chk1 (CST), anti-Chk1 Phospho (pS345) (1 : 500; CST), anti-Chk2 Phospho (pT68) (CST), anti-CREB (CST), anti-CREB Phospho (pS133)/anti-ATF-1 (phospho) (CST), anti-histone H2A.X Phospho (pS139) (Millipore, Billerica, MA, USA), anti-Hsp27 (CST), anti-Hsp27 Phospho (pS78) (1 : 500; CST), anti-PARP1 (Santa Cruz Biotechnology), anti-PARP1 cleaved (1 : 500; CST), anti-p16 (1 : 500; Santa Cruz Biotechnology), anti-p21 (Santa Cruz Biotechnology), anti-p38 (CST), anti-p38 Phospho (pThr180/Tyr182), anti-p44/42 Erk1/2 (CST), anti-p44/42 Erk1/2 Phospho (pThr202/Tyr204) (CST), anti-p53 (Santa Cruz Biotechnology), anti-Rb (1 : 500; Epitomics), anti-Rb (pS780) (CST), anti-tubulin (1 : 10 000; Sigma-Aldrich, St Louis, MO, USA), anti-PKCβII Phospho (pT641) (CST), anti-PKCδ (CST), anti-PKCζ/λ (CST) and anti-PKCζ/λ Phospho (pT410/pT403) (CST). Unless otherwise stated, antibody dilution was 1 : 1000.

Immunofluorescence microscopy. MRC-5 cells grown on cover slips over night ($\approx 1 \times 10^4$ cells) were irradiated and immunohistochemically stained with primary (1 : 500 mouse anti-histone H2A.X Phospho (S139) immunoglobulin G1 (IgG1) (Millipore) or 1 : 500 rabbit anti-53BP1 IgG1 (Santa Cruz Biotechnology)) and secondary antibodies (1 : 250 FITC- or cyanine 3-conjugated IgG anti-mouse IgG (Jackson ImmunoResearch Laboratories, West Grove, PA, USA) or 1 : 250 Alexa Fluor 488-conjugated anti-rabbit IgG (Invitrogen)).

Flow cytometry. Cell cycle analysis of IR-treated or -untreated MRC-5 cells was performed using standard ethanol fixation/PI-staining protocol and flow cytometry analysis (FACS) with a Dako CyAn ADP flow cytometer (Dako, North America, Carpinteria, CA, USA). For sub-G1 peak analysis of IMR-90, cell debris and necrotic cells were gated out according to the protocol of Riccardi and Nicoletti.[58] Annexin V staining was performed using the FITC Annexin V apoptosis detection kit (BD Biosciences, San Jose, CA, USA) and a Dako CyAn ADP flow cytometer (Dako).

RNA extraction and real-time PCR analysis. Total RNA was reverse transcribed using High-Capacity cDNA Reverse Transcription kit (Applied Biosystems; Life Technologies). Real-time PCR was performed using SYBR green premixed buffer and analyzed by the Rotor-Gene Q cycler (Qiagen, Hilden, Germany).

Conflict of Interest

JT was Zeptosens Technology Manager at Bayer Technology Services GmbH and is currently Group Head for Process Analytical Technologies at the same company. JvO was Head of Business Development at Zeptosens, a division of Bayer (Schweiz) AG. All the other authors declare no conflict of interest.

Acknowledgements. F Freimoser (University of Zurich) provided editorial assistance and critical input during the writing. We thank M Ehrat, G Balciunaite and J Grognux for technical assistance with protein arrays. This work was supported in part by the Kanton of Zurich (to MOH), Oncosuisse (KLS 02396-02-2009) and the UBS foundation.

Author contributions

AB, NK, JT and MOH designed the experiments; AB, NK and KM performed and analyzed the experiments; and JvO, HR, MB and MOH supervised the study. All authors contributed to the preparation of the manuscript.

1. Harper JW, Elledge SJ. The DNA damage response: ten years after. *Mol Cell* 2007; **28**: 739–745.
2. Shiloh Y. ATM and related protein kinases: safeguarding genome integrity. *Nate Rev Cancer* 2003; **3**: 155–168.
3. Bonner WM, Redon CE, Dickey JS, Nakamura AJ, Sedelnikova OA, Solier S *et al.* GammaH2AX and cancer. *Nat Rev Cancer* 2008; **8**: 957–967.
4. Surova O, Zhivotovsky B. Various modes of cell death induced by DNA damage. *Oncogene* 2012; E-pub ahead of print; doi: 10.1038/onc.2012.556.
5. Roos WP, Kaina B. DNA damage-induced cell death by apoptosis. *Trends Mol Med* 2006; **12**: 440–450.
6. Sabin RJ, Anderson RM. Cellular senescence – its role in cancer and the response to ionizing radiation. *Genome Integr* 2011; **2**: 7.
7. Bennetzen M, Larsen D, Bunkenborg J, Bartek J, Lukas J, Andersen J. Site-specific phosphorylation dynamics of the nuclear proteome during the DNA damage response. *Mol Cell Proteomics* 2010; **9**: 1314–1323.
8. Bensimon A, Schmidt A, Ziv Y, Elkon R, Wang SY, Chen DJ *et al.* ATM-dependent and -independent dynamics of the nuclear phosphoproteome after DNA damage. *Sci Signal* 2010; **3**: rs3.
9. Beli P, Lukashchuk N, Wagner SA, Weinert BT, Olsen JV, Baskcomb L *et al.* Proteomic investigations reveal a role for RNA processing factor THRAP3 in the dna damage response. *Mol Cell* 2012; **46**: 212–225.
10. Lee MJ, Ye AS, Gardino AK, Heijink AM, Sorger PK, MacBeath G *et al.* Sequential application of anticancer drugs enhances cell death by rewiring apoptotic signaling networks. *Cell* 2012; **149**: 780–794.
11. Tentner AR, Lee MJ, Ostheimer GJ, Samson LD, Lauffenburger DA, Yaffe MB. Combined experimental and computational analysis of DNA damage signaling reveals context-dependent roles for Erk in apoptosis and G1/S arrest after genotoxic stress. *Mol Syst Biol* 2012; **8**: 568.
12. van Oostrum J, Voshol H. Antibody-based proteomics to study cellular signalling networks. *Eur Pharmaceut Rev* 2008; **2**: 31–35.
13. Paweletz CP, Charboneau L, Bichsel VE, Simone NL, Chen T, Gillespie JW *et al.* Reverse phase protein microarrays which capture disease progression show activation of pro-survival pathways at the cancer invasion front. *Oncogene* 2001; **20**: 1981–1989.
14. Nishizuka S, Ramalingam S, Spurrier B, Washburn FL, Krishna R, Honkanen P *et al.* Quantitative protein network monitoring in response to DNA damage. *J Proteome Res* 2008; **7**: 803–808.
15. Hudson ME, Pozdnyakova I, Haines K, Mor G, Snyder M. Identification of differentially expressed proteins in ovarian cancer using high-density protein microarrays. *Proc Natl Acad Sci USA* 2007; **104**: 17494–17499.
16. Kuhne M, Riballo E, Rief N, Rothkamm K, Jeggo PA, Lobrich M. A double-strand break repair defect in ATM-deficient cells contributes to radiosensitivity. *Cancer Res* 2004; **64**: 500–508.
17. Lobrich M, Shibata A, Beucher A, Fisher A, Ensminger M, Goodarzi AA *et al.* gammaH2AX foci analysis for monitoring DNA double-strand break repair: strengths, limitations and optimization. *Cell Cycle* 2010; **9**: 662–669.
18. Yoshida K. Role for PKCδ on apoptosis in the DNA damage response. In: Chen CC (eds). *Selected Tpics in DNA Repair*. InTech: San Diego, USA, 2011. pp 293–304.
19. Newton AC. Protein kinase C: poised to signal. *Am J Physiol Endocrinol Metab* 2010; **298**: E395–E402.
20. Jackson DN, Foster DA. The enigmatic protein kinase Cdelta: complex roles in cell proliferation and survival. *FASEB J* 2004; **18**: 627–636.
21. Kosar M, Bartkova J, Hubackova S, Hodny Z, Lukas J, Bartek J. Senescence-associated heterochromatin foci are dispensable for cellular senescence, occur in a cell type- and insult-dependent manner and follow expression of p16(ink4a). *Cell Cycle* 2011; **10**: 457–468.
22. Cosentino C, Grieco D, Costanzo V. ATM activates the pentose phosphate pathway promoting anti-oxidant defence and DNA repair. *EMBO J* 2011; **30**: 546–555.
23. Meek DW. Tumour suppression by p53: a role for the DNA damage response? *Nat Rev Cancer* 2009; **9**: 714–723.
24. Lavin MF, Gueven N. The complexity of p53 stabilization and activation. *Cell Death Differ* 2006; **13**: 941–950.
25. Parekh DB, Ziegler W, Parker PJ. Multiple pathways control protein kinase C phosphorylation. *EMBO J* 2000; **19**: 496–503.
26. Lonze BE, Riccio A, Cohen S, Ginty DD. Apoptosis, axonal growth defects, and degeneration of peripheral neurons in mice lacking CREB. *Neuron* 2002; **34**: 371–385.
27. Datta SR, Dudek H, Tao X, Masters S, Fu H, Gotoh Y *et al.* Akt phosphorylation of BAD couples survival signals to the cell-intrinsic death machinery. *Cell* 1997; **91**: 231–241.
28. Adams JM, Cory S. The Bcl-2 apoptotic switch in cancer development and therapy. *Oncogene* 2007; **26**: 1324–1337.
29. Vogler M, Dinsdale D, Dyer MJ, Cohen GM. Bcl-2 inhibitors: small molecules with a big impact on cancer therapy. *Cell Death Differ* 2009; **16**: 360–367.
30. Lawless C, Wang C, Jurk D, Merz A, Zglinicki T, Passos JF. Quantitative assessment of markers for cell senescence. *Exp Gerontol* 2010; **45**: 772–778.
31. Torudd J, Protopopova M, Sarimov R, Nygren J, Eriksson S, Markova E *et al.* Dose–response for radiation-induced apoptosis, residual 53BP1 foci and DNA-loop relaxation in human lymphocytes. *Int J Radiat Biol* 2005; **81**: 125–138.
32. Meyn RE, Munshi A, Haymach JV, Milas L, Ang KK. Receptor signaling as a regulatory mechanism of DNA repair. *Radiother Oncol* 2009; **92**: 316–322.
33. Bulavin DV, Higashimoto Y, Popoff IJ, Gaarde WA, Basrur V, Potapova O *et al.* Initiation of a G2/M checkpoint after ultraviolet radiation requires p38 kinase. *Nature* 2001; **411**: 102–107.
34. Manke IA, Nguyen A, Lim D, Stewart MQ, Elia AE, Yaffe MB. MAPKAP kinase-2 is a cell cycle checkpoint kinase that regulates the G2/M transition and S phase progression in response to UV irradiation. *Mol Cell* 2005; **17**: 37–48.
35. Martelli AM, Evangelisti C, Nyakern M, Manzoli FA. Nuclear protein kinase C. *Biochim Biophys Acta* 2006; **1761**: 542–551.
36. Xue Y, Ren J, Gao X, Jin C, Wen L, Yao X. GPS 2.0, a tool to predict kinase-specific phosphorylation sites in hierarchy. *Mol Cell Proteomics* 2008; **7**: 1598–1608.
37. Yoshida K. Protein kinase C, p53, and DNA damage. In: Kazanietz MG (eds). *Protein Kinase C in Cancer Signaling and Therapy*. Springer: Berlin, 2010. pp 253–265.
38. Yoshida K, Miki Y, Kufe D. Activation of SAPK/JNK signaling by protein kinase Cdelta in response to DNA damage. *J Biol Chem* 2002; **277**: 48372–48378.
39. Basu A, Pal D. Two faces of protein kinase Cdelta: the contrasting roles of PKCdelta in cell survival and cell death. *Scientific World J* 2010; **10**: 2272–2284.
40. Schmidt-Ullrich RK, Dent P, Grant S, Mikkelsen RB, Valerie K. Signal transduction and cellular radiation responses. *Radiat Res* 2000; **153**: 245–257.
41. Basker R, Balajee AS, Geard CR, Hande MP. Isoform-specific activation of protein kinase c in irradiated human fibroblasts and their bystander cells. *Int J Biochem Cell Biol* 2008; **40**: 125–134.
42. Jacobs JP, Jones CM, Baille JP. Characteristics of a human diploid cell designated MRC-5. *Nature* 1970; **227**: 168–170.
43. Nichols WW, Murphy DG, Cristofalo VJ, Toji LH, Greene AE, Dwight SA. Characterization of a new human diploid cell strain, IMR-90. *Science* 1977; **196**: 60–63.
44. Franken NA, Rodermond HM, Stap J, Haveman J, van Bree C. Clonogenic assay of cells *in vitro*. *Nat Protoc* 2006; **1**: 2315–2319.
45. Dimri GP, Lee X, Basile G, Acosta M, Scott G, Roskelley C *et al.* A biomarker that identifies senescent human cells in culture and in aging skin *in vivo*. *Proc Natl Acad Sci USA* 1995; **92**: 9363–9367.
46. Pawlak M, Schick E, Bopp MA, Schneider MJ, Oroszlan P, Ehrat M. Zeptosens' protein microarrays: a novel high performance microarray platform for low abundance protein analysis. *Proteomics* 2002; **2**: 383–393.
47. Voshol H, Ehrat M, Traenkle J, Bertrand E, van Oostrum J. Antibody-based proteomics: analysis of signaling networks using reverse protein arrays. *FEBS J* 2009; **276**: 6871–6879.
48. Bevington PR. *Data Reduction and Error Analysis for the Physical Sciences*. 3rd edn McGraw-Hill: New York, NY, 2002. p 352.
49. Saeed AI, Sharov V, White J, Li J, Liang W, Bhagabati N *et al.* TM4: a free, open-source system for microarray data management and analysis. *Biotechniques* 2003; **34**: 374–378.
50. Zar JH. *Biostatistical Analysis*. 5th edn Prentice-Hall: Upper Saddle River, NJ, 2009. p 960.
51. Herrero-Yraola A, Bakhit SM, Franke P, Weise C, Schweiger M, Jorcke D *et al.* Regulation of glutamate dehydrogenase by reversible ADP-ribosylation in mitochondria. *EMBO J* 2001; **20**: 2404–2412.
52. Schaefer CF, Anthony K, Krupa S, Buchoff J, Day M, Hannay T *et al.* PID: the Pathway Interaction Database. *Nucleic Acids Res* 2009; **37**: D674–D679.
53. Kanehisa M, Goto S, Furumichi M, Tanabe M, Hirakawa M. KEGG for representation and analysis of molecular networks involving diseases and drugs. *Nucleic Acids Res* 2010; **38**: D355–D360.
54. Ihaka R, Gentleman RR. A language for data analysis and graphics. *J Comput Graph Stat* 1996; **5**: 299–314.
55. Szklarczyk D, Franceschini A, Kuhn M, Simonovic M, Roth A, Minguez P *et al.* The STRING database in 2011: functional interaction networks of proteins, globally integrated and scored. *Nucleic Acids Res* 2011; **39**: D561–D568.
56. Shannon P, Markiel A, Ozier O, Baliga NS, Wang JT, Ramage D *et al.* Cytoscape: a software environment for integrated models of biomolecular interaction networks. *Genome Res* 2003; **13**: 2498–2504.
57. Schneider CA, Rasband WS, Eliceiri KW. NIH Image to ImageJ: 25 years of image analysis. *Nat Methods* 2012; **9**: 671–675.
58. Riccardi C, Nicoletti I. Analysis of apoptosis by propidium iodide staining and flow cytometry. *Nat Protoc* 2006; **1**: 1458–1461.

Supplementary Information accompanies the paper on Cell Death and Disease website (http://www.nature.com/cddis)

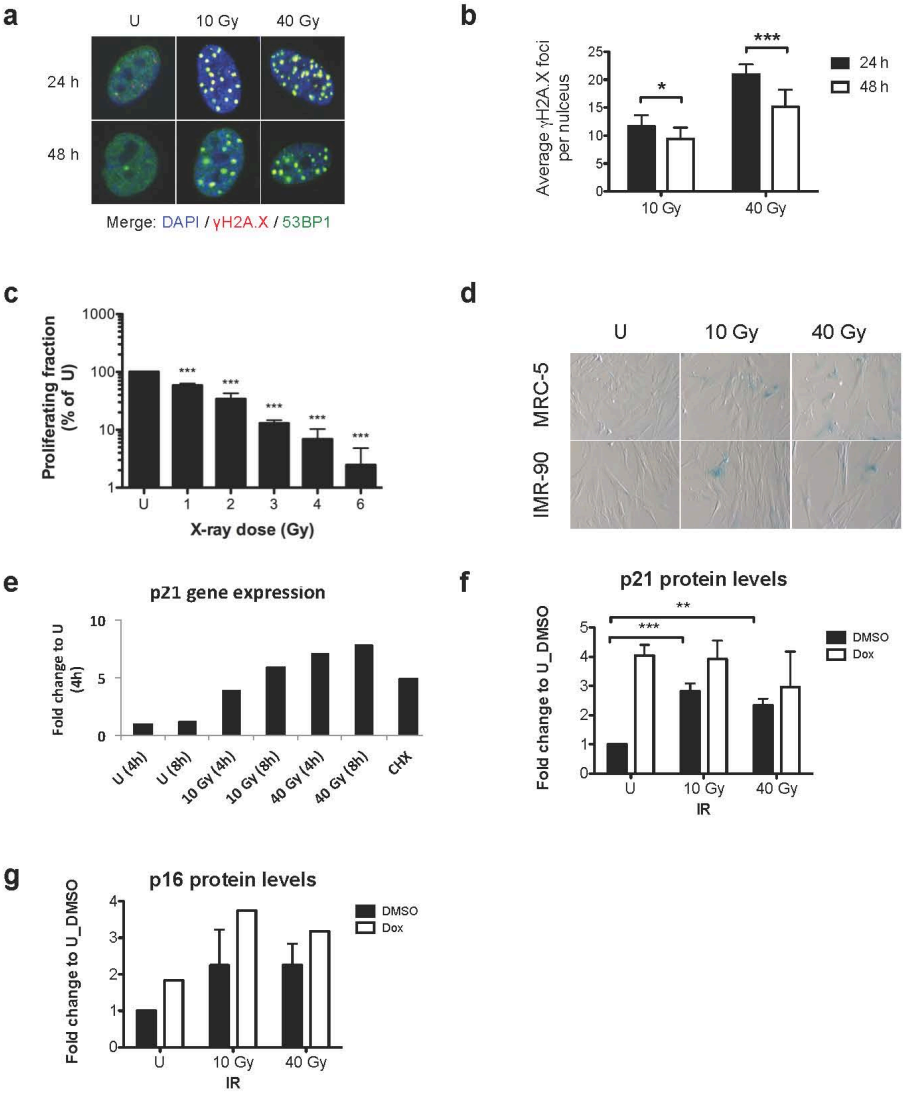

Figure S1. Irradiation increases senescence in response to 10 Gy or 40 Gy X-rays in NHFs. (a) Immunofluorescence staining of irradiated MRC-5 cells and of untreated control cells after 24 h and 48 h of recovery. Repair efficiency was determined using double staining with anti-γH2AX (Cy3) and 53BP1 (Alexa Fluor 488), which are recruited to particular foci (co-localization), marking sites of DNA double strand breaks. **(b)** Quantification of (a). The average number of γH2AX foci per cell was quantified with the spot detection function of Imaris (Bitplane) and identical image acquisition and foci detection parameters (n > 100 cell nuclei quantified per condition, n=5). **(c)** Colony forming assay of MRC-5 cells irradiated with X-ray doses of 1-6 Gy or left untreated (U) and recovered for 10 days (n=3). **(d)** SA-β-Gal staining of irradiated MRC-5 or IMR-90 after 72 h IR recovery with untreated (U) as control. **(e)** Gene expression analysis of senescence marker (p21) in MRC-5 in response to irradiation following 4-8 h IR recovery or cyclohexamide (CHX, 200 µM for 16 h). Quantification of WB analysis in IMR-90 of p21 **(f)** and p16 **(g)** protein level changes upon IR following 48 h recovery. Doxorubicin (0.5 µg/ml, 48 h) was used as positive control for induction of DNA damage (n=2-3). Statistical analysis was performed by Student's t-test, * p<0.05, ** p<0.01, *** p<0.001.

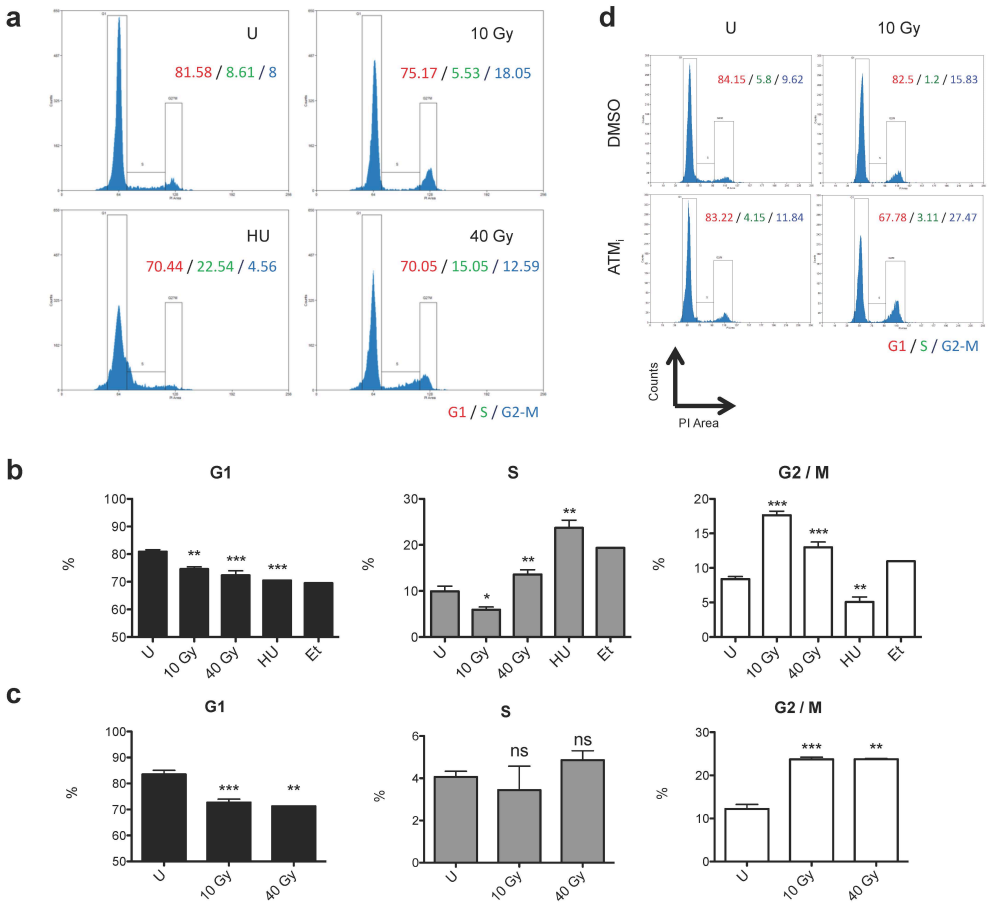

Figure S2. Irradiation increases the the G2/M cell cycle population 24-48 h after IR recovery in NHFs (a) Cell cycle analysis of irradiated MRC-5 by FACS analysis 24 h after irradiation (representative). To induce early S-phase arrest 2 mM hydroxyurea (HU) were incubated for 24 h prior to FACS analysis. **(b)** Quantification of cell cycle population changes in either G1, S or G2 / M 24 h after IR recovery or treatment with either hydroxyurea (2 mM) or etoposide (50 µM) (n=2-4). **(c)** Quantification of cell cycle population changes in either G1, S or G2 / M 48 h after IR recovery or treatment with either hydroxyurea (2 mM) or etoposide (50 µM) (n=2-4). **(d)** ATM-dependent cell cycle analysis in MRC-5. Cells were pretreated for 2h with ATM-specific inhibitor (KU-55933, 10 µM) prior to IR and FACS analysis 24 h after irradiation. Statistical analysis was performed by Student's t-test, * p<0.05, ** p<0.01, *** p<0.001.

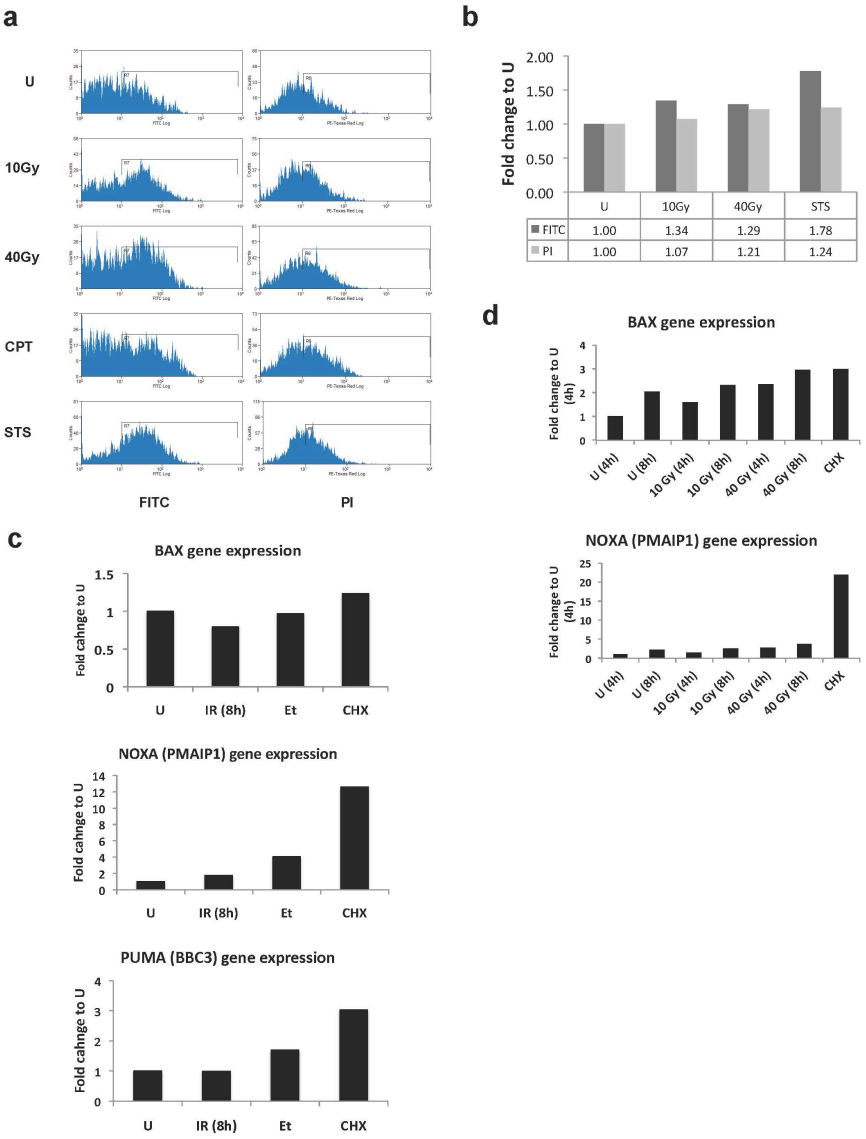

Figure S3. Irradiation does not induce early apoptosis in response to 10 Gy or 40 Gy X-rays in MRC-5. (a) Annexin V staining of MRC-5 irradiated (recovered for 8 h) or treated with camptothecin (CPT, 4 μM for 8 h) or staurosporin (STS, 1 μM, 2 h), prior to Annexin V staining and FACS analysis. **(b)** Quantification of Annexin V positive population (FITC) corresponding to early apoptosis and propidium iodide positive population (PI) corresponding to necrosis from (a). **(c)** Gene expression analysis of pro-apoptotic genes in response to irradiation (10 Gy, 8 h recovery), etoposide (Et, 50 μM for 8 h) or cyclohexamide (CHX, 200 μM for 16 h) with untreated (U) as control. **(d)** Gene expression analysis of pro-apoptotic genes in response to irradiation (4-8 h recovery) or cyclohexamide (CHX, 200 μM for 16 h) with untreated as control.

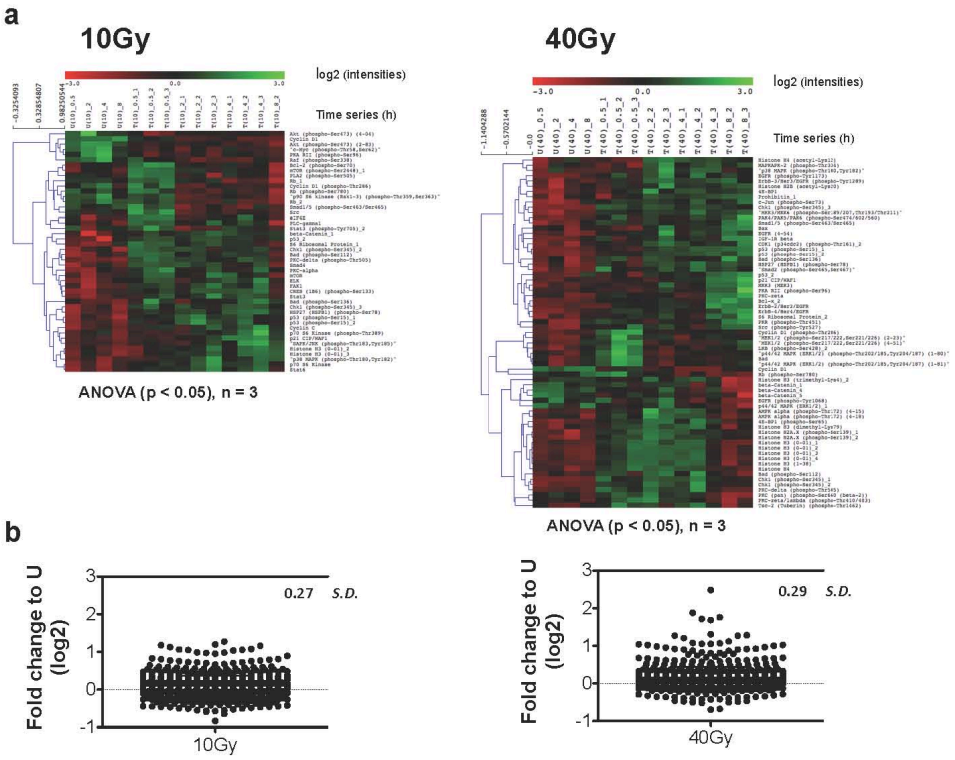

Figure S5. Significance analysis of IR-dependent proteome changes. (a) Relative fluorescence intensities (RFIs) (log2) for group 1 (untreated (U)_0.5 h, 2 h, 4 h, and 8 h), group 2 (biological triplicates of 10, T(10) or 40 Gy, T(40)_0.5 h), group 3 (biological triplicates of 10, T(10) or 40 Gy, T(40)_2 h), group 4 (biological triplicates of 10, T(10) or 40 Gy, T(40)_4 h) and group 5 (biological triplicates of 10, T(10) or 40 Gy, T(40)_8 h) were compared using F-statistics with $p < 0.05$. **(b)** Means of RFIs (replicates) were log2 transformed and fold changes (to U, group 1) were plotted individually for 10 and 40 Gy to determine the standard deviation, resulting in 0.27 S.D for 10 Gy and 0.29 for 40 Gy.

	Early induction	Late induction	Early reduction	Late reduction
10 Gy	Bad (phospho-S112)	Bad (phospho-S136)	Akt (phospho-S473) (2-83, 4-04)	Raf (phospho-S338)
	Bcl-2 (phospho-S70)	beta-Catenin_1/3/4/5	c-Myc (phospho-T58, S62)	Rb (phospho-S780)
	c-Jun (phospho-S70)	Caspase 9	Cyclin D1	Rb_1/2
	Chk1 (phospho-S345)_2/3	Cyclin C	PKA RII (phospho-S96)	
	CREB (phospho-S133)	H2A.X (phospho-S139)		
	eIF4E	H3 (0-01)_2/3		
	ELK	p21		
	FAK1	p38 (phospho-T180, Y182)		
	HSP27 (phospho-S78)	p53 (phospho-S15)_1/2		
	IRS-1	p53_1		
	mTOR	p70S6K		
	mTOR (phospho-S2448)_1	p70S6K (phospho-T389)		
	p53_2	JNK (phospho-T183, Y185)		
	PKC-alpha	Stat3		
	PKC-delta (phospho-T505)			
	PTEN			
	PLA2 (phospho-S505)			
	PLC-gamma1			
	rpS6 (phospho-S235, S236)			
	rpS6			
	Smad4			
	Src			
	Stat5			
	Stat6			
40 Gy	4E-BP1 (phospho-S65)	4E-BP1	beta-Catenin_1/4/5	H3 (trimethyl-K4)_2
	Bad	AMPK alpha (phospho-T172)_(4-15/18)	Cyclin D1	ERK1/2_1
	Chk1 (phospho-S345)_1/3	Bad (phospho-S112)	EGFR (phospho-Y1068)	
	Cyclin D1 (phospho-T286)	Bad (phospho-S136)		
	ErbB-4/Her-4	Bax		
	GSK-3-beta (phospho-S9)	Bcl-x_2		
	H2A.X (phospho-S139)_1/2	Caspase 7 (cleaved-Asp198)		
	H3	Caspase 9 (cleaved-Asp330)		
	H4	c-Jun (phospho-S73)		
	LKB (phospho-S428)	CDK1 (phospho-T161)_2		
	MEK1/2 (phospho-S217/222, S221/226) (2-23, 4-51)	Chk1 (phospho-S345)_2		
	MKK3/6 (phospho-S189/207, T193/211)	EGFR (4-54)		
	p44/42 (ERK1/2) (phospho-T202/185, Y204/187)	EGFR (phospho-Y1173)		
	p53 (phospho-S15)_2	eIF4E		
	PKC-delta (phospho-T505)	ErbB-2/Her-2		
	PKC-zeta/lambda (phospho-T410/403)	ErbB-3/Her-3		
	PKC-zeta	H3 (dimethyl-K79)		
	Smad2 (phospho-S465/467)	H4 (acetyl-K12)		
	Src (phospho-Y527)	Hsp27 (phospho-S78)		
		IGF-1R beta		
		MAPKAPK-2 (phospho-T334)		
		MKK3		
		mTOR (phospho-S2448)_2		
		p21		
		p38 (phospho-T180, Y182)		
		p53 (phospho-S15)_1		
		p53_2		
		PAK4/5/6 (phospho-S474, S602, S560)		
		PKA RII (phospho-S96)		
		PKR (phospho-T451)		
		Prohibitin_1		
		rpS6_2		

Figure S7. Significant proteome changes in response to 10 and 40 Gy IR. (Student's t-test, n=3, * = $p < 0.05$; ** = $p < 0.01$; *** = $p < 0.001$) Early induction / reduction, if 0.5 h time point significantly changed by at least $p < 0.05$; late induction or reduction, if one of the later time points (2-8 h) significantly changed by at least $p < 0.05$. Significant changes from Fig. S6, which are also represented in the heat map of Fig. 2b-c (ANOVA, $p < 0.05$, SD cut off = 1.5) are highlighted in green.

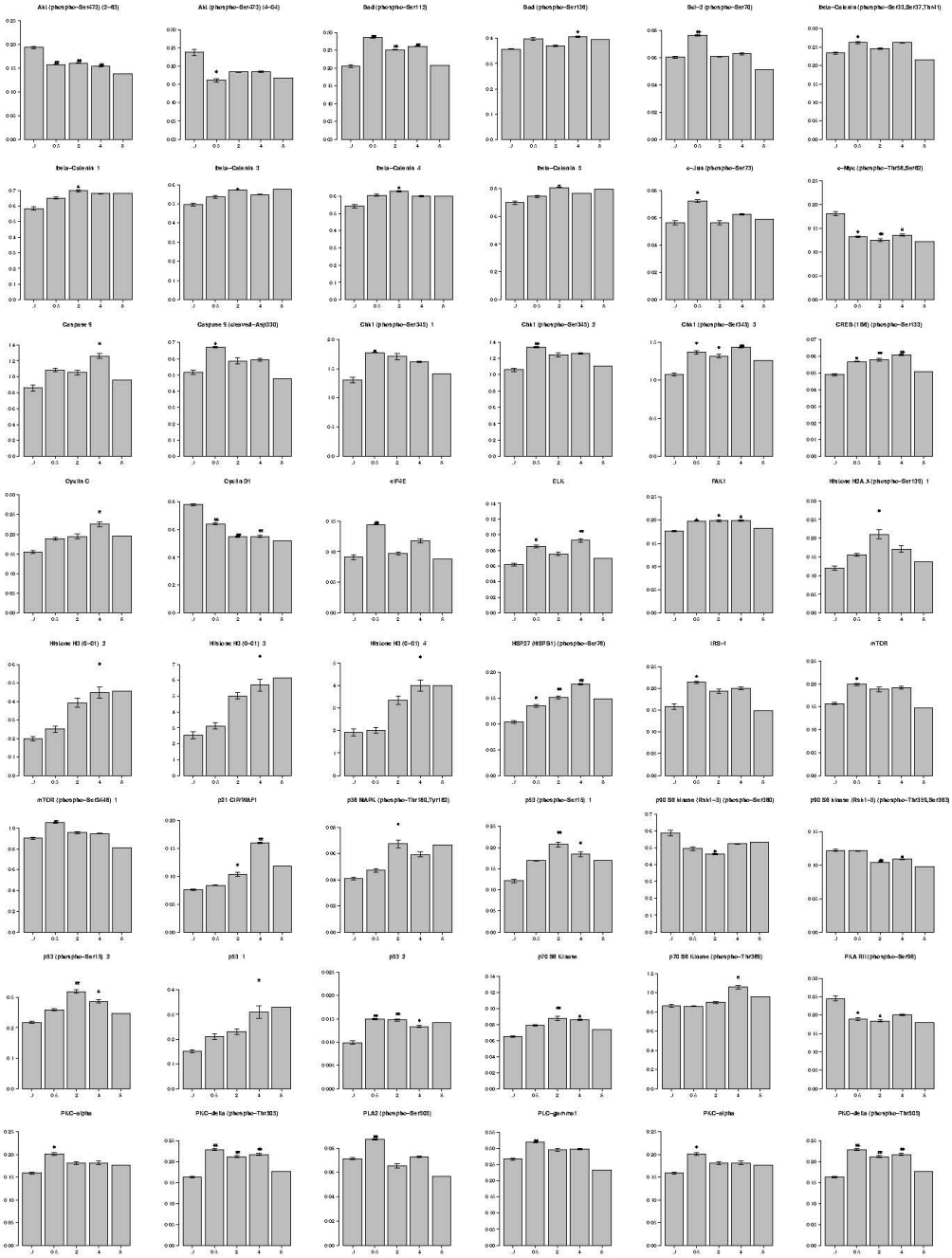
Akt (phospho-Ser473) (2-63)
Akt (phospho-Ser473) (41-64)
Bad (phospho-Ser112)
Bad (phospho-Ser136)
Bcl-2 (phospho-Ser70)
beta-Catenin (phospho-Ser33,Ser37,Thr41)
beta-Catenin 1
beta-Catenin 3
beta-Catenin 4
beta-Catenin 5
c-Jun (phospho-Ser73)
c-Myc (phospho-Thr58,Ser62)
Caspase 9
Caspase 9 (cleaved-Asp330)
Chk1 (phospho-Ser345) 1
Chk1 (phospho-Ser345) 2
Chk1 (phospho-Ser345) 3
CREB (1/66) (phospho-Ser133)
Cyclin C
Cyclin D1
eIF4E
ELK
FAK1
Histone H2A.X (phospho-Ser139) 1
Histone H3 (6-01) 2
Histone H3 (6-01) 3
Histone H3 (6-01) 4
HSP27 (HSP81) (phospho-Ser78)
IRS-1
mTOR
mTOR (phospho-Ser2448) 1
p21 CIP/WAF1
p38 MAPK (phospho-Thr180,Tyr182)
p53 (phospho-Ser15) 1
p90 S6 kinase (Rsk1-3) (phospho-Ser380)
p90 S6 kinase (Rsk1-3) (phospho-Thr359,Ser363)
p53 (phospho-Ser15) 2
p53 1
p53 2
p70 S6 Kinase
p70 S6 Kinase (phospho-Thr389)
PKA RII (phospho-Ser96)
PKC-alpha
PKC-delta (phospho-Thr505)
PLA2 (phospho-Ser505)
PLC-gamma1
PKC-alpha
PKC-delta (phospho-Thr505)

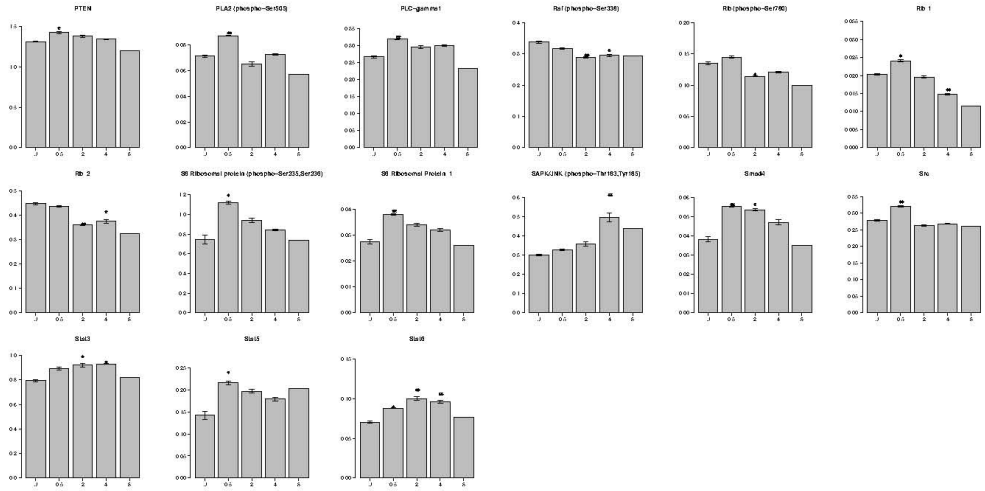

Figure S8. Significant proteome changes in response to 10Gy IR. Bar plots from Figure S7 (Student's t-test, n=3, * = $p < 0.05$; ** = $p < 0.01$; *** = $p < 0.001$).

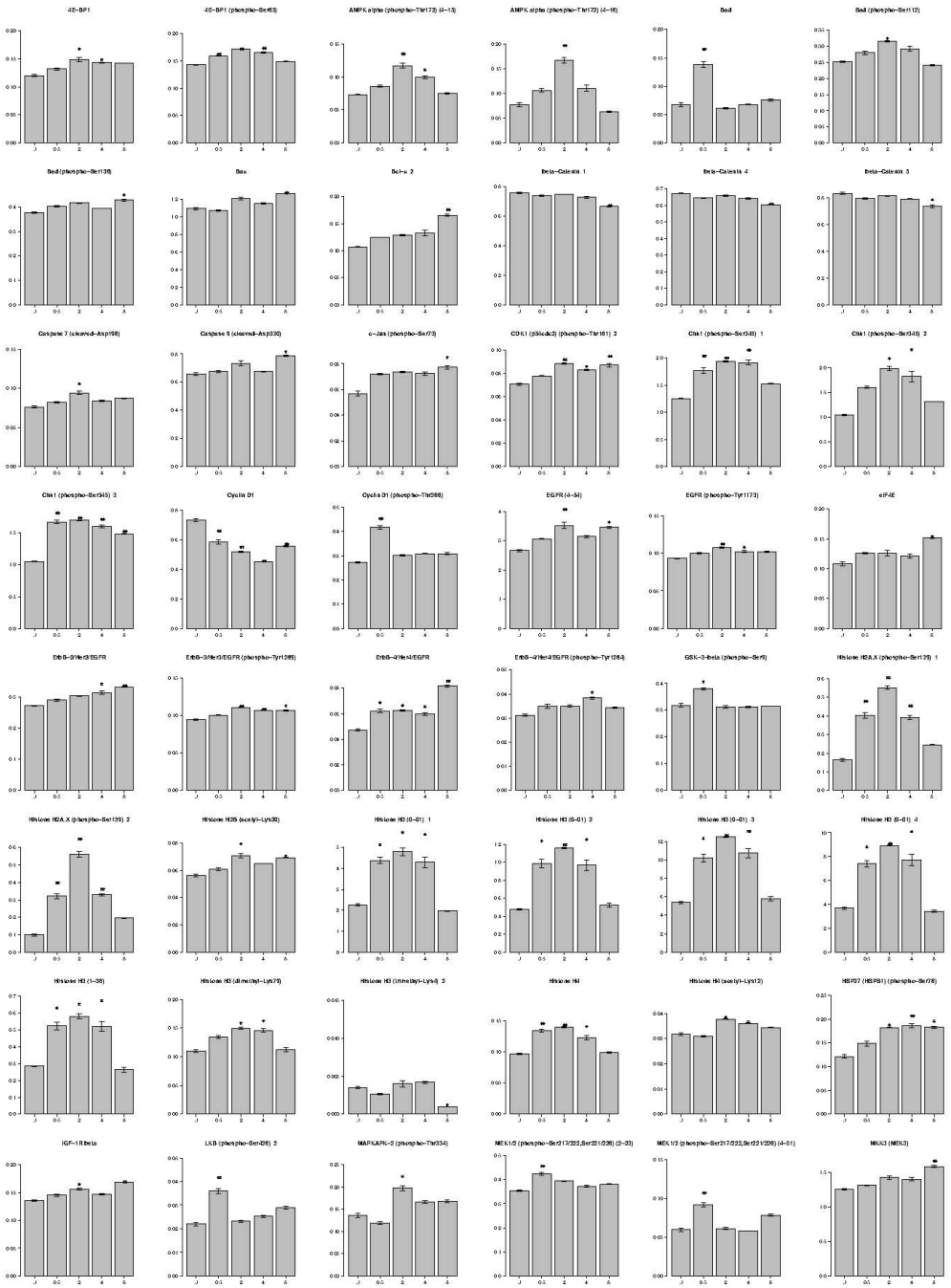

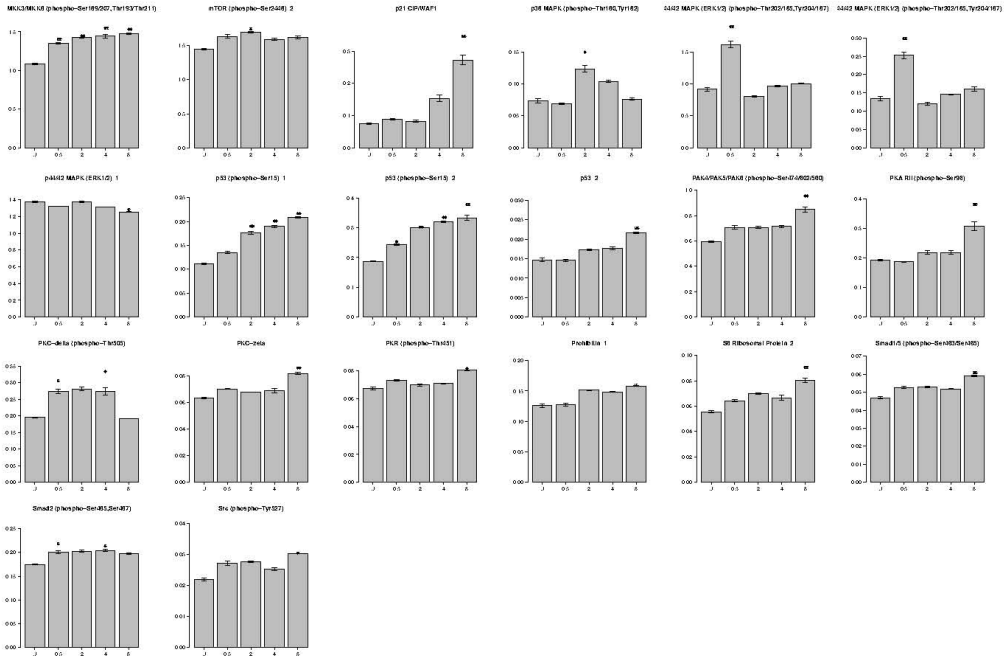

Figure S9. Significant proteome changes in response to 40Gy IR. Bar plots from Figure S7 (Student's t-test, n=3, * = p < 0.05; ** = p < 0.01; *** = p < 0.001).

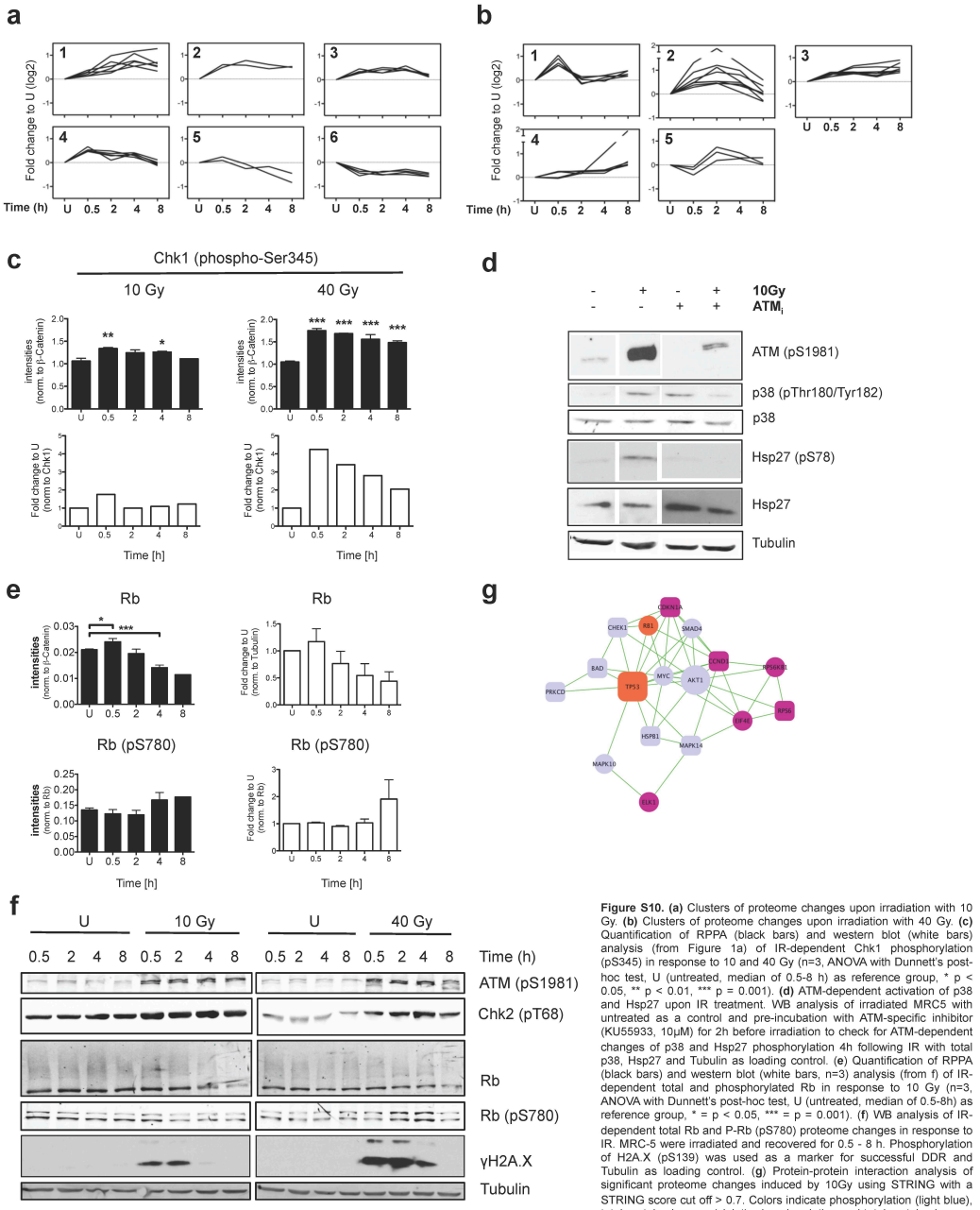

Figure S10. (a) Clusters of proteome changes upon irradiation with 10 Gy. **(b)** Clusters of proteome changes upon irradiation with 40 Gy. **(c)** Quantification of RPPA (black bars) and western blot (white bars) analysis (from Figure 1a) of IR-dependent Chk1 phosphorylation (pS345) in response to 10 and 40 Gy (n=3, ANOVA with Dunnett's post-hoc test, U (untreated, median of 0.5-8 h) as reference group, * $p < 0.05$, ** $p < 0.01$, *** $p = 0.001$). **(d)** ATM-dependent activation of p38 and Hsp27 upon IR treatment. WB analysis of irradiated MRC5 with untreated as a control and pre-incubation with ATM-specific inhibitor (KU55933, 10μM) for 2h before irradiation to check for ATM-dependent changes of p38 and Hsp27 phosphorylation 4h following IR with total p38, Hsp27 and Tubulin as loading control. (**e**) Quantification of RPPA (black bars) and western blot (white bars, n=3) analysis (from f) of IR-dependent total and phosphorylated Rb in response to 10 Gy (n=3, ANOVA with Dunnett's post-hoc test, U (untreated, median of 0.5-8h) as reference group, * = $p < 0.05$, *** = $p = 0.001$). (**f**) WB analysis of IR-dependent total Rb and P-Rb (pS780) proteome changes in response to IR. MRC-5 were irradiated and recovered for 0.5 - 8 h. Phosphorylation of H2A.X (pS139) was used as a marker for successful DDR and Tubulin as loading control. (**g**) Protein-protein interaction analysis of significant proteome changes induced by 10Gy using STRING with a STRING score cut off > 0.7. Colors indicate phosphorylation (light blue), total protein changes (violet), phosphorylation and total protein changes (orange). Circle represent unique changes and squares overlapping changes. Large symbols indicate proteins that interact with more than 14 members.

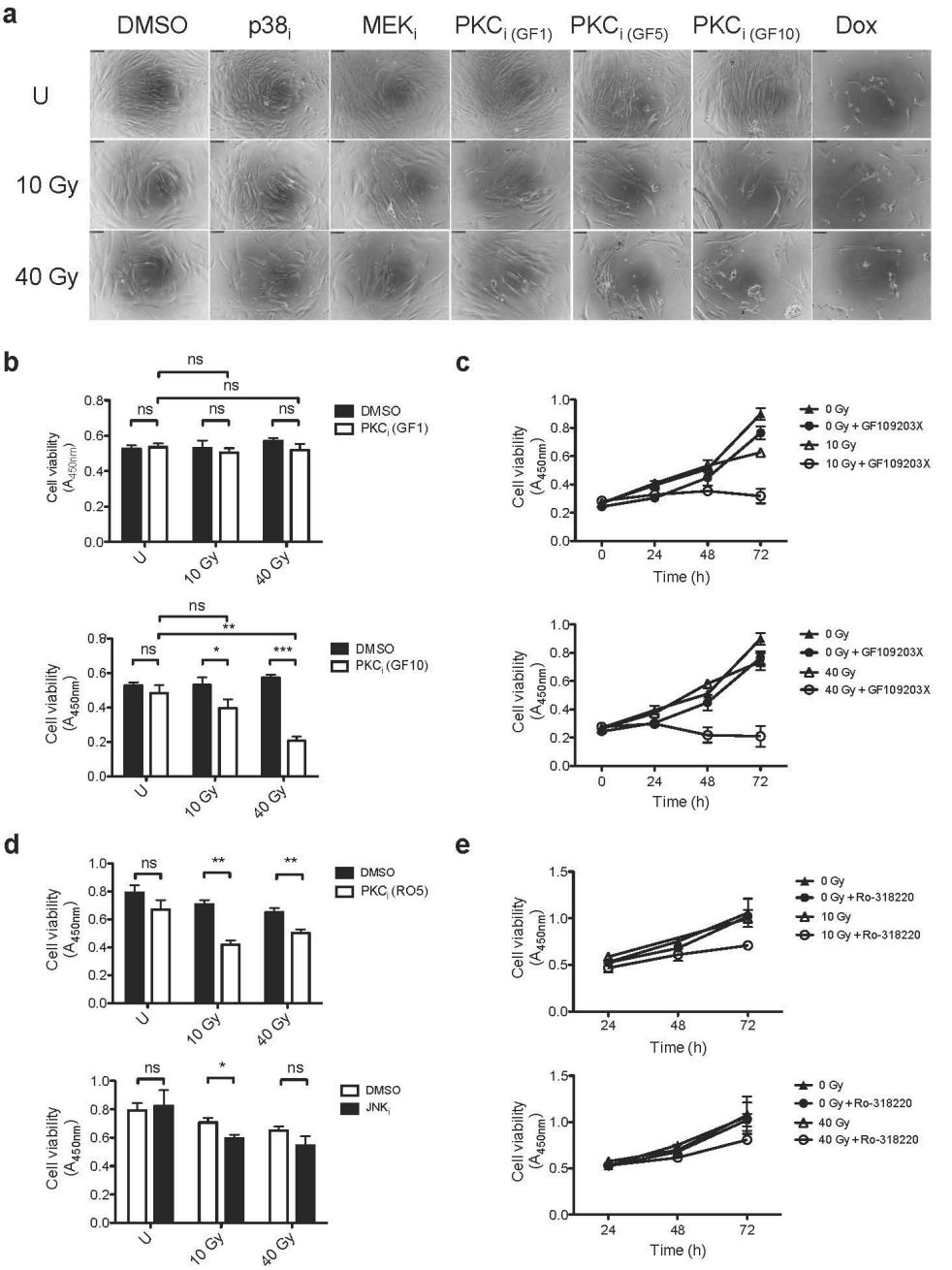

Figure S11. Radiosensitization of MRC-5 by pharmacological inhibition of PKC in response to IR. (a) PKC inhibition sensitizes MRC-5 to 10 and 40 Gy after 48 h. Phase contrast images of samples from (Figure 4), taken after 48 h recovery from IR. **(b)** Cell viability assay (WST-1) of MRC-5 (n=3) pretreated with PKC inhibitor (GF109203X, 1 or 10 µM) for 2 h before IR and recovery for the indicated time points (n=3). **(c)** Quantification of radiosensitization of MRC-5 by PKC inhibition (GF109203X, 10 µM) upon 10 and 40 Gy from (a). **(d)** Cell viability assay (WST-1) of MRC-5 (n=3) pretreated with PKC inhibitor (Ro-318220, 5 µM) or JNK inhibitor (SP600125, 10 µM) for 2 h before IR and recovery for the indicated time points (n=3). **(e)** Quantification of radiosensitization of MRC-5 by PKC inhibition (Ro-318220, 5 µM) upon 10 and 40 Gy from (d). Statistical analysis was performed by Student's t-test, * p<0.05, ** p<0.01, *** p<0.001, ns = not significant.

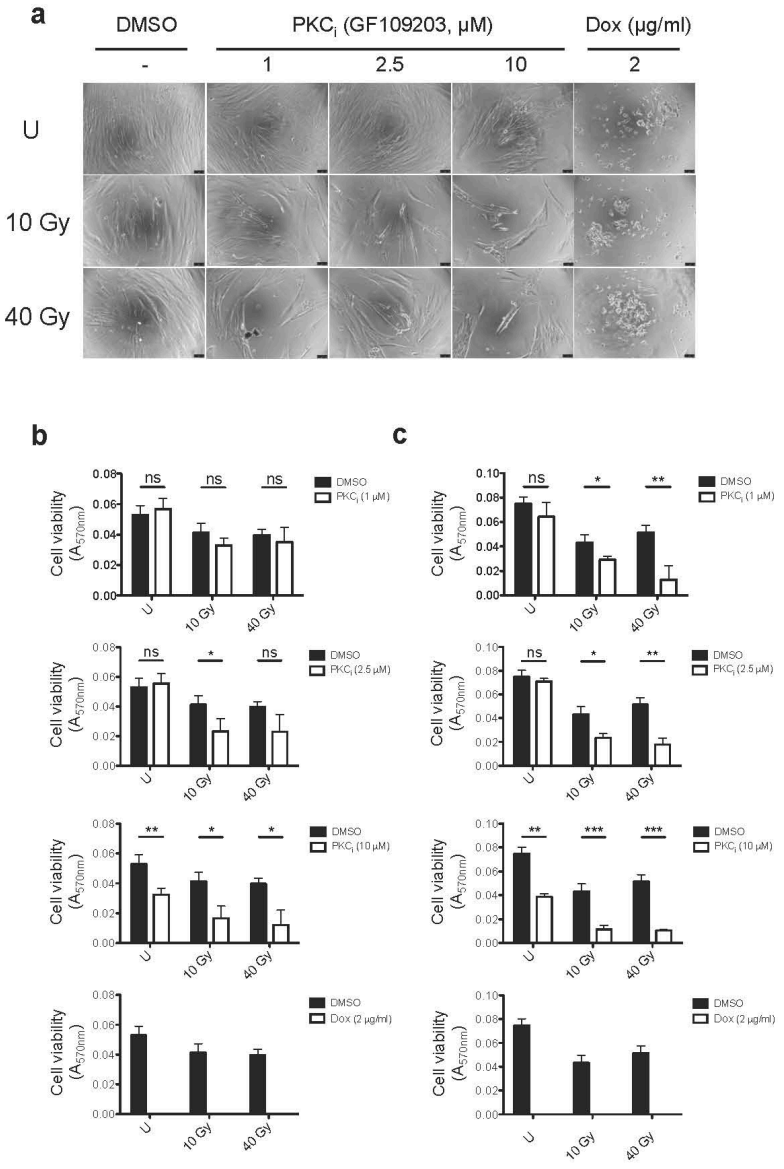

Figure S12. Radiosensitization of IMR-90 by pharmacological inhibition of PKC in response to IR. PKC inhibition sensitizes IMR-90 to 10 and 40 Gy after 48-72 h. **(a)** Phase contrast images of samples from (c), taken after 72 h recovery from IR. Cell viability assay (WST-1) of IMR-90 (n=3) pretreated with PKC inhibitor (GF109203X, 1, 2.5 and 10 µM) for 2 h before IR and recovery for 48 h **(b)** or 72 h **(c)** (n=3). Statistical analysis was performed by Student's t-test, * p<0.05, ** p<0.01, *** p<0.001), ns = not significant.

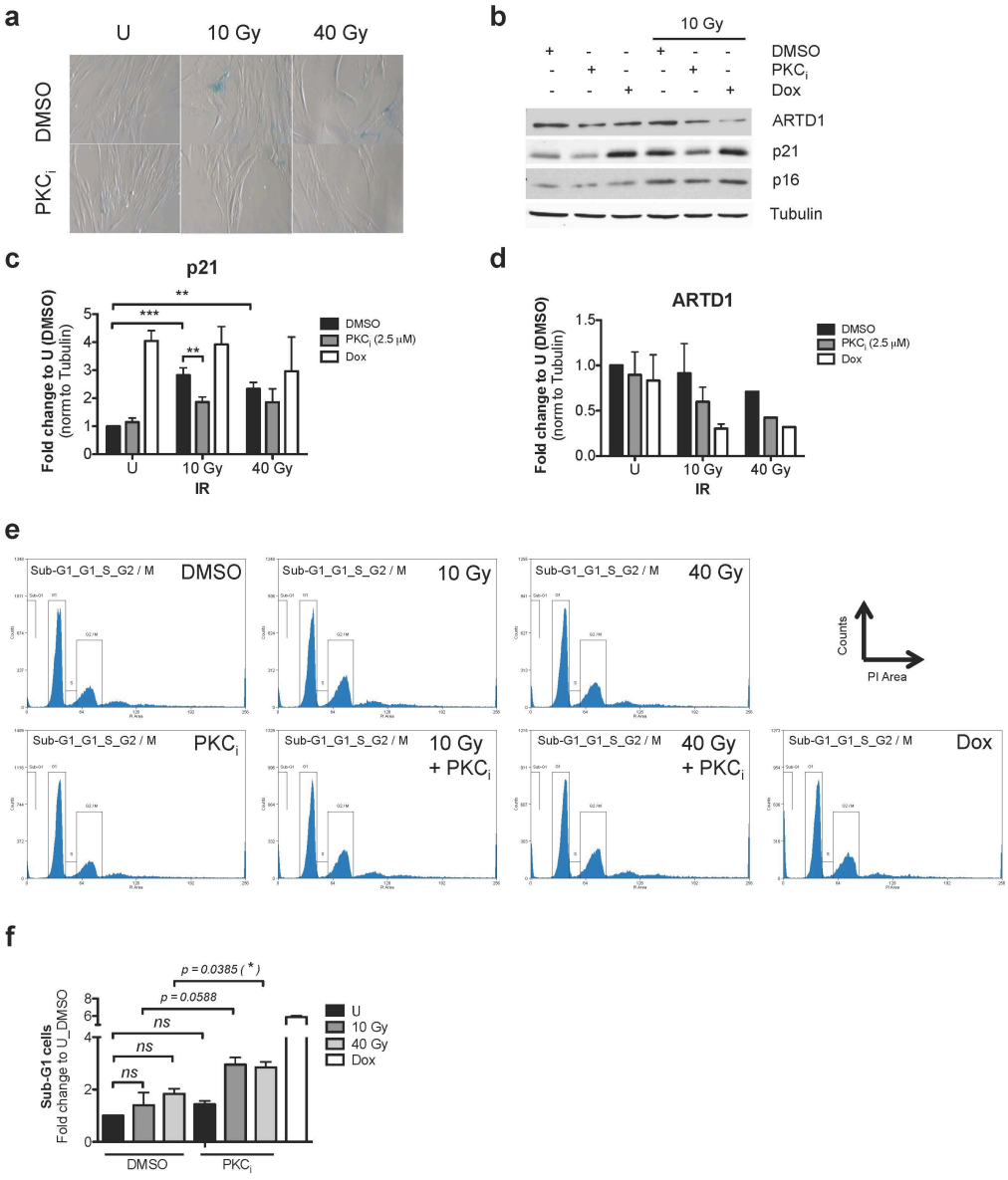

Figure S13. PKC inhibition reduces senescence and increases apoptosis in IMR-90 upon IR. (a) SA-β-Gal staining of irradiated IMR-90 in presence of PKC inhibitor (72 h recovery) with untreated (U) as control. **(b)** WB analysis of irradiated IMR-90 (48 h recovery) in presence of PKC inhibitor (GF109203X, 2.5 µM) or doxorubicin (0.5 µg/ml). Tubulin was used as loading control. Quantification of p21 protein **(c)** and ARTD1 levels **(d)** levels from (b) (n=2-3). **(e)** Sub-G1 peak analysis of irradiated IMR-90 (recovery for 48 h) in presence of PKC inhibitor (GF109203X, 2.5 µM) or DMSO as control. **(f)** Quantification from (e) (n=2). Statistical analysis was performed by Student's t-test, * p<0.05, ** p<0.01, *** p<0.001, ns = not significant.

3.1.2 Opposite regulation of ADP-ribosylation by PKC signaling: ARTD1 is activated by PKCα and inactivated by PKCδ

Opposite regulation of ADP-ribosylation by PKC signaling: ARTD1 is activated by PKCα and inactivated by PKCδ

Andrej Bluwstein[1,2], Nitin Kumar[3], Nicole Grosse[1], Jens Traenkle[4], Barbara van Loon[1], Michael Baudis[3], Michael O. Hottiger[1*]

Running title: PKCα is required for poly-ADP-ribose formation

[1]Institute of Veterinary Biochemistry and Molecular Biology, University of Zurich, Winterthurerstrasse 190, 8057 Zurich, Switzerland

[2]Cancer Biology PhD Program, Life Science Zurich Graduate School, University of Zurich,
Winterthurerstrasse 190, CH-8057 Zürich, Switzerland

[3]Institute for Molecular Life Science (IMLS) and Swiss Institute of Bioinformatics (SIB), University of Zurich, Winterthurerstrasse 190, Zurich, Switzerland

[4]Bayer Technology Services GmbH, Leverkusen, Germany

*Corresponding author: Email: hottiger@vetbio.uzh.ch

Abstract

ADP-ribosylation is a post-translational protein modification that consists of mono- and poly-ADP-ribose (PAR) molecules and which plays important functions in epigenetics, transcription and stress responses. Here, we aimed at identifying signaling pathways that are induced early upon the stimulation by oxidative stress (e.g., H_2O_2) and which regulate PAR formation. We performed a reverse phase protein array (RPPA) approach and in-depth kinetic analyses of key signaling components of the oxidative stress response. Even though H_2O_2 induces strong PAR formation within a few minutes, we identified positive and negative regulators of PAR formation. Functional analysis revealed that PKCδ acted as a negative modulator of ARTD1 activity, while calcium signaling and PKCα were required for H_2O_2-induced PAR formation. PKCα caused calcium-dependent DNA breaks, which are known to strongly activate PAR formation. These results implicate for the first time calcium- and PKCα-dependent induction of DNA lesions in PAR formation during the oxidative stress response.

Introduction

ADP-ribosylation is a post-translational protein modification that consists of mono- and poly-ADP-ribose (PAR) molecules that are covalently linked to specific residues of target proteins [1]. The linear or branched PAR polymer consists of 200-400 ADP-ribose moieties that are linked by O-glycosidic ribose-ribose 1'-2' bonds. These modifications are synthesized by a subfamily of ADP-ribosyltransferases (ARTs), which use NAD^+ as a substrate and belong to the ARTD (ADP-ribosyltransferase diphtheria toxin-like, originally PARP) family. In mammalians, the ARTD family is comprised of 18 proteins, which contain a catalytic ART domain conferring enzymatic activity [2]. The best-characterized ARTD family member is ARTD1 (originally PARP1), a 116 kDa nuclear enzyme consisting of an N-terminal DNA-binding domain (DBD), a central automodification domain (AMD), and a C-terminal catalytic domain (CAT) [3]. ARTD1 modifies itself *in cis* at the automodification domain [4] and other target proteins including histones, transcription factors and DNA-repair proteins, which points at an important function of ADP-ribosylation in epigenetics, transcriptional regulation and repair [5]. Indeed, ADP-ribosylation is implicated in the regulation of a plethora of cellular processes, biological phenomena and medical conditions [3,5,6].

ADP-ribosylation, in particular ARTD1, is strongly activated by oxidative stress [1]. The most frequent form of oxidative stress is exerted by reactive oxygen species (ROS), which originate from environmental sources (pollutants such as cigarette smoke, high doses of irradiation) as well as from endogenous oxygen metabolism (aerobic respiration in mitochondria, oxidases, cytochrome P450, NO synthases) [7]. ROS lead to the oxidation of organic macromolecules (e.g., proteins, lipids, DNA) and consecutively induce cytotoxicity in an uncontrollable manner. In the nucleus, ROS are thus believed to induce DNA damage and to expose DNA strand

breaks, which strongly stimulates the enzymatic activity of ARTD1. However, until now it is not clear whether ARTD1 is activated by DNA damage *in vivo* or if the stimulation of ADP-ribosylation in response to oxidative stress is the result of signaling events that are not directly linked to DNA damage.

ARTD1 has recently been termed a "cellular rheostat", because it integrates different types and levels of stress signals [3]. In response to mild or moderate stresses, it regulates transcription and DNA repair, while upon severe and sustained stress conditions, hyper-activation of ARTD1 leads to apoptosis or necrosis [8,9]. Interestingly, a series of studies showed ARTD1 automodification in the presence of specific DNA structures such as cruciform hairpins, indicating ARTD1 activation by higher-order DNA structures in a DNA damage-independent manner [10,11]. In line with these data, nucleosomes (intact DNA wrapped around core histones) were sufficient to induce ARTD1 activity and even to a stronger activation in comparison to activation by damaged DNA [12]. Moreover, ARTD1 activity could also be stimulated by cations (Mg^{2+}, Ca^{2+}), polyamines (spermine) and core histones (H1 and H3) alone or in combination, indicating DNA-independent mechanisms of ARTD1 activity *in vitro* [13]. Indeed, there is a growing body of evidence that indicates the involvement of intracellular signaling in the activation of ARTD1 in a DNA damage-independent manner [14].

Calcium signaling has been placed upstream of ARTD1 activity, but the exact mechanism of calcium-dependent regulation of ARTD1 activity is still unknown. ARTD1 activation was also observed as a consequence of PLC-IP3-dependent calcium mobilization in a DNA-independent manner [15], and the calcium/calmodulin-dependent kinase II (CaMKII) was identified as a positive regulator of ARTD1 activity in neurons [16,17]. Calcium-dependent stimulation of ARTD1 activity was also reported as a response to treatment with β-lapachone, which is an NQO1-dependent

ROS producer [18]. In contrast, other studies provide evidence for ARTD1-dependent calcium regulation in response to lethal hydrogen peroxide doses, thus placing calcium downstream of hydrogen peroxide induced ARTD1 activation [19,20].

Positive and direct regulation of ARTD1 activity was also described for the extracellular signal-regulated kinase (ERK) [21-23] as well as for c-Jun N-terminal kinase (JNK) [24], while opposing results for the involvement of protein kinase C (PKC) signaling in the regulation of ARTD1 have been obtained [25-28]. The PKC family of protein kinases is particularly interesting, because it comprises conventional, calcium-dependent enzymes, as well as novel and atypical kinases that act independent of calcium [29]. In mammalians, the PKC protein family is comprised of four conventional (PKCα, -βI/II and -γ), four novel (PKCδ, -ε, -η and -θ) and two atypical (PKCζ and -ι) isozymes [29]. Cellular signaling pathways thus have the potential to directly regulate ARTD1 activity by post-translational modification independent of DNA damage, even though the molecular mechanisms are still unknown. This is in contrast to the traditional view that considers ARTD1 as part of the DNA damage response, which is induced upon genotoxic or oxidative stress.

To resolve the conflicting information concerning PAR stimulating, the overall goal of this work was to identify cellular signaling pathways that are induced early upon the stimulation by oxidative stress (e.g., H_2O_2) and which regulate PAR formation. In order to address this question, we pursued a systemic reverse phase protein array (RPPA) approach and the in-depth molecular analysis of the key signaling components. Even though H_2O_2 induces strong PAR formation within a few minutes, our analysis identified both positive and negative regulators of PAR formation. Oxidative stress-induced PKCδ attenuated PAR levels, while calcium-dependent signaling mediated by CaMKIIδ and PKCα were required to stimulate PAR formation. Interestingly, our results suggest the calcium-dependent activation of

PKCα and the consecutive induction of DNA lesions as the mechanism, which stimulates PAR formation in response to oxidative stress. In addition to revealing an intricate and well-balanced interplay of counter-acting signaling pathways that fine-tune ARTD1 activity and PAR synthesis, these results for the first time directly implicate calcium- and PKCα-dependent DNA lesions in PAR formation and the response to oxidative stress.

Results

H_2O_2 treatment induces cytoplasmic kinases

To identify early H_2O_2-induced signaling events in protein extracts of MRC-5 primary human fibroblasts, which might regulate PAR formation, a proteomics screen using reverse phase protein arrays (RPPA) was performed at the 10 and 60 min time points after H_2O_2 treatment (0.5 and 2 mM) (Fig. 1a). These time-points were chosen because strong PAR formation is observed at the 10 min time-point, while no PAR is detectable at the 60 min time-point after H_2O_2 stimulation (Fig. 1b). Based on viability assays (24 h treatment), non-lethal (0.5 mM) and sub-lethal (2 mM) H_2O_2 doses were selected for further RPPA analysis (Fig. S1a). H_2O_2-induced PAR formation was completely inhibited by the PARP inhibitors ABT-888, Olaparib or PJ-34 as shown by immunofluorescence (IF) and western blotting (Fig. S1b and c). Significant protein changes were determined by statistical analysis using ANOVA ($p<0.05$, n=2) and untreated samples were used as a control group (Fig. 1c, S2 and S3a). The significantly changed proteins were clustered based on their temporal changes upon 0.5 or 2 mM H_2O_2 treatment using k-means clustering algorithm (Fig. 1d, S3b). Overall, the majority of significant protein reductions concerned total protein levels, while increases in response to H_2O_2 treatment were often observed for phosphorylation events (Fig. 1c, S3a). This could be explained by the H_2O_2-induced inhibition of translation [30], which causes a general reduction of the protein half-life. Interestingly, early activation clusters comprised kinases exclusively found in the cytoplasm that are known to be activated either directly by stress stimuli (p-p38, p-JNK) or by growth factor signals (ErbB-2, p-Akt). In addition, calcium signal transducers were found among the early-induced proteome changes (p-PKC, p-PLCγ, p-CaMKII, p-CREB, p-PLA2) (Fig. 1c-e, S3a-b). The majority of late activated signaling events included DNA damage response and cell cycle players such as p-

Aurora A, p-Chk1, p-Cyclin D, p-p53, p-p27 and gammaH2AX (Fig. 1e). However, the main hubs (Akt, p38, ERK2) in the protein-protein interaction network were rather cytoplasmic signaling components (except of p53) and that were mostly induced at the early time point, indicating cytoplasmic signaling events as the initial signaling events upon oxidative stress (Fig. 1f, S3c).

In summary, this systemic RPPA analysis of H_2O_2-induced proteome changes identified cytoplasmic kinases and signaling components as candidates that may regulate ARTD1 and early poly-ADP-ribosylation in the cell independent of the classical DNA damage response.

Oxidative stress induces positive and negative regulators of PAR formation

H_2O_2 treatment caused a short-lived induction of PAR in primary fibroblasts (Fig. 1b). In order to identify, which of the H_2O_2-induced early signaling pathways is responsible for the consecutive activation of ARTD1, a screen with small molecule inhibitors for a sub-set of the identified early-activated kinases was performed.

Primary IMR-90 fibroblasts or NIH/3T3 cells were treated with inhibitors against ARTDs (Olaparib), CAMKK (STO-609), CaMKII (KN-93), cyclophilin D (Cyclosporin A), IKK (IKK VII), AMPK (Dorsomorphin), MEK (PD985059), PKC (GF109203X), JNK (SP600125), p38 (SB203580), as well as with the calcium chelator (BABTA), to determine the overall contribution of calcium signaling, and PAR formation was assessed by IF analysis with the 10H anti-PAR antibody or western blotting (Fig. 2 and S4a-b). Even though the activation kinetics of p38 and Iκ-Bα (IKK) upon H_2O_2 treatment correlated with the enhanced PAR formation, their inhibition did not affect PAR levels (Fig. 2a-d and S4a). In agreement with observations by Zhang et al, inhibition of JNK reduced PAR formation [24] (Fig. 2c-d, S4a). However, we could not confirm this observation with JNK1/2 KO MEFs,

indicating an off-target effect of the JNK inhibitor SP600125 (Fig. S4c). In contrast, PAR formation was strongly reduced in H_2O_2 treated IMR-90 cells that were treated with a calcium chelator (BAPTA) or the CaMKII inhibitor KN-93. The identification of both, BAPTA and KN-93, as inhibitors of H_2O_2 induced PAR formation suggested that calcium signaling is a positive regulator of PAR formation upon oxidative stress that may directly activate ARTD1. This finding is in agreement with studies that implicated calcium signaling and CaMKII in the activation of ARTD1 [16-18]. In order to validate these results, the positive effect of CaMKIIδ on PAR formation was confirmed in more detail, since CaMKIIα and β were expressed at relatively low levels in NIH/3T3 cells (Fig. S5a). Down-regulation of CaMKIIδ by siRNA treatment of NIH/3T3 cells was efficient, did not affect ARTD1 protein levels (Fig. S5b), but led to slightly reduced PAR levels, less PAR foci and ARTD1 auto-modification (Fig. 2e and S5c-d). Unexpectedly, H_2O_2 treatment not only induced activators of PAR formation, but also negative regulators. The PKC inhibitor GF109203X induced a strong and significant hyperaccumulation of PAR in H_2O_2 treated human IMR-90 and NIH/3T3 cells (Fig. 2a-d), indicating that the entire PKC family or members thereof are negatively regulating PAR formation.

This inhibitor analysis thus demonstrated that H_2O_2 stimulation induced positive and negative regulators of PAR formation in human primary and mouse fibroblasts. CaMKIIδ positively regulated PAR formation under oxidative stress conditions, while PKC signaling seemed to interfere with PAR formation.

ARTD1 activity is attenuated by PKCδ-dependent phosphorylation

As indicated by our RPPA analysis and inhibitor screen, PKC negatively regulates PAR formation in response to treatment with H_2O_2. This recapitulates the results of earlier studies on PKC and ARTD1 [25-27]. In mammalians, the PKC protein

family is comprised of 10 proteins, which are classified into conventional (PKCα, -βI/II and -γ), novel (PKCδ, -ε, -η and -θ) and atypical isozymes (PKCζ and -ι) [29]. The four conventional PKCs are activated by calcium. To elucidate the molecular mechanism, by which PKC attenuates PAR formation in response to oxidative stress, the overall effect of the PKC signaling pathway on PAR formation was analyzed.

As shown before for IMR-90 cells (Fig. 2a-b), treatment of MRC-5 cells with the PKC inhibitor GF109203X led to enhanced PAR formation upon H_2O_2 treatment, thus confirming the negative regulation of PAR formation by PKC (Fig. 3a-b). Interestingly, in the presence of BAPTA, this effect was abolished; confirming that calcium signaling positively regulates PAR formation as shown by the inhibitor screen. In order to test if PKC family members generally attenuate PAR formation upon oxidative stress, individual members were specifically studied. First, we analyzed the involvement of the novel PKCδ in regulating H_2O_2-dependent PAR formation. PKCδ was selected because calcium signaling positively regulated PAR upon H_2O_2 stress, thus excluding a calcium-dependent PKC family member as a candidate for the negative regulation observed here (Fig. 2a-d). Among the two calcium-independent, DAG-dependent PKC family members, PKCδ showed the strongest expression in NIH/3T3 cells (Fig. S6a). Full-length ARTD1 was incubated with the catalytic domain of PKCδ and radioactive ATP. A strong signal corresponding to phosphorylated, full-length ARTD1 was only observed in the reactions containing PKCδ and in the absence of GF109203X (Fig. 3c). Phosphorylation of ARTD1 was evident for the N-terminal fragment comprising the first 214 amino acids, while all other fragments comprising amino acids 215 – 1014 did not reveal any significant phosphorylation by PKCδ (Fig. 3d). This result indicates selective motifs in the first two zinc fingers of ARTD1, comprising direct phosphorylation sites for PKCδ. Indeed, *in silico* analysis by the Motif Scan

prediction tool (ScanSite) identified Ser20 (NetPhos2.0 score = 0.99), Ser27 (NetPhos2.0 score = 0.61), Thr109 (NetPhos2.0 score = 0.87) and Thr127 (NetPhos2.0 score = 0.82), all located in first two zinc fingers of the ARTD1 DNA binding domain, as putative PKCδ phosphorylation sites in the ARTD1 full-length sequence. To further understand, whether phosphorylation of ARTD1 by PKCδ has a direct influence on ARTD1's enzymatic activity, phosphorylated ARTD1 was *in vitro* modified in presence or absence of DNA and radioactive labeled NAD. As expected, phosphorylation by PKCδ was able to attenuate the DNA-induced activation of ARTD1 (Fig. 3e), establishing ARTD1 phosphorylation in the N-terminal DNA binding domain by PKCδ as an important and powerful negative regulatory mechanism for ARTD1 activity and PAR formation.

To confirm PKC-dependent regulation of PAR formation as a response to oxidative stress, MRC-5 were transfected with siPKC pan with the goal to reduce the general protein expression of PKC family members. Unexpectedly, knockdown of all PKC family members led to a strong reduction in the number of PAR foci in the response to H_2O_2 stress (Fig. 3f-g). These results indicated a positive regulation of PAR formation by certain PKC family members, which is opposite to the effect observed for PKCδ, and thus imply attenuating and stimulating functions of PKC family members.

PKCα is required for poly-ADP-ribose formation during oxidative stress

In order to disentangle these unexpected, positive effects on PAR formation, individual PKC family members were specifically studied. The siPKC pan experiments have revealed that the calcium-dependent PKCα was predominantly down-regulated (Fig. 3g), while a significant reduction in PKCβ and PKCγ could not

be detected under these conditions (not shown). These analyses therefore focused mainly on PKCα.

Knockdown of the highly expressed, calcium-dependent PKCα (Fig. S6a), alone or in combination with PKCδ, led to a significant reduction in the number of PAR foci compared to the control (Fig. 4a-b), suggesting that PKCα is required for H_2O_2-induced PAR formation. In order to assess a possible direct regulation of ARTD1 activity by PKCα, full-length ARTD1 was incubated with PKCα and radioactive labeled ATP. A signal corresponding to phosphorylated, full-length ARTD1 was observed in the reactions containing PKCα (Fig. 4c), indicating that PKCα is able to directly phosphorylate ARTD1 *in vitro*. Incubation of different ARTD1 fragments with PKCα indicated that ARTD was phosphorylated unspecifically at various sites across the whole protein (Fig. 4d). In contrast to PKCδ, ARTD1 phosphorylation by PKCα did not significantly affect ARTD1's enzymatic activity (Fig. 4e). These results thus excluded direct PKCα-dependent phosphorylation of ARTD1 as the mechanism by which PAR formation is stimulated in a calcium-dependent manner upon H_2O_2 treatment and also suggested an indirect mechanism of ARTD1 activation mediated by PKCα. Since ARTD1 is strongly activated by DNA damage *in vitro*, it was hypothesized that calcium- and PKCα-dependent formation of DNA lesions may activate ARTD1. In order to test this hypothesis, NIH/3T3 cells were treated with the calcium chelator BAPTA or siPKCα and DNA integrity was assessed by the alkaline comet assay. BAPTA and siPKCα treatment both caused a significant reduction of the DNA tails in the comet assay, indicating that DNA strand breaks were induced by an enzyme regulated by PKCα and directly by reactive oxygen species (Fig. 4f-g and Fig. S6b). These results thus suggest a calcium-dependent activation of PKCα and the consecutive induction of

DNA lesions as the mechanism, which stimulates PAR formation in response to oxidative stress in NIH/3T3 cells.

Altogether, our results indicate an opposite regulation of ARTD1 activity by calcium-dependent PKCα and calcium-independent PKCδ in response to oxidative stress. Based on the findings presented here, we propose a model of calcium-dependent activation of PKCα and PKCα-dependent formation of DNA lesions for the regulation of ARTD1 activity in response to oxidative stress. In addition to PKCα, which is required for PAR formation under the tested conditions, other PKC isoforms such as PKCδ act as modulators of PAR formation in response to H_2O_2 treatment (Fig. S6b).

Discussion

Oxidative stress is a potent activator of PAR formation in different cell types, but a coherent picture of the molecular events that lead to ARTD1 activation and PAR formation does not exist. Although it is assumed that ARTD1 is indirectly activated by oxidative stress via the induction of DNA damage, a mechanism explaining such an activation has not been reported and ample evidence suggests the direct modification of ARTD1 enzymatic activity. The work described here identified cellular signaling pathways that were induced in MRC-5 human fibroblasts early after the induction of oxidative stress and whose kinetics correlated with PAR formation. Consecutive validation and in-depth analyses revealed that PKCδ attenuates PAR formation upon the exposure to oxidative stress, while PKCα was required for PAR formation under the same conditions. In addition, our results suggest the calcium-dependent activation of PKCα and the consecutive induction of DNA lesions as a novel mechanism, which stimulates PAR formation in response to oxidative stress. This study thus identifies opposing, calcium-dependent and -independent regulatory mechanisms for PAR formation upon oxidative stress within the PKC family of proteins.

These results are confirmatory of earlier findings that documented positive regulation of ARTD1 and PAR formation by calcium signaling and which implicated PKC and the MEK-ERK pathway in the regulation of ADP-ribosylation. In contrast to these earlier findings, our results indicate that positively and negatively regulating pathways are activated at the same time during oxidative stress in human primary fibroblasts as well as in murine NIH/3T3 cells. However, in contrast to reports on a positive regulation of ARTD1 by PKC and MEK-ERK, the results presented here also point at a negative regulation under the oxidative stress conditions of this study. Our systemic study thus integrates and extends the previous results and implies a complex

signaling network of simultaneously present and counter-acting components that regulate and fine-tune the nuclear PAR levels.

Inhibition of PKC signaling by a small molecule inhibitor (GF109203X, BIM 1) led to a significant increase in PAR induction upon H_2O_2 treatment, identifying PKC signaling as a negative modulator upon H_2O_2 stress. This result is in agreement with data obtained upon MNNG stress [26], indicating a general regulatory mechanism of ARTD1 activity by PKCs in response to genotoxic stress. Our *in vitro* experiments showed that phosphorylation of ARTD1 by PKCδ directly attenuates ADP-ribosyltransferase activity in the presence of DNA (Fig. 4e). Indeed, PKC has been previously shown to phosphorylate ARTD1 *in vitro* [27] and its inhibition resulted in increased PAR induction upon alkylation stress [26]. In contrast, there are also studies, which reported a positive regulation of ARTD1 by the Ca^{2+}-independent PKCδ isoform in response to histamine and we did not observe a stimulation of ARTD1 by PMA treatment alone (data not shown) [28,31]. However, our results document that the calcium-dependent isoform PKCα and the consecutive DNA strand break formation are required for PAR synthesis. This study thus identified for the first time opposing, isoform-specific functions of PKC family proteins under the same conditions.

Here, we describe stimulation and attenuation of ARTD1 activity upon *in vitro* phosphorylation by PKCα and PKCδ, respectively. We localized the phosphorylation by PKCδ to the N-terminal DBD of ARTD1, with a strong preference for the region encompassing the first two zinc fingers (Fig. 4d-e). Based on *in silico* analysis, sequence-stretches around Ser20 in the N-terminal DBD of ARTD1 match the consensus-motif of the two Ca^{2+}-independent PKC isoforms PKCδ and PKCε (Motif Scan, ScanSite) and also show a high probability score for phosphorylation. Indeed, based on two recently published structures of ARTD1 zinc finger domains bound to DNA, Ser20 stabilizes the interaction with the DNA backbone by forming a hydrogen

bond with a phosphate of a phosphodiester bond [32,33]. It can thus be speculated that phosphorylation of Ser20 by PKCδ destabilizes the interaction of the first ADRT1 zinc finger with the DNA backbone due to the negative charge of the phosphorylation, eventually resulting in less activity in response to H_2O_2. Previous studies have already shown ARTD1 phosphorylation by PKCα and PKCβ, and identified Ser504, Ser519 and Thr656 as preferential phosphorylation targets of PKCβ in full length ARTD1 [34]. In contrast, we only observed weak phosphorylation of PKCα that could not be localized to a specific domain and which did not alter ARTD1 enzymatic activity *in vitro*. It is currently unknown and almost impossible to assess if PKCα specifically phosphorylates ARTD1 *in vivo*. The weak phosphorylation without effect on enzymatic activity makes an *in vivo* phosphorylation of ARTD1 by PKCα doubtful. The results presented here rather suggest that a yet unidentified enzyme is activated by PKCα upon oxidative stress and consecutively induces DNA strand breaks. Likely candidates for this activity are calcium- and PKCα-dependent endonucleases or topoisomerases. Interestingly, activation of topoisomerases by PKC has been reported, although PKCα has not been studied specifically [35]. In contrast to the strongly reduced PAR formation upon siPKCα treatment, the DNA lesions, as determined by the alkaline comet assay, were only slightly, but significantly, reduced. BAPTA treatment, on the other hand, affected both, DNA lesions and the number of PAR foci. This indicates that not all observed DNA lesions might contribute to PAR formation and that the lesions that are formed following PKCα activation are those responsible for the activation of ARTD1. BAPTA treatment therefore not only abolishes PKCα activity, but also inhibits processes that cause additional types of DNA lesions that are distinct of those induced by the PKCα-dependent process. Interestingly, these results also indicate that cells respond to oxidative stress by the early, controlled induction of DNA lesions, which is thus likely a beneficial response.

For example, early activation of ARTD1 likely changes the metabolic state of the nucleus and provides a platform for the recruitment of proteins. These effects may explain the benefit of the early, controlled induction of DNA lesions in response to oxidative stress and represent a priming step that prepares and shields the DNA from the forthcoming effect of radicals that are formed upon the continued emanation of oxidative stress. It remains to be clarified where in the genome DNA lesions are induced.

Opposite regulation and specific phosphorylation of ARTD1 by PKCα and PKCδ has important biological consequences and may explain functional differences among the PKC isoforms. For example, depending on the cell type and its sub-cellular localization, PKCα is implicated in a variety of biological phenomena such as proliferation, apoptosis, differentiation and inflammation [36]. Interestingly, so far PKCα has not been linked to the regulation of PAR metabolism and ARTD1 activity and was only studied as a factor affected by PARP inhibition [37]. Interestingly, in the absence of Ca^{2+}, ARTD1 activity was reduced in response to nitrosative and oxidative stress [18,38]. Therefore, PKC-dependent regulation can either reduce ARTD1 activity through phosphorylation in the DBD independent of Ca^{2+} (e.g., by PKCδ) or lead to Ca^{2+}-dependent DNA break formation and thereby activate ARTD1 (e.g., by PKCα). Whether the stimulation of ARTD1 activity due to PKCα-induced DNA damage in addition includes effects via other calcium-dependent processes or PKC family members *in vivo* remains to be determined.

In summary, the here presented study identified the concurrent, H_2O_2-dependent activation of stimulatory and attenuating regulators of nuclear PAR formation. These findings thus highlight the complexity of the signaling network regulating PAR levels in the nucleus and identify key players determining and fine-tuning the nuclear PAR pool. Most importantly, the results presented here link

cytoplasmic signaling components and pathways to the formation of DNA strand breaks as a consequence of the calcium-dependent activation of PKCα. These findings for the first time explain how ARTD1 activity can be activated in the nucleus under conditions that are not directly linked to DNA damage formation by reactive oxygen species or irradiation. These results thus revealed a new mechanism for the intricate regulation of ARTD1 and ADP-ribosylation and thereby hopefully stimulate a more comprehensive view and study of the cellular functions of ADP-ribosylation.

Methods

Cell culture, IR treatment, siRNA transfection, lysis and proliferation assay

The MRC-5 and IMR-90 human lung fibroblast cell strains [39,40] were obtained from the American Type Culture Collection (ATCC) and cultured in supplemented MEM (Invitrogen). NIH/3T3 were obtained from American Type Culture Collection (ATCC) and cultured in supplemented DMEM (Invitrogen). JNK1/2 WT and (-/-) MEFs were a kind gift of the Roger Davies lab and were cultured in cultured in supplemented DMEM (Invitrogen). Cells were preincubated with inhibitors or activators (stocks dissolved in DMSO) for 1 h prior to H_2O_2 treatment in FCS-free media, which was also used as a vehicle for H_2O_2.. All inhibitors were obtained from Enzo Life Sciences, except from Olaparib (AstraZeneca), PD98059 (Santa Cruz), IKK VII and KN-93 and PMA (Merck Millipore) and used at a final concentration as indicated in the figures or figure legends. To reduce isoform specific ARTD1, PARG, CaMKIIδ/γ and siPKCα/δ and siPKC pan expression, $2x10^5$ NIH/3T3 or $1x10^5$ MRC-5 cells were transfected using mouse siARTD1 (QIAGEN, SI02731428), siPARG (QIAGEN, SI01369571), siCaMKIIδ (QIAGEN, SI00940415), siCaMKIIγ (QIAGEN, SI00940443), siPKCα (QIAGEN, SI01388583), siPKCδ (QIAGEN, SI01388744) or siPKC pan (Santa Cruz Biotechnology, sc-29449) or siCtl. (scrambled sequence, lacking significant homology to any known human or mouse gene sequence) with Lipofectamine RNAiMAX transfection reagent (Invitrogen) according to manual's instructions over 3-4 days, prior to H_2O_2 treatment. Whole cell extracts were prepared with standard RIPA lysis buffer (50 mM Tris/pH8, 400mM NaCl, 0.5% NP-40, 1% DOC, 0.1% SDS supplemented with proteinase inhibitor cocktail (Roche), 10 mM β-glycerolphosphate, 1mM NaF and DTT) and total protein concentration determined using standard Lowry method. Cell viability was determined by the MTT assay (Sigma).

Reverse phase protein arrays (RPPA)

RPPA were prepared as described [41]. In brief, whole cell extracts were spotted onto hydrophobically coated Zeptosens Chips (Bayer Technology Services GmbH). Serially diluted lysates (100, 75, 50 and 25%) were arrayed in duplicates onto hydrophobic Zeptosens Chips using the Nanoplotter NP2.0 (GeSiM), followed by blocking in an ultrasonic nebulizer (ZeptoFOG, Bayer Technology Services GmbH). Antibody incubation (Invitrogen), microarray data acquisition (ZeptoREADER, Bayer Technology Services GmbH) and data analysis (ZeptoVIEW version 3.1.0.2, Bayer Technology Services GmbH) was performed exactly as described [42]. The eight data points (100, 75, 50, 25% lysate amount in duplicates) were fitted using a weighted linear least squares fit [43] and the relative fluorescence intensity determined by interpolating at the median protein concentration or modification. To correct for small variations in protein content, relative intensities were normalized to the signals of β-Catenin, which did not show any significant variation (ANOVA, $p < 0.05$) in response to H_2O_2 over 10-60 min..

Significance and clustering analysis

To identify significant proteome changes in response to IR, relative fluorescence intensities were imported to MeV version 4.6 [44]. Relative fluorescence intensities were log2 transformed and normalized, before performing statistical analysis using One-way ANOVA as described in [45]. The mean transformed fluorescence intensities for group 1 (biological duplicates of untreated_10 min), group 2 (biological duplicates of 0.5 mM or 2 mM_10 min), group 3 (biological duplicates of 0.5 mM or 2 mM_60 min) were compared using F-statistics with $p < 0.05$. For fold-change analysis, transformed means of the biological replicates were normalized to the untreated

sample (set as 1) and proteome changes were filtered (cut off set at 1x SD equal to log2 > 0.77 / < -0.77 for 0.5 mM or log2 > 0.72 / < -0.72 for 2 mM). Significant proteome changes in response to H_2O_2 were selected for clustering analysis (Fig. 1 b-c) if significant by one-way ANOVA ($p < 0.05$). To correct for potential false negatives or positives, significance analysis was performed using fold change cut off with thresholds described above or performing a quality control analysis by visualization (V.C.) for clustering analysis as shown Fig. 1e. Similar profiles of the fold changes over time were identified by clustering analysis using the k-means clustering algorithm and default parameters of MeV version 4.6 [44]. K-means based clustering analysis in Fig. 1e comprises significant proteome changes, identified by ANOVA (n=2, $p<0.05$), Fold change cut off (1 S.D.) and/or visual control (V.C.) and thus might slightly differ from the results obtained by k-means clustering using only ANOVA (n=2, $p<0.05$) in Fig. 1d and Fig. S3b.

Pathway and network analysis

Gene pathway memberships corresponding to 200 pathways from protein interaction database (PID [46]) and 211 from KEGG [47] was obtained. The background protein list consisted of all analyzed proteins in this study (unique IDs) and only, pathways with more than 5 proteins were considered in the statistical analysis. This selection resulted in 93 and 63 pathways from PID and KEGG respectively. Pathways significantly affected by irradiation (significant by ANOVA and fold-change) induced protein (modification) change were identified using Fisher's exact test, performed using R statistical framework [48]. A Benjamini-Hochberg corrected p value cut-off of 0.05 was used to identify significantly affected pathways. .

Protein-protein interaction analysis on significant protein changes (ANOVA + log2 fold change cut-off) was performed using STRING (v 9.0) [49]. Interactions with a

STRING score more than 0.7 were analyzed with the help of Cytoscape (http://www.cytoscape.org/) [50].

Immunoblotting

For Western Blot analysis, proteins were separated by SDS PAGE gel electrophoresis and bands were visualized by either using horseradish peroxidase-conjugated antibodies (1:5000, GE Healthcare) and ECL detection (GE Healthcare) or by using IR-Dye-conjugated antibodies (1:15000, LI-COR) and detection by the Odyssey infrared imaging system (LI-COR). For quantification, bands were analyzed by ImageJ 1.46 (35) and the Odyssey imaging software (LI-COR).

Antibodies used for Western blotting were anti-ARTD1 (Santa Cruz), anti-CaMKIIdelta (Santa Cruz), anti-CREB Phospho (pS133)/ATF-1 Phospho (CST), anti-JNK1/2 (CST), anti-JNK1/2 Phospho (CST), anti-PAR (10H, homemade), anti-PKCα (CST), antiPKC-δ (CST), anti-Tubulin (1:10'000, Sigma). If not else stated, antibody dilution was 1:1000.

Immunofluorescence (IF) microscopy

For PAR- IF analysis 1.5x105 NIH/3T3 and 2.5x104 MEF, MRC-5 and IMR-90 cells were grown on cover slips overnight prior to inhibitor/activator preincubation and H_2O_2 treatment. Afterwards cells were washed with PBS (1x), fixed with ice-cold methanol and acetic acid (3:1) for 10 min at 4°C, washed with PBS (3x), blocked in 5% milk/0.05% Tween-20 in PBS for 30 min and stained immunohistochemically with primary mouse anti-poly(ADP-ribose) IgG, 1:250 (10H, homemade). Next, cells were washed with PBS (3x) before hybridization with a secondary antibody (1:250 Cy3 conjugated anti-mouse IgG, Jackson ImmunoResearch or 1:250 Alexa Fluor 488 ocnjugated anti-rabbit IgG, Invitrogen). Eventually, cells were mounted on glass

slides using DAPI-containing VECTASHIELD (Vector Labs) and images acquired using an inverted fluorescence microscope at 40x, oil immersion (Leica). Fluorescence intensity or foci number were quantified using ImageJ (v. 1.46r) or Imaris (v. 7.6.0, Bitplane) and equal set-up between the images and experiments.

RNA extraction and real-time PCR analysis

Total RNA was reverse transcribed using High-Capacity cDNA Reverse Transcription kit (Applied Biosystems). Real-time PCR was performed using SYBR green premixed buffer and analysed by the Rotor-Gene Q cycler (QIAGEN).

***In vitro* kinase and ARTD1 automodification assay**

For CaMKII kinase assay, experiment was performed according to the vendors recommendations (New England BioLabs, NEB, P6060) using 100 µM ATP (Sigma) spiked with 0.74 MBq gamma-labeled ATP (20 nM), 125 units CaMKII (NEB) and 1 µg recombinant ARTD1 fl. or ARTD1 deletion fragments (ARTD1 fr.) per reaction incubating for the indicated time points. Prior to the kinase reaction in the CaMKII kinase buffer, CaMKII was activated by 1.2 µM calmodulin according to the manual instructions. For PKCδ kinase assay, experiment was performed using 0.2 µl recombinant PKC catalytic subunit of the PKCδ isoform from rat brain (Sigma, P1609) and 1 µg ARTD1 fl. or ARTD1 fr. in PKCδ kinase buffer (120 mM Tris/pH 7.5, 40 mM MgCl2, 2 mM CaCl2, 2 mM DTT) and 20 nM ATP (Sigma) spiked with 0.74 MBq gamma-labeled ATP (20 nM) and reaction time as indicated in the figure or figure legend. For PKCα kinase assay 100 ng recombinant PKCα (Enzo, BML-SE494-0005) were incubated in PKCα kinase buffer (25 mM MOPS/pH 7.2, 12.5 mM β-glycerophosphate, 25 mM $MgCl_2$, 5 mM EGTA, 2 mM EDTA and 0.25 mM DTT) with 100 µM ATP (Sigma) spiked with 0.74 MBq gamma-labeled ATP (20 nM) /

reaction and 1 µg recombinant ARTD1 fl. or ARTD1 deletion fragments (ARTD1 fr.) for 15 min. For ARTD1 automodification assay, the kinase assay reaction was supplemented with PARP reaction buffer (50 mM Tris-HCl/pH 8, 4 mM $MgCl_2$, 250 µM DTT, 1 µg pepstatin/bestatin/leupeptin), 100 µM NAD (Sigma) spiked with 100 nM gamma-labeled NAD and in some cases 0.5 pmol of EcoRI dsDNA linker to induce ARTD1 activity *in vitro*.

Alkaline comet assay

$5x10^5$ NIH/3T3s were grown over night in 6-well-plates before inhibitor/activator preincubation for 1 h followed by H_2O_2 treatment. NIH/3T3 cells were collected by Trypsin/EDTA (Invitrogen) accordingly, span down and diluted to $3\text{-}4x10^5$ for alkaline comet assay, which was performed according to the manufacture's recommendations (Trevigen). Picture acquisition was performed using an inverted fluorescence microscope at 20x (Leica). For tail DNA quantification the free software CASP, version 1.2.2, was used (casplab.com).

References

1 Hassa, P. O., Haenni, S., Elser, M. & Hottiger, M. O. Nuclear ADP-ribosylation reactions in mammalian cells: where are we today and where are we going? *Microbiol Mol Biol Rev* **70**, 789-829, (2006).

2 Hottiger, M. O., Hassa, P. O., Lüscher, B., Schüler, H. & Koch-Nolte, F. Toward a unified nomenclature for mammalian ADP-ribosyltransferases. *Trends Biochem Sci* **35**, 208-219, (2010).

3 Luo, X. & Kraus, W. L. On PAR with PARP: cellular stress signaling through poly(ADP-ribose) and PARP-1. *Genes Dev* **26**, 417-432, (2012).

4 Altmeyer, M., Messner, S., Hassa, P. O., Fey, M. & Hottiger, M. O. Molecular mechanism of poly(ADP-ribosyl)ation by PARP1 and identification of lysine residues as ADP-ribose acceptor sites. *Nucleic Acids Res* **37**, 3723-3738, (2009).

5 Krishnakumar, R. & Kraus, W. The PARP side of the nucleus: Molecular actions, physiological outcomes, and clinical targets. *Mol Cell* **39**, 8-24, (2010).

6 Schiewer, M. J. *et al.* Dual roles of PARP-1 promote cancer growth and progression. *Cancer Discov*, (2012).

7 Cai, H. & Harrison, D. G. Endothelial dysfunction in cardiovascular diseases: the role of oxidant stress. *Circ Res* **87**, 840-844, (2000).

8 Kraus, W. L. & Hottiger, M. O. PARP-1 and gene regulation: Progress and puzzles. *Mol Aspects Med*, (2013).

9 David, K. K., Andrabi, S. A., Dawson, T. M. & Dawson, V. L. Parthanatos, a messenger of death. *Front Biosci* **14**, 1116-1128, (2009).

10 Lonskaya, I. *et al.* Regulation of poly(ADP-ribose) polymerase-1 by DNA structure-specific binding. *J Biol Chem* **280**, 17076-17083, (2005).

11 Potaman, V. N., Shlyakhtenko, L. S., Oussatcheva, E. A., Lyubchenko, Y. L. & Soldatenkov, V. A. Specific binding of poly(ADP-ribose) polymerase-1 to cruciform hairpins. *J Mol Biol* **348**, 609-615, (2005).

12 Kim, M., Mauro, S., Gévry, N., Lis, J. & Kraus, W. NAD+-dependent modulation of chromatin structure and transcription by nucleosome binding properties of PARP-1. *Cell* **119**, 803-814, (2004).

13 Kun, E., Kirsten, E., Mendeleyev, J. & Ordahl, C. Regulation of the enzymatic catalysis of poly(ADP-ribose) polymerase by dsDNA, polyamines, Mg2+, Ca2+, histones H1 and H3, and ATP. *Biochemistry* **43**, 210-216, (2004).

14 Burkle, A. & Virag, L. Poly(ADP-ribose): PARadigms and PARadoxes. *Mol Aspects Med*, (2013).

15 Homburg, S. *et al.* A fast signal-induced activation of Poly(ADP-ribose) polymerase: a novel downstream target of phospholipase c. *J Cell Biol* **150**, 293-307, (2000).

16 Ju, B.-G. *et al.* Activating the PARP-1 sensor component of the groucho/ TLE1 corepressor complex mediates a CaMKinase IIdelta-dependent neurogenic gene activation pathway. *Cell* **119**, 815-829, (2004).

17 Midorikawa, R., Takei, Y. & Hirokawa, N. KIF4 motor regulates activity-dependent neuronal survival by suppressing PARP-1 enzymatic activity. *Cell* **125**, 371-383, (2006).

18 Bentle, M., Reinicke, K., Bey, E., Spitz, D. & Boothman, D. Calcium-dependent modulation of poly(ADP-ribose) polymerase-1 alters cellular metabolism and DNA repair. *J Biol Chem* **281**, 33684-33696, (2006).

19 Blenn, C., Wyrsch, P., Bader, J., Bollhalder, M. & Althaus, F. Poly(ADP-ribose)glycohydrolase is an upstream regulator of Ca(2+) fluxes in oxidative cell death. *Cell Mol Life Sci*, (2010).

20 Wyrsch, P., Blenn, C., Bader, J. & Althaus, F. R. Cell death and autophagy under oxidative stress: roles of poly(ADP-Ribose) polymerases and Ca(2+). *Mol Cell Biol* **32**, 3541-3553, (2012).

21 Cohen-Armon, M. PARP-1 activation in the ERK signaling pathway. *Trends Pharmacol Sci* **28**, 556-560, (2007).

22 Cohen-Armon, M. *et al.* DNA-independent PARP-1 activation by phosphorylated ERK2 increases Elk1 activity: a link to histone acetylation. *Mol Cell* **25**, 297-308, (2007).

23 Kauppinen, T. *et al.* Direct phosphorylation and regulation of poly(ADP-ribose) polymerase-1 by extracellular signal-regulated kinases 1/2. *Proc Natl Acad Sci USA* **103**, 7136-7141, (2006).

24 Zhang, S. *et al.* c-Jun N-terminal kinase mediates hydrogen peroxide-induced cell death via sustained poly(ADP-ribose) polymerase-1 activation. *Cell Death Differ* **14**, 1001-1010, (2007).

25 Bauer, P. I. *et al.* Inhibition of DNA binding by the phosphorylation of poly ADP-ribose polymerase protein catalysed by protein kinase C. *Biochem Biophys Res Commun* **187**, 730-736, (1992).

26 Hegedus, C. *et al.* Protein kinase C protects from DNA damage-induced necrotic cell death by inhibiting poly(ADP-ribose) polymerase-1. *FEBS Lett* **582**, 1672-1678, (2008).

27 Tanaka, Y., Koide, S. S., Yoshihara, K. & Kamiya, T. Poly (ADP-ribose) synthetase is phosphorylated by protein kinase C in vitro. *Biochem Biophys Res Commun* **148**, 709-717, (1987).

28 Mizuguchi, H. *et al.* Involvement of protein kinase Cdelta/extracellular signal-regulated kinase/poly(ADP-ribose) polymerase-1 (PARP-1) signaling pathway in histamine-induced up-regulation of histamine H1 receptor gene expression in HeLa cells. *J Biol Chem* **286**, 30542-30551, (2011).

29 Newton, A. C. Protein kinase C: poised to signal. *Am J Physiol Endocrinol Metab* **298**, E395-402, (2010).

30 Vogel, C., Silva, G. M. & Marcotte, E. M. Protein expression regulation under oxidative stress. *Mol Cell Proteomics* **10**, M111 009217, (2011).

31 Mizuguchi, H. *et al.* PMA-induced dissociation of Ku86 from the promoter causes transcriptional up-regulation of histamine H(1) receptor. *Sci Rep* **2**, 916, (2012).

32 Langelier, M. F., Planck, J. L., Roy, S. & Pascal, J. M. Structural basis for DNA damage-dependent poly(ADP-ribosyl)ation by human PARP-1. *Science* **336**, 728-732, (2012).

33 Ali, A. A. *et al.* The zinc-finger domains of PARP1 cooperate to recognize DNA strand breaks. *Nat Struct Mol Biol* **19**, 685-692, (2012).

34 Gagne, J. P. *et al.* Proteomic investigation of phosphorylation sites in poly(ADP-ribose) polymerase-1 and poly(ADP-ribose) glycohydrolase. *J Proteome Res* **8**, 1014-1029, (2009).

35 Corbett, A. H., Fernald, A. W. & Osheroff, N. Protein kinase C modulates the catalytic activity of topoisomerase II by enhancing the rate of ATP hydrolysis: evidence for a common mechanism of regulation by phosphorylation. *Biochemistry* **32**, 2090-2097, (1993).

36 Nakashima, S. Protein kinase C alpha (PKC alpha): regulation and biological function. *J Biochem* **132**, 669-675, (2002).

37 Bartha, E. *et al.* PARP inhibition delays transition of hypertensive cardiopathy to heart failure in spontaneously hypertensive rats. *Cardiovasc Res* **83**, 501-510, (2009).

38 Virag, L. *et al.* Requirement of intracellular calcium mobilization for peroxynitrite-induced poly(ADP-ribose) synthetase activation and cytotoxicity. *Mol Pharmacol* **56**, 824-833, (1999).

39 Jacobs, J. P., Jones, C. M. & Baille, J. P. Characteristics of a human diploid cell designated MRC-5. *Nature* **227**, 168-170, (1970).

40 Nichols, W. W. *et al.* Characterization of a new human diploid cell strain, IMR-90. *Science* **196**, 60-63, (1977).

41 Pawlak, M. *et al.* Zeptosens' protein microarrays: a novel high performance microarray platform for low abundance protein analysis. *Proteomics* **2**, 383-393, (2002).

42 Voshol, H., Ehrat, M., Traenkle, J., Bertrand, E. & van Oostrum, J. Antibody-based proteomics: analysis of signaling networks using reverse protein arrays. *FEBS J* **276**, 6871-6879, (2009).

43 Bevington, P. R. Data Reduction and Error Analysis for the Physical Sciences. 3rd Ed. edn, (McGraw-Hill, 2002).

44 Saeed, A. I. *et al.* TM4: a free, open-source system for microarray data management and analysis. *Biotechniques* **34**, 374-378, (2003).

45 Zar, J. H. Biostatistical Analysis 5th Ed. edn, (Prentice Hall, 2009).

46 Schaefer, C. F. *et al.* PID: the Pathway Interaction Database. *Nucleic Acids Res* **37**, D674-679, (2009).

47 Kanehisa, M., Goto, S., Furumichi, M., Tanabe, M. & Hirakawa, M. KEGG for representation and analysis of molecular networks involving diseases and drugs. *Nucleic Acids Res* **38**, D355-360, (2010).

48 Ihaka, R. & Genleman, R. R. A language for data analysis and graphics. *J Comput Graph Stat* **5**, 299-314, (1996).

49 Szklarczyk, D. *et al.* The STRING database in 2011: functional interaction networks of proteins, globally integrated and scored. *Nucleic Acids Res* **39**, D561-568, (2011).

50 Shannon, P. *et al.* Cytoscape: a software environment for integrated models of biomolecular interaction networks. *Genome Res* **13**, 2498-2504, (2003).

Conflict of interest

JT was Zeptosens Technology Manager at Bayer Technology Services GmbH and is currently Group Head for Process Analytical Technologies at the same company.

Acknowledgements

We are grateful to Roger Davies (University of Massachusetts Medical School) for providing JNK1/2 WT and JNK1/2$^{-/-}$ MEFs and to Raffaella Santoro (University of Zurich) for providing gene expression data for CaMKII and PKC family members. Markus Ehrat and Jan van Oostrum are acknowledged for helpful input during the planning of the studies. F. Freimoser (University of Zurich) provided editorial assistance and critical input during the writing. This work was supported by Oncosuisse (KLS 02396-02-2009), the Swiss National Science Foundation Grant 31-122421, the Mäxi-Foundation and the Kanton of Zurich (to M.O.H.).

Figure Legends

Figure 1. H_2O_2 treatment induces cytoplasmic kinases. **a)** Work flow for characterization of H_2O_2 induced proteome changes by reverse phase protein microarrays (RPPA). **b)** PAR immunofluorescence analysis of primary MRC-5 treated with 0.5 mM H_2O_2 for 10-60 min or left untreated (U, 10min). **c-d)** Time profile clustering of 0.5 mM H_2O_2-dependent proteome changes (ANOVA, n=2, $p<0.05$) by k-means algorithm showing protein expression and modification (green) or repression and de-modification (red). Modifications are indicated in brackets, antibodies which have been applied more than once are indicated by a 1-digit number at the end of the analyte name, antibodies from different vendors are indicated by a 3-digit number in brackets (e.g. 2-02). **e)** Identification of overlapping proteome changes induced by 0.5 or 2 mM H_2O_2 over time. Shown are overlapping changes of 0.5 and 2 mM H_2O_2 significant proteome (ANOVA, n=2, $p<0.05$ (green), fold change cut off (1 S.D.) + visual control (V.C.) (yellow), V.C. only (orange) or fold change cut off only (red)) assigned to cluster 1 & 2 & 3 (early activation), cluster 4 (late activation) or cluster 5 (repression). Numbers in the venn diagrams indicate unique and overlapping proteome changes induced by 0.5 and 2 mM. **f)** *In silico* protein-protein interaction analysis of significant proteome changes induced by 0.5 mM using STRING with a STRING score cut off > 0.7. Colors indicate phosphorylation (purple), total protein changes and phosphorylation (violet). Hubs (more ≥ 20 interactions) are enlarged.

Figure 2. Oxidative stress induces positive and negative regulators of PAR formation. **a)** PAR-immunofluorescence (PAR-IF) analysis of IMR-90 cells preincubated with selected kinase inhibitors or DMSO (control) followed by 0.1 mM H_2O_2 treatment or left untreated. Cells were fixed and immunostained with anti-

poly(ADP-ribose) (red) and counterstained with DAPI (blue) 10 min after H_2O_2 treatment. **b)** Quantification of PAR intensity per nucleus from a). 10-20 nuclei analyzed per area (n=10). **c)** PAR-IF analysis of NIH/3T3 preincubated with inhibitors against targets indicated left of the images using 10-50 μM followed by 0.5 mM H_2O_2 treatment for 10 min or untreated as control. **d)** Quantification of PAR intensity per nucleus from c). 50-100 nuclei analyzed per area (n = 3-5). **e)** PAR-immunofluorescence analysis of NIH/3T3 transfected with siRNA targeting CaMKIIdelta (siCtl., used as control) followed by 0.1 mM H_2O_2 treatment. For quantification of PAR foci or intensity from b) 50 nuclei analyzed / area (n=10-15) from 5 independent experiments. Inhibitors were used against ARTD1/2 (Olaparib, 1 μM), calcium (BAPTA, 10 μM), CaMKK (STO-609, 10 μM), CaMKII (KN-93, 5 μM), cyclophilin D (Cyclosporin A, 1 μM), IKK (IKK VII, 10 μM), AMPK (Dorsomorphin, 10 μM), MEK (PD985059, 20 μM), PKC (GF109203X, 10 μM), JNK (SP600125), p38 (SB203580). Data are mean +/- SD by t-test with *p<0.05, **p<0.01, ***p<0.001, n.s. not significant. Scale bars, 25 μm.

Figure 3. Negative modulation of ARTD1 activity by PKC δ . a) PAR-IF analysis of MRC-5 preincubated with 5 μM GF109203X (PKC-specific inhibitor) or 10 μM BAPTA (calcium chelator) prior to 0.1 mM H_2O_2 for 10 min. siCtl. and siARTD1 were used as control for not affecting or reducing ARTD1 protein levels, respectively. Scale: 25 μm. **b)** Quantification of a). **c)** PKC kinase assay in presence or absence of PKC inhibitor (GF109203X, 5 μM) using full length ARTD1 (CIP treated) as substrate and radiolabeled ATP. **d)** PKC δ kinase assay using ARTD1 deletion fragments as substrate and radiolabeled ATP (^{32}P) performed as in Fig. 2g. **e)** Experiment performed as in Fig. 2h in presence or absence of EcoRI linker (ds DNA)

and incubation for 10 min at 30°C. **f)** PAR-immunofluorescence staining of primary MRC-5, transfected with siPKC (pan), followed by H_2O_2 treatment for 10 min. Scale bar, 10 μm. **g)** Quantification of f) (50-100 cells/condition, n=2). KD confirmation by immunoblotting anti-ARTD1, anti-PKCalpha or anti-PKCdelta using anti-Tubulin as loading control, indicated in the right corner of the panel. Data are mean +/- SD by t-test with *p<0.05.

Figure 4. PKCα is required for poly-ADP-ribose formation during oxidative stress. **a)** PAR-IF analysis of NIH/3T3, transfected with siPKCα and/or siPKCδ or siARTD1 (positive ctl) and siCtl (negative control), followed by H_2O_2 (0.1 mM) treatment for 10 min (500 cell/condition, n=2). **b)** KD confirmation of a) by immunoblotting anti-ARTD1, anti-PKCalpha and/or anti-PKCdelta using anti-Tubulin as loading control. **c)** PKCα kinase assay using ARTD1 full length (CIP treated) and Pol beta (positive control) as substrates and radiolabeled ATP (^{32}P). Loading controlled by Coomassie blue staining of the gel (lower panel, CB). d) PKCα kinase assay using ARTD1 deletion fragments or full length ARTD1 as substrate and radiolabeled ATP (^{32}P) performed as in Fig. 2g. **e)** Experiment performed as in Fig. 2h in presence or absence of EcoRI linker (ds DNA) and incubation for 10 min at 30°C. **f)** Alkaline comet assay of NIH/3T3 preincubated with BAPTA (20 μM) followed by 100 μM H_2O_2 treatment for 3-20 min (50 nuclei analysed / independent experiment, n=2). **g)** Alkaline comet assay, performed as in f), using PKCα transfected NIH/3T3 or siCtl (negative control) followed by 100 μM H_2O_2 treatment. Data are mean +/- SD by t-test with *p<0.05, **p<0.01, ***p<0.001.

Supplementary Figure Legends

Figure S1. Sample preparation and workflow for identification of PAR-dependent proteome changes upon H_2O_2 by RPPA. a) MTT assay of MRC-5 treated with different doses of H_2O_2 and recovery for 24 h (n=3). **b)** PAR IF of MRC-5 preincubated with different PARP inhibitors using 1 μM for ABT-88 and Olaparib and 10 μM for PJ-34. **c)** Immunoblotting analysis of MRC-5 pretreated with 1 µM ABT-888 or DMSO (control) and H_2O_2 treatment for 10-60 min.

Figure S2. Significance analysis of H_2O_2-dependent proteome changes. **a-b)** Relative fluorescence intensities (RFIs) (log2) for group 1 (biological duplicates for untreated (U)_10 min), group 2 (biological duplicates for 0.5 / 2 mM _10 min), group 3 (biological duplicates for 0.5 / 2 mM _60 min) were compared using F-statistics (ANOVA) with $p < 0.05$. **c-d)** Means of RFIs (replicates) were log2 transformed and fold changes (to U, group 1) were plotted individually for 0.5 mM (c) and 2 mM (d) to determine the standard deviation, resulting in 1 S.D. = 0.77 for 0.5 mM and 1 S.D. = 0.72 for 2 mM. **e-f)** Statistical, fold change and quality control analysis of significant proteome changes in response to 0.5 mM H_2O_2 (e) and 2 mM (f) using ANOVA ($p < 0.05$, $n = 2$) (green) and cut off (1 S.D.) (dashed line). Proteome changes which passed the cut off filter (1 S.D.) and satisfied visual quality control are highlighted in yellow, proteome changes which only passed the cut off filter (1 S.D.) are highlighted in red, proteome changes which only passed the visual quality control are highlighted in orange.

Figure S3. Clustering, protein-protein interaction and pathway analysis of H_2O_2-dependent proteome changes. a-b) Time profile clustering of 2 mM H_2O_2-

dependent proteome changes (ANOVA, n=2, $p < 0.05$) by k-means algorithm showing protein expression and modification (green) or repression and de-modification (red). Modifications are indicated in brackets, antibodies which have been applied more than once are indicated by a 1-digit number at the end of the analyte name, antibodies from different vendors are indicated by a 3-digit number in brackets (e.g., 2-83). **c)** In-silico protein-protein interaction analysis of significant proteome changes induced by 2 mM using STRING with a STRING score cut off > 0.7. Colors indicate phosphorylation (purple), total protein changes and phosphorylation (violet). Hubs (more >= 20 interactions) are enlarged. **d-e)** Enrichment of pathways from the pathway interaction database (PID) with significant proteome changes (ANOVA, $p < 0.05$) induced by 0.5 mM (d) and 2 mM (e) using Fisher's exact test. (FDR corrected p-value cut off = 0.05).

Figure S4. Identification of signaling players upstream of PAR induction upon H_2O_2. a) PAR-immunoblotting analysis of NIH/3T3 preincubated with ARTD1/2 inhibitor (Olaparib, 10 μM), increasing amount of JNK inhibitor (SP600125, 10-30 μM and p38 inhibitor (SB203580, 10 μM) for 1h, followed by 0.5 mM H_2O_2 treatment for 10 min. **b)** Experiment performed as in a, using Ca^{2+} chelator (BAPTA, 10 μM) and increasing amount of AMPK inhibitor (Dorsomorphin, 10-50 μM). **c)** Immunoblotting analysis of JNK1/2 double KO or WT MEF pretreated with 30 μM SP600125 (JNK-specific inhibitor) followed by 0.5 mM H_2O_2 treatment. Anisomycin (10 μM) treatment used as control for inducing JNK signaling. ARTD1 used as loading control and JNK1/2 to control absence of JNK in JNK1/2 double KO MEF. PAR intensity normalized to Tubulin and reported as percent of H2O2 + DMSO.

Figure S5. Negative modulation of ARTD1 activity by PKC δ . a) Gene expression analysis of CamKII family members in NIH/3T3 (n=3). **b)** Knockdown confirmation of CaMKIIδ in NIH/3T3. siCtl, siARTD1, siRYR1, siIP31 and siIP3R2 were used as negative controls for not affecting CaMKIIδ levels. Tubulin was used as loading control. **c)** Immunoblotting analysis of NIH/3T3 transfected with increasing amount of siCaMKIIdelta (50 -100 nM) followed by cell lysis and immunostaining. Tubulin used as loading control. **d)** Quantification of CamKIIδ, ARTD1 and PAR levels from c). **e)** PAR-immunofluorescence analysis of calmodulin1-3 (CaM1-3) transfected NIH/3T3 followed by 0.5 mM H_2O_2 treatment for 10 min. Data are mean +/- SD by t-test with *p<0.05, **p<0.01, ***p<0.001.

Figure S6. PKCα is required for poly-ADP-ribose formation during oxidative stress. a) Gene expression analysis of PKCs with i) calcium-dependent, ii) DAG and calcium-dependent or iii) calcium and DAG-independent family members in NIH/3T3s (n=3). **b)** Schematic presentation of signaling-dependent regulation of ARTD1 activity induced by H_2O_2. Calcium- and DNA-break dependent activation of ARTD1 by PKCα is negatively fine-tuned through direct phosphorylation (+P) by PKCδ upon H_2O_2 exposure. Activation of ARTD1 activity can be perturbed by inhibition of calcium by BAPTA or knockdown by PKCα/siPKC pan dominantly over the inhibitory effect of GF109203X and knockdown of PKCδ.

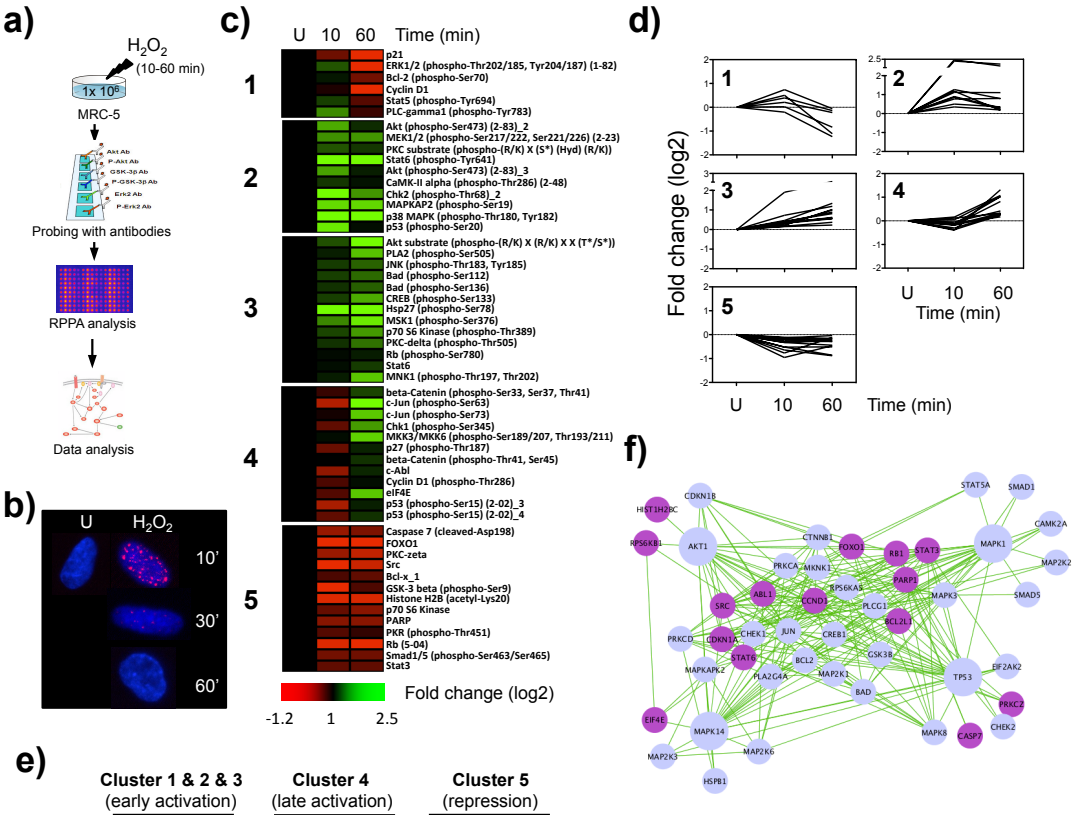

Cluster 1 & 2 & 3	Cluster 4	Cluster 5
Akt (p-Ser473)	Aurora A (p-Thr288)	ATM/ATR Substrate (p-Ser/Thr)
Akt substrate (p-(R/K)X(R/K)XX(T*/S*))	c-Abl	Caspase 7 (cleaved-Asp198)
AMPK alpha (p-Thr172)	c-Jun (p-Ser63)	eIF2a (p-Ser51)
Bad (p-Ser112)	Chk1 (p-Ser345)	FKHR (FoxO1)
Bcl-2 (p-Ser70)	Cyclin D1 (p-Thr286)	Histone H2B (acetyl-Lys20)
c-Jun (pSer73)	eIF4E	MAPKAPK-2
CDK1 (p-Tyr15)	Histone H2A.X (p-Ser139)	PDK-1
Chk2 (p-Thr68)	p27 (p-Thr187)	Rb (p-Ser807,Ser811)
CREB (p-Ser133)	p53 (p-Ser15)	Smad6
ErbB-2 (p-Tyr1248/Tyr1173)		Src
Histone H3		Src (p-Tyr527)
Histone H3 (p-Ser10)		Stat3
Histone H4		
HSP27 (p-Ser78)		
IkB-alpha (p-Ser32)		
IkB-alpha		
MAPKAPK-2 (p-Thr334)		
MEK1/2 (p-Ser217/222,Ser221/226) (2-23)		
MKK3/MKK6 (p-Ser189/207,Thr193/Thr211)		
MNK1 (MKNK) (pThr197,Thr202)		
MSK1 (p-Ser376)		
p21 CIP/WAF1 (p-Thr145)		
p38 MAPK (p-Thr180,Tyr182)		
p44/42 MAPK (ERK1/2) (p-Thr202/185,Tyr204/187)		
p53 (p-Ser20)		
PKC substrate (p-(R/K)X(S*)(Hyd)(R/k))		
PKC-delta (p-Thr505)		
PLA2 (p-Ser505)		
PLC-gamma1 (p-Tyr783)		
Rb (p-Ser780)		
JNK (p-Thr183,Tyr185)		
Stat5 (p-Tyr694)		
Stat6 (p-Tyr641)		

ANOVA (n=2, p<0.05)

Fold change cut off (1 S.D.) + V.C.

V.C.

Fold change cut off (1 S.D.)

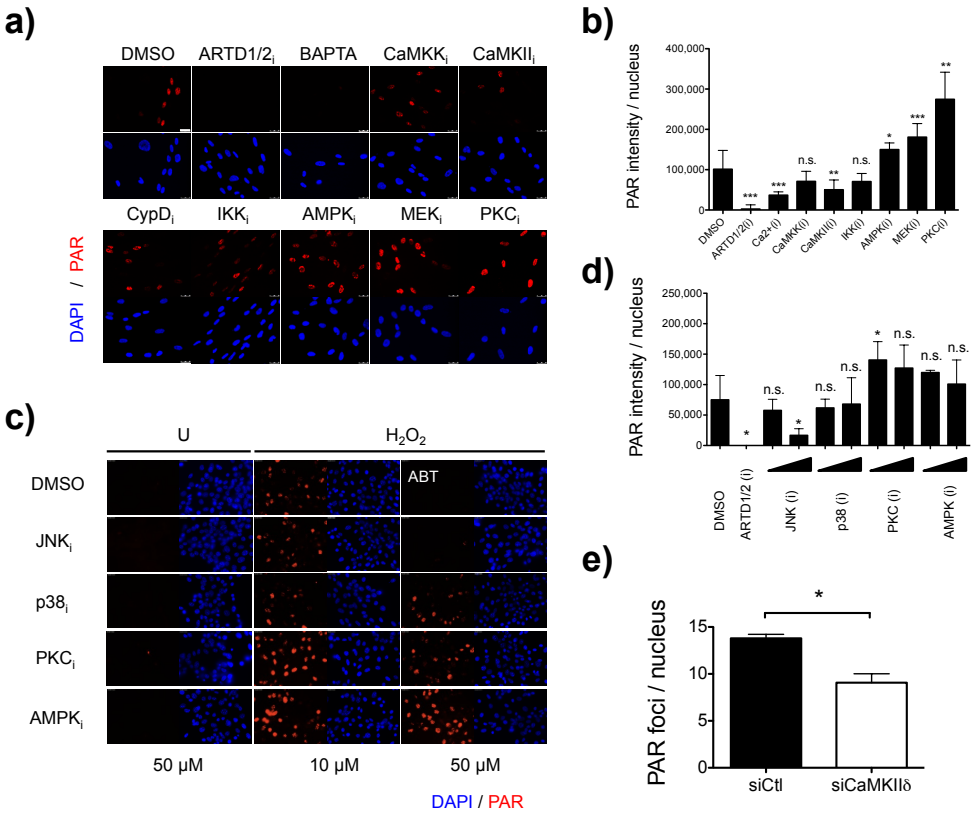
a)
DMSO
ARTD1/2i
BAPTA
CaMKKi
CaMKIIi
CypDi
IKKi
AMPKi
MEKi
PKCi
DAPI / PAR
b)
PAR intensity / nucleus
400,000
300,000
200,000
100,000
0
DMSO
ARTD1/2(i)
Ca2+(i)
CaMKK(i)
CaMKII(i)
IKK(i)
AMPK(i)
MEK(i)
PKC(i)
c)
U
H2O2
DMSO
JNKi
p38i
PKCi
AMPKi
ABT
50 µM
10 µM
50 µM
DAPI / PAR
d)
PAR intensity / nucleus
250,000
200,000
150,000
100,000
50,000
0
DMSO
ARTD1/2 (i)
JNK (i)
p38 (i)
PKC (i)
AMPK (i)
e)
PAR foci / nucleus
15
10
5
0
siCtl
siCaMKIIδ

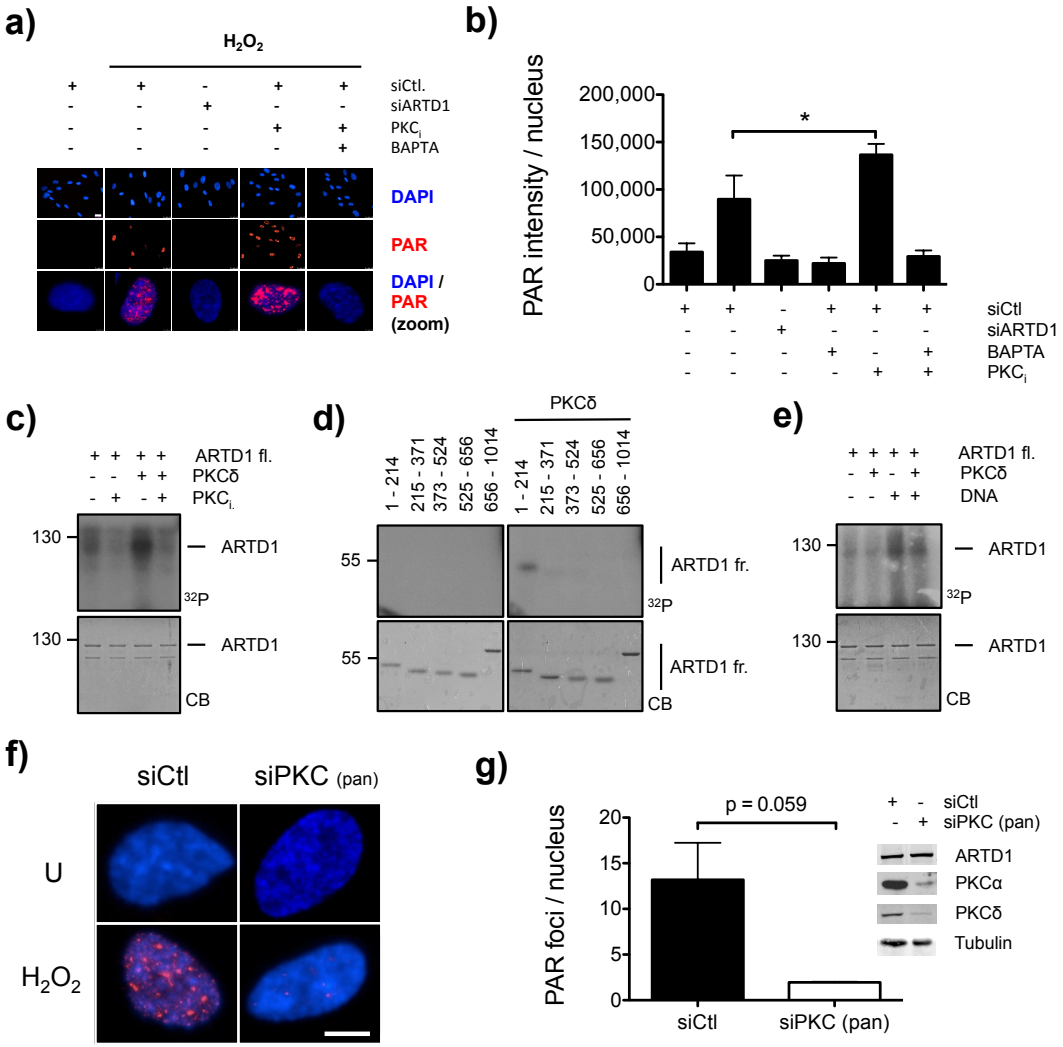
a)
H_2O_2
siCtl.
siARTD1
PKC_i
BAPTA
DAPI
PAR
DAPI / PAR (zoom)
b)
PAR intensity / nucleus
200,000
150,000
100,000
50,000
0
*
siCtl
siARTD1
BAPTA
PKC_i
c)
ARTD1 fl.
PKCδ
PKC_i
130
ARTD1
^{32}P
CB
d)
PKCδ
1 - 214
215 - 371
373 - 524
525 - 656
656 - 1014
55
ARTD1 fr.
^{32}P
CB
e)
ARTD1 fl.
PKCδ
DNA
f)
siCtl
siPKC (pan)
U
H_2O_2
g)
PAR foci / nucleus
p = 0.059
siCtl
siPKC (pan)
ARTD1
PKCα
PKCδ
Tubulin

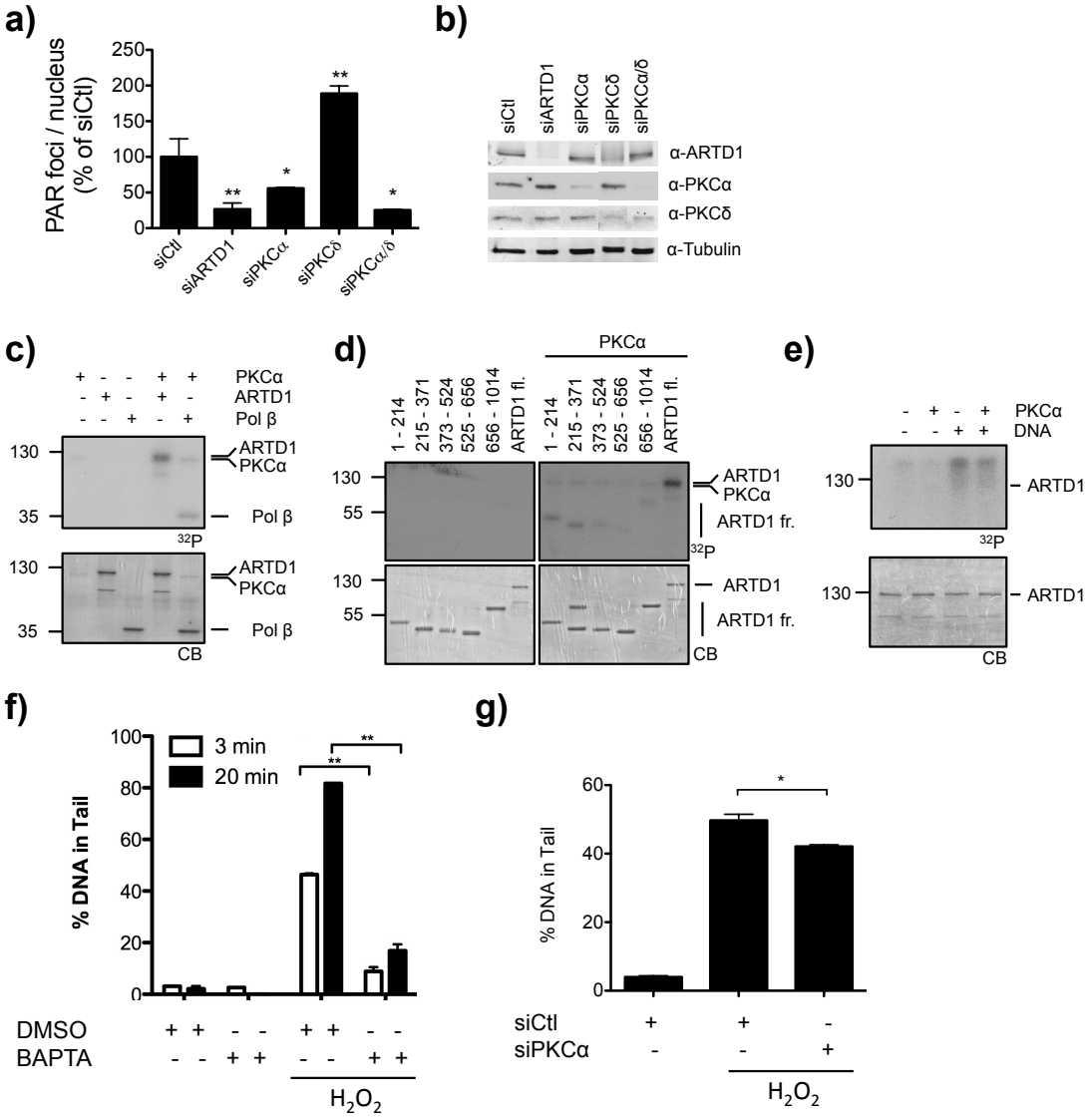
a)
PAR foci / nucleus (% of siCtl)
250
200
150
100
50
0
**
**
*
*
siCtl
siARTD1
siPKCα
siPKCδ
siPKCα/δ
b)
siCtl
siARTD1
siPKCα
siPKCδ
siPKCα/δ
α-ARTD1
α-PKCα
α-PKCδ
α-Tubulin
c)
PKCα
ARTD1
Pol β
130
35
ARTD1
PKCα
Pol β
32P
130
35
ARTD1
PKCα
Pol β
CB
d)
PKCα
1 - 214
215 - 371
373 - 524
525 - 656
656 - 1014
ARTD1 fl.
130
55
ARTD1
PKCα
ARTD1 fr.
32P
130
55
ARTD1
ARTD1 fr.
CB
e)
PKCα
DNA
130
ARTD1
32P
130
ARTD1
CB
f)
3 min
20 min
% DNA in Tail
100
80
60
40
20
0
**
**
DMSO
BAPTA
H2O2
g)
% DNA in Tail
60
40
20
0
*
siCtl
siPKCα
H2O2

a)

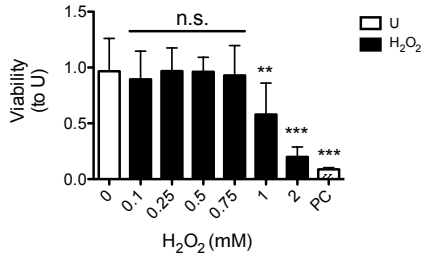
n.s.
U
H2O2
Viability (to U)
1.5
1.0
0.5
0.0
**
***
***
0
0.1
0.25
0.5
0.75
1
2
PC
H2O2 (mM)

b)

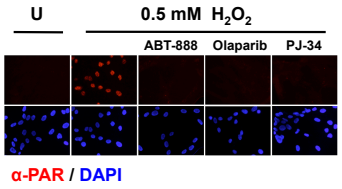
U
0.5 mM H2O2
ABT-888
Olaparib
PJ-34
α-PAR / DAPI

c)

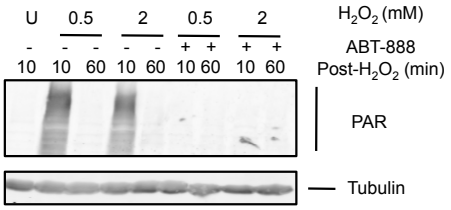
U
0.5
2
0.5
2
H2O2 (mM)
- - - - + + + +
ABT-888
10 10 60 10 60 10 60 10 60
Post-H2O2 (min)
PAR
Tubulin

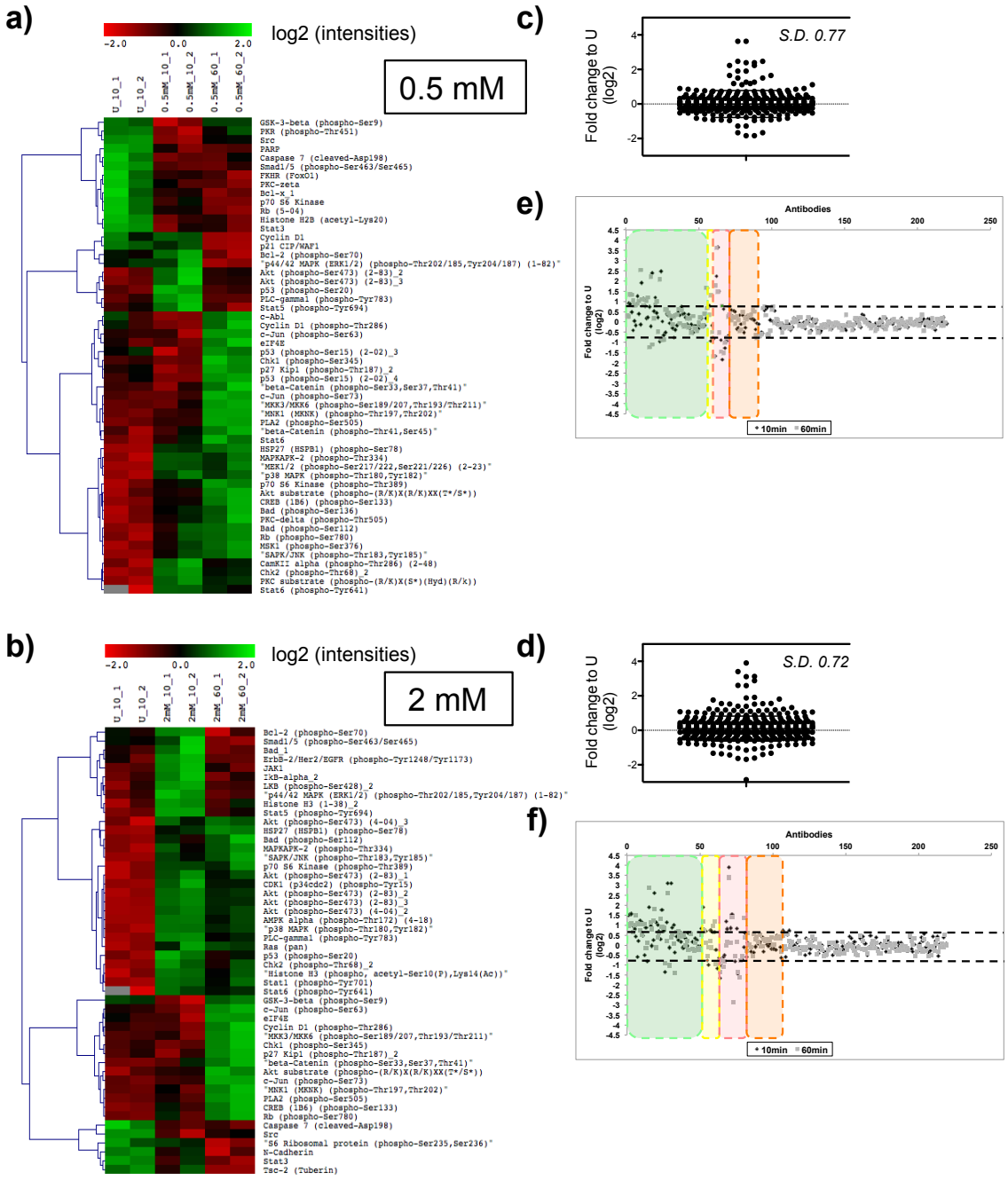
a)
log2 (intensities)
0.5 mM
U_10_1
U_10_2
0.5mM_10_1
0.5mM_10_2
0.5mM_60_1
0.5mM_60_2
GSK-3-beta (phospho-Ser9)
PKR (phospho-Thr451)
Src
PARP
Caspase 7 (cleaved-Asp198)
Smad1/5 (phospho-Ser463/Ser465)
FKHR (FoxO1)
PKC-zeta
Bcl-x_1
p70 S6 Kinase
Rb (S-04)
Histone H2B (acetyl-Lys20)
Stat3
Cyclin D1
p21 CIP/WAF1
Bcl-2 (phospho-Ser70)
"p44/42 MAPK (ERK1/2) (phospho-Thr202/185,Tyr204/187) (1-82)"
Akt (phospho-Ser473) (2-83)_2
Akt (phospho-Ser473) (2-83)_3
p53 (phospho-Ser20)
PLC-gamma1 (phospho-Tyr783)
Stat5 (phospho-Tyr694)
c-Abl
Cyclin D1 (phospho-Thr286)
c-Jun (phospho-Ser63)
eIF4E
p53 (phospho-Ser15) (2-02)_3
Chk1 (phospho-Ser345)
p27 Kip1 (phospho-Thr187)_2
p53 (phospho-Ser15) (2-02)_4
"beta-Catenin (phospho-Ser33,Ser37,Thr41)"
c-Jun (phospho-Ser73)
"MKK3/MKK6 (phospho-Ser189/207,Thr193/Thr211)"
"MNK1 (MKNK) (phospho-Thr197,Thr202)"
PLA2 (phospho-Ser505)
"beta-Catenin (phospho-Thr41,Ser45)"
Stat6
HSP27 (HSPB1) (phospho-Ser78)
MAPKAPK-2 (phospho-Thr334)
"MEK1/2 (phospho-Ser217/222,Ser221/226) (2-23)"
"p38 MAPK (phospho-Thr180,Tyr182)"
p70 S6 Kinase (phospho-Thr389)
Akt substrate (phospho-(R/K)X(R/K)XX(T*/S*))
CREB (1B6) (phospho-Ser133)
Bad (phospho-Ser136)
PKC-delta (phospho-Thr505)
Bad (phospho-Ser112)
Rb (phospho-Ser780)
MSK1 (phospho-Ser376)
"SAPK/JNK (phospho-Thr183,Tyr185)"
CamKII alpha (phospho-Thr286) (2-48)
Chk2 (phospho-Thr68)_2
PKC substrate (phospho-(R/K)X(S*)(Hyd)(R/k))
Stat6 (phospho-Tyr641)
c)
S.D. 0.77
Fold change to U (log2)
e)
Antibodies
Fold change to U (log2)
10min
60min
b)
log2 (intensities)
2 mM
U_10_1
U_10_2
2mM_10_1
2mM_10_2
2mM_60_1
2mM_60_2
Bcl-2 (phospho-Ser70)
Smad1/5 (phospho-Ser463/Ser465)
Bad_1
ErbB-2/Her2/EGFR (phospho-Tyr1248/Tyr1173)
JAK1
IkB-alpha_2
LKB (phospho-Ser428)_2
"p44/42 MAPK (ERK1/2) (phospho-Thr202/185,Tyr204/187) (1-82)"
Histone H3 (1-38)_2
Stat5 (phospho-Tyr694)
Akt (phospho-Ser473) (4-04)_3
HSP27 (HSPB1) (phospho-Ser78)
Bad (phospho-Ser112)
MAPKAPK-2 (phospho-Thr334)
"SAPK/JNK (phospho-Thr183,Tyr185)"
p70 S6 Kinase (phospho-Thr389)
Akt (phospho-Ser473) (2-83)_1
CDK1 (p34cdc2) (phospho-Tyr15)
Akt (phospho-Ser473) (2-83)_2
Akt (phospho-Ser473) (2-83)_3
Akt (phospho-Ser473) (4-04)_2
AMPK alpha (phospho-Thr172) (4-18)
"p38 MAPK (phospho-Thr180,Tyr182)"
PLC-gamma1 (phospho-Tyr783)
Ras (pan)
p53 (phospho-Ser20)
Chk2 (phospho-Thr68)_2
"Histone H3 (phospho, acetyl-Ser10(P),Lys14(Ac))"
Stat1 (phospho-Tyr701)
Stat6 (phospho-Tyr641)
GSK-3-beta (phospho-Ser9)
c-Jun (phospho-Ser63)
eIF4E
Cyclin D1 (phospho-Thr286)
"MKK3/MKK6 (phospho-Ser189/207,Thr193/Thr211)"
Chk1 (phospho-Ser345)
p27 Kip1 (phospho-Thr187)_2
"beta-Catenin (phospho-Ser33,Ser37,Thr41)"
Akt substrate (phospho-(R/K)X(R/K)XX(T*/S*))
c-Jun (phospho-Ser73)
"MNK1 (MKNK) (phospho-Thr197,Thr202)"
PLA2 (phospho-Ser505)
CREB (1B6) (phospho-Ser133)
Rb (phospho-Ser780)
Caspase 7 (cleaved-Asp198)
Src
"S6 Ribosomal protein (phospho-Ser235,Ser236)"
N-Cadherin
Stat3
Tsc-2 (Tuberin)
d)
S.D. 0.72
Fold change to U (log2)
f)
Antibodies
Fold change to U (log2)
10min
60min

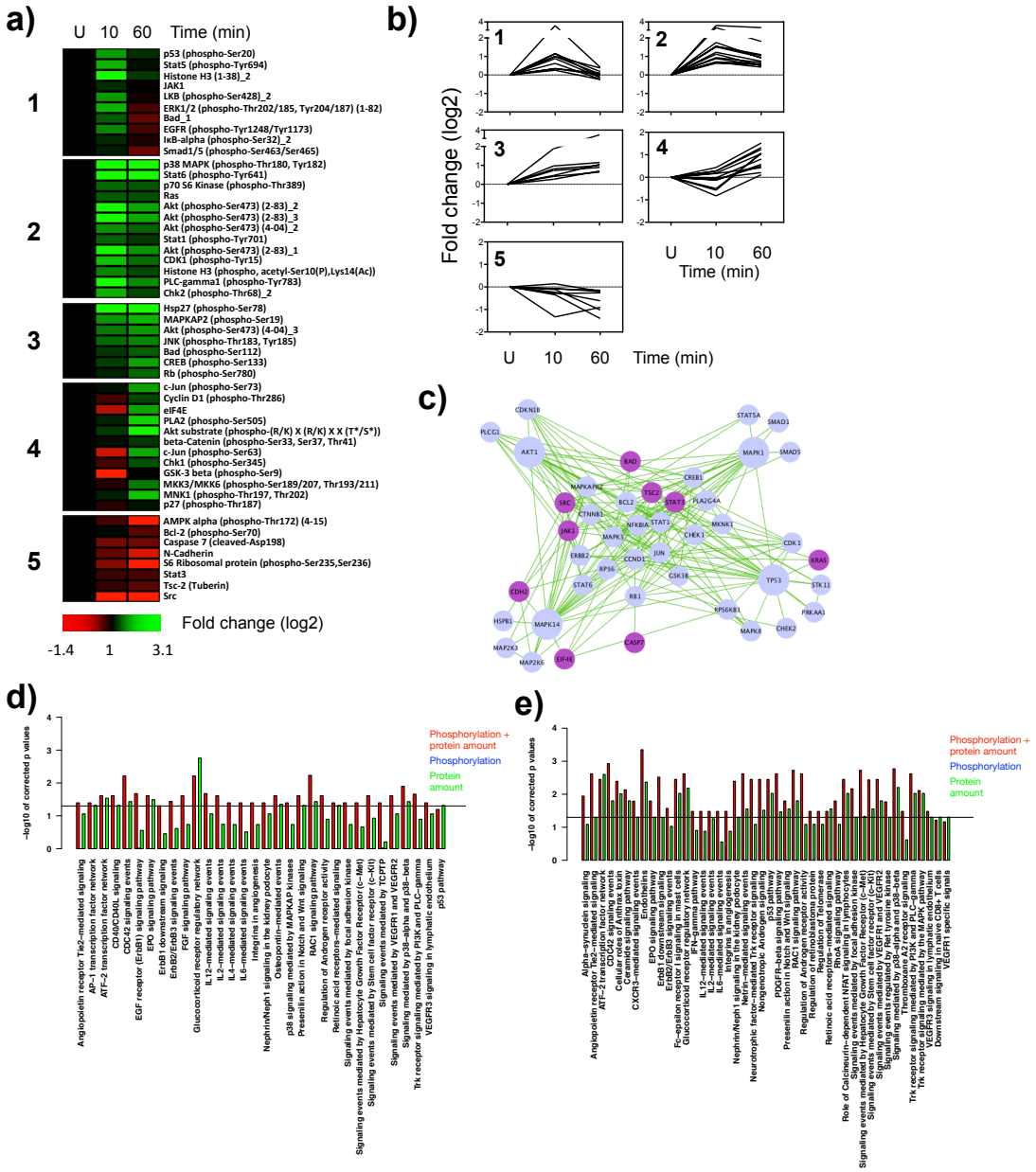
a)
U 10 60 Time (min)
1
p53 (phospho-Ser20)
Stat5 (phospho-Tyr694)
Histone H3 (1-38)_2
JAK1
LKB (phospho-Ser428)_2
ERK1/2 (phospho-Thr202/185, Tyr204/187) (1-82)
Bad_1
EGFR (phospho-Tyr1248/Tyr1173)
IκB-alpha (phospho-Ser32)_2
Smad1/5 (phospho-Ser463/Ser465)
2
p38 MAPK (phospho-Thr180, Tyr182)
Stat6 (phospho-Tyr641)
p70 S6 Kinase (phospho-Thr389)
Ras
Akt (phospho-Ser473) (2-83)_2
Akt (phospho-Ser473) (2-83)_3
Akt (phospho-Ser473) (4-04)_2
Stat1 (phospho-Tyr701)
Akt (phospho-Ser473) (2-83)_1
CDK1 (phospho-Tyr15)
Histone H3 (phospho, acetyl-Ser10(P),Lys14(Ac))
PLC-gamma1 (phospho-Tyr783)
Chk2 (phospho-Thr68)_2
3
Hsp27 (phospho-Ser78)
MAPKAP2 (phospho-Ser19)
Akt (phospho-Ser473) (4-04)_3
JNK (phospho-Thr183, Tyr185)
Bad (phospho-Ser112)
CREB (phospho-Ser133)
Rb (phospho-Ser780)
4
c-Jun (phospho-Ser73)
Cyclin D1 (phospho-Thr286)
eIF4E
PLA2 (phospho-Ser505)
Akt substrate (phospho-(R/K) X (R/K) X X (T*/S*))
beta-Catenin (phospho-Ser33, Ser37, Thr41)
c-Jun (phospho-Ser63)
Chk1 (phospho-Ser345)
GSK-3 beta (phospho-Ser9)
MKK3/MKK6 (phospho-Ser189/207, Thr193/211)
MNK1 (phospho-Thr197, Thr202)
p27 (phospho-Thr187)
5
AMPK alpha (phospho-Thr172) (4-15)
Bcl-2 (phospho-Ser70)
Caspase 7 (cleaved-Asp198)
N-Cadherin
S6 Ribosomal protein (phospho-Ser235,Ser236)
Stat3
Tsc-2 (Tuberin)
Src
Fold change (log2)
-1.4 1 3.1
b)
Fold change (log2)
1
2
3
4
5
U 10 60 Time (min)
U 10 60 Time (min)
c)
CDKN1B
PLCG1
AKT1
BAD
STAT5A
SMAD1
MAPK1
SMAD5
CREB1
MAPKAPK2
SRC
CTNNB1
BCL2
TSC2
STAT3
PLA2G4A
JAK1
NFKBIA
STAT1
MKNK1
MAPK3
CHEK1
CDK1
ERBB2
CCND1
JUN
KRAS
RPS6
CSK1E
TP53
STK11
CDH1
STAT6
RB1
RPS6KB1
PRKAA1
HSPB1
MAPK14
MAPK8
CHEK2
MAP2K3
CASP2
MAP2K6
EIF4E
d)
–log10 of corrected p values
Phosphorylation + protein amount
Phosphorylation
Protein amount
Angiopoietin receptor Tie2–mediated signaling
AP–1 transcription factor network
ATF–2 transcription factor network
CD40/CD40L signaling
CDC42 signaling events
EGF receptor (ErbB1) signaling pathway
EPO signaling pathway
ErbB1 downstream signaling
ErbB2/ErbB3 signaling events
FGF signaling pathway
Glucocorticoid receptor regulatory network
IL12–mediated signaling events
IL2–mediated signaling events
IL4–mediated signaling events
IL6–mediated signaling events
Integrins in angiogenesis
NephrinNeph1 signaling in the kidney podocyte
Osteopontin–mediated events
p38 signaling mediated by MAPKAP kinases
Presenilin action in Notch and Wnt signaling
RAC1 signaling pathway
Regulation of Androgen receptor activity
Retinoic acid receptors–mediated signaling
Signaling events mediated by focal adhesion kinase
Signaling events mediated by Hepatocyte Growth Factor Receptor (c–Met)
Signaling events mediated by Stem cell factor receptor (c–Kit)
Signaling events mediated by TCPTP
Signaling events mediated by VEGFR1 and VEGFR2
Signaling mediated by p38-alpha and p38-beta
Trk receptor signaling mediated by PI3K and PLC-gamma
VEGFR3 signaling in lymphatic endothelium
p53 pathway
e)
–log10 of corrected p values
Phosphorylation + protein amount
Phosphorylation
Protein amount
Alpha–synuclein signaling
Angiopoietin receptor Tie2–mediated signaling
ATF–2 transcription factor network
CD40/CD40L signaling
CDC42 signaling events
Cellular roles of Anthrax toxin
CXCR3–mediated signaling events
EGF receptor (ErbB1) signaling pathway
EPO signaling pathway
ErbB1 downstream signaling
ErbB2/ErbB3 signaling events
Fc–epsilon receptor I signaling in mast cells
Glucocorticoid receptor regulatory network
IL12–mediated signaling events
IL2–mediated signaling events
IL6–mediated signaling events
Integrins in angiogenesis
NephrinNeph1 signaling in the kidney podocyte
Netrin–mediated signaling events
Neurotrophic factor–mediated Trk receptor signaling
Nongenotropic Androgen signaling
p53 pathway
PDGFR–beta signaling pathway
Presenilin action in Notch and Wnt signaling
RAC1 signaling pathway
Regulation of Androgen receptor activity
Regulation of nucleotidase protein
Regulation of Telomerase
Retinoic acid receptors–mediated signaling
RhoA signaling pathway
Role of Calcineurin–dependent NFAT signaling in lymphocytes
Signaling events mediated by Hepatocyte Growth Factor Receptor (c–Met)
Signaling events mediated by Stem cell factor receptor (c–Kit)
Signaling events mediated by VEGFR1 and VEGFR2
Signaling events regulated by Ret tyrosine kinase
Thromboxane A2 receptor signaling
Trk receptor signaling mediated by PI3K and PLC–gamma
Trk receptor signaling mediated by the MAPK pathway
VEGFR3 signaling in lymphatic endothelium
Downstream signaling in naive CD8+ T cells
VEGFR1 specific signals

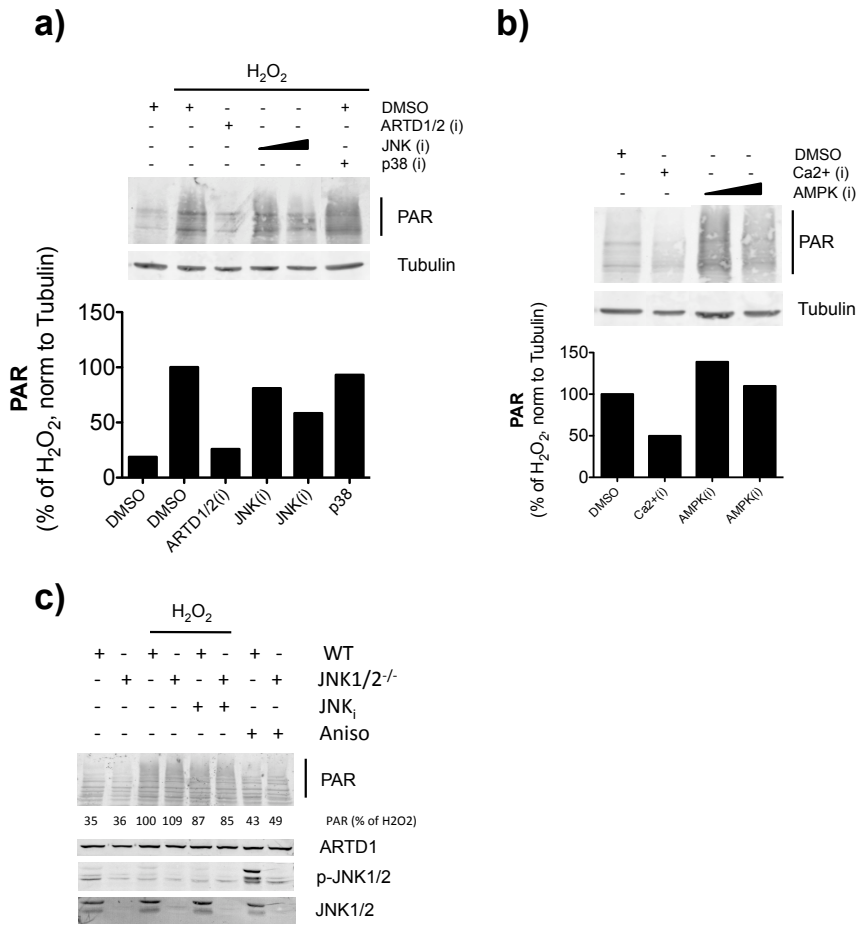
a)
H_2O_2
DMSO
ARTD1/2 (i)
JNK (i)
p38 (i)
PAR
Tubulin
PAR (% of H_2O_2, norm to Tubulin)
150
100
50
0
DMSO
DMSO
ARTD1/2(i)
JNK(i)
JNK(i)
p38
b)
DMSO
Ca2+ (i)
AMPK (i)
PAR
Tubulin
PAR (% of H_2O_2, norm to Tubulin)
150
100
50
0
DMSO
Ca2+(i)
AMPK(i)
AMPK(i)
c)
H_2O_2
WT
JNK1/2$^{-/-}$
JNK$_i$
Aniso
PAR
35 36 100 109 87 85 43 49
PAR (% of H2O2)
ARTD1
p-JNK1/2
JNK1/2

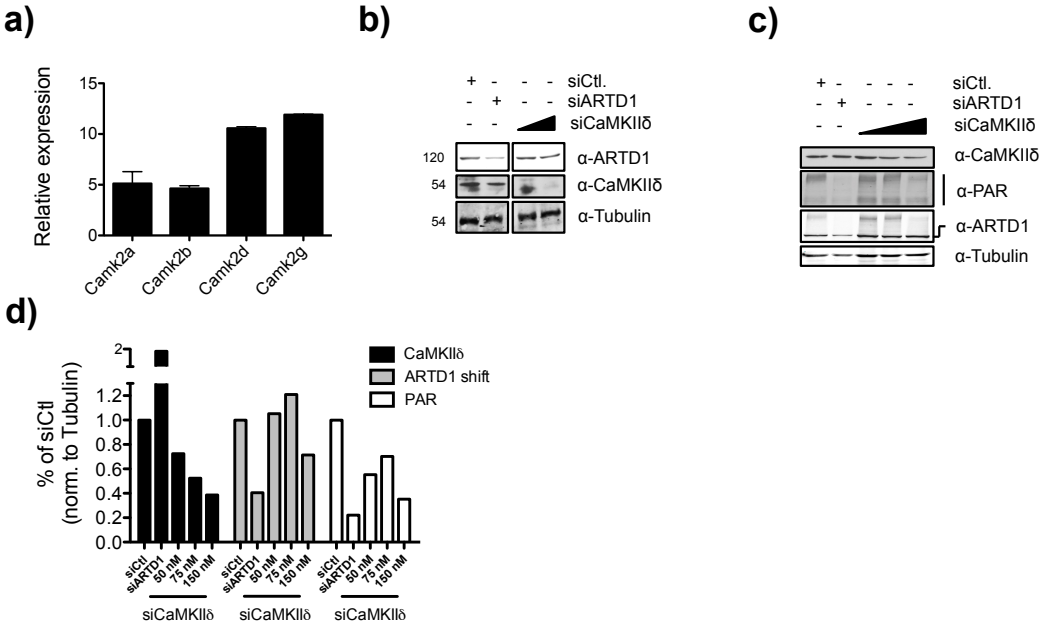
a)
Relative expression
15
10
5
0
Camk2a
Camk2b
Camk2d
Camk2g
b)
siCtl.
siARTD1
siCaMKIIδ
120
54
54
α-ARTD1
α-CaMKIIδ
α-Tubulin
c)
siCtl.
siARTD1
siCaMKIIδ
α-CaMKIIδ
α-PAR
α-ARTD1
α-Tubulin
d)
% of siCtl (norm. to Tubulin)
2
1.2
1.0
0.8
0.6
0.4
0.2
0.0
CaMKIIδ
ARTD1 shift
PAR
siCtl
siARTD1
50 nM
75 nM
150 nM
siCaMKIIδ

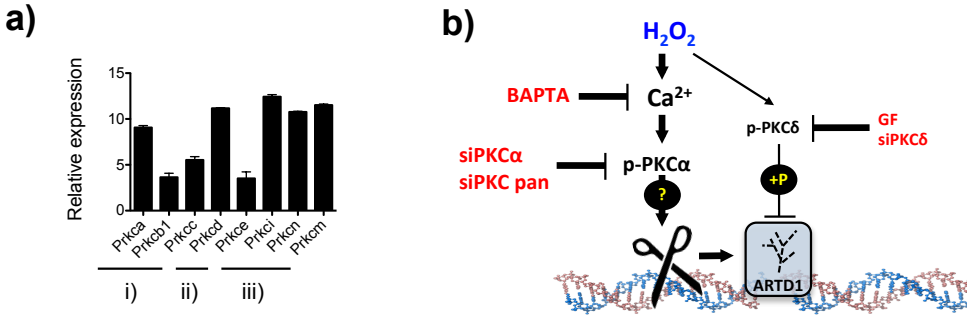
a)
Relative expression
15
10
5
0
Prkca
Prkcb1
Prkcc
Prkcd
Prkce
Prkci
Prkcn
Prkcm
i)
ii)
iii)
b)
H2O2
BAPTA
Ca2+
siPKCα
siPKC pan
p-PKCα
?
p-PKCδ
GF
siPKCδ
+P
ARTD1

3.1.3 Oxidative stress induced poly-ADP-ribose formation is initiated by a Calcium dependent nuclease

Oxidative stress induced poly-ADP-ribose formation is initiated by a calcium-dependent nuclease

Andrej Bluwstein[1,2], Nicole Grosse[1], Karolin Léger[1,2], Barbara van Loon[1], Michael O. Hottiger[1*]

[1]Institute of Veterinary Biochemistry and Molecular Biology, University of Zurich, Winterthurerstrasse 190, 8057 Zurich, Switzerland

[2]Life Science Zurich Graduate School, University of Zurich, 8057, Switzerland

*Corresponding author: Email: hottiger@vetbio.uzh.ch

Running title: Calcium-dependent PAR formation

Key words: Poly-ADP-ribosylation, ARTD1, PARP-1, PARP-2, genotoxic stress response, Calcium, nuclease

Abstract

The human genome is continuously exposed to various DNA damaging agents, which induce many types of DNA lesions. A major portion of these lesions represents DNA damages induced by reactive oxygen species (ROS). DNA lesions, induced by oxidative DNA damage, are expected to be repaired by the base excision repair pathway which is accompanied by a strong but short wave of nuclear poly-ADP-ribose (PAR) formation. The molecular details of the signalling processes that mediate this PAR formation are still largely under debate.

The results presented here show that a sub-lethal dose of H_2O_2 induced temporal PAR accumulation that depended on PLC, IP_3R and calcium release from the endoplasmatic reticulum. ROS itself was not responsible for the observed PAR formation. Most importantly, our findings indicate that H_2O_2 treatment induced DNA lesions in a calcium- and calmodulin dependent manner. Furthermore, preliminary experiments towards the identification of the nuclease, revealed that inflammaosome-induced nucleases or the recently described ER released and calcium-dependent DNAS1L3 are both not involved in H_2O_2-induced PAR formation. The work described here thus reveals an H_2O_2-induced, calcium-dependent endonuclease pathway that stimulates PAR formation in the nucleus.

Introduction

Nuclear and mitochondrial DNA is continuously exposed to endogenous or exogenous DNA damaging agents, which induce many types of DNA lesions (1). Per day, about 20'000 DNA lesions are endogenously formed in mammalian cells. Among the most important endogenous DNA damaging agents are reactive oxygen species (ROS), which can be produced as a result of exposure to toxic agents such as irradiation and environmental pollutants. The cell itself also produces ROS as byproducts of oxygen consuming enzymatic reactions, such as the mitochondrial respiratory chain (2). ROS are implicated in the cellular response to a variety of inflammatory stimuli and are also implicated in mediating apoptosis or programmed cell death and ischaemic injury, including stroke and heart attack (2). ROS constantly attack DNA and depending on the type and the extent of exposure, ROS also modify other vital cellular macromolecules such as lipids, proteins and RNA. One of the best-characterized oxidative DNA lesions is 7,8-dihydro-8-oxoguanine (8-oxo-G) (1). Cells have evolved a plethora of mechanisms to launch a specific response to different types of genotoxic stress in order to prevent the inheritance or repair of DNA damage (3,4). Incorporation of incorrect bases and DNA strand breaks can be repaired by proteins that specifically recognize such mutations or lesions.

ADP-ribosyltransferases (ARTs) synthesize mono- and poly-ADP-ribose (PAR) modifications on specific residues of target proteins by using nicotinamide adenine dinucleotide (NAD^+) as a substrate (5). The 18 human ART family members are divided into diphtheria toxin-like ARTs (ARTDs) and cholera toxin-like ARTs (ARTCs) (6) and have been implicated in a variety of biological functions (7,8). ARTD1 (PARP1) is the best-studied nuclear ART and has been linked to many chromatin-associated processes (9,10). The current scenario of oxidative stress-induced PAR formation describes that ARTD1 is activated in response to oxidative

DNA damage. Beside the possibility that the oxidation of nucleotides (such as 8-oxoG) can induce DNA strand breaks directly by a fenton-reaction (11), this DNA modification can also trigger a chain of events that starts with the activation of glycosylases (OGG1) and leads to the formation of an ARTD1-activating nick in the DNA as part of the base excision repair process. The ADP-ribose polymers (PAR) formed by ARTD1 were suggested to serve as "flag" marking the site of DNA damage and to assist the recruitment of further DNA repair adaptor and effector proteins (12,13), defining ARTD1 as a integral component of the efficient DNA repair machinery. Thus, inhibition of PAR formation by PARP inhibitors or deletion of ARTD1 sensitizes cells to the cytotoxic effects of DNA-damaging agents and impairs the viability of cells that suffered DNA damage. On the other hand, excessive PAR formation might lead to cell death in a complex, cell-type- and stimulus-dependent manner. Strong or prolonged activation of PAR formation causes NAD^+ and ATP depletion, severely impairs the energy-dependent functions of a cell, and changes the cell death program from apoptosis to necrosis (14). Under these conditions, PARP inhibitors prevent the depletion of NAD^+ and ATP and partially restored the cell's ability to carry out metabolic processes. In the case of excessive and sustained PAR formation, the polymers might also leave the nucleus and trigger the release of apoptosis inducing factor (AIF) from the outer mitochondrial membrane, thus mediating caspase-independent cell death termed parthanatos (15-18).

Under physiological genotoxic stress conditions (approx. 20'000 oxidative lesions per day and cell), ARTD1 does however not appear to be required for the above described BER, since ARTD1 knockout mice are viable and healthy (19), while mice deficient in one components of the BER machinery are all lethal (20-22). In accordance, re-analysing the BER impairment in $ARTD1^{-/-}$ cells indicated that

ARTD1 is not required for BER, but that ARTD1 rather reduces the BER kinetics (23,24). These data support a model where BER of physiological DNA damage occurs in a single, coordinated step that is ARTD1 independent. However, following DNA damage induction above normal endogenous levels and exceeding the level of the BER capacity, ARTD1 might play an important role in the stress response (25). Although this enzyme is strongly activated by double-stranded DNA *in vitro*, a direct induction of PAR formation *in vivo* through DNA damage has only been analysed in a correlative manner.

Signaling via calcium is a universal mechanism both in excitable and non-excitable cells. In a model of oxidative stress-induced cytotoxicity, several laboratories have demonstrated that a calcium (Ca^{2+}) signal was required for the activation of ARTD1 (26,27). Cellular Ca^{2+} is mainly stored in the endoplasmatic reticulum (ER), an organelle additionally responsible for folding and assembly of membrane and secreted proteins, synthesis of lipids as well as sterols (28,29). Both, oxidative stress and ER stress through ROS generation may increase Ca^{2+} leakage from the ER lumen (30-32). Notably, the Ca^{2+} concentration in the ER is 1'000-times greater than in the cytosol. The ER Ca^{2+} levels are modulated by the ER located Ca^{2+} release channels, inositol-1.4.5-trisphophate receptor (IP_3R) and the ryanodine receptor (RyR) (33,34). Ca^{2+} uptake on the other hand is mediated through the Sarco/Endoplasmic Reticulum calcium ATPase (SERCA) and numerous ER-associated enzymatic cascades (35). Mitochondria and the ER form a delicate network that is fundamental for the maintenance of cellular homeostasis and survival. In addition to a structural connection (32), there is dynamic exchange of Ca^{2+} ions between these two organelles, which regulates processes such as ER chaperone-assisted folding of newly synthesized proteins, regulation of mitochondria-localized de-hydrogenases involved in the Krebs cycle, and the activation of Ca^{2+}-dependent

enzymes that execute cell death programs (36). ER stress has been shown to trigger Ca^{2+} release from the ER and subsequent Ca^{2+} uptake by mitochondria (32). The efficiency of this process depends on the proximity between ER and mitochondria (37).

Here, we characterize the oxidative stress induced signalling cascade important for the formation of PAR. Our data provide evidence that Ca^{2+} release from the ER, though the signalling of PLC-catalysed IP_3 is essential for nuclear PAR formation by ARTD1. Moreover, we provide evidence that ROS, either exogenous or endogenous, as a consequence of the treatment of cells by H_2O_2 is not responsible for PAR formation. Furthermore, comet assays provide strong evidence, that the Ca^{2+} release is responsible for inducing DNA strand breaks. Finally, we exclude that an inflammasome induced caspase-dependent nuclease or the recently described DNAS1L3, which is Ca^{2+}-dependent and released after ER stress are not involved in H_2O_2-induced PAR formation. The nuclease responsible for the induction of strand-breaks leading to PAR formation remains thus to be identified.

Results

A sub-lethal dose of H_2O_2 induces temporal PAR formation

Although oxidative, stress-induced PAR formation was reported by several laboratories using high doses of hydrogen peroxide (H_2O_2), the molecular mechanism leading to PAR formation under non-lethal doses was so far not studied in detail. To investigate the molecular mechanism of PAR formation in response to sub-lethal oxidative stress, human primary fibroblasts (MRC-5) were pulse-treated with 0.1 or 0.5 mM H_2O_2. PAR formation was analyzed by immunofluorescence staining using the 10H anti-PAR antibody and data were collected by conventional fluorescence microscopy. PAR staining was observed as soon as 5 min after treatment and was no longer detectable at the 30 min time-point, independent on the dose used (Fig. 1A). To elucidate whether the applied doses induce cell death, cell viability was measured 24 hours after H_2O_2 treatment by the MTT assay and the proliferation ability after 10 days with a colony-forming assay (CFA). H_2O_2 doses of 1 mM or higher reduced cell viability significantly after 24 hours and did not allow the formation of colonies after 10 days (Fig. 1B,C). In contrast, H_2O_2 doses below 1 mM did not affect cell viability, but only impaired cell proliferation, suggesting that oxidative stress induced by concentrations below 1 mM H_2O_2 only induced a cell cycle arrest and possibly senescence (Fig. 1B,C). Repetition of these experiments with NIH/3T3 cells confirmed these observations, although these cells seemed to be more resistant to H_2O_2 (2 mM H_2O_2 was not lethal, Suppl. Fig. 1A,B). This experiment suggested, that the extent of PAR formation would be co-regulated by the ability of the cell to detoxify applied H_2O_2 molecules. Inhibition of catalase by 3-AT indeed extended PAR formation up to 40 min, indicating that the activity of this enzyme is strongly contributing to the kinetics of the induced PAR levels (Fig. 1D). A second treatment with the same H_2O_2 dose after 30 min also prolonged PAR formation, indicating that

the cells were not refractory after the first oxidative stress response and that the first H_2O_2 treatment did not deplete the NAD^+ pool to such an extent, that PAR formation was abrogated. To understand whether the half-life of H_2O_2 was also influencing cell viability, MRC-5 were treated with H_2O_2 in the presence of increasing amount of serum, which has been reported to scavenge H_2O_2 molecules (38). Indeed, cell viability improved from 0 – 1 % and almost completely abolished the cytotoxic effect of H_2O_2 even in response to 10 mM (Fig. 1E). Interestingly, PAR formation was also inhibited by increasing amount of serum (data not shown), suggesting a direct correlation between the amount of H_2O_2 molecules, the PAR signal and cell viability in response to H_2O_2.

H_2O_2-induced PAR formation depends on PLC, IP_3 and calcium release from the endoplasmic reticulum.

Oxidative stress induces cytosolic calcium accumulation as a fast response. To test whether early induction of PAR is influenced by calcium, human fibroblast were treated with a sub-lethal dose of H_2O_2 in the presence of small molecule inhibitors of components that are involved in Ca^{2+} signaling. Subsequent treatment with a sub-lethal H_2O_2 dose revealed that pretreatment with the endogenous calcium chelator BAPTA diminished PAR formation to comparable extent as the PARP inhibitor Olaparib (Fig. 2A,B). A direct effect of BAPTA on ARTD1 activity can be excluded, since ARTD1 automodification was not affected by the addition of BAPTA to the *in vitro* reaction (Suppl. Fig. S2A). Moreover, the inhibition of the IP_3 (IP_3R) or the Ryanodine receptor (RyR), two receptors located in the ER and involved in Ca^{2+} signaling, reduced PAR formation (Fig. 2A,B), confirming that Ca^{2+} is released from the ER upon H_2O_2 treatment. Assessing PAR formation by immunoblot analysis confirmed the above observations (Suppl. Fig. 2B). To exclude that the observed

effects were not due to an off-target effect of the tested inhibitors, the levels of all above-mentioned proteins were reduced by siRNA treatment and PAR formation was analyzed. Knocking-down ARTD1, IP_3R or RyR indeed reduced PAR formation upon H_2O_2 treatment significantly, confirming these proteins as part of the oxidative stress-induced signaling cascade that induces PAR formation through the release of Ca^{2+} (Fig. 2C,D and Suppl. Fig. 2C). To strengthen the conclusion, that IP_3 production by PLC at the cellular membrane is responsible for the observed PAR formation, PLC was inhibited and PAR formation subsequently induced by H_2O_2. Inhibition of phospholipase C (PLC) indeed reduced PAR formation substantially, indicating that oxidative events at the membrane may initiate a signaling cascade, which leads to the synthesis of IP_3 and the subsequent release of Ca^{2+} from the ER (Fig. 2A).

H_2O_2-induced calcium release is essential for PAR formation.

Calmodulin (CaM) is an important Ca^{2+} binding protein and calcium signal transducer (39). Application of small molecule inhibitors of CaM reduced PAR levels to the same extent as BAPTA, thus indicating its crucial involvement in regulating PAR formation upon H_2O_2 stress (Suppl. Fig. 2A). Moreover, knockdown of CaM3 almost completely abolished PAR formation upon H_2O_2 treatment and thus confirmed the results with the specific CaM inhibitor (Suppl. Fig. 2C,D). Inhibition of Cyclophilin D (CypD) and Complex I (NADH dehydrogenase), two mitochondrial proteins, did not affect H_2O_2-induced PAR formation, indicating that the mitochondrial permeability transition pore and electron transport chain are unlikely involved in these early signaling events (Fig. 2A,B and Suppl. Fig. 2B). Interestingly, also the scavenging of endogenous ROS by the treatment with NAC did not reduced PAR formation within the first 30 min, revealing that a possible perturbation of

mitochondria by Ca^{2+} and the subsequent release of endogenous ROS do not contribute to the observed PAR formation within the first few minutes after H_2O_2 treatment (Fig. 2E). Together these results suggested, that the initiating signal leading to PAR formation is not originating from the mitochondrial, but more likely generated by events at the plasma membrane. Under physiological conditions, Ca^{2+} is constantly leaking from the ER and needs to be pumped back to avoid the induction of mitochondrial ROS production, the activation ER-stress, or caspase dependent cell death (40,41). Inhibition of SERCA by thapsigargin (Tg) was reported to increase intracellular Ca^{2+} levels (42). Indeed, pre-treatment of cells with Tg prolonged the observed PAR formation up to 60 minutes, while treatment with the inhibitor alone was not able to induce PAR formation (Fig. 2F and Suppl. Fig. 2E). Together, these results provide strong evidence that the physiological fluctuation of Ca^{2+} is not sufficient to induce PAR formation, but that the enhanced release of Ca^{2+} by IP_3 is required to reach an intra-cellular Ca^{2+} threshold, which is important for PAR formation.

Sublethal doses of H_2O_2 induce the anti-oxidant response but not the unfolded protein response in ER.

H_2O_2 is reported to induce ER-stress and to activate the anti-oxidant response (43). To test whether this is the case under the conditions tested here, NIH/3T3 were treated with H_2O_2 for 10 min and the expression of marker genes involved in ER-stress (Calreticulin, BIP, Grp94) and the anti-oxidant response (SOD, GSR) was analyzed (11,44). As expected, ER-stress was affected by Tg treatment alone, but the response to H_2O_2 was not significant and combination of Tg and H_2O_2 did not affect the expression of the tested genes as compared to Tg treatment alone (Fig. 2G). BAPTA treatment alone, or in combination with H_2O_2, did not cause significant changes in

gene expression neither (Suppl. Fig. 2F). These results indicated, that ER-stress is not induced or enhanced by H_2O_2 treatment within the first 10 min, and therefore cannot contribute to calcium-dependent activity of ARTD1. In contrast, H_2O_2 treatment led to a fast expression of genes involved in the anti-oxidant response, which was also inhibited by BAPTA, indicating calcium-dependent activation of oxidative stress (Fig. 2H and Suppl. Fig. 2G). In summary, our data provide evidence for an early-induced oxidative stress response that leads to the release of Ca^{2+} via the PLC-IP_3R/RyR pathway and consecutive PAR formation.

The base excision repair pathway is not involved in PAR formation.

ARTD1 was described to be only activated in BER in cases where the number of DNA lesions exceeds the endogenous BER capacity (4). We thus analyzed the number of PAR foci induced upon H_2O_2 treatment in cells depleted of XRCC1 (which reduces the BER repair capacity). Oxidative stress induced the same amount of PAR foci in siXRCC1 and siMock treated cells (Fig. 3A), indicating that the initial activation of ARTD1 after H_2O_2 treatment is not dependent on the BER capacity. To analyze whether initiation of the BER pathway is required for initial PAR formation, WT and OGG1 MEFs were treated with H_2O_2 and PAR formation analyzed. Induction of PAR formation was comparable in both cell types. Kinetic experiments however revealed that removal of PAR was delayed at the 60 min time point, indicating that the presence of OGG1 is positively affecting PAR formation, but only at a late time point after treatment and that the initial strong PAR formation is induced by a mechanism distinct from BER (Fig. 3B).

H_2O_2 induces DNA lesions in a calcium dependent manner.

The current model of ARTD1 activation foresees that DNA is damaged by ROS either directly (e.g., induction of single strand breaks) or indirectly (e.g., induction of oxidative DNA lesions), which are subsequently repaired by BER (45). To confirm that treatment of cells with H_2O_2 indeed induces DNA strand breaks, cells were treated with different doses of H_2O_2 for either 3 or 20 min. Treatment with 50 μM H_2O_2 for 3 min already induced detectable DNA lesions as observed by the alkaline comet assay (Fig. 3C). Increasing the H_2O_2 concentration lead to an increased number of DNA lesions. Interestingly, extending the treatment period to 20 min led to no dramatic increase in DNA damage, indicating that the detoxification system reacted comparably to a 3 or 20 min H_2O_2 exposure (Fig. 3C). Moreover, there was no evidence for DNA breaks below 50 μM H_2O_2, which correlates with the minimal dose of H_2O_2 (50 μM) required to induce PAR (Suppl. Fig. 1A). In conclusion, we observed a positive correlation between the formation of DNA lesions and PAR formation in response to H_2O_2.

Since the alkaline comet assay does not distinguish between single or double-strand break formation, DNA damage was further analyzed by investigating markers of true DNA double strand breaks. The observed H_2O_2-induced DNA damage was very unlikely the accumulation of DNA double-strand breaks (DSBs), as treatment of cells with 6 Gy IR, which arrested cells in a CFA experiment, and induced early γH2AX and 53BP1 foci formation (DSB markers), was not able to induce PAR formation at all (Suppl. Fig 3A, B). In contrast, H_2O_2 treatment led to a delayed induction of γH2AX foci formation (peaking after 60 min), while showing no sign of 53BP1 foci formation at all (Fig. 3D-E). Together, these experiments indicated that H_2O_2 might induce single-strand DNA lesions which are converted into double-strand

DNA lesions (after 60 min) and which are different from a classical DNA damage response (DDR) induced upon irradiation.

To confirm that the induced DNA breaks are dependent on the Ca^{2+} release from the ER, the alkaline comet assay was performed in the presence of BAPTA. Co-treatment of cells with BAPTA and H_2O_2 significantly reduced DNA damage at two different time points (3 and 20 min; Fig. 3F). Interestingly, irradiation of cells with 5 or 20 Gy induced detectable DNA damage, which was however not inhibited by BAPTA, again indicating that the mechanism responsible for the DNA damage upon H_2O_2 treatment is not activated upon irradiation (Fig. 3G). Interestingly, BAPTA treatment also reduced γH2AX foci formation after 60 min recovery from IR, providing strong evidence that these foci are indeed generated from the single-strand lesions observed already at 3-10 min (Fig. 3H). Moreover, inhibition of ROS by NAC did not lead to a reduction in DNA break formation, which is in line with slightly elevated PAR formation upon NAC pretreatment, thus excluding ROS as a direct inducer of PAR upon H_2O_2 treatment (Fig. 3I). Finally, addition of H_2O_2 to irradiated cells led to a strong DNA break induction, which was abrogated in presence of BAPTA to the level of IR-induced DNA breaks (Fig. 3I). These results confirm calcium dependent formation of H_2O_2 induced SSBs rather than IR-induced DSBs and strongly correlate with PAR formation.

Inflammasome-induced nucleases or the ER released endonuclease, DNAS1L3, are not involved in H_2O_2-induced PAR formation.

The above reported findings eliminated the possibility that ROS directly induce DNA damage and rather pointed at a nuclease, which is either Ca^{2+}-dependent or which translocates to the nucleus in a Ca^{2+}-dependent manner. Several endonucleases have already been published to contribute to chromatin degradation during apoptosis in a

Ca^{2+}-dependent manner (46,47). Caspase-activated DNases (CAD) are the most favourable candidates (48). A calcium sensor (CasR) was recently described to be an important component linking Ca^{2+}release from the ER to the inflammasome and the activation caspase-1 (49). To investigate whether a CasR is involved in the observed H_2O_2-induced DNA damage, CasR was depleted by siRNA and PAR formation induced by H_2O_2 treatment. Knockdown of CasR did not reduce PAR formation, indicating that the inflammasome-induced nuclease is unlikely to induce PAR formation (data not shown). Furthermore, alkaline comet formation was analysed in cells treated with H_2O_2 in the presence of Z-VAD, a Pan Caspase inhibitor. The addition of Z-VAD did not inhibit DNA damage upon H_2O_2 treatment, indicating that CADs are unlikely involved in this process (Fig. 4A). Recently, an ER-released Ca^{2+}-dependent endonuclease was described to be important in internucleosomal DNA fragmentation including DNAS1L3 (50). Preliminary results did however not show an effect on PAR formation upon deletion of DNAS1L3 by siRNA, indicating that DNAS1L3 was neither involved in this process (data not shown).

Discussion

The results presented here show that a sub-lethal dose of H_2O_2 induced temporal PAR accumulation with fast kinetics and independent of the redox system of the cell. H_2O_2-induced PAR formation was dependent on PLC, IP_3R and calcium release from the endoplasmatic reticulum. Our findings indicate that H_2O_2 induces single-stranded DNA lesions in a calcium-dependent manner. Furthermore, we show that these DNA lesions were not generated by inflammasome-induced nucleases or the ER-released endonuclease DNAS1L3. The work described here thus reveals an H_2O_2-induced, Ca^{2+}-dependent endonuclease pathway that stimulates PAR formation in the nucleus.

Although the H_2O_2 dose was chosen not to induce immediate cell death, the reduction of colony formation after treatment indicates that the induced DNA lesions indeed affected long-term cell proliferation. This growth phenotype could be caused by defects in sister chromatid exchange or by the activation of cell cycle check points and the consecutive induction of senescence. Whether this phenotype was induced by the initial BER independent induction of DNA lesions, or by additional DNA lesions (e.g. OGG1-dependent DNA lesions, induced after 60 minutes), requires further experimental analysis. Moreover, Ca^{2+}-induced DNA lesions might be single-stranded DNA strand breaks, that are during S-Phase converted into double stranded DNA lesions (after 60 minutes) as observed by the induction of γH2AX foci. This hypothesis is strengthened by the observation, that γH2AX foci formation could also be inhibited by BAPTA, indicate that the Ca^{2+}-induced number of DNA lesions either exceeded the endogenous repair capacity for single-stranded DNA strand breaks or that the cellular repair system was not able to recognize or repair the induced single-strand DNA lesion due to other constrains. The S-phase induced conversion of single-strand to double-strand DNA breaks would thus provide an alternative way for

proliferating cells to repair the induced single strand breaks by double strand break repair pathways.

ARTD1 and its induced PAR formation have in general been traditionally implicated in the response to DNA damage. An important cornerstone for this model is the activation of ARTD1 by DNA *in vitro* and the detection of PAR upon treatment of cells with genotoxic compounds. A causative link between DNA lesions and the activation of ARTD1 *in vivo*, remained however on the correlative level. The first evidence for a fast activation of ARTD1 by signals evoked in the cell membrane, involving IP_3 and Ca^{2+} mobilization, was observed in neurons (51). In contrast to the above-presented data, these studies with neurons did not observe DNA breaks. Comparable to our studies, treatment of thymocytes with low concentrations of peroxynitrite induced rapid Ca^{2+} mobilization (1 to 3 min), DNA single-strand breakage and activation of ARTD1 (27), suggesting signals that can induce PAR formation originate at the plasma membrane, traverse the cytoplasm and finally reach the nucleus, where DNA strand breaks are induced and PAR formation is stimulated.

Whether the described signal pathway is the only required pathway for the induction of nuclear PAR formation remains to be confirmed, as PLC not only generates IP_3 , but also diacetylglycerol (DAG) which was described induce the PKC kinase family. Recent own observation indicated that the PKC family shows a dual role in the regulation of ARTD1 activity (manuscript submitted). While knockdown of the DAG-dependent PKCδ enhanced ARTD1 activity upon H_2O_2 treatment, knockdown of the calcium-dependent PKCα strongly reduced H_2O_2-induced PAR formation, indicating a calcium-dependent and DNA-independent regulation of ARTD1-induced PAR formation upon oxidative stress. Similarly, Ca^{2+}- signaling was essential for PAR formation as confirmed by the elimination of its formation after knockdown of Calmodulin. Whether Calmodulin is directly involved in the induction

of the endonuclease or activating a so far unidentified pathway that is additionally required (e.g. phosphorylation of ARTD1) needs additional clarification. Based on our own studies (manuscript submitted) we identified the calmodulin-dependent kinase IIδ (CaMKIIδ) as a positive regulator of ARTD1 activity upon oxidative stress, which is in line with previous observations in neurons (52,53) and may explain an alternative mechanism of ARTD1 modulation by kinase signaling.

ARTD1 and PARG have both been described to control extracellular Ca^{2+} fluxes, although as upstream regulators, through melastatin-like transient receptor potential 2 channels (TRPM2) in a cell death-signalling pathway (54). TRPM2 activation accounted for essentially the entire Ca^{2+} influx into the cytosol, activating caspases and causing the translocation of apoptosis inducing factor (AIF) from the inner mitochondrial membrane to the nucleus followed by cell death. ADP-ribose-loading of cells induced Ca^{2+} fluxes in the absence of oxidative damage, suggesting that ADP-ribose is the key metabolite of the ARTD1/PARG system regulating TRPM2, controlling a cell death signal pathway including different cell compartments.

β-lapachone (β-lap) was the first chemotherapeutic agent shown to elicit a Ca^{2+}-mediated cell death by ARTD1 hyperactivation at clinically relevant doses in cancer cells expressing elevated NAD(P)H:quinone oxidoreductase 1 (NQO1) levels (26). β-lap induced the NQO1-dependent generation of ROS and DNA breaks, and triggered Ca^{2+}-dependent γ-H2AX formation and ARTD1 hyperactivation. Reduction of ARTD1 activity or Ca^{2+} chelation protected cells. The same group reported that Ca^{2+} chelation abrogated H_2O_2, but not MNNG-induced ARTD1 hyperactivation and cell death suggesting hat the MNNG and H_2O_2-induced PAR formation might not be induced by a common mechanism (26). In contrast, own MNNG experiments revealed that also MNNG induced PAR formation can be strongly reduced by

BAPTA (data not shown), suggesting that MNNG, might induce also a Ca^{2+}-induced nuclease comparable to H_2O_2. Interestingly, the required minimal doses of MNNG to induce PAR, also induced cell death, suggesting that PAR formation might be induced as a secondary effect after alkylating DNA mutation. Moreover, MNNG induced PAR formation appeared later the H2O2-induced PAR formation and also remained longer (data not shown).

These studies provide strong evidence that H_2O_2 treatment induced an endonuclease that cleaves DNA and thereby induces PAR formation. Initial efforts to identify the responsible endonuclease revealed that the inflammasome-induced pathways and the ER-release DNAS1L3 are not involved in PAR formation. Several other possible nuclease candidates can however be foreseen, and should be experimentally analazed.

Together, these studies provide evidence that H_2O_2 treatment induces PAR formation not through oxidative damage of the DNA during the first 30 minutes, but rather induces through Ca^{2+} signaling an endonuclease, that induces single-strand lesions.

Experimental procedures

Cell culture, IR treatment, siRNA transfection and lysis

The MRC-5 and IMR-90 human lung fibroblast cell strains (20, 21) were obtained from the American Type Culture Collection (ATCC) and cultured in supplemented MEM (Invitrogen). NIH/3T3 from ATCC, shXRCC1 HeLa (kind gift of Dr. Roberta Minotti), OGG1 WT and KO MEFs (kind gift of Dr. Michaelo Razumenko) were cultured in supplemented DMEM (Invitrogen). Cells were preincubated with inhibitors (stocks dissolved in DMSO) for 1h prior to H_2O_2 treatment in FCS-free media, which was also used as a vehicle for H_2O_2. All inhibitors were obtained from Enzo Life Sciences, except from Olaparib (AstraZeneca), 3-AT (Sigma), and used at a final concentration as indicated in the figures or figure legends. To reduce isoform specific ARTD1, IP_3R or CaM expression, $2x10^5$ NIH/3T3 cells were transfected using mouse siARTD1 (AAGGGCAAGCACAGTGTCAAA, QIAGEN, SI02731428), siIP3R1 (CAGGGAAATGATGACCAAAGA, QIAGEN, SI01079085), siIP3R2 (CAGCCTGGGATTACAGAAATA, QIAGEN, SI02694293), siIP3R3 (CACCATGGAGTTCGTAGAAGA QIAGEN, SI01079099), siCaM1 (TAGAAGTGTGTTGCATTTAAA, QIAGEN, SI00940009), siCaM2 (CACAACTTGCCTCAAATCCAT, QIAGEN, SI00940044), siCaM-like3 (ATGGTGAATGAAATTGACAAA, QIAGEN, SI00940142) or siCtl. (scrambled sequence, lacking significant homology to any known mouse gene sequence) with Lipofectamine RNAiMAX transfection reagent (Invitrogen) according to manual's instructions over 3-4 days, prior to H_2O_2 treatment. Whole cell extracts were prepared with standard RIPA lysis buffer (50 mM Tris/pH8, 400mM NaCl, 0.5% NP-40, 1% DOC, 0.1% SDS supplemented with proteinase inhibitor cocktail (Roche), 10 mM β-glycerolphosphate, 1mM NaF and DTT) and total protein concentration determined using standard Lowry method.

Immunoblotting

For immunoblot analysis, proteins were separated by SDS PAGE gel electrophoresis and bands were visualized by either using horseradish peroxidase-conjugated antibodies (1:5000, GE Healthcare) and ECL detection (GE Healthcare) or by using IR-Dye-conjugated antibodies (1:15000, LI-COR) and detection by the Odyssey

infrared imaging system (LI-COR). For quantification, bands were analyzed by ImageJ 1.46 (35) and the Odyssey imaging software (LI-COR).
Antibodies used for immuneblotting were anti-PARP1/2 (Santa Cruz), anti-PAR (10H, homemade), anti-Tubulin (1:10'000, Sigma), anti-β-Actin (CST). If not else stated, antibody dilution was 1:1000.

Immunofluorescence (IF) microscopy

For PAR- IF analysis $1.5x10^5$ NIH/3T3 and Raw 264.1 or $2.5x10^4$ MEF, MRC-5 and IMR-90 cells were grown on cover slips overnight prior to inhibitor/activator preincubation and H_2O_2 treatment. Afterwards cells were washed with PBS (1x), fixed with ice-cold methanol and acetic acid (3:1) for 10 min at 4°C, washed with PBS (3x), blocked in 5% milk/0.05% Tween-20 in PBS for 30 min and stained immunohistochemically with primary mouse anti-poly(ADP-ribose) IgG, 1:250 (10H, homemade) or anti-PARP1/2 rabbit IgG, 1:250 (Santa Cruz). Next, cells were washed with PBS (3x) before hybridization with a secondary antibody (1:250 Cy3 conjugated anti-mouse IgG, Jackson ImmunoResearch or 1:250 Alexa Fluor 488 ocnjugated anti-rabbit IgG, Invitrogen). Eventually, cells were mounted on glass slides using DAPI-containing VECTASHIELD (Vector Labs) and images acquired using an inverted fluorescence microscope at 40x, oil immersion (Leica). Fluorescence intensity or foci number were quantified using ImageJ (v. 1.46r) or Imaris (v. 7.6.0, Bitplane) and equal set-up between the images and experiments. For γH2A.X or 8-OxoG- IF analysis, experiment performed as described above using ice cold methanol for fixation, blocking with 10% FCS in PBS and immunostaining with primary mouse anti-Histone H2A.X Phospho (Ser139) IgG1, 1:500 (Millipore) or mouse anti-8-oxoguanine IgM, 1:250 (Millipore) and secondary FITC conjugated anti-mouse IgG,1:250 or TexasRed AffiniPure F(ab')$_2$ fragment donkey anti-mouse IgM μ chain, 1:250 (Jackson ImmunoResearch). For 53BP1- IF analysis, experiment performed as described above fixing cells with 4% paraformaldehyde (PFA), washing with PBS (2x) and permeabilization by 0.25% Triton X100 in PBS for 5 min followed by brief washing (2x) before applying blocking solution (5% milk/0.05% Tween-20 in PBS) and immunostaining with primary rabbit anti-53BP1 IgG, 1:300 (Santa Cruz) and secondary Cy3 conjugated anti-rabbit IgG, 1:250 (Jackson ImmunoResearch).

RNA extraction and real-time PCR analysis

Cells were harvested either by trypsin or directly lysed on the plate in lysis buffer. RNA extraction was performed with the NucleoSpin® RNA II kit (Macherey-Nagel, Düren, Germany). RNA was quantified with a NanoDrop (ThermoFisherScintific, Waltham, MS, USA) and reverse transcribed according to the supplier's protocol (High Capacity cDNA Reverse Transcription Kit, Applied Biosystems, Foster City, CA, United States).

Quantitative-real-time polymerase chain reactions (qPCR) were performed with SYBR® green SensiMix SYBR Hi-ROX Kit (Bioline Reagents Ltd, London, UK) and a Rotor-Gene Q 2plex HRM System (Qiagen, Hilden, Germany).

Alkaline Comet assay

5x105 Raw 264.1 or NIH/3T3s were grown over night in 6-well-plates before inhibitor/activator preincubation for 1 h followed by H2O2 treatment. Raw and NIH/3T3 cells were collected by scrapping and Trypsin/EDTA (Invitrogen) accordingly, span down and diluted to 3-4x105 for Comet Assay, which was performed according to the manufacture's recommendations (Trevigen).

Cell proliferation and viability assay

Cell proliferation was determined by the clonogenic assay as described elsewhere (55). AlamarBlue® assay (Invitrogen, Carlsbad, CA, USA) or MTT assay (Sigma) were used to measure cell viability.

References

1. Markkanen, E., Hubscher, U. and van Loon, B. (2012) Regulation of oxidative DNA damage repair: the adenine:8-oxo-guanine problem. *Cell Cycle*, **11**, 1070-1075.
2. Cai, H. and Harrison, D.G. (2000) Endothelial dysfunction in cardiovascular diseases: the role of oxidant stress. *Circ Res*, **87**, 840-844.
3. Zhou, B.B. and Elledge, S.J. (2000) The DNA damage response: putting checkpoints in perspective. *Nature*, **408**, 433-439.
4. Dianov, G.L. and Hubscher, U. (2013) Mammalian base excision repair: the forgotten archangel. *Nucleic Acids Res*.
5. Hassa, P.O., Haenni, S., Elser, M. and Hottiger, M.O. (2006) Nuclear ADP-ribosylation reactions in mammalian cells: where are we today and where are we going? *Microbiol Mol Biol Rev*, **70**, 789-829.
6. Hottiger, M.O., Hassa, P.O., Lüscher, B., Schüler, H. and Koch-Nolte, F. (2010) Toward a unified nomenclature for mammalian ADP-ribosyltransferases. *Trends Biochem Sci*, **35**, 208-219.
7. Luo, X. and Kraus, W.L. (2012) On PAR with PARP: cellular stress signaling through poly(ADP-ribose) and PARP-1. *Genes Dev*, **26**, 417-432.
8. Schreiber, V., Dantzer, F., Ame, J.-C. and De Murcia, G. (2006) Poly(ADP-ribose): novel functions for an old molecule. *Nat Rev Mol Cell Biol*, **7**, 517-528.
9. Kraus, W.L. and Hottiger, M.O. (2013) PARP-1 and gene regulation: Progress and puzzles. *Mol Aspects Med*.
10. Hassa, P.O. and Hottiger, M.O. (2008) The diverse biological roles of mammalian PARPs, a small but powerful family of poly-ADP-ribose polymerases. *Front Biosci*, **13**, 3046-3082.

11. Jones, D.P. (2008) Radical-free biology of oxidative stress. *Am J Physiol Cell Physiol*, **295**, C849-C868.
12. De Vos, M., Schreiber, V. and Dantzer, F. (2012) The diverse roles and clinical relevance of PARPs in DNA damage repair: Current state of the art. *Biochem Pharmacol*, **84**, 137-146.
13. Trucco, C., Oliver, F., de Murcia, G. and Ménissier-de Murcia, J. (1998) DNA repair defect in poly(ADP-ribose) polymerase-deficient cell lines. *Nucleic Acids Res*, **26**, 2644-2649.
14. Berger, N.A., Sims, J.L., Catino, D.M. and Berger, S.J. (1983) Poly(ADP-ribose) polymerase mediates the suicide response to massive DNA damage: studies in normal and DNA-repair defective cells. *Princess Takamatsu Symp*, **13**, 219-226.
15. Andrabi, S.A., Kim, N.S., Yu, S.W., Wang, H., Koh, D.W., Sasaki, M., Klaus, J.A., Otsuka, T., Zhang, Z., Koehler, R.C. *et al.* (2006) Poly(ADP-ribose) (PAR) polymer is a death signal. *Proc Natl Acad Sci USA*, **103**, 18308-18313.
16. Wang, Y., Kim, N.S., Haince, J.F., Kang, H.C., David, K.K., Andrabi, S.A., Poirier, G.G., Dawson, V.L. and Dawson, T.M. (2011) Poly(ADP-ribose) (PAR) binding to apoptosis-inducing factor is critical for PAR polymerase-1-dependent cell death (Parthanatos). *Sci Signal*, **4**, ra20.
17. Yu, S.-W., Andrabi, S., Wang, H., Kim, N., Poirier, G., Dawson, T. and Dawson, V. (2006) Apoptosis-inducing factor mediates poly(ADP-ribose) (PAR) polymer-induced cell death. *Proc Natl Acad Sci USA*, **103**, 18314-18319.
18. Yu, S.-W., Wang, H., Poitras, M., Coombs, C., Bowers, W., Federoff, H., Poirier, G., Dawson, T. and Dawson, V. (2002) Mediation of poly(ADP-ribose) polymerase-1-dependent cell death by apoptosis-inducing factor. *Science*, **297**, 259-263.

19. Wang, Z., Auer, B., Stingl, L., Berghammer, H., Haidacher, D., Schweiger, M. and Wagner, E. (1995) Mice lacking ADPRT and poly(ADP-ribosyl)ation develop normally but are susceptible to skin disease. *Genes Dev*, **9**, 509-520.
20. Gu, H., Marth, J.D., Orban, P.C., Mossmann, H. and Rajewsky, K. (1994) Deletion of a DNA polymerase beta gene segment in T cells using cell type-specific gene targeting. *Science*, **265**, 103-106.
21. Tebbs, R.S., Flannery, M.L., Meneses, J.J., Hartmann, A., Tucker, J.D., Thompson, L.H., Cleaver, J.E. and Pedersen, R.A. (1999) Requirement for the Xrcc1 DNA base excision repair gene during early mouse development. *Dev Biol*, **208**, 513-529.
22. Xanthoudakis, S., Smeyne, R.J., Wallace, J.D. and Curran, T. (1996) The redox/DNA repair protein, Ref-1, is essential for early embryonic development in mice. *Proc Natl Acad Sci USA*, **93**, 8919-8923.
23. Strom, C.E., Johansson, F., Uhlen, M., Szigyarto, C.A., Erixon, K. and Helleday, T. (2011) Poly (ADP-ribose) polymerase (PARP) is not involved in base excision repair but PARP inhibition traps a single-strand intermediate. *Nucleic Acids Res*, **39**, 3166-3175.
24. Allinson, S.L., Dianova, II and Dianov, G.L. (2003) Poly(ADP-ribose) polymerase in base excision repair: always engaged, but not essential for DNA damage processing. *Acta Biochim Pol*, **50**, 169-179.
25. Woodhouse, B. and Dianov, G. (2008) Poly ADP-ribose polymerase-1: an international molecule of mystery. *DNA Repair (Amst)*, **7**, 1077-1086.
26. Bentle, M., Reinicke, K., Bey, E., Spitz, D. and Boothman, D. (2006) Calcium-dependent modulation of poly(ADP-ribose) polymerase-1 alters cellular metabolism and DNA repair. *J Biol Chem*, **281**, 33684-33696.

27. Virag, L., Scott, G.S., Antal-Szalmas, P., O'Connor, M., Ohshima, H. and Szabo, C. (1999) Requirement of intracellular calcium mobilization for peroxynitrite-induced poly(ADP-ribose) synthetase activation and cytotoxicity. *Mol Pharmacol*, **56**, 824-833.

28. Gething, M.J. and Sambrook, J. (1992) Protein folding in the cell. *Nature*, **355**, 33-45.

29. Kaufman, R.J. (1999) Stress signaling from the lumen of the endoplasmic reticulum: coordination of gene transcriptional and translational controls. *Genes Dev*, **13**, 1211-1233.

30. Berridge, M.J., Bootman, M.D. and Roderick, H.L. (2003) Calcium signalling: dynamics, homeostasis and remodelling. *Nat Rev Mol Cell Biol*, **4**, 517-529.

31. Gorlach, A., Klappa, P. and Kietzmann, T. (2006) The endoplasmic reticulum: folding, calcium homeostasis, signaling, and redox control. *Antioxid Redox Signal*, **8**, 1391-1418.

32. Giorgi, C., De Stefani, D., Bononi, A., Rizzuto, R. and Pinton, P. (2009) Structural and functional link between the mitochondrial network and the endoplasmic reticulum. *Int J Biochem Cell Biol*, **41**, 1817-1827.

33. Hajnoczky, G., Csordas, G., Madesh, M. and Pacher, P. (2000) Control of apoptosis by IP(3) and ryanodine receptor driven calcium signals. *Cell Calcium*, **28**, 349-363.

34. Hanson, C.J., Bootman, M.D. and Roderick, H.L. (2004) Cell signalling: IP3 receptors channel calcium into cell death. *Curr Biol*, **14**, R933-R935.

35. Csordas, G. and Hajnoczky, G. (2009) SR/ER-mitochondrial local communication: calcium and ROS. *Biochim Biophys Acta*, **1787**, 1352-1362.

36. Franzini-Armstrong, C. (2007) ER-mitochondria communication. How privileged? *Physiology*, **22**, 261-268.

37. de Brito, O.M. and Scorrano, L. (2008) Mitofusin 2 tethers endoplasmic reticulum to mitochondria. *Nature*, **456**, 605-610.

38. Oowada, S., Endo, N., Kameya, H., Shimmei, M. and Kotake, Y. (2012) Multiple free-radical scavenging capacity in serum. *J Clin Biochem Nutr*, **51**, 117-121.

39. Hoeflich, K.P. and Ikura, M. (2002) Calmodulin in action: diversity in target recognition and activation mechanisms. *Cell*, **108**, 739-742.

40. Berridge, M.J. (2002) The endoplasmic reticulum: a multifunctional signaling organelle. *Cell Calcium*, **32**, 235-249.

41. Janssen, K., Horn, S., Niemann, M.T., Daniel, P.T., Schulze-Osthoff, K. and Fischer, U. (2009) Inhibition of the ER Ca2+ pump forces multidrug-resistant cells deficient in Bak and Bax into necrosis. *J Cell Sci*, **122**, 4481-4491.

42. Jones, K.T. and Sharpe, G.R. (1994) Thapsigargin raises intracellular free calcium levels in human keratinocytes and inhibits the coordinated expression of differentiation markers. *Exp Cell Res*, **210**, 71-76.

43. Malhotra, J.D. and Kaufman, R.J. (2007) Endoplasmic reticulum stress and oxidative stress: a vicious cycle or a double-edged sword? *Antioxid Redox Signal*, **9**, 2277-2293.

44. Zhang, K. and Kaufman, R.J. (2008) From endoplasmic-reticulum stress to the inflammatory response. *Nature*, **454**, 455-462.

45. Caldecott, K.W. (2008) Single-strand break repair and genetic disease. *Nat Rev Genet*, **9**, 619-631.

46. Lee, M.J., Kee, K.H., Suh, C.H., Lim, S.C. and Oh, S.H. (2009) Capsaicin-induced apoptosis is regulated by endoplasmic reticulum stress- and calpain-mediated mitochondrial cell death pathways. *Toxicology*, **264**, 205-214.

47. Norberg, E., Gogvadze, V., Vakifahmetoglu, H., Orrenius, S. and Zhivotovsky, B. (2010) Oxidative modification sensitizes mitochondrial apoptosis-inducing factor to calpain-mediated processing. *Free Radic Biol Med*, **48**, 791-797.

48. Nagata, S. (2000) Apoptotic DNA fragmentation. *Exp Cell Res*, **256**, 12-18.

49. Lee, G.S., Subramanian, N., Kim, A.I., Aksentijevich, I., Goldbach-Mansky, R., Sacks, D.B., Germain, R.N., Kastner, D.L. and Chae, J.J. (2012) The calcium-sensing receptor regulates the NLRP3 inflammasome through Ca2+ and cAMP. *Nature*, **492**, 123-127.

50. Errami, Y., Naura, A.S., Kim, H., Ju, J., Suzuki, Y., El-Bahrawy, A.H., Ghonim, M.A., Hemeida, R.A., Mansy, M.S., Zhang, J. *et al.* (2013) Apoptotic DNA fragmentation may be a cooperative activity between caspase-activated deoxyribonuclease and the poly(ADP-ribose) polymerase-regulated DNAS1L3, an endoplasmic reticulum-localized endonuclease that translocates to the nucleus during apoptosis. *J Biol Chem*, **288**, 3460-3468.

51. Homburg, S., Visochek, L., Moran, N., Dantzer, F., Priel, E., Asculai, E., Schwartz, D., Rotter, V., Dekel, N. and Cohen-Armon, M. (2000) A fast signal-induced activation of Poly(ADP-ribose) polymerase: a novel downstream target of phospholipase c. *J Cell Biol*, **150**, 293-307.

52. Ju, B.-G., Solum, D., Song, E., Lee, K.-J., Rose, D., Glass, C. and Rosenfeld, M. (2004) Activating the PARP-1 sensor component of the groucho/ TLE1 corepressor complex mediates a CaMKinase IIdelta-dependent neurogenic gene activation pathway. *Cell*, **119**, 815-829.

53. Midorikawa, R., Takei, Y. and Hirokawa, N. (2006) KIF4 motor regulates activity-dependent neuronal survival by suppressing PARP-1 enzymatic activity. *Cell*, **125**, 371-383.

54. Blenn, C., Wyrsch, P., Bader, J., Bollhalder, M. and Althaus, F.R. (2011) Poly(ADP-ribose)glycohydrolase is an upstream regulator of Ca2+ fluxes in oxidative cell death. *Cell Mol Life Sci*, **68**, 1455-1466.

55. Franken, N.A., Rodermond, H.M., Stap, J., Haveman, J. and van Bree, C. (2006) Clonogenic assay of cells in vitro. *Nature Protoc*, **1**, 2315-2319.

Author Contributions

A.B. designed and performed experiments; N.G. performed and analysed the comet assays; K.L. performed gene expression analysis; B.vL. and M.O.H. supervised the work and M.O.H. wrote the manuscript.

The authors declare that they have no conflict of interest.

Acknowledgements

Roberta Minotti (Former member of the IVBMB, University of Zurich, Switzerland) is acknowledged for providing the shXRCC1 HeLa cells. Mykhailo Razumenko (University Hospital Zurich, Switzerland) is acknowledged for providing the OGG1 WT and KO MEFs. Florian Freimoser (University of Zurich, Switzerland) provided editorial assistance and critical input during the writing. This work was supported in part by the Swiss National Science Foundation Grants 31-122421, Mäxi-Foundation and the Kanton of Zurich (to M.O.H.).

Figure Legends

Fig. 1. Induction of early PAR in response to low, non-lethal H_2O_2 doses depends on the cellular redox system. a) PAR-IF kinetic analysis of MRC-5 upon increasing dosage of H_2O_2. **b)** Viability assay (MTT) of primary MRC-5, pulse-treated with increasing dosage of H_2O_2 for 15 min and recovery for 24 h. **c)** Colony forming assay (CFA) of MRC-5 pulse-treated with increasing dosage of H_2O_2 for 15 min and recovery for 10 days. **d)** PAR-IF analysis of MRC-5 either directly treated with 0.5 mM H_2O_2 for 10-40 min or pretreated with 30 mM 3-AT (catalase inhibitor) prior to H_2O_2 treatment for 10-40 min. In another case, H_2O_2 treated cells (30 min) were boosted with 0.5 mM H_2O_2 (final) and fixed either 3 min ("30 min") or 10 min ("40 min") after stimulation with freshly added H_2O_2. e) Viability assay (MTT) of primary MRC-5, pulse-treated with increasing dosage of H_2O_2 (supplemented with increasing amount FCS) for 15 min and recovery for 24 h. Data are mean +/- SD by t-test with *p<0.05, **p<0.01, ***p<0.001, n.s. not significant. Significant only in case of reduction to control (U). Fold induction to U (untreated = 0 mM H_2O_2).

Fig. 2. H_2O_2-induced PAR formation is dependent on PLC, IP_3 and calcium release from the endoplasmic reticulum. a) PAR-IF analysis of IMR-90 preincubated with selected inhibitors or DMSO (control) followed by 0.1 mM H_2O_2 treatment or left untreated. **b)** Quantification of PAR intensity per nucleus from a). 10-20 nuclei analyzed per area (n=10). **c)** PAR-IF analysis of NIH/3T3 transfected with siRNA against IP_3R1-3 (siCtl. or siARTD1 used as control) followed by 0.5 mM H_2O_2 treatment. For quantification of PAR foci or intensity 50 nuclei analyzed / area (n=5). **d)** PAR-IF analysis of NIH/3T3 transfected with siRNA against RyR1 (siCtl. or siARTD1 used as control) followed by 0.5 mM H_2O_2 treatment. **e)** PAR-immunoblotting analysis of NIH/3T3, preincubated for 1 h with selected inhibitors or

DMSO (control) followed by 0.5 mM H_2O_2 treatment or left untreated. Tubulin was used as loading control. **f)** PAR-IF analysis of thapsigargin (Tg) treated NIH/3T3 for 1 h, before H_2O_2 treatment for 10-60 min. Quantification of PAR foci number over time determined by analyzing 100-200 nuclei per independent experiment (n=3). **g-h)** Gene expression analysis of ER-stress genes (Calreticulin, BIP, Grp94) and anti-oxidant response genes (SOD2, GSR) in NIH/3T3 treated with 0.5 mM H2O2 for 10 min, before RNA extraction. In some cases, cells were perincubated with 10 μM BAPTA or 1 μM thapsigargin for 1 h before addition of H_2O_2. DMSO was used as control. Data are mean +/- SD by t-test with *p<0.05, **p<0.01, ***p<0.001, n.s. not significant. Scale bars, 25 μm. Concentrations of inhibitors (μM, if not else stated) are indicated behind the compound name. Ola = Olaparib (ARTD1/2 inghibitor), BAPTA (Ca2+ chelator), 2-APB (IP3R inhibitor), Dn = Dantrolen (RyR inhibitor), D609 (PLC inhibitor), U73 = U73221 (PLC inhibitor), CsA = Cyclosporine A (Cyclophilin D inhibitor), FK506 (Calcineurin inhibitor), NAC (ROS inhibitor).

Fig. 3 H_2O_2 induces single-stranded DNA lesions in a calcium dependent manner. a) PAR-IF analysis of stably transduced HeLa with shXRCC1, treated with 0.5 mM H_2O_2 and recovery for 10 min. For quantification 50 nuclei per area were analyzed (n=3). **b)** PAR-IF analysis of OGG1 KO MEF treated with 0.5 mM H_2O_2 for the indicated time points. For quantification 50 nuclei per area were analyzed (n=3). **c)** Alkaline comet assay of NIH/3T3, treated with increasing concentration of H_2O_2 for the indicated time points (50 nuclei analyzed / independent experiment, n=2). **d)** IF analysis of MRC-5 treated with 0.5 mM H_2O_2 for 10-60 min followed by fixation and immunostaining with anti-PAR (red), anti-γH2A.X (green) or anti-53BP1 (red) and counterstaining with DAPI (blue). **e)** Quantification of PAR and γH2A.X foci

number from d) (10-20 nulcei analyzed / area, n=5). **f)** Alkaline comet assay of NIH/3T3 preincubated with BAPTA (10 μM) followed by 25 and 50 μM H_2O_2 treatment for 3-20 min (50 nuclei analyzed / independent experiment, n=2). **g)** Alkaline comet assay of NIH/3T3 preincubated with BAPTA (20 μM), PMA (0.2 μM), Olaparib (1 μM) or DMSO (control) followed by H_2O_2 treatment with 100 μM and incubation for 3 min before lysis (50 nuclei analyzed / independent experiment, n=2). In some cases cells were treated with KBrO3 (3 min) or 5-20 Gy X-rays (15 min recovery). **h)** γH2A.X-IF staining of NIH/3T3 preincubated with BAPTA (10 μM) or DMSO (control) followed by 0.1 mM H_2O_2 treatment for 10-60 min. **i)** Alkaline comet assay of NIH/3T3 preincubated with BAPTA (20 μM) or NAC (30 mM) followed by H_2O_2 treatment with 100 μM and incubation for 3 min before lysis (50 nuclei analyzed / independent experiment, n=2). In some cases cells were treated with KBrO3 (30 mM, 1 h) or MNNG (50 μM, 1 h) or 20 Gy X-rays (15 min recovery). For quantification 50 nuclei analyzed / area (n=6). Data are mean +/- SD by t-test with *p<0.05, **p<0.01, ***p<0.001, n.s. not significant.

Figure 4. Nuclease X is activated/released in a Calcium-dependent manner. a) Alkaline comet assay of NIH/3T3 preincubated with BAPTA (20 μM), Z-VAD (50 μM) or DMSO (control) followed by H_2O_2 treatment with 100 μM and incubation for 3 - 20 min before lysis and electrophoresis (50 nuclei analyzed / independent experiment, n=2). Data are mean +/- SD by t-test with *p<0.05, **p<0.01, ***p<0.001, n.s. not significant.

Supplementary Figure Legends

Supplementary Figure 1. Induction of early PAR in response to low, non-lethal H_2O_2 doses depends on the cellular redox system. **a)** PAR-IF kinetic analysis NIH/3T3 upon increasing dosage of of H_2O_2 treated for the indicated time points. **b)** Viability assay (AlamarBlue) of NIH/3T3, treated with increasing dosage of H_2O_2 for 24 h. Data are mean +/- SD by t-test with ***p<0.001. Scale bar = 25 μm.

Supplementary Figure 2. H_2O_2 induced calcium release from the ER positively regulates PAR induction and the cellular antioxidant response.

a) ARTD1 auto-modification assay in presence of increasing amount of BAPTA 1-10 μM using radioactive-labeled NAD. PJ-34 (1-10 μM) and DMSO (1-10 μl) were used as positive and negative control, respectively. Coomassie blue staining of the gel was used as loading control. **b)** PAR-immunoblotting analysis of NIH/3T3, preincubated for 1 h with selected inhibitors (indicated below the quantification bars) or DMSO (control) followed by 0.5 mM H_2O_2 treatment or left untreated. Tubulin was used as loading control. **c)** KD efficiency from transfections in Fig. 2c and from Suppl. Fig. 2d determined by quantitative PCR. For each siRNA ARTD1 expression levels were determined to rule out off-target effects due to reduced ARTD1 levels. **d)** PAR-immunofluorescence analysis of NIH/3T3 transfected with siRNA against CaM1-3 (siCtl. or siARTD1 used as control) followed by 0.5 mM H_2O_2 treatment. For quantification of PAR foci or intensity 50 nuclei analyzed / area (n=5). **e)** PAR-IF analysis of thapsigargin (Tg) treated NIH/3T3 for 1 h, before H_2O_2 treatment for 10-60 min. Quantification of PAR foci number over time determined by analyzing 100-200 nuclei per independent experiment (n=3). **f-g)** Gene expression analysis of ER-stress genes (Calreticulin, BIP, Grp94) and anti-oxidant response genes (SOD2, GSR)

in NIH/3T3 treated with 0.5 mM H_2O_2 for 10 min, before RNA extraction. In some cases, cells were perincubated with 10 μM BAPTA or 1 μM thapsigargin for 1 h before addition of H_2O_2. DMSO was used as control. Data are mean +/- SD by t-test with *p<0.05, **p<0.01, ***p<0.001, n.s. not significant. Scale bars, 25 μm. Concentrations of inhibitors (μM, if not else stated) are indicated behind the compound name.

Supplementary Figure 3. Early induction of DNA double-strand breaks upon IR. **a)** IF analysis of MRC-5 treated with 6 Gy X-rays for 10-60 min followed by fixation and immunostaining with anti-PAR (red), anti-γH2A.X (green) or anti-53BP1 (red) and counterstaining with DAPI (blue). **b)** Colony forming assay (CFA) of primary MRC-5 irradiated with an increasing dose of X-rays or untreated (control) and recovery for 10 days (n=8-16). Data are mean +/- SD by t-test with *p<0.05, **p<0.01, ***p<0.001, n.s. not significant.

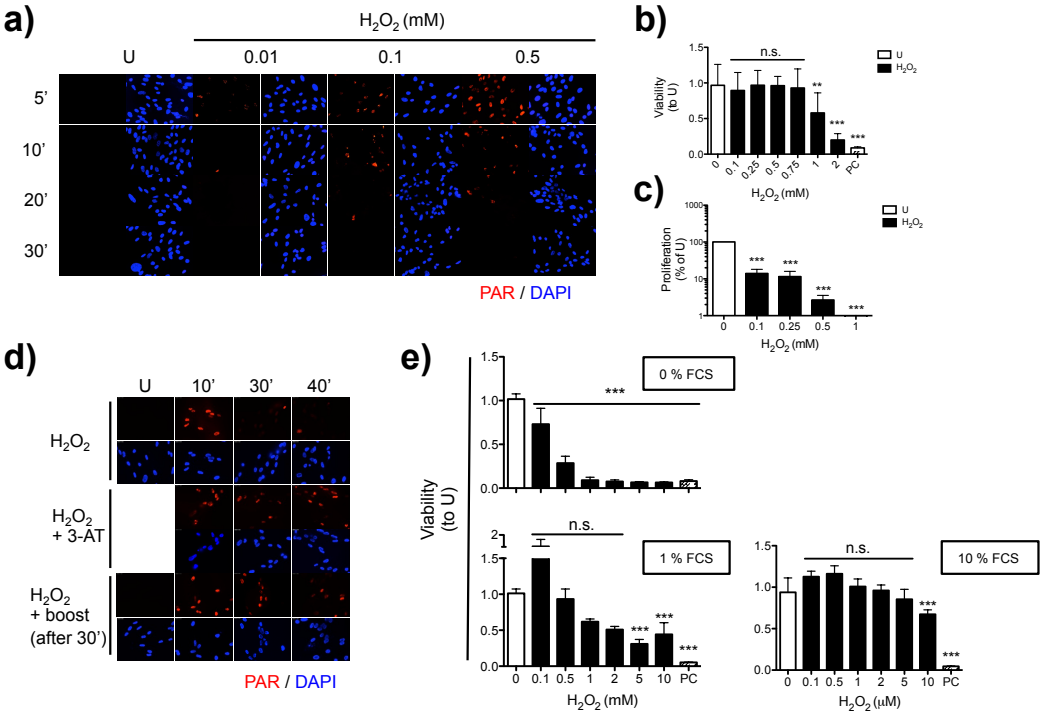
a)
H_2O_2 (mM)
U
0.01
0.1
0.5
5'
10'
20'
30'
PAR / DAPI
b)
Viability (to U)
n.s.
U
H_2O_2
H_2O_2 (mM)
c)
Proliferation (% of U)
H_2O_2 (mM)
d)
U
10'
30'
40'
H_2O_2
H_2O_2 + 3-AT
H_2O_2 + boost (after 30')
PAR / DAPI
e)
Viability (to U)
0 % FCS
1 % FCS
10 % FCS
n.s.
H_2O_2 (mM)
H_2O_2 (µM)
PC

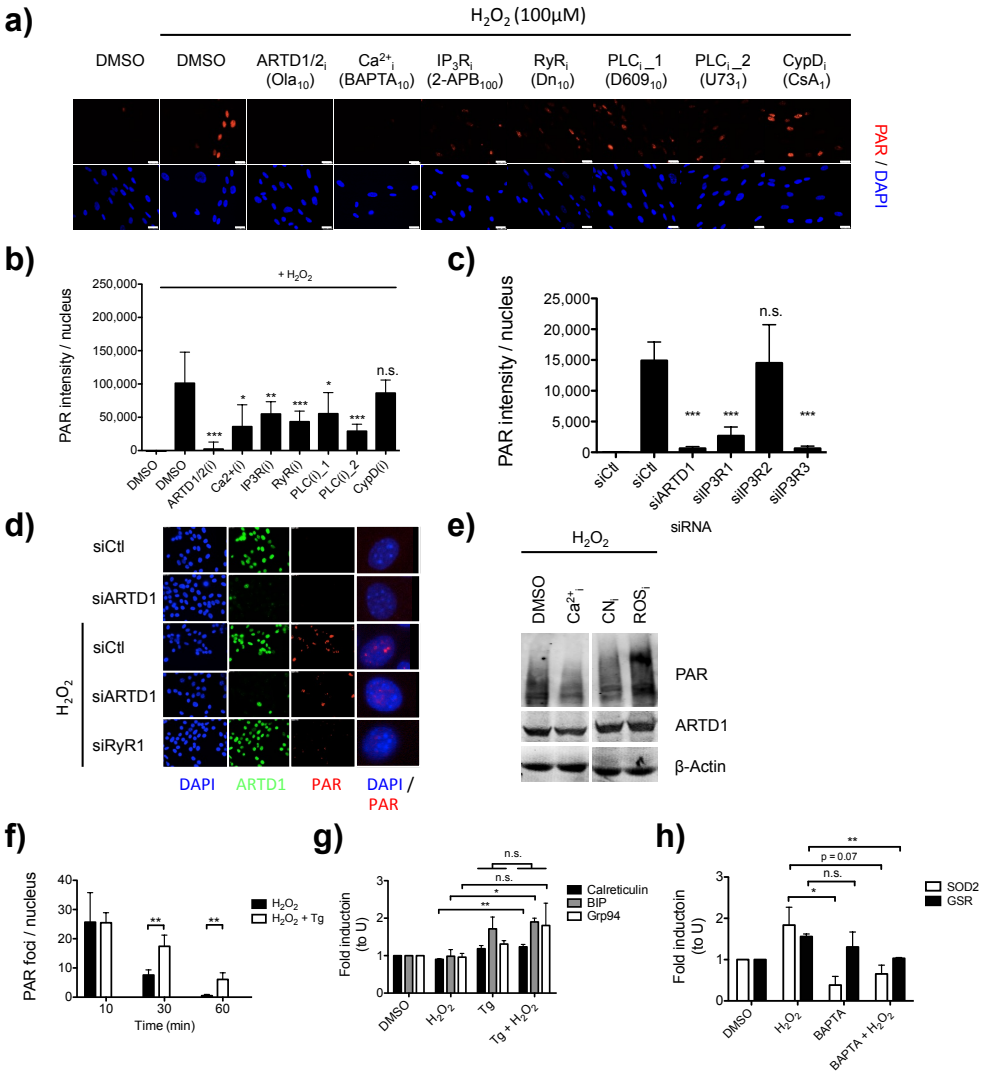
a)
H2O2 (100µM)
DMSO
DMSO
ARTD1/2i (Ola10)
Ca2+i (BAPTA10)
IP3Ri (2-APB100)
RyRi (Dn10)
PLCi_1 (D60910)
PLCi_2 (U731)
CypDi (CsA1)
PAR / DAPI
b)
+ H2O2
PAR intensity / nucleus
250,000
200,000
150,000
100,000
50,000
0
n.s.
DMSO
DMSO
ARTD1/2(i)
Ca2+(i)
IP3R(i)
RyR(i)
PLC(i)_1
PLC(i)_2
CypD(i)
c)
PAR intensity / nucleus
25,000
20,000
15,000
10,000
5,000
0
n.s.
siCtl
siCtl
siARTD1
siIP3R1
siIP3R2
siIP3R3
siRNA
d)
siCtl
siARTD1
siCtl
siARTD1
siRyR1
H2O2
DAPI
ARTD1
PAR
DAPI / PAR
e)
H2O2
DMSO
Ca2+i
CNi
ROSi
PAR
ARTD1
β-Actin
f)
PAR foci / nucleus
40
30
20
10
0
H2O2
H2O2 + Tg
10
30
60
Time (min)
g)
Fold inductoin (to U)
3
2
1
0
n.s.
n.s.
*
**
Calreticulin
BIP
Grp94
DMSO
H2O2
Tg
Tg + H2O2
h)
Fold inductoin (to U)
3
2
1
0
**
p = 0.07
n.s.
*
SOD2
GSR
DMSO
H2O2
BAPTA
BAPTA + H2O2

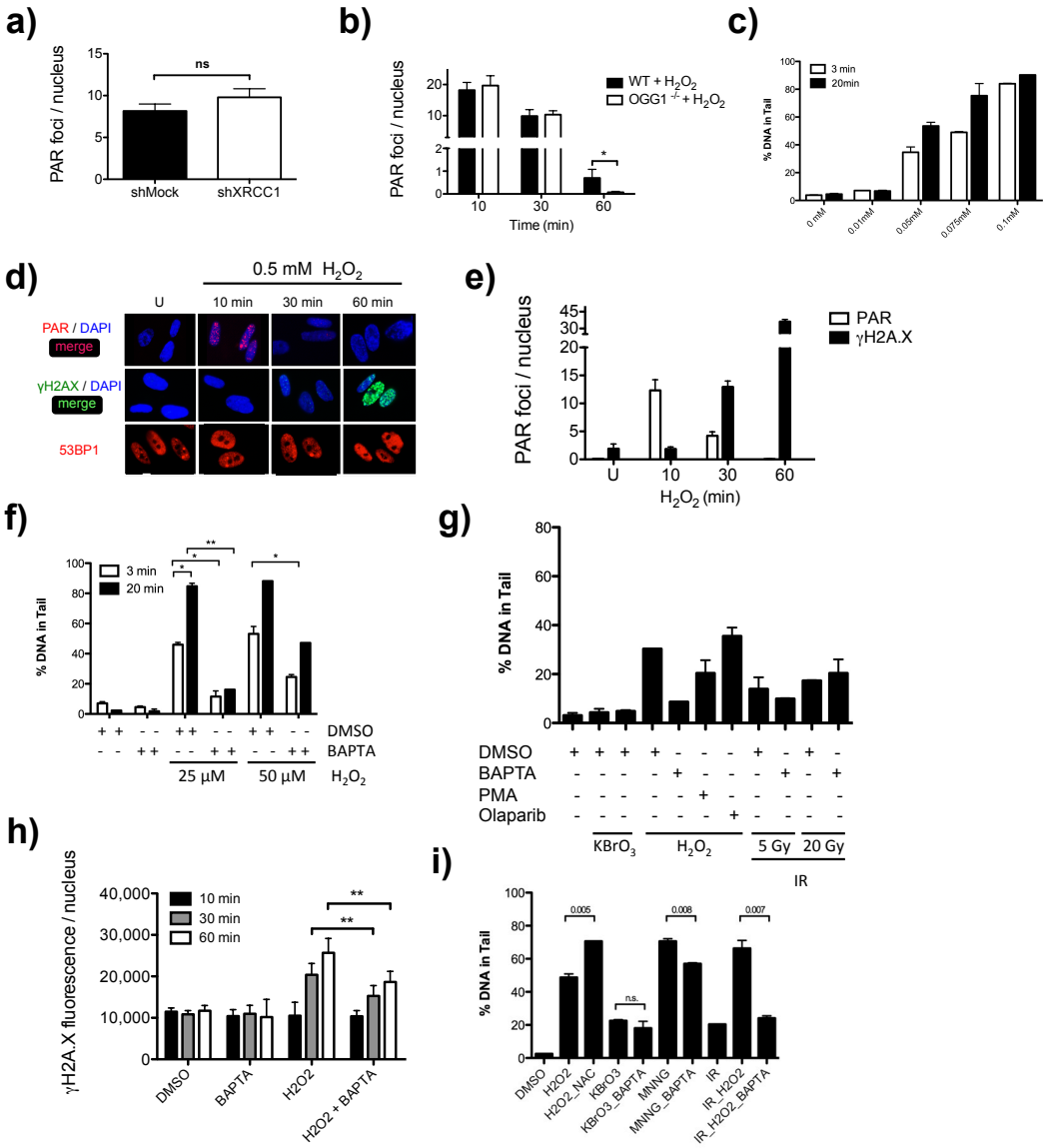
a)
PAR foci / nucleus
ns
shMock
shXRCC1
b)
PAR foci / nucleus
WT + H2O2
OGG1 -/- + H2O2
Time (min)
c)
% DNA in Tail
3 min
20min
0 mM
0.01mM
0.05mM
0.075mM
0.1mM
d)
0.5 mM H2O2
U
10 min
30 min
60 min
PAR / DAPI
merge
γH2AX / DAPI
merge
53BP1
e)
PAR foci / nucleus
PAR
γH2A.X
H2O2 (min)
f)
% DNA in Tail
3 min
20 min
DMSO
BAPTA
25 μM
50 μM
H2O2
g)
% DNA in Tail
DMSO
BAPTA
PMA
Olaparib
KBrO3
H2O2
5 Gy
20 Gy
IR
h)
γH2A.X fluorescence / nucleus
10 min
30 min
60 min
DMSO
BAPTA
H2O2
H2O2 + BAPTA
i)
% DNA in Tail
0.005
n.s.
0.008
0.007
DMSO
H2O2
H2O2_NAC
KBrO3
KBrO3_BAPTA
MNNG
MNNG_BAPTA
IR
IR_H2O2
IR_H2O2_BAPTA

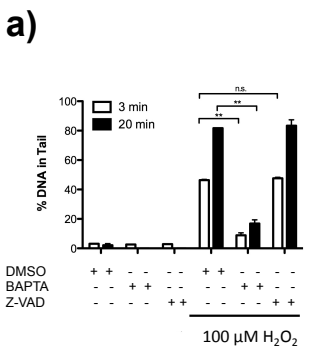
a)
% DNA in Tail
3 min
20 min
n.s.
DMSO
BAPTA
Z-VAD
100 μM H2O2

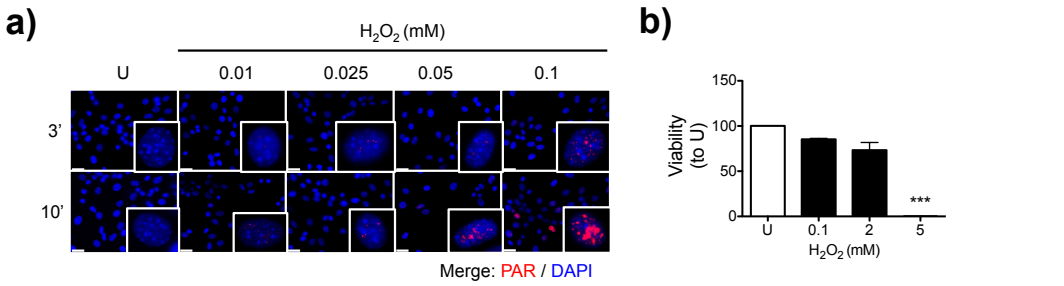
a)
H_2O_2 (mM)
U
0.01
0.025
0.05
0.1
3'
10'
Merge: PAR / DAPI
b)
Viability (to U)
150
100
50
0
U
0.1
2
5
***
H_2O_2 (mM)

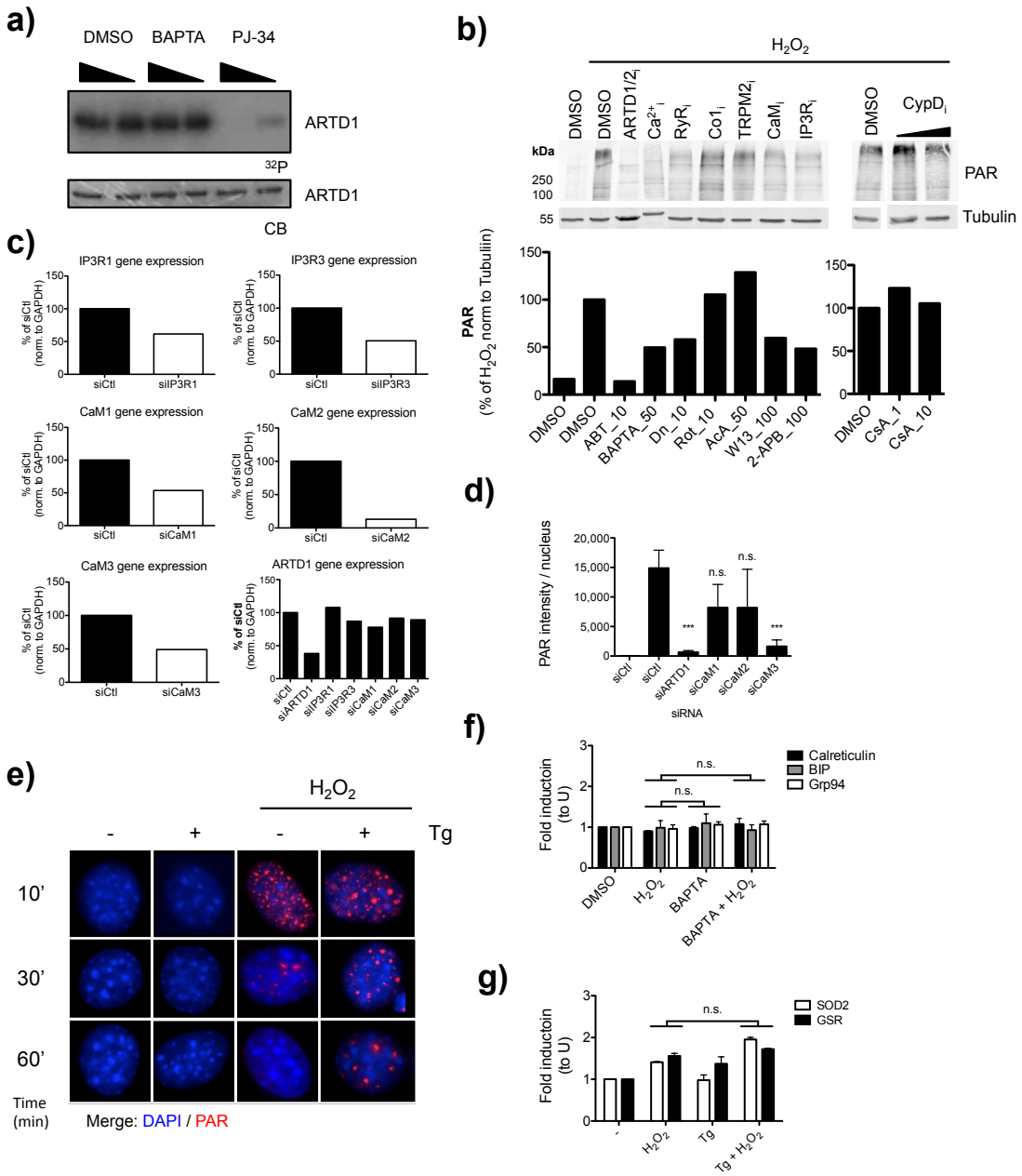
a)
DMSO
BAPTA
PJ-34
ARTD1
32P
ARTD1
CB
b)
H_2O_2
DMSO
DMSO
ARTD1/2i
Ca2+i
RyRi
Co1i
TRPM2i
CaMi
IP3Ri
DMSO
CypDi
kDa
250
100
55
PAR
Tubulin
PAR (% of H_2O_2 norm to Tubulin)
DMSO
DMSO
ABT_10
BAPTA_50
Dn_10
Rot_10
AcA_50
W13_100
2-APB_100
DMSO
CsA_1
CsA_10
c)
IP3R1 gene expression
IP3R3 gene expression
CaM1 gene expression
CaM2 gene expression
CaM3 gene expression
ARTD1 gene expression
% of siCtl (norm. to GAPDH)
siCtl
siIP3R1
siIP3R3
siCaM1
siCaM2
siCaM3
siARTD1
d)
PAR intensity / nucleus
20,000
15,000
10,000
5,000
0
n.s.
***
siRNA
e)
H_2O_2
-
+
-
+
Tg
10'
30'
60'
Time (min)
Merge: DAPI / PAR
f)
Fold inductoin (to U)
n.s.
Calreticulin
BIP
Grp94
DMSO
H_2O_2
BAPTA
BAPTA + H_2O_2
g)
Fold inductoin (to U)
n.s.
SOD2
GSR
H_2O_2
Tg
Tg + H_2O_2

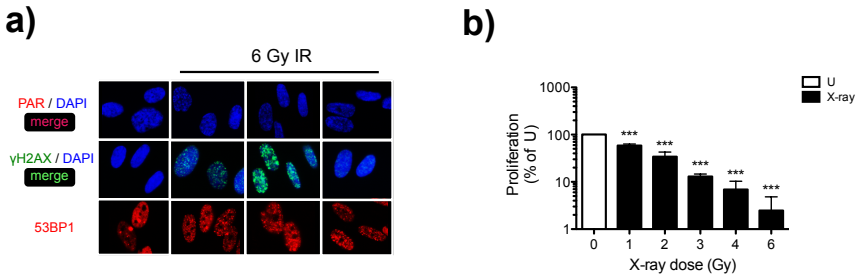
a)
6 Gy IR
PAR / DAPI
merge
γH2AX / DAPI
merge
53BP1
b)
U
X-ray
Proliferation
(% of U)
1000
100
10
1
***
***
***
***
***
0
1
2
3
4
6
X-ray dose (Gy)

3.2 Unpublished Results

Primary MRC-5 fibroblasts are more sensitive towards high doses of IR compared to immortalized counterparts

Human fibroblasts are extremely resistant towards stress induced by treatment with different types of DNA damaging agents and resist particularly high doses of double strand break-inducing ionizing irradiation (IR) (*240*). The aim of the first study "PKC signaling prevents irradiation-induced apoptosis in human fibroblasts" was to describe general proteome changes induced by high doses of IR in order to identify the mechanisms, which are employed by human fibroblasts to overcome severe DNA damages.

To assess the repair capacity of human fibroblasts upon IR-induced DNA damage, primary human MRC-5 cells were treated with increasing concentrations of X-rays. Proliferation and survival was monitored using colony forming assays (CFA) to test for clonogenicity (ability of cells to form colonies from a single cell) over a time period of 10 days (Fig. 1a-b). Irradiation induced a dose-dependent decrease in proliferation, with an LD_{50} (dose at which 50% of the population are impaired in proliferation) of 2 Gy (Fig. 1a-b). In strong contrast to that, immortalized MRC-5 showed a LD_{50} of 6 Gy, thus being more resistant to IR compared to primary MRC-5. These findings indicate that presence of loss- or gain-of-function mutations in immortalized MRC-5 might have increased resistance towards ionizing radiation. Indeed, immortalized MRC-5 showed a faster reproduction rate and reduced cell size in comparison to primary cells (data not shown), indicating the presence of mutations, which might affect growth, doubling rate or alter the metabolism of these cells. Interestingly, the induction of the DDR as measured by γH2A.X foci formation, was comparable in both cell strains (Fig 1c and Fig. 1 of first manuscript for data for primary MRC-5). However, it remains to be clarified, whether primary MRC-5 have a reduced repair capacity compared to immortalized MRC-5 cells, which would explain their sensitivity towards irradiation. DSBs have been described as a potent inducer of ARTD1 activity *in vitro* and in cells induced upon laser damage (*190, 217*). To check, whether IR is also able to induce PAR formation, immortalized MRC-5 were irradiated with increasing dosage of X-rays. PAR formation was significantly induced in response to IR doses between 10-40 Gy (Fig. 1d). Interestingly, doses above 10-40 Gy lead to a marked decrease in proliferation and cells above 20 Gy showed no sign

of proliferation at all (Fig. 1b). Altogether, these results indicate that PAR formation was only induced by lethal doses of IR.,

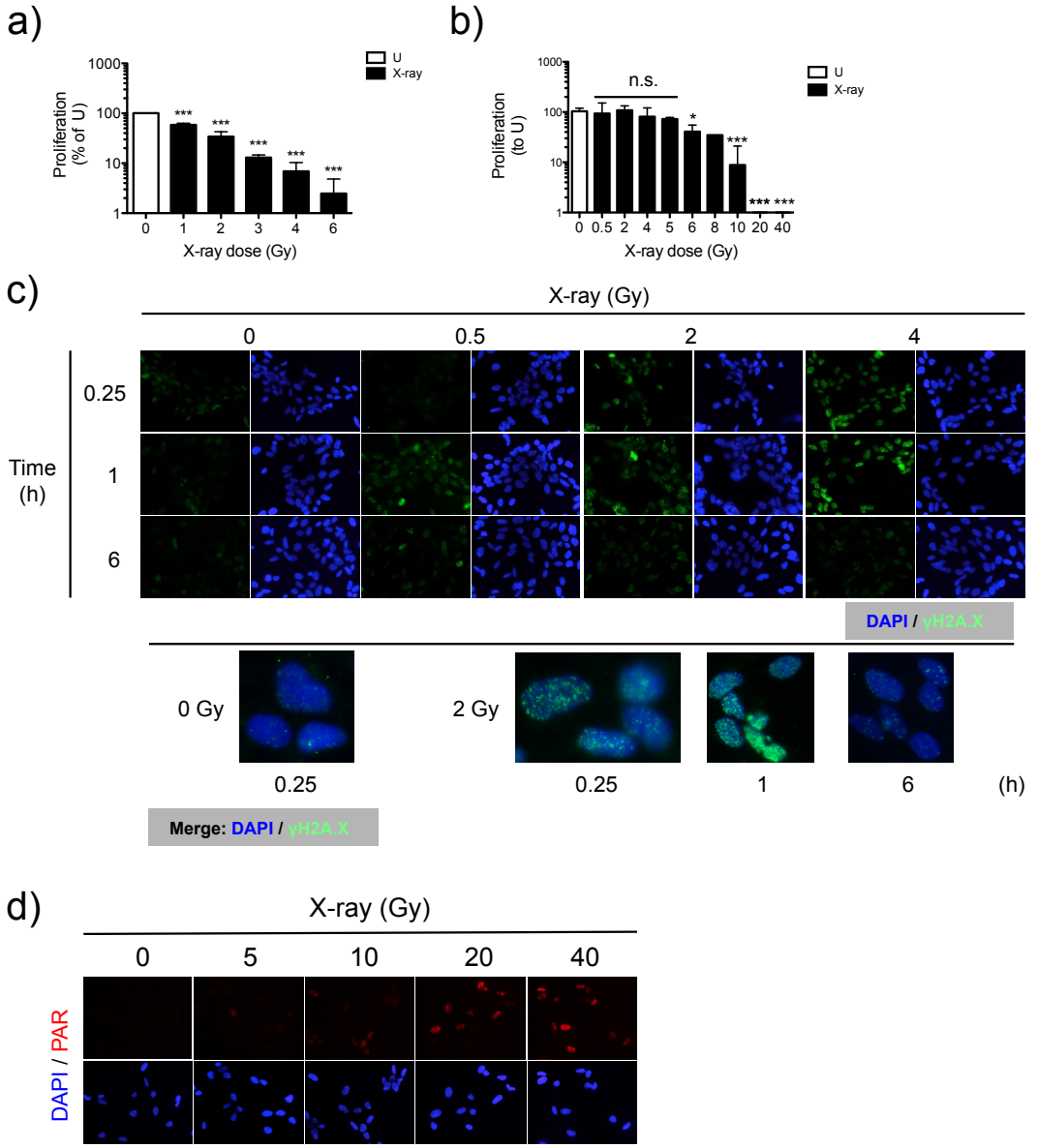

Fig. 1. PAR formation in response to lethal IR doses. a-b) Colony forming assay (CFA) of primary a) or immortalized b) MRC-5 irradiated with an increasing dose of X-rays or untreated (U) and recovery for 10 days (n=8-16 for (a) or n=2-6 for (b)). **c)** γH2A.X-IF of immortalized MRC5 irradiated with increasing dosage of X-rays and recovery for 15 min – 6 h. Lower panel is a 63x acquisition of γH2A.X and DAPI positive stained and merged nuclei. **d)** PAR-IF of immortalized MRC-5, irradiated with increasing dosage of X-rays and recovery for 3 min. Data are mean +/- SD by t-test with *p<0.05, **p<0.01, ***p<0.001, n.s. not significant. Significant only in case of reduction to control (U).

Doxorubicin and IR treatment of immortalized MRC-5 cells induce a DDR but nor PAR formation

It was the aim of the second and third manuscripts (in preparation) to understand the network signaling and the regulatory mechanisms of ARTD1 activation by oxidative stress. ARTD1 activity is strongly induced by genotoxic sress and was previously

linked to oxidative stress-induced DNA damage repair (*190, 217*). To identify a potent inducer of ARTD1 activity, primary as well as immortalized MRC-5 cells were treated with DNA intercalating agents (doxorubicin) and DNA alkylating compounds (MNNG). Cell proliferation and cytotoxicity were measured as in Fig. 1 by clonogenic assay, as well as with the MTT assay, which measures the metabolic activity of living cells and thus indicates reduced viability.

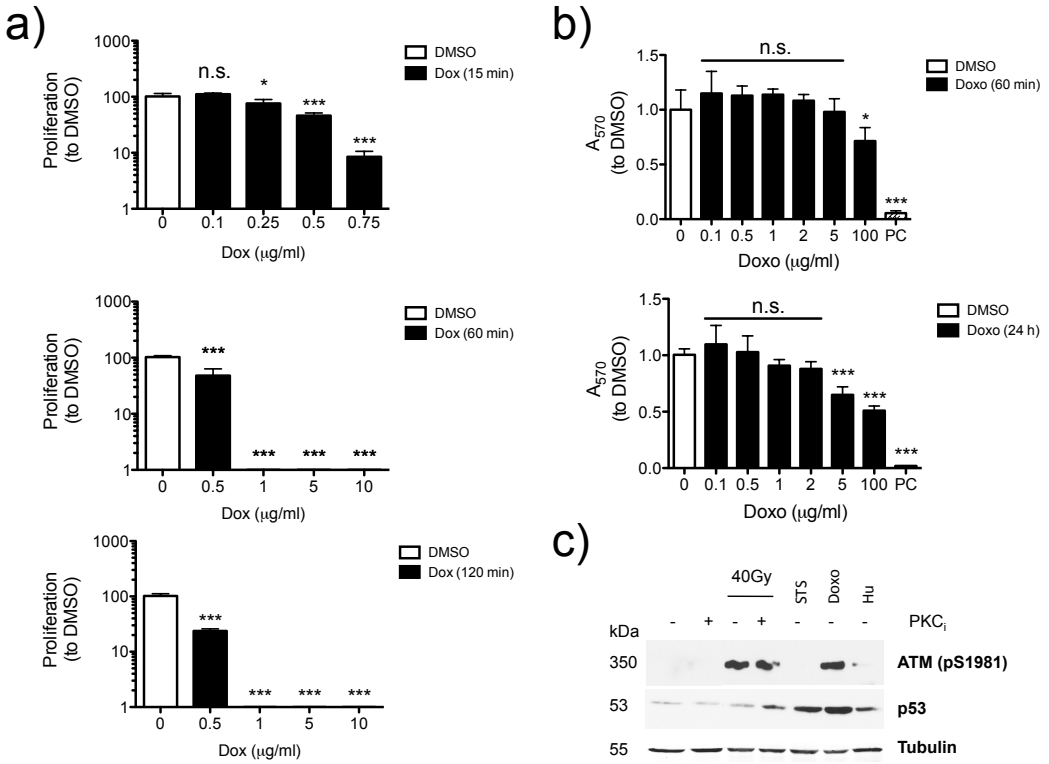

Fig. 2. Doxorubicin treatment reduces survival of immortalized MRC-5 in a dose- and time-dependent manner and leads to the induction of a DDR. a) CFA of immortalized MRC-5 pulse-treated with increasing concentration of doxorubicin or DMSO (control) for 15-120 min and recovery for 10 days (n=3). **b)** MTT assay of immortalized MRC-5 pulse-treated with increasing concentration of doxorubicin or DMSO (control) for 60 min - 24 h and recovery for 24 h (n=4). **c)** Immunoblot analysis of IR (40 Gy), staurosporine (STS, 1μM), doxorubicin (Doxo, 0.5 μg/ml) or hydroxyurea (HU, 2 mM) treated primary MCR-5 for 20 h, before cell lysis. In some cases, cells were preincubated for 1 h with PKC inhibitor (GF109203X, 10 μM). Data are mean +/- SD by t-test with *p<0.05, **p<0.01, ***p<0.001, n.s. not significant. Significant only in case of reduction to control (DMSO).

Pulse-treatment of doxorubicin from 15-120 min abolished proliferation above 0.5 μg/ml following 10 days recovery. (Fig. 2a). Interestingly, short-term recovery (24 h instead of 10 days) from pulsed and constitutive doxorubicin treatment (60min - 24h) revealed a much higher tolerance of immortalized MRC-5 towards Doxorubicin as confirmed by the MTT assay (Fig. 2b). These results indicate that treated cells survived a short-term period (24 h), while leading to deficiency in colony formation over a long period of repair recovery (10 d). These observations also suggest a delayed induction of cell cycle arrest or apoptosis, which is not seen within the first

24 h. Doxorubicin treatment (0.5 μg/ml) was able to induce a strong DNA damage response shown by the induction of ATM phosphorylation and p53 stabilization (Fig. 2c), but failed to induce early PAR formation, even in response to doses above 0.5 μg/ml (data not shown).

MNNG treatment induces a proliferation stop and is sufficient for the induction of calcium-dependent PAR formation

To check for survival and PAR formation upon alkylating stress, primary MRC-5 were treated with increasing amount of MNNG and clonogenicity as well as PAR formation determined as described above. In response to an increasing dose of MNNG, clonogenicity was reduced in a dose-dependent manner. Primary MRC-5 were resistant to MNNG doses of 15 μM and showed a significant, but rather mild proliferation stop upon 25 μM following 10 days recovery (Fig. 3a). However, doses above 50 μM led to a strong reduction in proliferation, reducing clonogenicity to 10 % compared to non-treated cells. Strikingly, the induction of PAR upon MNNG exposure was only obvious upon doses, which led to a strong reduction of clonogenicity (Fig. 3b). Similar findings were also made in immortalized MRC-5, showing a correlation between PAR induction and reduced proliferation upon MNNG treatment (Fig. 3c-d). Hence our results suggest, that the induction of PAR requires MNNG doses, which either induce a permanent cell cycle arrest or lead to apoptosis. Interestingly, these data are in strong contrast to H_2O_2-induced PAR formation, which could be readily induced upon doses, which did not show any sign of proliferation stop or significant reduction in viability (Fig. 1b, third manuscript). Moreover, MNNG-induced PAR revealed a long half-life, showing comparable signal intensity between 3 – 20 min of MNNG treatment. In contrast, H_2O_2 induced PAR formation was transient, showing already 10 min after adding peroxide a gradual decrease in the PAR signal (Fig. 1a, third manuscript). Altogether, these data indicate a distinct nature of PAR in response to MNNG compared to H_2O_2. Most likely the difference in the response is due to differences in the triggered cellular stress and introduction of DNA lesions between MNNG and H_2O_2. Calcium sequestration by BAPTA (Ca^{2+} chelator) led to a strong reduction in MNNG-induced PAR formation, indicating a similar mechanism of calcium-dependent activation of ARTD1/2 (Fig. 3f, third manuscript) as observed for oxidative stress.

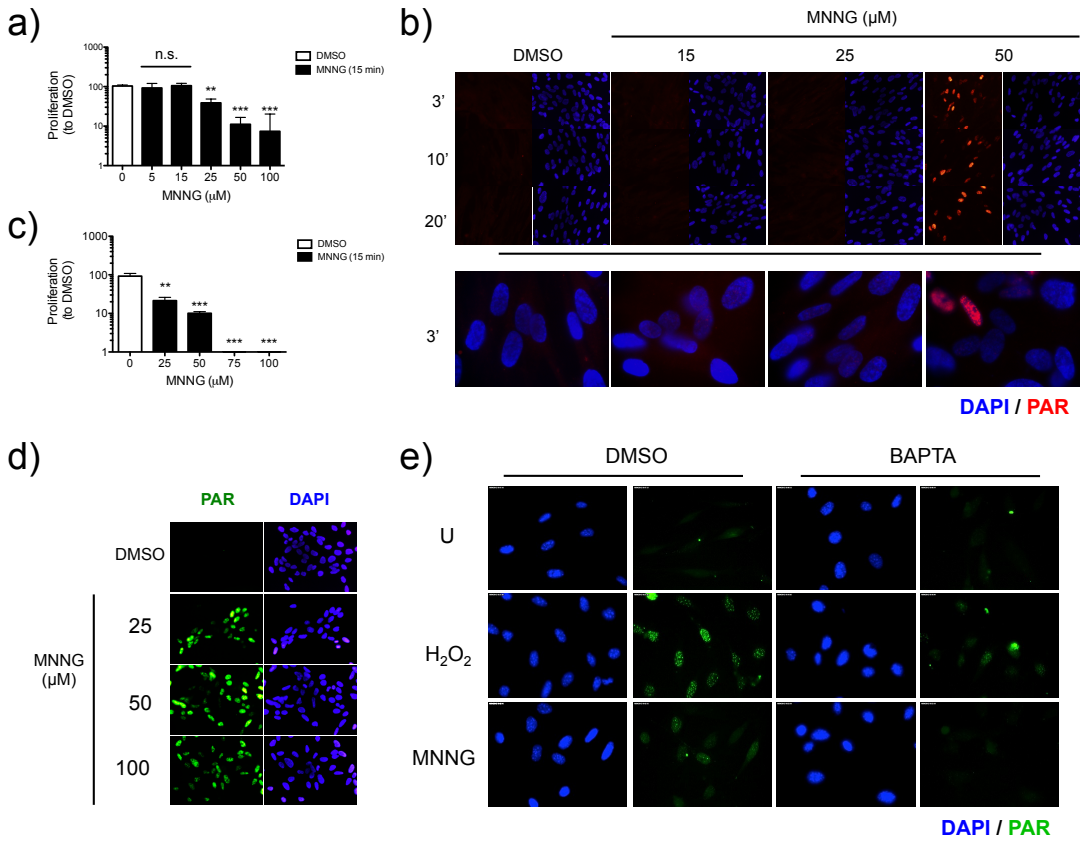

Fig. 3 Direct correlation between reduction in proliferation and induced PAR formation upon MNNG treatment. a) CFA of primary MRC-5 pulse-treated with increasing concentration of MNNG for 15 min or DMSO (control) (n=4-8) **b)** PAR IF of primary MRC-5 pulse-treated with increasing concentration of MNNG for 30 min and recovery in drug-free media for additional 10 min before fixation and immunostaining with anti-PAR (green) and counterstaining with DAPI (blue) to detect the nucleus. **c)** CFA of immortalized MRC-5 pulse-treated with increasing concentration of MNNG for 15 min or DMSO (control) (n=3). **d)** Experiment performed as in b) using immortalized MRC-5 pulse treated fwith increasing dose of MNNG and recovery for 15 min. **e)** PAR IF of H_2O_2 (0.5 mM, 10 min w/o recovery) or MNNG (50 μM, 30 min w/o recovery) treated MEF in presence of BAPTA or DMSO (control) preincubation for 1 h. Data are mean +/- SD by t-test with *p<0.05, **p<0.01, ***p<0.001, n.s. not significant. Significant only in case of reduction to control (DMSO).

Knockdown of CDK2 reduces ARTD1 protein levels and leads to reduced PAR formation in response to H_2O_2

For the inhibitor screen described in the second manuscript, we observed a reduced PAR formation in presence of the JNK inhibitor SP600125. However, this could not be confirmed by treating WT and JNK1/2 KO MEFs with H_2O_2 (as shown by PAR WB and IF, second manuscript). This is in contrast to earlier studies which documented the regulation of PAR induction by JNK upon H_2O_2 treatment (*236*), although a direct involvement of JNK in the regulation of ARTD1 activity has so far not been shown. Others and we observed a rather delayed induction of JNK in

response to H_2O_2, peaking 30-60 min upon treatment (second manuscript, (*241*)). In contrast to this observation, PAR formation is induced very early (first 5 minutes) and reaches again basal levels after 30 min, Fig. 1a, third manuscript). Hence, our results based on the JNK inhibitor SP600125 as well as reported by Zhang et al., would rather point to an off target effect of this inhibitor, that reduces PAR formation upon H_2O_2 treatment. Indeed, SP600125 has been described to target other kinases as potently as JNK itself (*242*). Based on the JNK off-targets identified by Bain et al., we performed a small-scale siRNA screen for JNK-off targets and assessed PAR formation by IF and WB using NIH/3T3.

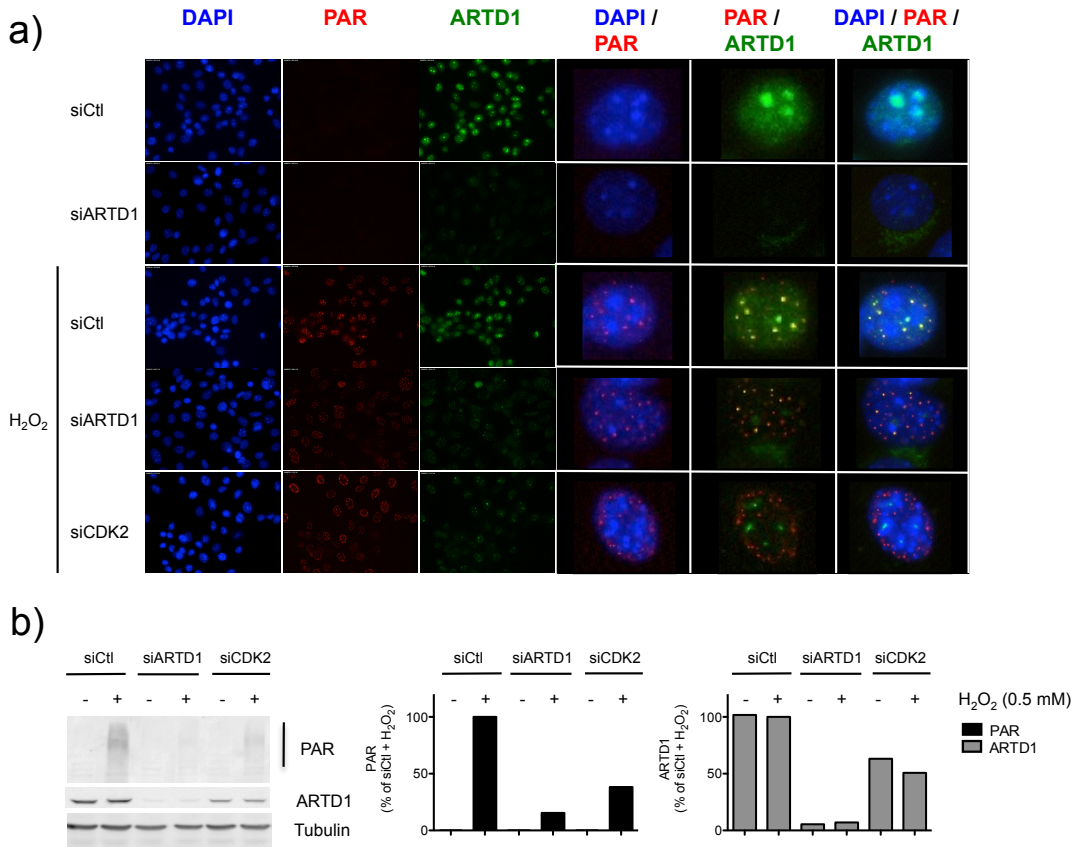

Fig. 5. KD of CDK2 reduces ARTD1 protein levels and leads to reduced PAR formation in response to H_2O_2. a) Immunofluorescence analysis of siCDK2 transfected NIH/3T3 (4 days) or siCtl and siARTD1 for not affecting or reducing ARTD1 protein levels as control and immunostaining with anti-PAR or anti-ARTD1 (control). **b)** Immunoblotting analysis of siCDK2 transfected NIH/3T3 as in a) and immunostaining with anti-PAR. anti-ARTD1 was used as control to confirm ARTD1 protein level reduction upon siARTD1. anti-Tubulin was used as loading control. Quantification is shown on the right-hand site of the blots.

Knockdown (KD) of CDK2 by siRNA in NIH/3T3 cells, reduced ARTD1 protein and H_2O_2-induced PAR formation by IF (Fig. 5a and b). These data indicate that CDK2 acts upstream of PAR formation by regulating ARTD1 protein levels or transcription. To clarify whether the residual activity is due to the incomplete reduction of ARTD1 upon CDK2 KD, we transfected NIH/3T3 with siCDK2 in combination with ARTD1.

Since other ARTD members, such as TNKS1 (ARTD5) or TNKS2 (ARTD6) have been described to posses poly-ADP-ribosylation activity (*187*), we also combined KD of CDK2 with KD of either TNKS1, TNKS2 or in combination with both (Fig. 6). Interestingly, siTNKS-1, but not siARTD1 or siTNKS-2, led to a complete reduction of PAR formation in the siCDK-2 background, indicating that CDK2 might regulate PAR formation in response to H_2O_2 through ARTD1 and that TNKS-1 might also contribute to PAR formation upon H_2O_2 treatment.

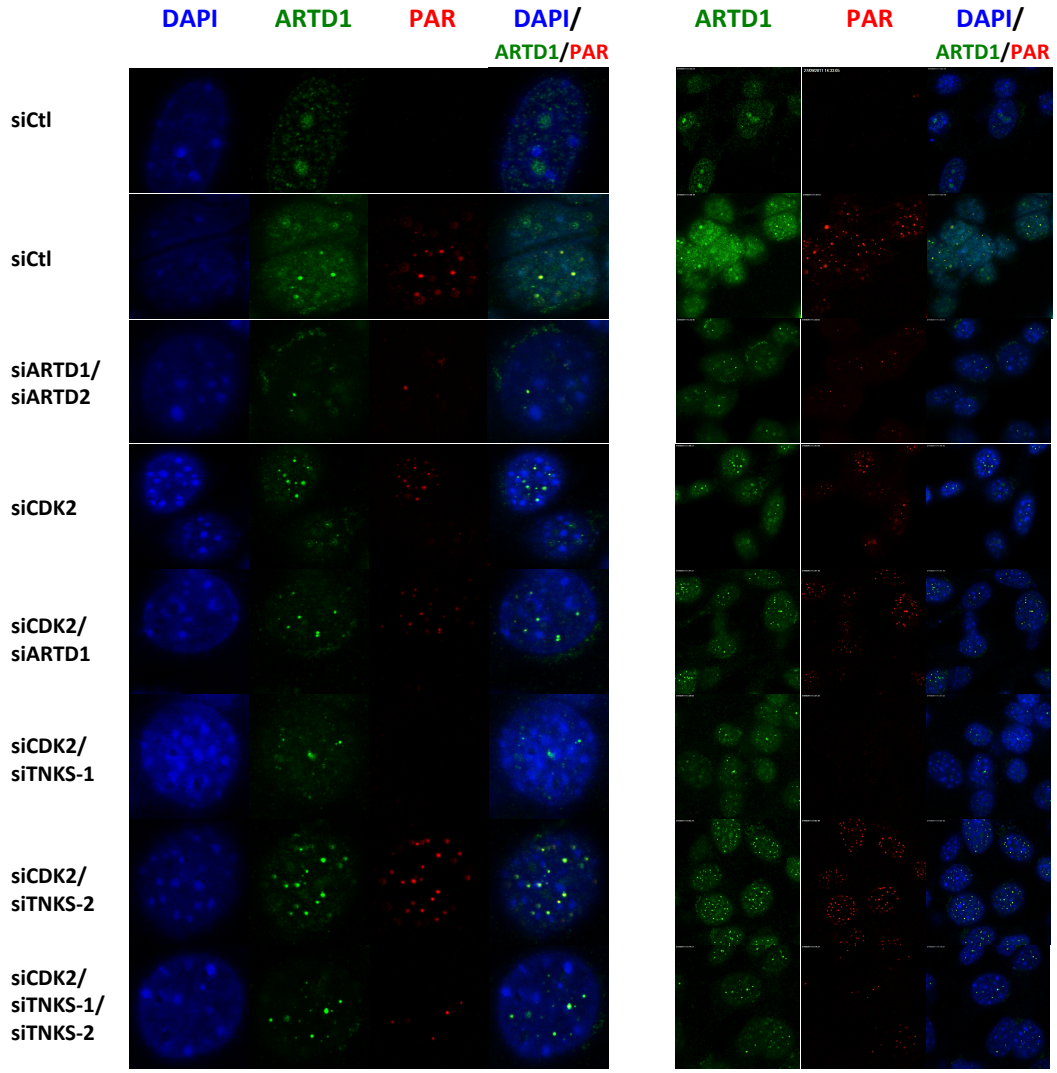

Fig. 6. KD of TNKS-1 in combination with CDK2 leads to a complete reduction of PAR fromation upon H_2O_2 treatment. Confocal immunofluorescence analysis of siCDK2 combined with siTNKS-1 and siTNKS-2 transfected NIH/3T3 and immunostaining with anti-PAR. siCtl and siARTD1 transfection were used as control for not affecting or reducing ARTD1 protein levels, respectively.

Another candidate, who has been shown to be a potent off-target of SP600125, is Chk1 (*242*).

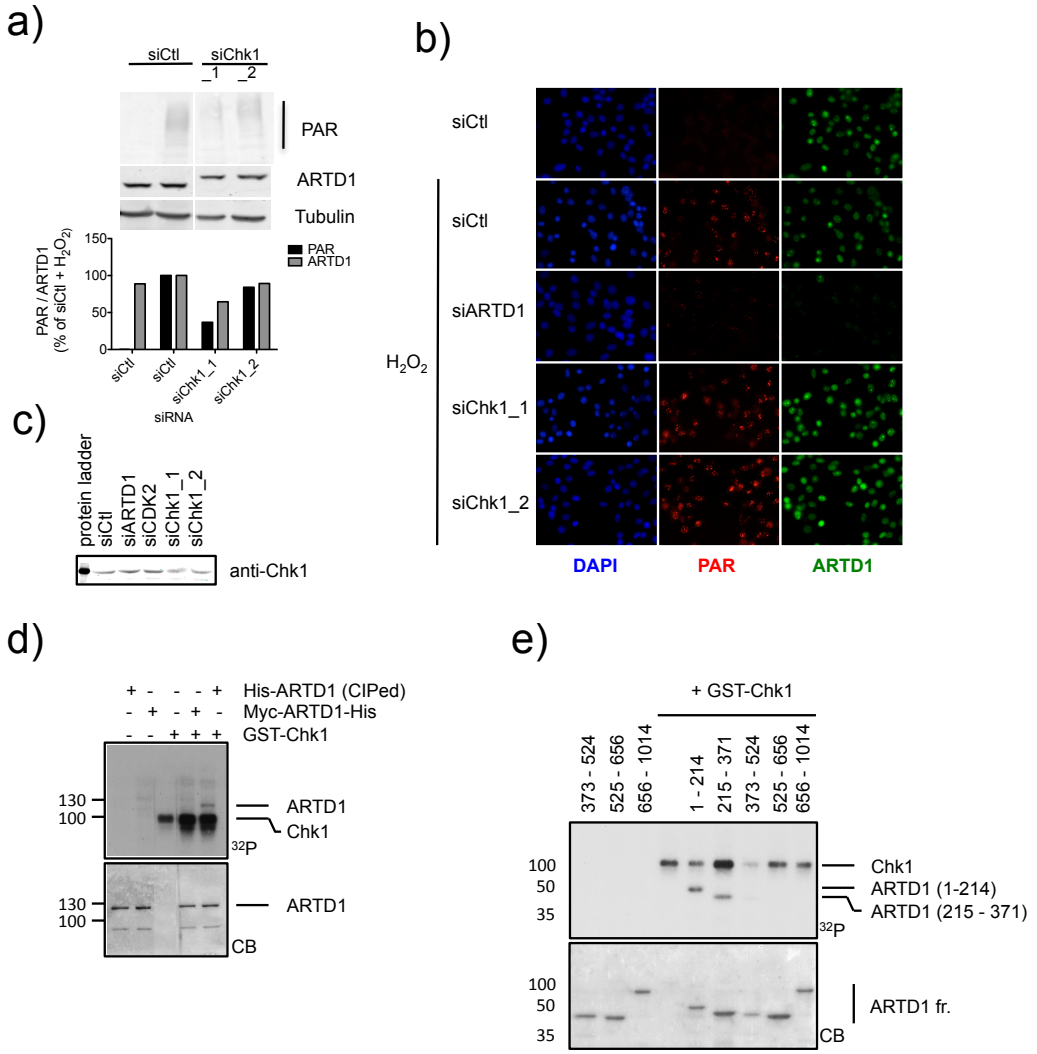

Fig. 7. Knockdown of Chk1 does not reduce PAR formation induced by H_2O_2. a) Immunoblotting analysis of siChk1 transfected NIH/3T3 using two different siRNA oligos targeting siChk1 (_1 and _2) and immunostaining with anti-PAR and anti-ARTD1. anti-Tubulin was used as loading control and for quantification PAR was normalized to Tubulin protein levels. Quantification is shown below the blots. **b)** Immunofluorescence analysis of siChk1 transfected NIH/3T3 using two different siRNA oligos (_1 and _2) or siCtl and siARTD1 for not affecting or reducing ARTD1 protein levels as control and immunostaining with anti-PAR or anti-ARTD1 (control) **c)** KD confirmation of siChk1 transfected NIH/3T3 by immunoblotting from b). siCtl, siARTD1 and siCDK2 were used as control for not affecting Chk1 protein levels. **d)** Chk1 kinase assay using GST-tagged Chk1 and two purified ARTD1 constructs (full length and CIP treated for His-ARTD1) as substrates and gamma-labeled ATP. e) Experiment performed as in d) using instead ARTD1 deletion fragments either in presence (1-1014, lane 5-9) or in absence of GST-Chk1 (373-1014, lane 1-3). GST-Chk1 alone (lane 4) was used as negative control.

siChk1 transfected NIH/3T3 cells exhibited reduced PAR formation after H_2O_2 treatment. However, these reduced PAR levels correlated with reduced ARTD1 protein levels, which might explain this effect (Fig. 7a).

To confirm the reduction of PAR upon Chk1 KD, the experiment was performed exactly as in Fig. 7a, however, using PAR-IF as a readout. However, reduction of Chk1 did not show any significant difference in PAR levels between siControl and siChk1 transfected cells (Fig. 7b). The experiment was well controlled, since siARTD1 treatment led to a complete reduction of PAR levels comparable to untreated cells (Fig. 7b). It could be argued that a difference was not observed due to a weak KD as confirmed by WB (Fig. 7c). However, we have also noticed strong induction of cell death upon siChk1 treatment, indicating that the observed phenotype in a) might be an artifact of cell death. Independent of the discrepancies regarding Chk1's role in regulating ARTD1 activity, ARTD1 was phosphorylated by Chk1 *in vitro* and we could pin-point the phosphorylation site to the N-terminal zinc-finger DNA binding domain (Fig. 6d-e). It remains to be clarified, whether Chk1 might also play a role in the regulation of ARTD1 activity *in vivo*.

4. Discussion and Perspectives

4.1 Summary of results

To elucidate the molecular mechanism regulating the resistance of primary human fibroblasts to high doses of ionizing irradiation of up to 80 Gy (*240, 243*), we performed a proteome-wide analysis using RPPAs. Based on the kinetics of cytoplasmic and nuclear phosphorylation events affected by IR, we discovered a significant activation of protein kinase C (PKC) family members, including PKCβII, PKCδ and PKCζ in MRC5 fibroblasts. Inhibition of PKC signaling by a broad-range PKC inhibitor (GF109203X) or down-regulation of PKC protein levels sensitized primary fibroblasts to IR, led to the activation of pro-apoptotic signaling (ARTD1 cleavage, stabilization of p53, upregulation of Bad), as well as to inhibition of pro-survival signaling (CREB and Bad dephosphorylation). This analysis thus identified a molecular switch, which is responsible for the radio-resistance of primary human fibroblasts.

To identify possible regulatory mechanisms of ARTD1 activation in response to oxidative stress, we again used RPPA analysis. The results of this broad analysis were validated and followed up using a small molecule inhibitor screen and IF with PAR formation as a readout. This analysis identified calcium (Ca^{2+}) and CaMKII as positive and PKC as negative regulators of ARTD1 activity. Moreover, knockdown of CaMKIIδ led to reduced PAR levels upon H_2O_2 exposure and we confirmed the direct phosphorylation and activation of ARTD1 by CaMKIIδ in *in vitro* kinase assays. In contrast, PKCδ-dependent phosphorylation of ARTD1 *in vitro* led to a decrease of its automodification in the presence of DNA. More importantly, knockdown of the Ca^{2+}-dependent PKCα isoform and a general depletion of PKC protein expression strongly reduced the number of PAR foci induced by H_2O_2.

Our results also indicated an early induction of Ca^{2+} signaling upon H_2O_2 exposure, which pointed at a possible important upstream regulation of ARTD1 activity by Ca^{2+}. Indeed, inhibition of Ca^{2+} signaling by BAPTA completely abolished H_2O_2 induced PAR formation. Using small molecule inhibitors and siRNA, we further identified PLC-dependent production of IP3 and subsequent activation of ER-based IP3R and RyR receptors to be responsible for the Ca^{2+} release from the ER. Moreover, H_2O_2-induced DNA breaks, as observed by an alkaline Comet assay, could be

prevented by BAPTA, which on the other hand, had no influence on IR or $KBrO_3$ induced DNA break induction, indicating a link between Ca^{2+}-dependent induction of DNA lesions and PAR formation upon H_2O_2 treatment.

4.2 PKC signaling prevents irradiation-induced apoptosis of primary human fibroblasts

Dependent on the severity of DNA damage, the DDR either leads to survival of the cell or to cell death by apoptosis (*34, 96*). In contrast to epithelial or cancerous cells, human fibroblasts are highly resistant towards IR and thus a perfect model to study the molecular signaling events regulating the decision in response to severe DNA damage (*240*). We were able to describe an early signaling network, encompassing cytoplasmic pro-survival and pro-proliferation pathways including phosphorylation of MEK-ERK, LKB-AMPK, PKC-CREB as well as phosphorylation of the Akt-substrate Bad (Fig. 2b/c, Supp. Fig. S7-S9). Interestingly, mounting evidence indicates the involvement of cytoplasmic signaling events in the regulation of survival and DNA break repair upon IR (*244*). Using human tumor cells, a series of studies identified the importance of EGFR-Akt signaling-dependent activation of DNA-PKcs upon IR for protecting tumor cells from irradiation induced cell death (*245-247*). Similarly, the direct translocation of Akt into the nucleus leads to the activation of the DDR via DNA-PKcs (*86*). Interestingly, compared to early signaling events mentioned above, we observed a delayed activation of the γH2A.X-p53-p21 pathway, as well as the non-canonical MKK3/6-p38-MAPKAP2-Hsp27 DDR kinase signaling pathway (Fig. 2b/c, Supp. Fig. S7-S9). It thus remains to be clarified whether cytoplasmic signaling directly affects the DDR upon IR.

The MEK-ERK signaling pathway, also identified as an early-induced event in our screen, was confirmed by others as a positive regulator of ATM activation and homologues recombination (HR) efficiency in response to UV-C irradiation (*248*). Compared to cytoplasmic signaling-dependent regulation of the DDR, a recent proteomics study identified over 700 proteins, including cytoplasmic kinases, carrying the ATM/ATR recognition motif (SQ/TQ motif), which indicates regulation of a broad phospho-proteome by the DDR (*62*). One interesting example from this screen is the enrichment of members of the AKT/PKB signaling network. This signaling cascade is typically activated by cell membrane-bound PDK1 or Pi3K, which trigger AKT signaling upon extracellular stimuli such as insulin (*6*). Although not tested for

AKT, we could show ATM-dependent activation of two MAPK pathways, including the p38-Hsp27 (Suppl. Fig. S10d) and the MEK-ERK pathway (data not show). For a direct activation of these kinases, ATM would have to translocate to the cytoplasm. Indeed, such a translocation event of the ATM kinase has been described for the activation of the NF-κB pathway upon IR (*82*).

Systemic analyses of DSB-induced proteome changes have been performed previously (*63, 77, 78*). In strong contrast to our study, however, nuclear phosphorylation events dominated the identified proteome changes, indicating the nucleus as the dominant organelle for the DDR. Major findings included phosphorylation of RNA processing and splicing, as well as epigenetic phospho-proteome changes. Besides the confirmation of the already described activation of the p38-MAPK and NF-κB pathways, cytoplasmic kinase signaling was identified in none of these studies as a significant component of the DDR (*78, 82, 249*). One important explanation for the failure to detect cytoplasmic kinase signaling as an element of the DDR could be the experimental set-up of the studies cited above. While Bennetzen et al. excluded the cytoplasm from the proteomics analysis, Beli et al. did not analyze earlier time points than 1 h after treatment (*250*). In contrast, we investigated phospho-proteome changes upon early recovery from IR, including a 30 min time point. Moreover, our studies were based on whole cell extracts and a strong bias to canonical cytoplasmic signaling pathways, which might explain the enrichment for cytoplasmic signaling events identified here.

The key observation of our study was the early induction of protein kinase C family members (PKCζ, PKCδ and PKCβII) and their role in preventing IR-induced apoptosis upon high doses of IR exposure (Fig. 4 and 5). Indeed, PKCδ activation was previously linked to the DDR, being targeted by the c-Abl kinase for phosphorylation and nuclear translocation upon IR (*251*). Our study using two broad PKC inhibitors (GF109203X, RO-318220), which target the PKC family members PKCα-γ, PKCδ-ε and PKCζ (*29, 252, 253*), revealed a protective role of PKC signaling in the DDR upon IR (Fig. 4 and 5). Prevention of apoptosis upon IR could be also confirmed by the down-regulation of PKCδ (novel) and PKCζ/λ (atypical) protein levels (Fig. 5d and h). PKCδ is described to be a double edged sword regarding its involvement in survival and apoptosis upon genotoxic stress (*254*). PKCδ null mice are resistant to apoptosis and p53 phosphorylation by PKCδ has been shown to be important for apoptosis (*255, 256*). Regulation of apoptosis by PKCδ also requires its direct

activation by phosphorylation, proteolytic cleavage by Caspase 3 and nuclear as well as mitochondrial shuttling (*257-261*). Besides a pro-apoptotic function, PKCδ as well as members from the canonical and atypical PKCζ pathway, have also been shown to promote survival (*254*). Interestingly, many tumors overexpress PKCδ and sensitization of chemotherapy treated tumors with PKC inhibitors as well as antisense oligonucleotides, enhances chemotherapy induced apoptosis (*262, 263*). While there is a vast amount of information on the involvement of PKCδ in survival and apoptosis, only little information is present about the regulation of these mechanisms for the Ca^{2+}-dependent members of the PKC family. Nevertheless, a recent study linked integrin αv dependent up-regulation of PKCα and PKCα-dependent re-localization of p53 from the nucleus to survival in melanoma (*264*). Other studies identified PKCα protein expression as a prerequisite for survival and proliferation of malignant glioma and PKCβ expression in tumor microenvironment to support growth of adjacent malignant B cells (*265, 266*).

In our study, we treated primary fibroblasts with IR, hence not directly addressing the question whether acquired radioresistance in cancer cells might be dependent on similar survival cues. On the other hand, fibroblasts are part of the tumor microenvironment and recent studies indicate a link between senescence and tumor progression (*267-270*). Even though senescence is a well-accepted barrier for tumor formation due to permanent cell cycle arrest *in vivo*, co-culture and conditioned medium studies could show the secretion of pro-survival and pro-angiogenic chemokines by senescent fibroblasts, leading to tumor progression of nearby premalignant cells (*267-270*). Moreover, a recent study could show the importance of cancer-associated fibroblasts in promoting resistance of tumors to chemotherapy. Irradiation of prostate fibroblasts led to the release of WNT16B, which supported survival and invasion of adjacent cancer cells by paracrine NF-κB/Wnt pathway activation (*271*). Reducing the expression of WNT16B in tumor-associated fibroblasts led to tumor volume shrinkage and attenuated chemoresistance. Prospectively, our results open up an avenue for new treatment strategies by sensitizing the tumor-associated microenvironment for apoptosis by combined radiotherapy and PKC inhibition.

4.3 Opposite regulation of ADP-ribosylation by PKC signaling: ARTD1 is activated by PKCα and inactivated by PKCδ

The enzymatic activity of ARTD1 has been previously shown to be regulated by phosphorylation events *in vitro* (*225*). So far only two phosphorylation sites have been confirmed to be functionally relevant *in vivo* (*233*). Here, we reported the identification of different positive and negative modulators of ARTD1 enzymatic activity in response to oxidative stress in human and mouse fibroblasts. Inhibition of PKC by a small molecule inhibitor (GF109203X, BIM 1) led to a significant increase in PAR induction upon H_2O_2 treatment, identifying PKC as a negative modulator upon H_2O_2 stress. This observation could also be strengthened by *in vitro* experiments showing a reduced enzymatic activity of ARTD1 upon phosphorylation by PKCδ in the presence of DNA. Indeed, PKC has been previously shown to phosphorylate ARTD1 *in vitro* (*237*) and its inhibition resulted in increased PAR induction upon alkylation stress (*239*). In contrast, there are also studies, which reported a positive regulation of ARTD1 by the Ca^{2+}-independent PKCδ isoform in response to histamine (*272, 273*). Indeed, our results identified Ca^{2+}-dependent PKCα as a positive regulator of PAR formation in response to H_2O_2 treatment. Independent of the precise mechanism of ARTD1 activation *in vivo*, we could confirm the negative regulation of ARTD1 activity upon phosphorylation by PKCδ by *in vitro* experiments and were able to localize the phosphorylation site of ARTD1 by PKCδ to the region encompassing the first two zinc fingers of N-terminal DBD (Fig. 4). Based on *in silico* analysis, sequence-stretches around Ser20 and Thr109 in the N-terminal DBD of ARTD1 match the consensus-motif of two Ca^{2+}-independent PKC isoforms including PKCδ and PKCε, respectively (Motif Scan, ScanSite). Interestingly, both sites also show a high probability score for phosphorylation using another prediction tool (NetPhos 2.0, with 0.993 for Ser20 and 0.872 for Thr109). Indeed, based on two recently published structures of ARTD1 zinc finger domains bound to DNA, Ser20 stabilizes the interaction with the DNA backbone by forming a hydrogen bond with a phosphate of a phosphodiester bond (*197, 198*). It can thus be speculated that phosphorylation of Ser20 by PKC destabilizes the interaction of the ADRT1 first zinc finger with the DNA backbone due to a highly negative charge of the added phosphate group, eventually resulting in less activity in response to H_2O_2 exposure. In contrast, other laboratories identified Ser504, Ser519 and Trh656 as preferential phospho-targets of PKC in full length ARTD1 (*274*). Indeed, based on *in silico*

prediction Ser504 can be modified by Ca^{2+}-dependent PKCs (Motif Scan, ScanSite). One explanation for the difference of the modified region could be the use of different PKC isoforms for the *in vitro* kinase assay. While Gagne et al. relied on a Ca^{2+}-dependent PKCβ, we performed the assay using PKCδ, which is not Ca^{2+}-dependent (*274*). Indeed, chelation of Ca^{2+} was reported to reduce ARTD1 activity in response to nitrosative and oxidative stress (*226, 227*). Therefore, PKC could either reduce ARTD1 activity through phosphorylation in the DBD by a Ca^{2+}-independent member (e.g., PKCδ) or lead to stimulation through modification in the AMD by a Ca^{2+}-dependent PKC member (e.g., PKCβ). It remains to be clarified which PKC isoform is responsible for enhancing or inhibiting ARTD1 enzymatic activity in response to different stimuli *in vivo*. Based on our data, knockdown of the Ca^{2+}-dependent PKCα alone, in combination with the calcium-independent PKCδ in murine NIH/3T3, as well as a general depletion of PKC protein expression in human MRC-5, strongly reduced the number of PAR foci. Interestingly, single knockdown of PKCδ enhanced PAR formation upon H_2O_2 treatment, thus confirming the *in vitro* kinase data mentioned above. Altogether, these results indicate a dual role of PKC family members in the regulation of PAR formation upon oxidative stress. While PKCδ is a direct negative modulator of ARTD1 activity, the Ca^{2+} -dependent PKCα seems to be an essential kinase for the activity of ARTD1 upon oxidative stress-induced Ca^{2+} accumulation in the cytoplasm.

Besides PKCδ, activation of three additional kinases led to enhanced PAR formation upon their inhibition including AMPK, GSK3 and MEK. Interestingly, all three kinases were induced as early as 10 min after stimulation with H_2O_2 (Fig. 1e). Based on *in silico* prediction analysis, AMPK and GSK3 are predicted to phosphorylate Ser257 and Thr368, respectively (Motif Scan, ScanSite). Interestingly, Ser257, comparable to Ser20, is crucial for the interaction of ARTD1 with the DNA by stabilizing an interaction of ZnF3 with the backbone of the DNA (*197*). Strikingly, phosphorylation of ARTD1 by AMPK could be shown *in vitro,* specifically in the third zinc finger, indicating a realistic possibility of a direct regulation of ARTD1 by AMPK *in vivo* (Kassner et al, 2012; doctoral thesis). GSK3 inhibition by GSK3 kinase inhibitors (SB-415286) enhanced PAR formation after H_2O_2 treatment, indicating GSK3 as a negative upstream regulator of PAR formation upon H_2O_2 treatment (data not shown). Moreover, knockdown of GSK3α and GSK3β enhanced ARTD1 activity, while combinatorial knockdown of both isoforms showed no

additive effect of this phenotype (data not shown). However, based on preliminary *in vitro* kinase analysis, ARTD1 was not phosphorylated by GSK3β, thus indicating an indirect mechanism of ARTD1 activity modulation by GSK3 (data not shown). Interestingly, two studies recently provided evidence for negative regulation of the GSK3β kinase activity by ARTD10-dependent mono-ADP ribosylation (*275, 276*). Whether there is a biologically relevant link between ARTD10 and GSK3β-dependent regulation of ARTD1 still remains to be solved.

Based on reports by others (*231, 232*), PAR formation was shown to be positively regulated by CaMKII, which is a Ca^{2+}-dependent kinase and therefore a potential candidate for a DNA-independent mechanism of ARTD1 activation. Indeed, we could show direct phosphorylation of ARTD1 by CaMKII, which led to automodification of ARTD1 in the absence of DNA *in vitro* (data not shown). However, based on a CaMKII-specific inhibitor or CaMKIIδ siRNA, we could not detect a complete inhibition of ARTD1 activity, indicating an alternative or additional mechanism of ARTD1 activation upon non-lethal doses of H_2O_2.

Most of the identified negative and positive regulators of ARTD1 activity are able (i) to translocate into the nucleus (PKC, AMPK, MEK-ERK, CaMKII) (*232, 277-279*), (ii) to act in the same pathway (PKC-GSK3 / PKC-MEK) (*280, 281*) and are (iii) readily activated upon oxidative stress (second manuscript). To get a better insight into the direct modulation of ARTD1 activity by kinase signaling, one could try to identify possible phosphorylation sites for the above-mentioned kinases using mass spectrometry. Based on ARTD1 phospho-dead or –mimicking mutants, one could look at transcriptional, epigenetic or cell survival changes to understand their biological relevance in response to oxidative stress, but also other stimuli, such as inflammation, using models suited for the corresponding question. Since there is a group of negative regulators, some of which are described to act in a pathway (PKC-GSK3 or PKC-MEK), it would be also interesting to understand whether they act dependent on each other upon oxidative stress. Most importantly, the identification of the most prominent terminal kinase, which directly modifies ARTD1 and influences its activity, would be very interesting. Our proteomics and inhibitor screen analyses were biased towards signaling- and phosphorylation-dependent candidates. Thus, the activity of ARTD1 is also likely regulated by other posttranslational modifications, as has been shown for acetylation, ubiquitinylation or SUMOylation, even though without a direct effect on its enzymatic activity (*184*).

4.4 Oxidative stress induced poly-ADP-ribose formation is initiated by a Calcium dependent nuclease

Oxidative stress, for example reactive oxygen species (ROS), is an important stimulus for Ca^{2+} release from the ER, upon which the divalent ion can unleash its signaling potential (*137*). ARTD1 activity is strongly stimulated upon oxidative stress, which is so far believed to be exclusively due to the introduction of DNA breaks by direct oxidation of the DNA (*45*). Here, we report a Ca^{2+}-dependent activation mechanism of ARTD1 in a DNA break-dependent, but oxidation damage-independent manner. Inhibition of endogenous Ca^{2+} by a cell permeable Ca^{2+} chelator (BAPTA) reduced PAR formation to nearly basal levels. Moreover, inhibition or knockdown of IP3- or ryanodine receptors, as well as the IP3 producing enzyme PLC, all led to a significant reduction in PAR formation upon H_2O_2 treatment, indicating that the induction of PAR in response to H_2O_2 is dependent on the Ca^{2+} release from the ER. Indeed, Ca^{2+} signaling has been linked to ARTD1 activity in response to various stimuli ranging from growth factors to membrane depolarization, interestingly in all cases in a DNA break-independent manner (*230-232*). In contrast, we observed early break formation (after 3 min) in response to H_2O_2, which could be prevented by the addition of BAPTA. Interestingly, introduction of DNA breaks in response to ionizing radiation as well as oxidation of the DNA by $KBrO_3$ was Ca^{2+}-independent, indicating an H_2O_2-specific type of DNA breaks. Others have already reported the induction of DNA SSBs after H_2O_2 treatment as an upstream regulatory event of ARTD1, which was prevented in presence of BAPTA (*226*). In contrast to others, we were, however, able to identify the source of Ca^{2+} and excluded ROS formation as an upstream inducer of PAR formation using NAC (*226*). Altogether, our data point to a Ca^{2+}-dependent regulation of ARTD1 activity by a DNA nuclease induced upon oxidative stress. Even though BAPTA was described to be highly selective ($>10^5$) for Ca^{2+} over Mg^{2+} (*282*), two early studies challenged BAPTA's selectivity and could even show its preference for metal ions such as ferric iron (Fe^{3+}) (*283, 284*). Removal of extracellular Ca^{2+} by EGTA reduced H_2O_2-induced cytosolic and nuclear Ca^{2+}, but could not prevent DNA break induction (*283*). Interestingly, both BAPTA as well as selective membrane permeable metal ion chelators such as TPEN and PHEN prevented DNA breakage, while only BAPTA reduced intracellular Ca^{2+} levels, indicating metal ions as crucial mediators of H_2O_2-induced DNA break formation

(*283*). Whether metal ions are directly involved in DNA break formation has to be further investigated, however, it is well accepted that in the presence of ferrous (Fe^{2+}) or ferric (Fe^{3+}) iron, H_2O_2 is transformed into highly reactive hydroxyl free radicals (HO) via the Fenton reaction (*106*). Free hydroxyl radicals, on the other hand, could react with macromolecules such as the DNA and induce DNA breakage. Iron-dependent formation of free radicals, leading to DNA breaks and PAR formation, would insofar make sense, since direct DNA breakage by $KBrO_3$ or IR was BAPTA-independent. On the other hand, inhibition or knockdown of Ca^{2+} signaling modulators (such as PLC or IP_3R) strongly reduced PAR levels, indicating that the release of intracellular Ca^{2+} is an important regulatory component of PAR formation. Moreover, another laboratory recently observed a reduction in SSB formation upon nitrosative stress by using two additional Ca^{2+} chelators (cell permeable ester of EGTA and Quin-2), indicating the crucial role of Ca^{2+} in DNA break formation (*226*). Interestingly, increasing the cytosolic Ca^{2+} concentration by inhibiting the Ca^{2+} pump SERCA with the inhibitor thapsigargin prolonged PAR formation upon H_2O_2 exposure in this study, again strongly supporting the role of Ca^{2+} as a positive regulator of PAR formation. Thus, it cannot yet be excluded that both Ca^{2+} and iron metal ions contribute to ARTD1 activity and DNA break formation upon H_2O_2 treatment. Indeed, Golconda et al. reported both Ca^{2+} and iron to play a role in the formation of DNA breaks upon H_2O_2 treatment (*285*). A major consequence of a cytosolic Ca^{2+} rise is the depletion of intracellular Ca^{2+} stores in the ER and lysosomes, leading to Ca^{2+} overload in the mitochondria and the induction of caspase-dependent apoptosis (*138*). Importantly, early hallmarks of apoptosis are characterized by DNA fragmentation, which is initiated by a family of caspase-activated DNases (CADs) (*286*). Interestingly, early studies have already linked accumulation of cytosolic Ca^{2+} to DNA fragmentation in response to oxidative stress (*285, 287*). Hence, it would be interesting to test whether a Ca^{2+}-dependent nuclease might be involved in inducing PAR formation. Inhibition of caspases by Z-VAD revealed no significant changes of DNA break induction upon H_2O_2 exposure, suggesting that caspase-dependent DNAases are not playing a crucial role in DNA break formation.

Finally, inhibition of H_2O_2-induced DNA breaks and PAR formation in presence of BAPTA might be two independent processes, as we can currently not determine if the induced DNA breaks and PAR formation indeed co-localize.

An important aspect for future analysis is the question whether Ca^{2+} signaling is indeed a general regulator of ARTD1 activity, especially considering the versatile role of ARTD1 in different cell processes (*183*). To rule out or identify the crucial nuclease, one could perform an unbiased siRNA screen with PAR as a readout upon H_2O_2 exposure, however, also here one would have to consider technical pitfalls of such an approach, as has been nicely shown by others (*288*).

References

1. Amit, I., Citri, A., Shay, T., Lu, Y., Katz, M., Zhang, F., Tarcic, G., Siwak, D., Lahad, J., Jacob-Hirsch, J., Amariglio, N., Vaisman, N., Segal, E., Rechavi, G., Alon, U., Mills, G. B., Domany, E., and Yarden, Y. (2007) A module of negative feedback regulators defines growth factor signaling, *Nature genetics 39*, 503-512.
2. Westheimer, F. H. (1987) Why nature chose phosphates, *Science 235*, 1173-1178.
3. Hunter, T. (2012) Why nature chose phosphate to modify proteins, *Philosophical transactions of the Royal Society of London. Series B, Biological sciences 367*, 2513-2516.
4. Freeman, M. (2000) Feedback control of intercellular signalling in development, *Nature 408*, 313-319.
5. Dikic, I., and Giordano, S. (2003) Negative receptor signalling, *Current opinion in cell biology 15*, 128-135.
6. Hunter, T. (2000) Signaling--2000 and beyond, *Cell 100*, 113-127.
7. Hubbard, S. R., and Till, J. H. (2000) Protein tyrosine kinase structure and function, *Annual review of biochemistry 69*, 373-398.
8. Hubbard, S. R. (1997) Crystal structure of the activated insulin receptor tyrosine kinase in complex with peptide substrate and ATP analog, *Embo J 16*, 5572-5581.
9. Lemmon, M. A., and Schlessinger, J. (2010) Cell signaling by receptor tyrosine kinases, *Cell 141*, 1117-1134.
10. Pawson, T., and Nash, P. (2003) Assembly of cell regulatory systems through protein interaction domains, *Science 300*, 445-452.
11. Kolch, W. (2005) Coordinating ERK/MAPK signalling through scaffolds and inhibitors, *Nat Rev Mol Cell Biol 6*, 827-837.
12. Hazzalin, C. A., and Mahadevan, L. C. (2002) MAPK-regulated transcription: a continuously variable gene switch?, *Nat Rev Mol Cell Biol 3*, 30-40.
13. Ferguson, K. M., Lemmon, M. A., Sigler, P. B., and Schlessinger, J. (1995) Scratching the surface with the PH domain, *Nature structural biology 2*, 715-718.
14. Toker, A., and Cantley, L. C. (1997) Signalling through the lipid products of phosphoinositide-3-OH kinase, *Nature 387*, 673-676.
15. Karin, M. (2006) Nuclear factor-kappaB in cancer development and progression, *Nature 441*, 431-436.
16. Liscovitch, M., and Cantley, L. C. (1994) Lipid second messengers, *Cell 77*, 329-334.
17. Berridge, M. J., Bootman, M. D., and Roderick, H. L. (2003) Calcium signalling: dynamics, homeostasis and remodelling, *Nat Rev Mol Cell Biol 4*, 517-529.
18. Amit, I., Wides, R., and Yarden, Y. (2007) Evolvable signaling networks of receptor tyrosine kinases: relevance of robustness to malignancy and to cancer therapy, *Molecular systems biology 3*, 151.
19. Pastor-Satorras, R., Smith, E., and Sole, R. V. (2003) Evolving protein interaction networks through gene duplication, *Journal of theoretical biology 222*, 199-210.
20. Newton, A. C. (2010) Protein kinase C: poised to signal, *Am J Physiol Endocrinol Metab 298*, E395-402.
21. Le Good, J. A., Ziegler, W. H., Parekh, D. B., Alessi, D. R., Cohen, P., and Parker, P. J. (1998) Protein kinase C isotypes controlled by phosphoinositide 3-kinase through the protein kinase PDK1, *Science 281*, 2042-2045.
22. Ikenoue, T., Inoki, K., Yang, Q., Zhou, X., and Guan, K. L. (2008) Essential function of TORC2 in PKC and Akt turn motif phosphorylation, maturation and signalling, *Embo J 27*, 1919-1931.
23. Balendran, A., Hare, G.R.m Kieloch, M.R., Alessi, D.R. (2000) Further evidence that 3-phosphoinositide-dependent protein kinase-1 (PDK1) is required for the stability and phosphorylation of protein kinase C (PKC) isoforms., *FEBS Lett. 484*, 217-223.
24. Schechtman, D., and Mochly-Rosen, D. (2001) Adaptor proteins in protein kinase C-mediated signal transduction, *Oncogene 20*, 6339-6347.
25. Giorgione, J. R., Lin, J. H., McCammon, J. A., and Newton, A. C. (2006) Increased membrane affinity of the C1 domain of protein kinase Cdelta compensates for the lack of involvement of its C2 domain in membrane recruitment, *J Biol Chem 281*, 1660-1669.
26. Hansra, G., Garcia-Paramio, P., Prevostel, C., Whelan, R. D., Bornancin, F., and Parker, P. J. (1999) Multisite dephosphorylation and desensitization of conventional protein kinase C isotypes, *The Biochemical journal 342 (Pt 2)*, 337-344.
27. Huang, F. L., Yoshida, Y., Cunha-Melo, J. R., Beaven, M. A., and Huang, K. P. (1989) Differential down-regulation of protein kinase C isozymes, *J Biol Chem 264*, 4238-4243.

28. Leontieva, O. V., and Black, J. D. (2004) Identification of two distinct pathways of protein kinase Calpha down-regulation in intestinal epithelial cells, *J Biol Chem 279*, 5788-5801.
29. Toullec, D., Pianetti, P., Coste, H., Bellevergue, P., Grand-Perret, T., Ajakane, M., Baudet, V., Boissin, P., Boursier, E., Loriolle, F., and et al. (1991) The bisindolylmaleimide GF 109203X is a potent and selective inhibitor of protein kinase C, *J Biol Chem 266*, 15771-15781.
30. Cameron, A. J., Escribano, C., Saurin, A. T., Kostelecky, B., and Parker, P. J. (2009) PKC maturation is promoted by nucleotide pocket occupation independently of intrinsic kinase activity, *Nat Struct Mol Biol 16*, 624-630.
31. Hoeijmakers, J. H. (2001) Genome maintenance mechanisms for preventing cancer, *Nature 411*, 366-374.
32. Freedman, N. D., Leitzmann, M. F., Hollenbeck, A. R., Schatzkin, A., and Abnet, C. C. (2008) Cigarette smoking and subsequent risk of lung cancer in men and women: analysis of a prospective cohort study, *The lancet oncology 9*, 649-656.
33. Bartek, J., and Lukas, J. (2001) Mammalian G1- and S-phase checkpoints in response to DNA damage, *Current opinion in cell biology 13*, 738-747.
34. Surova, O., and Zhivotovsky, B. (2012) Various modes of cell death induced by DNA damage, *Oncogene*.
35. Shiloh, Y. (2003) ATM and related protein kinases: safeguarding genome integrity, *Nat Rev Cancer 3*, 155-168.
36. Hanawalt, P. C., and Spivak, G. (2008) Transcription-coupled DNA repair: two decades of progress and surprises, *Nat Rev Mol Cell Biol 9*, 958-970.
37. Waters, L. S., Minesinger, B. K., Wiltrout, M. E., D'Souza, S., Woodruff, R. V., and Walker, G. C. (2009) Eukaryotic translesion polymerases and their roles and regulation in DNA damage tolerance, *Microbiology and molecular biology reviews : MMBR 73*, 134-154.
38. van Loon, B., Markkanen, E., and Hubscher, U. (2010) Oxygen as a friend and enemy: How to combat the mutational potential of 8-oxo-guanine, *DNA repair 9*, 604-616.
39. Cooke, M. S., Evans, M. D., Dizdaroglu, M., and Lunec, J. (2003) Oxidative DNA damage: mechanisms, mutation, and disease, *FASEB journal : official publication of the Federation of American Societies for Experimental Biology 17*, 1195-1214.
40. McKinnon, P. J., and Caldecott, K. W. (2007) DNA strand break repair and human genetic disease, *Annual review of genomics and human genetics 8*, 37-55.
41. Lobrich, M., Shibata, A., Beucher, A., Fisher, A., Ensminger, M., Goodarzi, A. A., Barton, O., and Jeggo, P. A. gammaH2AX foci analysis for monitoring DNA double-strand break repair: strengths, limitations and optimization, *Cell Cycle 9*, 662-669.
42. Smyth, M. S., and Martin, J. H. (2000) x ray crystallography, *Mol Pathol 53*, 8-14.
43. Doi, K. (2007) Computer-aided diagnosis in medical imaging: historical review, current status and future potential, *Comput Med Imaging Graph 31*, 198-211.
44. Bernier, J., Hall, E. J., and Giaccia, A. (2004) Radiation oncology: a century of achievements, *Nat Rev Cancer 4*, 737-747.
45. Caldecott, K. W. (2008) Single-strand break repair and genetic disease, *Nature reviews. Genetics 9*, 619-631.
46. Harper, J. W., and Elledge, S. J. (2007) The DNA damage response: ten years after, *Mol Cell 28*, 739-745.
47. Ciccia, A., and Elledge, S. J. (2010) The DNA damage response: making it safe to play with knives, *Molecular cell 40*, 179-204.
48. Meek, K., Dang, V., and Lees-Miller, S. P. (2008) DNA-PK: the means to justify the ends?, *Advances in immunology 99*, 33-58.
49. You, Z., and Bailis, J. M. (2010) DNA damage and decisions: CtIP coordinates DNA repair and cell cycle checkpoints, *Trends in cell biology 20*, 402-409.
50. Zhou, B. B., and Elledge, S. J. (2000) The DNA damage response: putting checkpoints in perspective, *Nature 408*, 433-439.
51. Shiloh, Y. (2006) The ATM-mediated DNA-damage response: taking shape, *Trends Biochem Sci 31*, 402-410.
52. Abraham, R. T. (2004) PI 3-kinase related kinases: 'big' players in stress-induced signaling pathways, *DNA repair 3*, 883-887.
53. Brown, E. J., and Baltimore, D. (2000) ATR disruption leads to chromosomal fragmentation and early embryonic lethality, *Genes Dev 14*, 397-402.
54. O'Driscoll, M., Ruiz-Perez, V. L., Woods, C. G., Jeggo, P. A., and Goodship, J. A. (2003) A splicing mutation affecting expression of ataxia-telangiectasia and Rad3-related protein (ATR) results in Seckel syndrome, *Nature genetics 33*, 497-501.

55. Jazayeri, A., Falck, J., Lukas, C., Bartek, J., Smith, G. C., Lukas, J., and Jackson, S. P. (2006) ATM- and cell cycle-dependent regulation of ATR in response to DNA double-strand breaks, *Nat Cell Biol 8*, 37-45.
56. Uziel, T., Lerenthal, Y., Moyal, L., Andegeko, Y., Mittelman, L., and Shiloh, Y. (2003) Requirement of the MRN complex for ATM activation by DNA damage, *Embo J 22*, 5612-5621.
57. Bakkenist, C. J., and Kastan, M. B. (2003) DNA damage activates ATM through intermolecular autophosphorylation and dimer dissociation, *Nature 421*, 499-506.
58. Lee, J. H., and Paull, T. T. (2005) ATM activation by DNA double-strand breaks through the Mre11-Rad50-Nbs1 complex, *Science 308*, 551-554.
59. Kinner, A., Wu, W., Staudt, C., and Iliakis, G. (2008) Gamma-H2AX in recognition and signaling of DNA double-strand breaks in the context of chromatin, *Nucleic acids research 36*, 5678-5694.
60. Guo, Z., Kozlov, S., Lavin, M. F., Person, M. D., and Paull, T. T. (2010) ATM activation by oxidative stress, *Science 330*, 517-521.
61. Guo, Z., Deshpande, R., and Paull, T. T. (2010) ATM activation in the presence of oxidative stress, *Cell Cycle 9*, 4805-4811.
62. Matsuoka, S., Ballif, B. A., Smogorzewska, A., McDonald, E. R., 3rd, Hurov, K. E., Luo, J., Bakalarski, C. E., Zhao, Z., Solimini, N., Lerenthal, Y., Shiloh, Y., Gygi, S. P., and Elledge, S. J. (2007) ATM and ATR substrate analysis reveals extensive protein networks responsive to DNA damage, *Science 316*, 1160-1166.
63. Bensimon, A., Schmidt, A., Ziv, Y., Elkon, R., Wang, S. Y., Chen, D. J., Aebersold, R., and Shiloh, Y. (2010) ATM-dependent and -independent dynamics of the nuclear phosphoproteome after DNA damage, *Science signaling 3*, rs3.
64. Rogakou, E. P., Pilch, D. R., Orr, A. H., Ivanova, V. S., and Bonner, W. M. (1998) DNA double-stranded breaks induce histone H2AX phosphorylation on serine 139, *J Biol Chem 273*, 5858-5868.
65. Bonner, W. M., Redon, C. E., Dickey, J. S., Nakamura, A. J., Sedelnikova, O. A., Solier, S., and Pommier, Y. (2008) GammaH2AX and cancer, *Nat Rev Cancer 8*, 957-967.
66. Stiff, T., O'Driscoll, M., Rief, N., Iwabuchi, K., Lobrich, M., and Jeggo, P. A. (2004) ATM and DNA-PK function redundantly to phosphorylate H2AX after exposure to ionizing radiation, *Cancer research 64*, 2390-2396.
67. Stucki, M., Clapperton, J. A., Mohammad, D., Yaffe, M. B., Smerdon, S. J., and Jackson, S. P. (2005) MDC1 directly binds phosphorylated histone H2AX to regulate cellular responses to DNA double-strand breaks, *Cell 123*, 1213-1226.
68. Lou, Z., Minter-Dykhouse, K., Franco, S., Gostissa, M., Rivera, M. A., Celeste, A., Manis, J. P., van Deursen, J., Nussenzweig, A., Paull, T. T., Alt, F. W., and Chen, J. (2006) MDC1 maintains genomic stability by participating in the amplification of ATM-dependent DNA damage signals, *Molecular cell 21*, 187-200.
69. Stewart, G. S., Wang, B., Bignell, C. R., Taylor, A. M., and Elledge, S. J. (2003) MDC1 is a mediator of the mammalian DNA damage checkpoint, *Nature 421*, 961-966.
70. van Attikum, H., and Gasser, S. M. (2009) Crosstalk between histone modifications during the DNA damage response, *Trends in cell biology 19*, 207-217.
71. Tjeertes, J. V., Miller, K. M., and Jackson, S. P. (2009) Screen for DNA-damage-responsive histone modifications identifies H3K9Ac and H3K56Ac in human cells, *Embo J 28*, 1878-1889.
72. Huyen, Y., Zgheib, O., Ditullio, R. A., Jr., Gorgoulis, V. G., Zacharatos, P., Petty, T. J., Sheston, E. A., Mellert, H. S., Stavridi, E. S., and Halazonetis, T. D. (2004) Methylated lysine 79 of histone H3 targets 53BP1 to DNA double-strand breaks, *Nature 432*, 406-411.
73. Markham, D., Munro, S., Soloway, J., O'Connor, D. P., and La Thangue, N. B. (2006) DNA-damage-responsive acetylation of pRb regulates binding to E2F-1, *EMBO Rep 7*, 192-198.
74. Carr, S. M., Munro, S., Kessler, B., Oppermann, U., and La Thangue, N. B. (2011) Interplay between lysine methylation and Cdk phosphorylation in growth control by the retinoblastoma protein, *Embo J 30*, 317-327.
75. Tang, Y., Zhao, W., Chen, Y., Zhao, Y., and Gu, W. (2008) Acetylation is indispensable for p53 activation, *Cell 133*, 612-626.
76. Pradhan, S., Chin, H. G., Esteve, P. O., and Jacobsen, S. E. (2009) SET7/9 mediated methylation of non-histone proteins in mammalian cells, *Epigenetics : official journal of the DNA Methylation Society 4*, 383-387.
77. Bennetzen, M. V., Larsen, D. H., Bunkenborg, J., Bartek, J., Lukas, J., and Andersen, J. S. (2010) Site-specific phosphorylation dynamics of the nuclear proteome during the DNA damage response, *Mol Cell Proteomics 9*, 1314-1323.

78. Beli, P., Lukashchuk, N., Wagner, S. A., Weinert, B. T., Olsen, J. V., Baskcomb, L., Mann, M., Jackson, S. P., and Choudhary, C. (2012) Proteomic Investigations Reveal a Role for RNA Processing Factor THRAP3 in the DNA Damage Response, *Mol Cell 46*, 212-225.
79. Tentner, A. R., Lee, M. J., Ostheimer, G. J., Samson, L. D., Lauffenburger, D. A., and Yaffe, M. B. (2012) Combined experimental and computational analysis of DNA damage signaling reveals context-dependent roles for Erk in apoptosis and G1/S arrest after genotoxic stress, *Molecular systems biology 8*, 568.
80. Bluwstein, A., Kumar, N., Leger, K., Traenkle, J., Oostrum, J., Rehrauer, H., Baudis, M., and Hottiger, M. O. (2013) PKC signaling prevents irradiation-induced apoptosis of primary human fibroblasts, *Cell death & disease 4*, e498.
81. Stilmann, M., Hinz, M., Arslan, S. C., Zimmer, A., Schreiber, V., and Scheidereit, C. (2009) A nuclear poly(ADP-ribose)-dependent signalosome confers DNA damage-induced IkappaB kinase activation, *Molecular cell 36*, 365-378.
82. Hinz, M., Stilmann, M., Arslan, S. C., Khanna, K. K., Dittmar, G., and Scheidereit, C. (2010) A cytoplasmic ATM-TRAF6-cIAP1 module links nuclear DNA damage signaling to ubiquitin-mediated NF-kappaB activation, *Molecular cell 40*, 63-74.
83. Wu, Z. H., Wong, E. T., Shi, Y., Niu, J., Chen, Z., Miyamoto, S., and Tergaonkar, V. (2010) ATM- and NEMO-dependent ELKS ubiquitination coordinates TAK1-mediated IKK activation in response to genotoxic stress, *Molecular cell 40*, 75-86.
84. Kharbanda, S., Pandey, P., Yamauchi, T., Kumar, S., Kaneki, M., Kumar, V., Bharti, A., Yuan, Z. M., Ghanem, L., Rana, A., Weichselbaum, R., Johnson, G., and Kufe, D. (2000) Activation of MEK kinase 1 by the c-Abl protein tyrosine kinase in response to DNA damage, *Molecular and cellular biology 20*, 4979-4989.
85. Tang, D., Wu, D., Hirao, A., Lahti, J. M., Liu, L., Mazza, B., Kidd, V. J., Mak, T. W., and Ingram, A. J. (2002) ERK activation mediates cell cycle arrest and apoptosis after DNA damage independently of p53, *J Biol Chem 277*, 12710-12717.
86. Bozulic, L., Surucu, B., Hynx, D., and Hemmings, B. A. (2008) PKBalpha/Akt1 acts downstream of DNA-PK in the DNA double-strand break response and promotes survival, *Mol Cell 30*, 203-213.
87. Manke, I. A., Nguyen, A., Lim, D., Stewart, M. Q., Elia, A. E., and Yaffe, M. B. (2005) MAPKAP kinase-2 is a cell cycle checkpoint kinase that regulates the G2/M transition and S phase progression in response to UV irradiation, *Molecular cell 17*, 37-48.
88. Wang, X., McGowan, C. H., Zhao, M., He, L., Downey, J. S., Fearns, C., Wang, Y., Huang, S., and Han, J. (2000) Involvement of the MKK6-p38gamma cascade in gamma-radiation-induced cell cycle arrest, *Molecular and cellular biology 20*, 4543-4552.
89. Bensimon, A., Aebersold, R., and Shiloh, Y. (2011) Beyond ATM: the protein kinase landscape of the DNA damage response, *FEBS letters 585*, 1625-1639.
90. Bartek, J., and Lukas, J. (2001) Mammalian G1- and S-phase checkpoints in response to DNA damage, *Curr Opin Cell Biol 13*, 738-747.
91. Malumbres, M., and Barbacid, M. (2001) To cycle or not to cycle: a critical decision in cancer, *Nat Rev Cancer 1*, 222-231.
92. Santra, M. K., Wajapeyee, N., and Green, M. R. (2009) F-box protein FBXO31 mediates cyclin D1 degradation to induce G1 arrest after DNA damage, *Nature 459*, 722-725.
93. Mailand, N., Falck, J., Lukas, C., Syljuasen, R. G., Welcker, M., Bartek, J., and Lukas, J. (2000) Rapid destruction of human Cdc25A in response to DNA damage, *Science 288*, 1425-1429.
94. Meek, D. W. (2009) Tumour suppression by p53: a role for the DNA damage response?, *Nat Rev Cancer 9*, 714-723.
95. Stein, G. H., Drullinger, L. F., Soulard, A., and Dulic, V. (1999) Differential roles for cyclin-dependent kinase inhibitors p21 and p16 in the mechanisms of senescence and differentiation in human fibroblasts, *Mol Cell Biol 19*, 2109-2117.
96. Campisi, J. (2001) Cellular senescence as a tumor-suppressor mechanism, *Trends in cell biology 11*, S27-31.
97. Hanahan, D., and Weinberg, R. A. (2011) Hallmarks of cancer: the next generation, *Cell 144*, 646-674.
98. Donzelli, M., and Draetta, G. F. (2003) Regulating mammalian checkpoints through Cdc25 inactivation, *EMBO Rep 4*, 671-677.
99. Reinhardt, H. C., and Yaffe, M. B. (2009) Kinases that control the cell cycle in response to DNA damage: Chk1, Chk2, and MK2, *Current opinion in cell biology 21*, 245-255.
100. Kinzler, K. W., and Vogelstein, B. (1997) Cancer-susceptibility genes. Gatekeepers and caretakers, *Nature 386*, 761, 763.

101. Vogelstein, B., and Kinzler, K. W. (2004) Cancer genes and the pathways they control, *Nature medicine 10*, 789-799.
102. Knudson, A. G., Jr. (1971) Mutation and cancer: statistical study of retinoblastoma, *Proc Natl Acad Sci U S A 68*, 820-823.
103. Cai, H., and Harrison, D. G. (2000) Endothelial dysfunction in cardiovascular diseases: the role of oxidant stress, *Circulation research 87*, 840-844.
104. Nathan, C. (2003) Specificity of a third kind: reactive oxygen and nitrogen intermediates in cell signaling, *The Journal of clinical investigation 111*, 769-778.
105. D'Autreaux, B., and Toledano, M. B. (2007) ROS as signalling molecules: mechanisms that generate specificity in ROS homeostasis, *Nat Rev Mol Cell Biol 8*, 813-824.
106. Jones, D. P. (2008) Radical-free biology of oxidative stress, *American journal of physiology. Cell physiology 295*, C849-868.
107. Fridovich, I. (1997) Superoxide anion radical (O2-.), superoxide dismutases, and related matters, *J Biol Chem 272*, 18515-18517.
108. Thomas, D. D., Liu, X., Kantrow, S. P., and Lancaster, J. R., Jr. (2001) The biological lifetime of nitric oxide: implications for the perivascular dynamics of NO and O2, *Proc Natl Acad Sci U S A 98*, 355-360.
109. Hidalgo, E., and Demple, B. (1994) An iron-sulfur center essential for transcriptional activation by the redox-sensing SoxR protein, *Embo J 13*, 138-146.
110. Zheng, M., Aslund, F., and Storz, G. (1998) Activation of the OxyR transcription factor by reversible disulfide bond formation, *Science 279*, 1718-1721.
111. Kim, S. O., Merchant, K., Nudelman, R., Beyer, W. F., Jr., Keng, T., DeAngelo, J., Hausladen, A., and Stamler, J. S. (2002) OxyR: a molecular code for redox-related signaling, *Cell 109*, 383-396.
112. Winter, J., Linke, K., Jatzek, A., and Jakob, U. (2005) Severe oxidative stress causes inactivation of DnaK and activation of the redox-regulated chaperone Hsp33, *Molecular cell 17*, 381-392.
113. Graf, P. C., Martinez-Yamout, M., VanHaerents, S., Lilie, H., Dyson, H. J., and Jakob, U. (2004) Activation of the redox-regulated chaperone Hsp33 by domain unfolding, *J Biol Chem 279*, 20529-20538.
114. Klatt, P., and Lamas, S. (2000) Regulation of protein function by S-glutathiolation in response to oxidative and nitrosative stress, *European journal of biochemistry / FEBS 267*, 4928-4944.
115. den Hertog, J., Groen, A., and van der Wijk, T. (2005) Redox regulation of protein-tyrosine phosphatases, *Archives of biochemistry and biophysics 434*, 11-15.
116. Mohr, S., Hallak, H., de Boitte, A., Lapetina, E. G., and Brune, B. (1999) Nitric oxide-induced S-glutathionylation and inactivation of glyceraldehyde-3-phosphate dehydrogenase, *J Biol Chem 274*, 9427-9430.
117. Qanungo, S., Starke, D. W., Pai, H. V., Mieyal, J. J., and Nieminen, A. L. (2007) Glutathione supplementation potentiates hypoxic apoptosis by S-glutathionylation of p65-NFkappaB, *J Biol Chem 282*, 18427-18436.
118. Sykes, M. C., Mowbray, A. L., and Jo, H. (2007) Reversible glutathiolation of caspase-3 by glutaredoxin as a novel redox signaling mechanism in tumor necrosis factor-alpha-induced cell death, *Circulation research 100*, 152-154.
119. Lander, H. M., Milbank, A. J., Tauras, J. M., Hajjar, D. P., Hempstead, B. L., Schwartz, G. D., Kraemer, R. T., Mirza, U. A., Chait, B. T., Burk, S. C., and Quilliam, L. A. (1996) Redox regulation of cell signalling, *Nature 381*, 380-381.
120. Choi, Y., Chen, H. V., and Lipton, S. A. (2001) Three pairs of cysteine residues mediate both redox and zn2+ modulation of the nmda receptor, *The Journal of neuroscience : the official journal of the Society for Neuroscience 21*, 392-400.
121. Fratelli, M., Demol, H., Puype, M., Casagrande, S., Eberini, I., Salmona, M., Bonetto, V., Mengozzi, M., Duffieux, F., Miclet, E., Bachi, A., Vandekerckhove, J., Gianazza, E., and Ghezzi, P. (2002) Identification by redox proteomics of glutathionylated proteins in oxidatively stressed human T lymphocytes, *Proc Natl Acad Sci U S A 99*, 3505-3510.
122. Leichert, L. I., Gehrke, F., Gudiseva, H. V., Blackwell, T., Ilbert, M., Walker, A. K., Strahler, J. R., Andrews, P. C., and Jakob, U. (2008) Quantifying changes in the thiol redox proteome upon oxidative stress in vivo, *Proc Natl Acad Sci U S A 105*, 8197-8202.
123. Brigelius-Flohe, R., Banning, A., and Schnurr, K. (2003) Selenium-dependent enzymes in endothelial cell function, *Antioxid Redox Signal 5*, 205-215.
124. Malhotra, J. D., and Kaufman, R. J. (2007) Endoplasmic reticulum stress and oxidative stress: a vicious cycle or a double-edged sword?, *Antioxid Redox Signal 9*, 2277-2293.

125. Chakravarthi, S., Jessop, C. E., and Bulleid, N. J. (2006) The role of glutathione in disulphide bond formation and endoplasmic-reticulum-generated oxidative stress, *EMBO Rep 7*, 271-275.
126. Hwang, C., Sinskey, A. J., and Lodish, H. F. (1992) Oxidized redox state of glutathione in the endoplasmic reticulum, *Science 257*, 1496-1502.
127. Gross, E., Kastner, D. B., Kaiser, C. A., and Fass, D. (2004) Structure of Ero1p, source of disulfide bonds for oxidative protein folding in the cell, *Cell 117*, 601-610.
128. Ellgaard, L., and Helenius, A. (2003) Quality control in the endoplasmic reticulum, *Nat Rev Mol Cell Biol 4*, 181-191.
129. Schroder, M., and Kaufman, R. J. (2005) The mammalian unfolded protein response, *Annual review of biochemistry 74*, 739-789.
130. Bertolotti, A., Zhang, Y., Hendershot, L. M., Harding, H. P., and Ron, D. (2000) Dynamic interaction of BiP and ER stress transducers in the unfolded-protein response, *Nat Cell Biol 2*, 326-332.
131. Harding, H. P., Zhang, Y., Zeng, H., Novoa, I., Lu, P. D., Calfon, M., Sadri, N., Yun, C., Popko, B., Paules, R., Stojdl, D. F., Bell, J. C., Hettmann, T., Leiden, J. M., and Ron, D. (2003) An integrated stress response regulates amino acid metabolism and resistance to oxidative stress, *Molecular cell 11*, 619-633.
132. Yamamoto, K., Sato, T., Matsui, T., Sato, M., Okada, T., Yoshida, H., Harada, A., and Mori, K. (2007) Transcriptional induction of mammalian ER quality control proteins is mediated by single or combined action of ATF6alpha and XBP1, *Developmental cell 13*, 365-376.
133. Zhang, K., and Kaufman, R. J. (2008) From endoplasmic-reticulum stress to the inflammatory response, *Nature 454*, 455-462.
134. Tu, B. P., and Weissman, J. S. (2004) Oxidative protein folding in eukaryotes: mechanisms and consequences, *The Journal of cell biology 164*, 341-346.
135. Gorlach, A., Klappa, P., and Kietzmann, T. (2006) The endoplasmic reticulum: folding, calcium homeostasis, signaling, and redox control, *Antioxid Redox Signal 8*, 1391-1418.
136. Ryter, S. W., Kim, H. P., Hoetzel, A., Park, J. W., Nakahira, K., Wang, X., and Choi, A. M. (2007) Mechanisms of cell death in oxidative stress, *Antioxid Redox Signal 9*, 49-89.
137. Berridge, M. J., Lipp, P., and Bootman, M. D. (2000) The versatility and universality of calcium signalling, *Nat Rev Mol Cell Biol 1*, 11-21.
138. Hanson, C. J., Bootman, M. D., and Roderick, H. L. (2004) Cell signalling: IP3 receptors channel calcium into cell death, *Current biology : CB 14*, R933-935.
139. Miyazaki, S., Shirakawa, H., Nakada, K., and Honda, Y. (1993) Essential role of the inositol 1,4,5-trisphosphate receptor/Ca2+ release channel in Ca2+ waves and Ca2+ oscillations at fertilization of mammalian eggs, *Dev Biol 158*, 62-78.
140. Gilland, E., Miller, A. L., Karplus, E., Baker, R., and Webb, S. E. (1999) Imaging of multicellular large-scale rhythmic calcium waves during zebrafish gastrulation, *Proc Natl Acad Sci U S A 96*, 157-161.
141. Creton, R., Speksnijder, J. E., and Jaffe, L. F. (1998) Patterns of free calcium in zebrafish embryos, *Journal of cell science 111 (Pt 12)*, 1613-1622.
142. Creton, R., Kreiling, J. A., and Jaffe, L. F. (2000) Presence and roles of calcium gradients along the dorsal-ventral axis in Drosophila embryos, *Dev Biol 217*, 375-385.
143. Mackenzie, L., Bootman, M. D., Berridge, M. J., and Lipp, P. (2001) Predetermined recruitment of calcium release sites underlies excitation-contraction coupling in rat atrial myocytes, *The Journal of physiology 530*, 417-429.
144. Berridge, M. J. (1998) Neuronal calcium signaling, *Neuron 21*, 13-26.
145. Buonanno, A., and Fields, R. D. (1999) Gene regulation by patterned electrical activity during neural and skeletal muscle development, *Current opinion in neurobiology 9*, 110-120.
146. Lu, K. P., and Means, A. R. (1993) Regulation of the cell cycle by calcium and calmodulin, *Endocrine reviews 14*, 40-58.
147. Crabtree, G. R. (1999) Generic signals and specific outcomes: signaling through Ca2+, calcineurin, and NF-AT, *Cell 96*, 611-614.
148. Chawla, S., Hardingham, G. E., Quinn, D. R., and Bading, H. (1998) CBP: a signal-regulated transcriptional coactivator controlled by nuclear calcium and CaM kinase IV, *Science 281*, 1505-1509.
149. Hardingham, G. E., Chawla, S., Cruzalegui, F. H., and Bading, H. (1999) Control of recruitment and transcription-activating function of CBP determines gene regulation by NMDA receptors and L-type calcium channels, *Neuron 22*, 789-798.
150. Smith, M. R., Court, D. W., Kim, H. K., Park, J. B., Rhee, S. G., Rhim, J. S., and Kung, H. F. (1998) Overexpression of phosphoinositide-specific phospholipase Cgamma in NIH 3T3 cells promotes transformation and tumorigenicity, *Carcinogenesis 19*, 177-185.

151. Rizzo, M. T., and Weber, G. (1994) 1-Phosphatidylinositol 4-kinase: an enzyme linked with proliferation and malignancy, *Cancer research 54*, 2611-2614.
152. Hajnoczky, G., Csordas, G., Madesh, M., and Pacher, P. (2000) Control of apoptosis by IP(3) and ryanodine receptor driven calcium signals, *Cell Calcium 28*, 349-363.
153. Bootman, M. D., and Lipp, P. (1999) Ringing changes to the 'bell-shaped curve', *Current biology : CB 9*, R876-878.
154. Clapham, D. E. (2007) Calcium signaling, *Cell 131*, 1047-1058.
155. Kelley, G. G., Reks, S. E., Ondrako, J. M., and Smrcka, A. V. (2001) Phospholipase C(epsilon): a novel Ras effector, *Embo J 20*, 743-754.
156. Lee, H. C. (2012) Cyclic ADP-ribose and nicotinic acid adenine dinucleotide phosphate (NAADP) as messengers for calcium mobilization, *J Biol Chem 287*, 31633-31640.
157. Lange, I., Penner, R., Fleig, A., and Beck, A. (2008) Synergistic regulation of endogenous TRPM2 channels by adenine dinucleotides in primary human neutrophils, *Cell Calcium 44*, 604-615.
158. Kolisek, M., Beck, A., Fleig, A., and Penner, R. (2005) Cyclic ADP-ribose and hydrogen peroxide synergize with ADP-ribose in the activation of TRPM2 channels, *Molecular cell 18*, 61-69.
159. Bers, D. M. (2004) Macromolecular complexes regulating cardiac ryanodine receptor function, *Journal of molecular and cellular cardiology 37*, 417-429.
160. Ramsey, I. S., Delling, M., and Clapham, D. E. (2006) An introduction to TRP channels, *Annual review of physiology 68*, 619-647.
161. Newmeyer, D. D., and Ferguson-Miller, S. (2003) Mitochondria: releasing power for life and unleashing the machineries of death, *Cell 112*, 481-490.
162. Rapizzi, E., Pinton, P., Szabadkai, G., Wieckowski, M. R., Vandecasteele, G., Baird, G., Tuft, R. A., Fogarty, K. E., and Rizzuto, R. (2002) Recombinant expression of the voltage-dependent anion channel enhances the transfer of Ca2+ microdomains to mitochondria, *The Journal of cell biology 159*, 613-624.
163. Vanden Abeele, F., Skryma, R., Shuba, Y., Van Coppenolle, F., Slomianny, C., Roudbaraki, M., Mauroy, B., Wuytack, F., and Prevarskaya, N. (2002) Bcl-2-dependent modulation of Ca(2+) homeostasis and store-operated channels in prostate cancer cells, *Cancer Cell 1*, 169-179.
164. Nutt, L. K., Chandra, J., Pataer, A., Fang, B., Roth, J. A., Swisher, S. G., O'Neil, R. G., and McConkey, D. J. (2002) Bax-mediated Ca2+ mobilization promotes cytochrome c release during apoptosis, *J Biol Chem 277*, 20301-20308.
165. Nutt, L. K., Pataer, A., Pahler, J., Fang, B., Roth, J., McConkey, D. J., and Swisher, S. G. (2002) Bax and Bak promote apoptosis by modulating endoplasmic reticular and mitochondrial Ca2+ stores, *J Biol Chem 277*, 9219-9225.
166. Niki, I., Yokokura, H., Sudo, T., Kato, M., and Hidaka, H. (1996) Ca2+ signaling and intracellular Ca2+ binding proteins, *Journal of biochemistry 120*, 685-698.
167. Nakayama, S., and Kretsinger, R. H. (1994) Evolution of the EF-hand family of proteins, *Annual review of biophysics and biomolecular structure 23*, 473-507.
168. Hoeflich, K. P., and Ikura, M. (2002) Calmodulin in action: diversity in target recognition and activation mechanisms, *Cell 108*, 739-742.
169. Shen, X., Valencia, C. A., Szostak, J. W., Dong, B., and Liu, R. (2005) Scanning the human proteome for calmodulin-binding proteins, *Proc Natl Acad Sci U S A 102*, 5969-5974.
170. Swulius, M. T., and Waxham, M. N. (2008) Ca(2+)/calmodulin-dependent protein kinases, *Cellular and molecular life sciences : CMLS 65*, 2637-2657.
171. Pearson, R. B., and Kemp, B. E. (1991) Protein kinase phosphorylation site sequences and consensus specificity motifs: tabulations, *Methods Enzymol 200*, 62-81.
172. Hudmon, A., and Schulman, H. (2002) Structure-function of the multifunctional Ca2+/calmodulin-dependent protein kinase II, *The Biochemical journal 364*, 593-611.
173. Gaertner, T. R., Kolodziej, S. J., Wang, D., Kobayashi, R., Koomen, J. M., Stoops, J. K., and Waxham, M. N. (2004) Comparative analyses of the three-dimensional structures and enzymatic properties of alpha, beta, gamma and delta isoforms of Ca2+-calmodulin-dependent protein kinase II, *J Biol Chem 279*, 12484-12494.
174. Rosenberg, O. S., Deindl, S., Sung, R. J., Nairn, A. C., and Kuriyan, J. (2005) Structure of the autoinhibited kinase domain of CaMKII and SAXS analysis of the holoenzyme, *Cell 123*, 849-860.
175. Meyer, T., Hanson, P. I., Stryer, L., and Schulman, H. (1992) Calmodulin trapping by calcium-calmodulin-dependent protein kinase, *Science 256*, 1199-1202.

176. Miller, S. G., and Kennedy, M. B. (1986) Regulation of brain type II Ca2+/calmodulin-dependent protein kinase by autophosphorylation: a Ca2+-triggered molecular switch, *Cell 44*, 861-870.
177. Swaminathan, P. D., and Anderson, M. E. (2011) CaMKII inhibition: breaking the cycle of electrical storm?, *Circulation 123*, 2183-2186.
178. Tobimatsu, T., and Fujisawa, H. (1989) Tissue-specific expression of four types of rat calmodulin-dependent protein kinase II mRNAs, *J Biol Chem 264*, 17907-17912.
179. Griffith, L. C. (2004) Calcium/calmodulin-dependent protein kinase II: an unforgettable kinase, *The Journal of neuroscience : the official journal of the Society for Neuroscience 24*, 8391-8393.
180. Lisman, J., Yasuda, R., and Raghavachari, S. (2012) Mechanisms of CaMKII action in long-term potentiation, *Nature reviews. Neuroscience 13*, 169-182.
181. Miranti, C. K., Ginty, D. D., Huang, G., Chatila, T., and Greenberg, M. E. (1995) Calcium activates serum response factor-dependent transcription by a Ras- and Elk-1-independent mechanism that involves a Ca2+/calmodulin-dependent kinase, *Molecular and cellular biology 15*, 3672-3684.
182. Nair, J. S., DaFonseca, C. J., Tjernberg, A., Sun, W., Darnell, J. E., Jr., Chait, B. T., and Zhang, J. J. (2002) Requirement of Ca2+ and CaMKII for Stat1 Ser-727 phosphorylation in response to IFN-gamma, *Proc Natl Acad Sci U S A 99*, 5971-5976.
183. Gibson, B. A., and Kraus, W. L. (2012) New insights into the molecular and cellular functions of poly(ADP-ribose) and PARPs, *Nat Rev Mol Cell Biol 13*, 411-424.
184. Luo, X., and Kraus, W. L. (2012) On PAR with PARP: cellular stress signaling through poly(ADP-ribose) and PARP-1, *Genes Dev 26*, 417-432.
185. Krishnakumar, R., and Kraus, W. L. (2010) The PARP side of the nucleus: molecular actions, physiological outcomes, and clinical targets, *Molecular cell 39*, 8-24.
186. Hassa, P. O., Haenni, S. S., Elser, M., and Hottiger, M. O. (2006) Nuclear ADP-ribosylation reactions in mammalian cells: where are we today and where are we going?, *Microbiol Mol Biol Rev 70*, 789-829.
187. Hassa, P. O., and Hottiger, M. O. (2008) The diverse biological roles of mammalian PARPS, a small but powerful family of poly-ADP-ribose polymerases, *Frontiers in bioscience : a journal and virtual library 13*, 3046-3082.
188. Hottiger, M. O., Hassa, P. O., Luscher, B., Schuler, H., and Koch-Nolte, F. (2010) Toward a unified nomenclature for mammalian ADP-ribosyltransferases, *Trends in biochemical sciences 35*, 208-219.
189. Ame, J. C., Rolli, V., Schreiber, V., Niedergang, C., Apiou, F., Decker, P., Muller, S., Hoger, T., Menissier-de Murcia, J., and de Murcia, G. (1999) PARP-2, A novel mammalian DNA damage-dependent poly(ADP-ribose) polymerase, *J Biol Chem 274*, 17860-17868.
190. Altmeyer, M., Messner, S., Hassa, P. O., Fey, M., and Hottiger, M. O. (2009) Molecular mechanism of poly(ADP-ribosyl)ation by PARP1 and identification of lysine residues as ADP-ribose acceptor sites, *Nucleic acids research 37*, 3723-3738.
191. Boehler, C., Gauthier, L. R., Mortusewicz, O., Biard, D. S., Saliou, J. M., Bresson, A., Sanglier-Cianferani, S., Smith, S., Schreiber, V., Boussin, F., and Dantzer, F. (2011) Poly(ADP-ribose) polymerase 3 (PARP3), a newcomer in cellular response to DNA damage and mitotic progression, *Proc Natl Acad Sci U S A 108*, 2783-2788.
192. Rulten, S. L., Fisher, A. E., Robert, I., Zuma, M. C., Rouleau, M., Ju, L., Poirier, G., Reina-San-Martin, B., and Caldecott, K. W. (2011) PARP-3 and APLF function together to accelerate nonhomologous end-joining, *Molecular cell 41*, 33-45.
193. Kickhoefer, V. A., Siva, A. C., Kedersha, N. L., Inman, E. M., Ruland, C., Streuli, M., and Rome, L. H. (1999) The 193-kD vault protein, VPARP, is a novel poly(ADP-ribose) polymerase, *The Journal of cell biology 146*, 917-928.
194. Raval-Fernandes, S., Kickhoefer, V. A., Kitchen, C., and Rome, L. H. (2005) Increased susceptibility of vault poly(ADP-ribose) polymerase-deficient mice to carcinogen-induced tumorigenesis, *Cancer research 65*, 8846-8852.
195. Smith, S., Giriat, I., Schmitt, A., and de Lange, T. (1998) Tankyrase, a poly(ADP-ribose) polymerase at human telomeres, *Science 282*, 1484-1487.
196. Chang, P., Coughlin, M., and Mitchison, T. J. (2005) Tankyrase-1 polymerization of poly(ADP-ribose) is required for spindle structure and function, *Nat Cell Biol 7*, 1133-1139.
197. Langelier, M. F., Planck, J. L., Roy, S., and Pascal, J. M. (2012) Structural basis for DNA damage-dependent poly(ADP-ribosyl)ation by human PARP-1, *Science 336*, 728-732.
198. Ali, A. A., Timinszky, G., Arribas-Bosacoma, R., Kozlowski, M., Hassa, P. O., Hassler, M., Ladurner, A. G., Pearl, L. H., and Oliver, A. W. (2012) The zinc-finger domains of PARP1 cooperate to recognize DNA strand breaks, *Nat Struct Mol Biol 19*, 685-692.

199. Langelier, M. F., Ruhl, D. D., Planck, J. L., Kraus, W. L., and Pascal, J. M. (2010) The Zn3 domain of human poly(ADP-ribose) polymerase-1 (PARP-1) functions in both DNA-dependent poly(ADP-ribose) synthesis activity and chromatin compaction, *J Biol Chem 285*, 18877-18887.
200. Leung, C. C., and Glover, J. N. (2011) BRCT domains: easy as one, two, three, *Cell cycle 10*, 2461-2470.
201. Kiehlbauch, C. C., Aboul-Ela, N., Jacobson, E. L., Ringer, D. P., and Jacobson, M. K. (1993) High resolution fractionation and characterization of ADP-ribose polymers, *Analytical biochemistry 208*, 26-34.
202. Ogata, N., Ueda, K., and Hayaishi, O. (1980) ADP-ribosylation of histone H2B. Identification of glutamic acid residue 2 as the modification site, *J Biol Chem 255*, 7610-7615.
203. Kawaichi, M., Ueda, K., and Hayaishi, O. (1981) Multiple autopoly(ADP-ribosyl)ation of rat liver poly(ADP-ribose) synthetase. Mode of modification and properties of automodified synthetase, *J Biol Chem 256*, 9483-9489.
204. Haenni, S. S., Hassa, P. O., Altmeyer, M., Fey, M., Imhof, R., and Hottiger, M. O. (2008) Identification of lysines 36 and 37 of PARP-2 as targets for acetylation and auto-ADP-ribosylation, *The international journal of biochemistry & cell biology 40*, 2274-2283.
205. Chapman, J. D., Gagne, J. P., Poirier, G. G., and Goodlett, D. R. (2013) Mapping PARP-1 Auto-ADP-ribosylation Sites by Liquid Chromatography-Tandem Mass Spectrometry, *Journal of proteome research*.
206. Kanai, M., Hanashiro, K., Kim, S. H., Hanai, S., Boulares, A. H., Miwa, M., and Fukasawa, K. (2007) Inhibition of Crm1-p53 interaction and nuclear export of p53 by poly(ADP-ribosyl)ation, *Nat Cell Biol 9*, 1175-1183.
207. Kraus, W. L. (2008) Transcriptional control by PARP-1: chromatin modulation, enhancer-binding, coregulation, and insulation, *Current opinion in cell biology 20*, 294-302.
208. Meyer-Ficca, M. L., Meyer, R. G., Coyle, D. L., Jacobson, E. L., and Jacobson, M. K. (2004) Human poly(ADP-ribose) glycohydrolase is expressed in alternative splice variants yielding isoforms that localize to different cell compartments, *Experimental cell research 297*, 521-532.
209. Oka, S., Kato, J., and Moss, J. (2006) Identification and characterization of a mammalian 39-kDa poly(ADP-ribose) glycohydrolase, *J Biol Chem 281*, 705-713.
210. Kraus, W. L., and Hottiger, M. O. (2013) PARP-1 and gene regulation: Progress and puzzles, *Molecular aspects of medicine*.
211. David, K. K., Andrabi, S. A., Dawson, T. M., and Dawson, V. L. (2009) Parthanatos, a messenger of death, *Frontiers in bioscience : a journal and virtual library 14*, 1116-1128.
212. Eustermann, S., Videler, H., Yang, J. C., Cole, P. T., Gruszka, D., Veprintsev, D., and Neuhaus, D. (2011) The DNA-binding domain of human PARP-1 interacts with DNA single-strand breaks as a monomer through its second zinc finger, *J Mol Biol 407*, 149-170.
213. Potaman, V. N., Shlyakhtenko, L. S., Oussatcheva, E. A., Lyubchenko, Y. L., and Soldatenkov, V. A. (2005) Specific binding of poly(ADP-ribose) polymerase-1 to cruciform hairpins, *J Mol Biol 348*, 609-615.
214. Lonskaya, I., Potaman, V. N., Shlyakhtenko, L. S., Oussatcheva, E. A., Lyubchenko, Y. L., and Soldatenkov, V. A. (2005) Regulation of poly(ADP-ribose) polymerase-1 by DNA structure-specific binding, *J Biol Chem 280*, 17076-17083.
215. Ikejima, M., Noguchi, S., Yamashita, R., Ogura, T., Sugimura, T., Gill, D. M., and Miwa, M. (1990) The zinc fingers of human poly(ADP-ribose) polymerase are differentially required for the recognition of DNA breaks and nicks and the consequent enzyme activation. Other structures recognize intact DNA, *J Biol Chem 265*, 21907-21913.
216. Gradwohl, G., Menissier de Murcia, J. M., Molinete, M., Simonin, F., Koken, M., Hoeijmakers, J. H., and de Murcia, G. (1990) The second zinc-finger domain of poly(ADP-ribose) polymerase determines specificity for single-stranded breaks in DNA, *Proc Natl Acad Sci U S A 87*, 2990-2994.
217. Mortusewicz, O., Ame, J. C., Schreiber, V., and Leonhardt, H. (2007) Feedback-regulated poly(ADP-ribosyl)ation by PARP-1 is required for rapid response to DNA damage in living cells, *Nucleic acids research 35*, 7665-7675.
218. Strom, C. E., Johansson, F., Uhlen, M., Szigyarto, C. A., Erixon, K., and Helleday, T. (2011) Poly (ADP-ribose) polymerase (PARP) is not involved in base excision repair but PARP inhibition traps a single-strand intermediate, *Nucleic acids research 39*, 3166-3175.
219. Murai, J., Huang, S. Y., Das, B. B., Renaud, A., Zhang, Y., Doroshow, J. H., Ji, J., Takeda, S., and Pommier, Y. (2012) Trapping of PARP1 and PARP2 by Clinical PARP Inhibitors, *Cancer research 72*, 5588-5599.

220. Woodhouse, B. C., Dianova, II, Parsons, J. L., and Dianov, G. L. (2008) , *DNA Repair (Amst) 7*, 932-940.
221. de Murcia, J. M., Niedergang, C., Trucco, C., Ricoul, M., Dutrillaux, B., Mark, M., Oliver, F. J., Masson, M., Dierich, A., LeMeur, M., Walztinger, C., Chambon, P., and de Murcia, G. (1997) Requirement of poly(ADP-ribose) polymerase in recovery from DNA damage in mice and in cells, *Proc Natl Acad Sci U S A 94*, 7303-7307.
222. Wang, Z. Q., Auer, B., Stingl, L., Berghammer, H., Haidacher, D., Schweiger, M., and Wagner, E. F. (1995) Mice lacking ADPRT and poly(ADP-ribosyl)ation develop normally but are susceptible to skin disease, *Genes Dev 9*, 509-520.
223. Wang, Z. Q., Stingl, L., Morrison, C., Jantsch, M., Los, M., Schulze-Osthoff, K., and Wagner, E. F. (1997) PARP is important for genomic stability but dispensable in apoptosis, *Genes Dev 11*, 2347-2358.
224. Kim, M. Y., Mauro, S., Gevry, N., Lis, J. T., and Kraus, W. L. (2004) NAD+-dependent modulation of chromatin structure and transcription by nucleosome binding properties of PARP-1, *Cell 119*, 803-814.
225. Burkle, A., and Virag, L. (2013) Poly(ADP-ribose): PARadigms and PARadoxes, *Molecular aspects of medicine*.
226. Virag, L., Scott, G. S., Antal-Szalmas, P., O'Connor, M., Ohshima, H., and Szabo, C. (1999) Requirement of intracellular calcium mobilization for peroxynitrite-induced poly(ADP-ribose) synthetase activation and cytotoxicity, *Molecular pharmacology 56*, 824-833.
227. Bentle, M. S., Reinicke, K. E., Bey, E. A., Spitz, D. R., and Boothman, D. A. (2006) Calcium-dependent modulation of poly(ADP-ribose) polymerase-1 alters cellular metabolism and DNA repair, *J Biol Chem 281*, 33684-33696.
228. Blenn, C., Wyrsch, P., Bader, J., Bollhalder, M., and Althaus, F. R. (2011) Poly(ADP-ribose)glycohydrolase is an upstream regulator of Ca2+ fluxes in oxidative cell death, *Cellular and molecular life sciences : CMLS 68*, 1455-1466.
229. Wyrsch, P., Blenn, C., Bader, J., and Althaus, F. R. (2012) Cell death and autophagy under oxidative stress: roles of poly(ADP-Ribose) polymerases and Ca(2+), *Molecular and cellular biology 32*, 3541-3553.
230. Homburg, S., Visochek, L., Moran, N., Dantzer, F., Priel, E., Asculai, E., Schwartz, D., Rotter, V., Dekel, N., and Cohen-Armon, M. (2000) A fast signal-induced activation of Poly(ADP-ribose) polymerase: a novel downstream target of phospholipase c, *The Journal of cell biology 150*, 293-307.
231. Ju, B. G., Solum, D., Song, E. J., Lee, K. J., Rose, D. W., Glass, C. K., and Rosenfeld, M. G. (2004) Activating the PARP-1 sensor component of the groucho/ TLE1 corepressor complex mediates a CaMKinase IIdelta-dependent neurogenic gene activation pathway, *Cell 119*, 815-829.
232. Midorikawa, R., Takei, Y., and Hirokawa, N. (2006) KIF4 motor regulates activity-dependent neuronal survival by suppressing PARP-1 enzymatic activity, *Cell 125*, 371-383.
233. Kauppinen, T. M., Chan, W. Y., Suh, S. W., Wiggins, A. K., Huang, E. J., and Swanson, R. A. (2006) Direct phosphorylation and regulation of poly(ADP-ribose) polymerase-1 by extracellular signal-regulated kinases 1/2, *Proc Natl Acad Sci U S A 103*, 7136-7141.
234. Cohen-Armon, M., Visochek, L., Rozensal, D., Kalal, A., Geistrikh, I., Klein, R., Bendetz-Nezer, S., Yao, Z., and Seger, R. (2007) DNA-independent PARP-1 activation by phosphorylated ERK2 increases Elk1 activity: a link to histone acetylation, *Molecular cell 25*, 297-308.
235. Cohen-Armon, M. (2007) PARP-1 activation in the ERK signaling pathway, *Trends in pharmacological sciences 28*, 556-560.
236. Zhang, S., Lin, Y., Kim, Y. S., Hande, M. P., Liu, Z. G., and Shen, H. M. (2007) c-Jun N-terminal kinase mediates hydrogen peroxide-induced cell death via sustained poly(ADP-ribose) polymerase-1 activation, *Cell death and differentiation 14*, 1001-1010.
237. Tanaka, Y., Koide, S. S., Yoshihara, K., and Kamiya, T. (1987) Poly (ADP-ribose) synthetase is phosphorylated by protein kinase C in vitro, *Biochemical and biophysical research communications 148*, 709-717.
238. Bauer, P. I., Farkas, G., Buday, L., Mikala, G., Meszaros, G., Kun, E., and Farago, A. (1992) Inhibition of DNA binding by the phosphorylation of poly ADP-ribose polymerase protein catalysed by protein kinase C, *Biochemical and biophysical research communications 187*, 730-736.
239. Hegedus, C., Lakatos, P., Olah, G., Toth, B. I., Gergely, S., Szabo, E., Biro, T., Szabo, C., and Virag, L. (2008) Protein kinase C protects from DNA damage-induced necrotic cell death by inhibiting poly(ADP-ribose) polymerase-1, *FEBS letters 582*, 1672-1678.

240. Kuhne, M., Riballo, E., Rief, N., Rothkamm, K., Jeggo, P. A., and Lobrich, M. (2004) A double-strand break repair defect in ATM-deficient cells contributes to radiosensitivity, *Cancer Res 64*, 500-508.
241. Tobiume, K., Matsuzawa, A., Takahashi, T., Nishitoh, H., Morita, K., Takeda, K., Minowa, O., Miyazono, K., Noda, T., and Ichijo, H. (2001) ASK1 is required for sustained activations of JNK/p38 MAP kinases and apoptosis, *EMBO Rep 2*, 222-228.
242. Bain, J., McLauchlan, H., Elliott, M., and Cohen, P. (2003) The specificities of protein kinase inhibitors: an update, *The Biochemical journal 371*, 199-204.
243. Kosar, M., Bartkova, J., Hubackova, S., Hodny, Z., Lukas, J., and Bartek, J. (2011) Senescence-associated heterochromatin foci are dispensable for cellular senescence, occur in a cell type- and insult-dependent manner and follow expression of p16(ink4a), *Cell cycle 10*, 457-468.
244. Meyn, R. E., Munshi, A., Haymach, J. V., Milas, L., and Ang, K. K. (2009) Receptor signaling as a regulatory mechanism of DNA repair, *Radiother Oncol 92*, 316-322.
245. Dittmann, K., Mayer, C., and Rodemann, H. P. (2005) Inhibition of radiation-induced EGFR nuclear import by C225 (Cetuximab) suppresses DNA-PK activity, *Radiother Oncol 76*, 157-161.
246. Toulany, M., Kasten-Pisula, U., Brammer, I., Wang, S., Chen, J., Dittmann, K., Baumann, M., Dikomey, E., and Rodemann, H. P. (2006) Blockage of epidermal growth factor receptor-phosphatidylinositol 3-kinase-AKT signaling increases radiosensitivity of K-RAS mutated human tumor cells in vitro by affecting DNA repair, *Clinical cancer research : an official journal of the American Association for Cancer Research 12*, 4119-4126.
247. Toulany, M., Kehlbach, R., Florczak, U., Sak, A., Wang, S., Chen, J., Lobrich, M., and Rodemann, H. P. (2008) Targeting of AKT1 enhances radiation toxicity of human tumor cells by inhibiting DNA-PKcs-dependent DNA double-strand break repair, *Molecular cancer therapeutics 7*, 1772-1781.
248. Golding, S. E., Rosenberg, E., Neill, S., Dent, P., Povirk, L. F., and Valerie, K. (2007) Extracellular signal-related kinase positively regulates ataxia telangiectasia mutated, homologous recombination repair, and the DNA damage response, *Cancer Res 67*, 1046-1053.
249. Reinhardt, H. C., and Yaffe, M. B. (2009) Kinases that control the cell cycle in response to DNA damage: Chk1, Chk2, and MK2, *Curr Opin Cell Biol 21*, 245-255.
250. Olsen, J. V., Blagoev, B., Gnad, F., Macek, B., Kumar, C., Mortensen, P., and Mann, M. (2006) Global, in vivo, and site-specific phosphorylation dynamics in signaling networks, *Cell 127*, 635-648.
251. Yuan, Z. M., Utsugisawa, T., Ishiko, T., Nakada, S., Huang, Y., Kharbanda, S., Weichselbaum, R., and Kufe, D. (1998) Activation of protein kinase C delta by the c-Abl tyrosine kinase in response to ionizing radiation, *Oncogene 16*, 1643-1648.
252. Martiny-Baron, G., Kazanietz, M. G., Mischak, H., Blumberg, P. M., Kochs, G., Hug, H., Marme, D., and Schachtele, C. (1993) Selective inhibition of protein kinase C isozymes by the indolocarbazole Go 6976, *J Biol Chem 268*, 9194-9197.
253. Wilkinson, S. E., Parker, P. J., and Nixon, J. S. (1993) Isoenzyme specificity of bisindolylmaleimides, selective inhibitors of protein kinase C, *The Biochemical journal 294 (Pt 2)*, 335-337.
254. Basu, A., and Pal, D. (2010) Two faces of protein kinase Cdelta: the contrasting roles of PKCdelta in cell survival and cell death, *ScientificWorldJournal 10*, 2272-2284.
255. Miyamoto, A., Nakayama, K., Imaki, H., Hirose, S., Jiang, Y., Abe, M., Tsukiyama, T., Nagahama, H., Ohno, S., Hatakeyama, S., and Nakayama, K. I. (2002) Increased proliferation of B cells and auto-immunity in mice lacking protein kinase Cdelta, *Nature 416*, 865-869.
256. Yoshida, K., Liu, H., and Miki, Y. (2006) Protein kinase C delta regulates Ser46 phosphorylation of p53 tumor suppressor in the apoptotic response to DNA damage, *J Biol Chem 281*, 5734-5740.
257. Blass, M., Kronfeld, I., Kazimirsky, G., Blumberg, P. M., and Brodie, C. (2002) Tyrosine phosphorylation of protein kinase Cdelta is essential for its apoptotic effect in response to etoposide, *Molecular and cellular biology 22*, 182-195.
258. Datta, R., Kojima, H., Yoshida, K., and Kufe, D. (1997) Caspase-3-mediated cleavage of protein kinase C theta in induction of apoptosis, *J Biol Chem 272*, 20317-20320.
259. Majumder, P. K., Pandey, P., Sun, X., Cheng, K., Datta, R., Saxena, S., Kharbanda, S., and Kufe, D. (2000) Mitochondrial translocation of protein kinase C delta in phorbol ester-induced cytochrome c release and apoptosis, *J Biol Chem 275*, 21793-21796.
260. Basu, A., Woolard, M. D., and Johnson, C. L. (2001) Involvement of protein kinase C-delta in DNA damage-induced apoptosis, *Cell death and differentiation 8*, 899-908.

261. Ghayur, T., Hugunin, M., Talanian, R. V., Ratnofsky, S., Quinlan, C., Emoto, Y., Pandey, P., Datta, R., Huang, Y., Kharbanda, S., Allen, H., Kamen, R., Wong, W., and Kufe, D. (1996) Proteolytic activation of protein kinase C delta by an ICE/CED 3-like protease induces characteristics of apoptosis, *The Journal of experimental medicine 184*, 2399-2404.
262. Clark, A. S., West, K. A., Blumberg, P. M., and Dennis, P. A. (2003) Altered protein kinase C (PKC) isoforms in non-small cell lung cancer cells: PKCdelta promotes cellular survival and chemotherapeutic resistance, *Cancer research 63*, 780-786.
263. McCracken, M. A., Miraglia, L. J., McKay, R. A., and Strobl, J. S. (2003) Protein kinase C delta is a prosurvival factor in human breast tumor cell lines, *Molecular cancer therapeutics 2*, 273-281.
264. Smith, S. D., Enge, M., Bao, W., Thullberg, M., Costa, T. D., Olofsson, H., Gashi, B., Selivanova, G., and Stromblad, S. (2012) Protein kinase Calpha (PKCalpha) regulates p53 localization and melanoma cell survival downstream of integrin alphav in three-dimensional collagen and in vivo, *J Biol Chem 287*, 29336-29347.
265. Cameron, A. J., Procyk, K. J., Leitges, M., and Parker, P. J. (2008) PKC alpha protein but not kinase activity is critical for glioma cell proliferation and survival, *Int J Cancer 123*, 769-779.
266. Lutzny, G., Kocher, T., Schmidt-Supprian, M., Rudelius, M., Klein-Hitpass, L., Finch, A. J., Durig, J., Wagner, M., Haferlach, C., Kohlmann, A., Schnittger, S., Seifert, M., Wanninger, S., Zaborsky, N., Oostendorp, R., Ruland, J., Leitges, M., Kuhnt, T., Schafer, Y., Lampl, B., Peschel, C., Egle, A., and Ringshausen, I. (2013) Protein kinase c-beta-dependent activation of NF-kappaB in stromal cells is indispensable for the survival of chronic lymphocytic leukemia B cells in vivo, *Cancer Cell 23*, 77-92.
267. Bavik, C., Coleman, I., Dean, J. P., Knudsen, B., Plymate, S., and Nelson, P. S. (2006) The gene expression program of prostate fibroblast senescence modulates neoplastic epithelial cell proliferation through paracrine mechanisms, *Cancer research 66*, 794-802.
268. Coppe, J. P., Kauser, K., Campisi, J., and Beausejour, C. M. (2006) Secretion of vascular endothelial growth factor by primary human fibroblasts at senescence, *J Biol Chem 281*, 29568-29574.
269. Krtolica, A., Parrinello, S., Lockett, S., Desprez, P. Y., and Campisi, J. (2001) Senescent fibroblasts promote epithelial cell growth and tumorigenesis: a link between cancer and aging, *Proc Natl Acad Sci U S A 98*, 12072-12077.
270. Martens, J. W., Sieuwerts, A. M., Bolt-deVries, J., Bosma, P. T., Swiggers, S. J., Klijn, J. G., and Foekens, J. A. (2003) Aging of stromal-derived human breast fibroblasts might contribute to breast cancer progression, *Thrombosis and haemostasis 89*, 393-404.
271. Sun, Y., Campisi, J., Higano, C., Beer, T. M., Porter, P., Coleman, I., True, L., and Nelson, P. S. (2012) Treatment-induced damage to the tumor microenvironment promotes prostate cancer therapy resistance through WNT16B, *Nature medicine 18*, 1359-1368.
272. Mizuguchi, H., Terao, T., Kitai, M., Ikeda, M., Yoshimura, Y., Das, A. K., Kitamura, Y., Takeda, N., and Fukui, H. (2011) Involvement of protein kinase Cdelta/extracellular signal-regulated kinase/poly(ADP-ribose) polymerase-1 (PARP-1) signaling pathway in histamine-induced up-regulation of histamine H1 receptor gene expression in HeLa cells, *J Biol Chem 286*, 30542-30551.
273. Mizuguchi, H., Miyagi, K., Terao, T., Sakamoto, N., Yamawaki, Y., Adachi, T., Ono, S., Sasaki, Y., Yoshimura, Y., Kitamura, Y., Takeda, N., and Fukui, H. (2012) PMA-induced dissociation of Ku86 from the promoter causes transcriptional up-regulation of histamine H(1) receptor, *Scientific reports 2*, 916.
274. Gagne, J. P., Moreel, X., Gagne, P., Labelle, Y., Droit, A., Chevalier-Pare, M., Bourassa, S., McDonald, D., Hendzel, M. J., Prigent, C., and Poirier, G. G. (2009) Proteomic investigation of phosphorylation sites in poly(ADP-ribose) polymerase-1 and poly(ADP-ribose) glycohydrolase, *Journal of proteome research 8*, 1014-1029.
275. Feijs, K. L., Kleine, H., Braczynski, A., Forst, A. H., Herzog, N., Verheugd, P., Linzen, U., Kremmer, E., and Luscher, B. (2013) ARTD10 substrate identification on protein microarrays: regulation of GSK3beta by mono-ADP-ribosylation, *Cell Commun Signal 11*, 5.
276. Rosenthal, F., Feijs, K. L., Frugier, E., Bonalli, M., Forst, A. H., Imhof, R., Winkler, H. C., Fischer, D., Caflisch, A., Hassa, P. O., Luscher, B., and Hottiger, M. O. (2013) Macrodomain-containing proteins are new mono-ADP-ribosylhydrolases, *Nat Struct Mol Biol 20*, 502-507.
277. Schmalz, D., Hucho, F., and Buchner, K. (1998) Nuclear import of protein kinase C occurs by a mechanism distinct from the mechanism used by proteins with a classical nuclear localization signal, *Journal of cell science 111 (Pt 13)*, 1823-1830.
278. Kodiha, M., Rassi, J. G., Brown, C. M., and Stochaj, U. (2007) Localization of AMP kinase is regulated by stress, cell density, and signaling through the MEK-->ERK1/2 pathway, *American journal of physiology. Cell physiology 293*, C1427-1436.

279. Jaaro, H., Rubinfeld, H., Hanoch, T., and Seger, R. (1997) Nuclear translocation of mitogen-activated protein kinase kinase (MEK1) in response to mitogenic stimulation, *Proc Natl Acad Sci U S A 94*, 3742-3747.
280. Fang, X., Yu, S., Tanyi, J. L., Lu, Y., Woodgett, J. R., and Mills, G. B. (2002) Convergence of multiple signaling cascades at glycogen synthase kinase 3: Edg receptor-mediated phosphorylation and inactivation by lysophosphatidic acid through a protein kinase C-dependent intracellular pathway, *Molecular and cellular biology 22*, 2099-2110.
281. Ueda, Y., Hirai, S., Osada, S., Suzuki, A., Mizuno, K., and Ohno, S. (1996) Protein kinase C activates the MEK-ERK pathway in a manner independent of Ras and dependent on Raf, *J Biol Chem 271*, 23512-23519.
282. Tsien, R. Y. (1980) New calcium indicators and buffers with high selectivity against magnesium and protons: design, synthesis, and properties of prototype structures, *Biochemistry 19*, 2396-2404.
283. Jornot, L., Petersen, H., and Junod, A. F. (1998) Hydrogen peroxide-induced DNA damage is independent of nuclear calcium but dependent on redox-active ions, *The Biochemical journal 335 (Pt 1)*, 85-94.
284. Britigan, B. E., Rasmussen, G. T., and Cox, C. D. (1998) Binding of iron and inhibition of iron-dependent oxidative cell injury by the "calcium chelator" 1,2-bis(2-aminophenoxy)ethane N,N,N',N'-tetraacetic acid (BAPTA), *Biochemical pharmacology 55*, 287-295.
285. Golconda, M. S., Ueda, N., and Shah, S. V. (1993) Evidence suggesting that iron and calcium are interrelated in oxidant-induced DNA damage, *Kidney international 44*, 1228-1234.
286. Nagata, S. (2000) Apoptotic DNA fragmentation, *Experimental cell research 256*, 12-18.
287. Ueda, N., and Shah, S. V. (1992) Endonuclease-induced DNA damage and cell death in oxidant injury to renal tubular epithelial cells, *The Journal of clinical investigation 90*, 2593-2597.
288. Adamson, B., Smogorzewska, A., Sigoillot, F. D., King, R. W., and Elledge, S. J. (2012) A genome-wide homologous recombination screen identifies the RNA-binding protein RBMX as a component of the DNA-damage response, *Nat Cell Biol 14*, 318-328.

Curriculum Vitae

Andrej Bluwstein

Guggachstr. 25
CH-8057 Zürich

+41 77 4359967
andrej.bluwstein@vetbio.uzh.ch

Personal Information

Date of Birth	27.03.1984
Place of Birth	Surgut, Russia
Nationality	German

Education

01/2010 – today	University of Zurich (UZH), Switzerland Int. **PhD program in Cancer Biology**, Life Science Zurich Graduate School Currently employed in the lab of Prof. Michael O. Hottiger, IVBMB
08/2007 – 11/2009	Technical University of Munich (TUM), Germany **Master's studies in Molecular Biotechnology** Degree: Master of Science - **Ø 1,3 (passed with distinction, ECTS-Grade: A)**
08/2007 – 06/2008	Uppsala University (UU), Sweden **Exchange studies** (majors: **Functional Genomics and Microbiology**) Erasmus-Exchange-Program
10/2004 – 08/2007	Technical University of Munich (TUM), Germany **Bachelor's studies in Molecular Biotechnology** Degree: Bachelor of Science - **Ø 1,9 (passed with merit, ECTS-Grade: B)**
09/1995 – 07/2004	Lessing-Gymnasium Karlsruhe, Germany **Abitur** (German school leaving examination) - Ø 2,2 Foreign languages: English Intensive courses: Biology and Chemistry

Languages

German:	Excellent
English:	Excellent (**TOEFL iBT**, 10/2008 at F+U Heidelberg, **total score: 102**)
Russian:	Fluent, written and spoken
French:	Basics

Personal Interests

News papers (World affairs, Environment and Public health), Travelling, Snowboarding, Cooking, Nature, Friends

Fellowships

08/2007 – 06/2008	SOCRATES / ERASMUS Sholarship

List of Publications

Lemeer S, Bluwstein A, Wu Z, Leberfinger J, Müller K, Kramer K, Kuster B. **Phosphotyrosine mediated protein interactions of the discoidin domain receptor 1.** J Proteomics. 2012 Jun 27;75(12):3465-77.

Bluwstein A, Kumar N, Léger K, Traenkle J, Oostrum Jv, Rehrauer H, Baudis M, Hottiger MO. **PKC signaling prevents irradiation-induced apoptosis of primary human fibroblasts.** Cell Death Dis. 2013 Feb 14;4:e498.

Acknowledgements

My special thanks go to my supervisor Michael Hottiger for providing the topic of my thesis, continuous support, critical comments and wise suggestions during fruitful discussions. Many thanks go to Karo, who supported me scientifically, during the personal group meetings, as well as for her open ears during difficult phases of the four years. Of course I also would like to thank all the group members of the Hottiger lab for the great time during the daily routine in the lab, but also happy moments outside of the lab! Moreover, I would like to thank the whole institute for the great atmosphere in and outside of the lab.

Many thanks to Nitin Kumar, Nicole Grosse and colleagues of Zeptosens (now Bayer AG) for great collaborations and support during experiments and data analysis. Many thanks for my thesis committee members, Michael Hottiger, Alessandro Sartori, Lars French and Markus Ehrat for scientific support during thesis committee reports.

Thanks to my friends outside and around Zurich, who made it possible never to forget that there is also life outside of the lab. Finally and especially I would like to thank to my mom and dad, my brother and Steph and in particular to my love, Nina, for their tireless support, love, comprehension and trust especially during the whole period and the tough moments of the seemingly never-ending writing phase.